Higher-dimensional black holes: Braneworld stars and Hawking radiation.

Creek, Simon

Higher-Dimensional Black Holes: Braneworld Stars and Hawking Radiation.

Simon Creek

A Thesis presented for the degree of
Doctor of Philosophy

The Centre for Particle Theory
Department of Mathematical Sciences
University of Durham
England

November 2007

Acknowledgements

Although a thesis must ultimately be attributed to an individual, it is a pleasure to acknowledge those who have contributed throughout, not just financially or scientifically, but also in helping to preserve my sanity.

Foremost I would like to thank my supervisor Panagiota Kanti for years of guidance, encouragement and support. There are few PhD students as fortunate as I to have benefitted from such counsel and been guided through as fruitful a series of research projects. For this I am extremely grateful. I would like to extend thanks to my closest collaborators: Ruth Gregory, Bina Mistry, Kyriakos Tamvakis and Orestis Efthimiou for their many hours of discussion and analysis. I must also offer sincere thanks to the Particle Physics and Astronomy Research Council for their financial support, as without studentship PPA/S/S/2004/03815 none of this would have been possible.

Thanks go to my officemates for much needed distraction, and in particular Andy and his infinite supply of games and puzzles to while away the day; also to all the guys upstairs for coffee time distraction and the latest update on the plight of the 'Boro. Then there are the residents of 7 Dickens Wynd. John, James, Kemal and Martyn – some of the greatest pleasures I take away from my time in Durham are the memories that have followed from making your acquaintance. It is often said that really close friends are hard to come by. I guess I must have been impossibly lucky to find so many in the same place, and at the same time.

I'd like to thank my family, in particular my parents for their support and many hours of discussion, even when none of us really knew what we were talking about.

Finally I'd like to thank Izy. For listening, for understanding, for being there when I needed you; but most of all – for waiting.

Declaration

The work in this thesis is based on research carried out at the Centre for Particle Theory, Department of Mathematical Sciences, University of Durham, England. No part of this thesis has been submitted elsewhere for any other degree or qualification and it is all my own work unless referenced to the contrary in the text.

Chapters 1 and 2 of this thesis present an introduction to extra-dimensional theories and review of braneworld models. Chapter 3 is original work, focusing on my contribution to a publication that resulted from collaboration with Prof. Ruth Gregory, Bina Mistry and my supervisor, Prof. Panagiota Kanti [1]. Chapter 4 contains background material required in the study of Hawking radiation from higher-dimensional black holes. Chapters 5–7 comprise new material researched in collaboration with Prof. Panagiota Kanti, Prof. Kyriakos Tamvakis and Orestis Efthimiou [2–5].

Higher-Dimensional Black Holes: Braneworld Stars and Hawking Radiation.

Simon Creek

Submitted for the degree of Doctor of Philosophy
November 2007

Abstract

In this thesis two aspects of braneworld models are studied. A new attempt at finding the metric of a braneworld black hole within the second Randall-Sundrum model is explored. Branes containing distributions of perfect fluid are embedded in a variety of 5-dimensional $SO(4)$-symmetric bulk spacetimes so that the Israel junction conditions are satisfied. A particular class of time-dependent embeddings are studied and shown to be unable to describe the braneworld black hole. Static trajectories are then investigated in five-dimensional anti-de Sitter and Schwarzschild backgrounds. These reveal a wide variety of permissible trajectories which are classified according to their energy-momentum profiles. The static embedding of branes in a Schwarzschild-anti-de Sitter spacetime is then explored, revealing objects with possible interpretation as "braneworld stars".

The evaporation of higher-dimensional rotating black holes, both on the brane and in the bulk is studied from an analytical perspective. A matching technique is employed to derive the solution for the radial component of the fields of scalars, fermions and gauge bosons propagating in the brane-induced line-element of a higher-dimensional rotating black hole. These solutions are used to calculate Hawking radiation spectra from a black hole in the spin-down phase of its lifetime within the Arkani-Hamed-Dimopoulos-Dvali model. The same method is used to calculate the emission of scalar fields into the bulk spacetime of a higher-dimensional rotating black hole and a comparison is made between brane and bulk emission rates. Finally the matching technique is applied to the problem of graviton emission in the bulk from a higher-dimensional Schwarzschild black hole.

For my parents

Contents

Chapter 1

Introduction

Since 1865 when James Clerk Maxwell unified the equations of electricity and magnetism, physicists have remained acutely aware that a deeper order may lie beneath the multitude of seemingly fundamental forces. One hundred years later the uniting of electromagnetism and the weak force by Weinberg and Salam reduced the number of independent forces further and gave tantalising suggestion that a route to the unification of all known forces may exist. To this day great effort is expended in the search for "Grand Unification", consolidating the electroweak and strong forces into a single framework and simplifying the somewhat arbitrary structure of the Standard Model of Particle Physics.

At its most basic level the Standard Model consists of a menagerie of particles: 12 force carriers, 48 matter particles and the (as yet undiscovered) Higgs boson. The electroweak and strong forces are described by gauge theories, arising from the symmetry group $SU(3) \times SU(2) \times U(1)$. Upon careful selection of around 20 adjustable parameters the Standard Model obtains extraordinarily accurate predictive power when compared with experiment at energies up to 1 TeV. Despite this power the theory has a failure so critical that it remains an impossible endpoint for theoretical particle physics: there is no mention of the oldest known force.

The classical theory of gravity is Einstein's general relativity [6] where the background upon which physics plays becomes a dynamical arena. Matter causes spacetime to curve and this curvature determines the motion of particles along spacetime geodesics. According to Einstein the structure and evolution of our four-dimensional

universe is governed by the equation

$$R_{\mu\nu} - \frac{1}{2}Rg_{\mu\nu} = 8\pi {}^{(4)}G_N T_{\mu\nu}\,, \tag{1.1}$$

where $R_{\mu\nu}$ and R are the Ricci tensor and scalar respectively, $g_{\mu\nu}$ is the spacetime metric, ${}^{(4)}G_N$ is Newton's gravitational constant and $T_{\mu\nu}$ is the energy-momentum tensor describing the matter content of the universe. The Einstein equations (1.1) can be derived from variation of the Einstein-Hilbert action [7,8]

$$S = \frac{1}{16\pi {}^{(4)}G_N}\int \sqrt{-g}Rd^4x + S_M\,, \tag{1.2}$$

where

$$T_{\mu\nu} = -\frac{2}{\sqrt{-g}}\frac{\delta S_M}{\delta g^{\mu\nu}}\,, \qquad \text{and} \qquad g = \det g_{\mu\nu}\,.$$

A major obstacle in the union of gravity and particle physics is that general relativity is a classical theory whereas the Standard Model is quantum in nature. Given the success of quantum theory it is generally believed that some method of quantising gravity is required to successfully describe physics beyond the classically valid regime. Unfortunately, direct efforts to achieve this have met with results that are either incalculable or unpredictive [9–11]. On a practical level this is not a problem as the energy at which quantum gravity effects become significant is given by the Planck scale, ${}^{(4)}M_P = \sqrt{\frac{\hbar c}{{}^{(4)}G_N}} \sim 10^{19}$ GeV, which is far beyond the anticipated reach of even the most powerful present-day particle accelerators[1]. While this is a convenient situation for existing theory to enjoy, the lack of experimental results in the quantum gravity regime acts as a hindrance to development of the correct quantum theory of gravity. The situation also poses the question – why is the fundamental scale of gravity sixteen orders of magnitude larger than the electroweak scale of Standard Model forces, $M_w \sim 1$ TeV? On a conceptual level, the absence of a consistent method of quantising gravity is deeply unsatisfactory and a number of new theories have been proposed as candidate quantum gravity descriptions. In parallel there has been a concerted effort to explain the disturbing hierarchy present

[1]When operational it is anticpated the Large Hadron Collider will conduct experiments with centre of mass energy $\sim 1.4 \times 10^4$ GeV.

in the energy scales of the fundamental forces. Out of these investigations string theory has emerged as a leading contender.

String theory [12–14] is a quantum theory in which all particles are unified as the particular vibrational modes of elementary microscopic strings. Among the many quantum vibrational states of the relativistic string, one closed-string mode can be identified as the particle of gravity, and consequently the theory may be viewed as a consistent quantum theory of gravity. Realistic models of string theory incorporate supersymmetry and by the mid 1980s five distinct superstring theories had been discovered. Many interrelations between these theories have been discovered and it is believed that they all arise as different limits of a single theory, known as M-theory [15–17]. A somewhat surprising calculational result is that M-theory operates in eleven dimensions, while the superstrings it contains are ten-dimensional in nature.

1.1 Extra Dimensions

At first sight a fundamentally eleven-dimensional spacetime is at odds with both the Standard Model, explicitly constructed to operate in four dimensions, and the predictions of general relativity, where a Newtonian inverse-square gravitational force is intimately tied to the existence of only three accessible spatial dimensions. To see this consider a generalisation of the static, non-relativistic, weak-field limit of Einstein's equations governing the gravitational potential ${}^{(4+n)}V$ when n extra dimensions are introduced

$$\nabla^2 {}^{(4+n)}V = S_{(3+n)}\, {}^{(4+n)}G_N\, \rho_m \,, \tag{1.3}$$

where $S_{(D)} = 2\pi^{D/2}/\Gamma(D/2)$ is the surface area of the unit sphere in D spatial dimensions, ${}^{(4+n)}G_N$ is the higher-dimensional generalisation of Newton's constant and ρ_m is the matter density sourcing the gravitational field. If the matter density is taken to be a point particle of mass m then application of the (4+n)-dimensional Gauss law gives the gravitational force per unit mass exerted by this particle as

$${}^{(4+n)}F(r) = -\frac{{}^{(4+n)}G_N\, m}{r^{n+2}} \,. \tag{1.4}$$

Dilution of gravity into the larger volume of extra-dimensional space weakens its effect between two bodies separated by all but the smallest of distances. This result is in conflict with experience of the long range nature of the gravitational force and seemingly excludes the possibility of extra dimensions.

Turning a momentary blind eye to empirical evidence, the calculational prediction of the number of dimensions may also be viewed as a strength of string theory. Historically the number of spatial dimensions has been regarded as yet another parameter to be entered into a theory by hand. However, it now seems plausible that this number is not arbitrary, but determined by underlying theoretical consistency. For string theory to be a serious candidate for a unified theory it is clearly necessary to hide the extra dimensions from everyday view, thereby resolving the conflict between their existence and physical experience.

1.2 Kaluza-Klein Compactification

One method proposed by Kaluza in 1921 (and subsequently extended by Klein) [18, 19] was motivated by a desire to unify gravity and electromagnetism. Kaluza considered a five-dimensional universe in which the extra spatial dimension is compactified on a circle of radius L through the identification $y \sim y + 2\pi kL$ where k takes all integer values. When the 5-d metric is expanded in a Fourier series as

$$g_{AB}(x^\mu, y) = \sum_k e^{\frac{iky}{L}} g^k_{AB}(x^\mu)\,, \tag{1.5}$$

where $g^k_{AB}(x^\mu)$ are the amplitudes of the Kaluza-Klein modes, it can be seen that the 5-d nature of the universe is manifested in the 4-d effective theory as an infinite number of fields with masses $|k|/L$. If the radius of the compact dimension is sufficiently small (eg. of order the Planck length, ${}^{(4)}l_P = \sqrt{\frac{\hbar\, {}^{(4)}G_N}{c^3}} \sim 10^{-33}$ cm) so that the energy of the first Kaluza-Klein mode ($k = 1$) is greater than that accessible by particle physics experiments, then the effective low-energy theory contains massless modes only and the effective metric can be assumed independent of the extra dimension, y. Under these conditions Kaluza and Klein showed that the action for five-dimensional gravity, calculated truncating the five-dimensional metric at the zero mode in the

Fourier expansion, naturally reproduces the action for four-dimensional gravity and electromagnetism coupled to a scalar field. This demonstrated that extra dimensions could be present in the universe but hidden from experimental view providing they are compactified on a very small scale.

1.3 Braneworlds

An alternative method of ensuring the known results of particle physics are preserved is to confine the Standard Model, a priori, to a four-dimensional slice of a higher-dimensional spacetime. With all conventional matter fixed by some mechanism to a hypersurface of appropriate dimension the additional dimensions need no longer be curled tightly out of sight, but may be large or even infinite in extent. Such a hypersurface upon which our everyday universe resides is commonly referred to as a "brane". A critical feature of braneworld models is that while matter is confined to the brane, gravity, being the dynamics of spacetime itself, must necessarily be higher-dimensional in nature and permeate both the brane and the extra dimensions of the bulk. At the same time it remains of utmost importance that any viable theory including extra dimensions must produce a phenomenologically acceptable four-dimensional theory of gravity and cosmology. It was shown in equation (1.4) that the observed Newtonian inverse-square law relies heavily on the presence of exactly three spatial dimensions. A major task of braneworld models is finding an extra-dimensional configuration that recovers this result.

1.3.1 Arkani-Hamed-Dimopoulos-Dvali (ADD) Braneworlds

In 1998 the ADD model [20–22] was proposed as a framework for solving the hierarchy problem. It achieved this by suggesting that the fundamental scales of gravity and Standard Model forces are, in fact, the same. According to the model, gravitational and gauge interactions become united at the weak scale, M_w, which is then the only fundamental short distance scale in nature. This is possible because there exists a number of large (in comparison to the Planck length) extra dimensions and the observed Planck mass, ${}^{(4)}M_P \sim 10^{19}$ GeV, is only an effective scale whose relative

enormity is purely a consequence of our four-dimensional viewpoint.

To see how this might arise it is necessary to relate the observed Planck mass, ${}^{(4)}M_P$, to that of the higher-dimensional theory, ${}^{(4+n)}M_P \sim 1$ TeV, by pursuing a simple Gauss' law calculation and dimensional analysis argument. To begin with, the relationship between ${}^{(4+n)}G_N$ and ${}^{(4)}G_N$ (the full and effective Newton's constants) must be established. Suppose that the n extra dimensions are compactified as in the Kaluza-Klein case: $y_\alpha \sim y_\alpha + 2\pi kL$, and a point mass, m, is placed at some origin in the spacetime. This situation is equivalent to an infinite n-dimensional lattice of "image masses" in an uncompactified spacetime. The force on a test particle at a distance $r \ll 2\pi L$ from the mass will be essentially higher-dimensional in nature, as in equation (1.4), owing to the minimal contributions from the image masses. At much larger distances, $r \gg 2\pi L$ the resolution between discrete image masses will be lost and they will appear as continuous infinite strings of uniform mass density in each of the extra dimensions. The gravitational field at such a distant point can then be found by performing a Gauss' law integration over a cylinder centred around the n-dimensional line of mass, with side length l and three-dimensional spheres of radius r forming the ends. Such an integration gives the effective four-dimensional force per unit mass on a test particle as

$$ {}^{(4)}F(r) = -S_{(3+n)}\frac{{}^{(4+n)}G_N\, m}{4\pi(2\pi L)^n r^2} = -\frac{{}^{(4)}G_N\, m}{r^2}\,. \tag{1.6} $$

From this it is clear that the fundamental and effective Newton's constants are related by the volume of the extra-dimensional space: ${}^{(4+n)}G_N \sim L^n\, {}^{(4)}G_N$.

The Planck mass may be defined in arbitrary dimension as the unique combination of the fundamental constants c, $\hbar$ and ${}^{(4+n)}G_N$ that has units of mass. From equation (1.4) the dimensionality of ${}^{(4+n)}G_N$ clearly varies with the dimensionality of spacetime, in particular

$$ \left[{}^{(4+n)}G_N\right] : \frac{L^{3+n}}{MT^2}\,, \qquad [c] : \frac{L}{T}\,, \qquad [\hbar] : \frac{ML^2}{T}\,. $$

From this ${}^{(4+n)}M_P$ can be calculated as

$$ {}^{(4+n)}M_P = \left[\frac{\hbar c}{{}^{(4+n)}G_N}\left(\frac{\hbar}{c}\right)^n\right]^{\frac{1}{2+n}}\,, \tag{1.7} $$

and substituting for ${}^{(4+n)}G_N$ yields

$$ {}^{(4+n)}M_P^{2+n} \sim \frac{1}{L^n}\frac{\hbar c}{{}^{(4)}G_N}\left(\frac{\hbar}{c}\right)^n = \frac{{}^{(4)}M_P^2}{L^n}, \tag{1.8} $$

where in the last equality natural units have been adopted by setting $\hbar = c = 1$. So the fundamental and effective scales of the gravitational interaction are also related by the volume of extra dimensional space: ${}^{(4)}M_P^2 \sim L^n\,{}^{(4+n)}M_P^{2+n}$.

The presence of massive Kaluza-Klein gravitons in extra dimensional theories modifies the cross-sections of Standard Model particle interactions, but this imposes only very mild constraints on the possible size of extra dimensions. Torsion balance experiments have sought to observe extra dimensions directly through modifications to Newton's law at small scales. Taking the fundamental Planck mass $\sim$ 1 TeV and the observed value of the effective 4-d Planck mass, if there exists just one extra dimension then the above relation would suggest its size is of order 10^{13}cm, implying deviations from Newtonian gravity over scales the size of the solar system. Such a result is excluded by experiment. If there are two extra dimensions then the limit to their size decreases to approximately 0.1 mm. The most recent torsion balance experiments [23–25] have demonstrated the accuracy of Newton's law down to $\approx 50\mu m$, suggesting $n = 2$ is excluded also.

It may be argued that the ADD model does not pose a satisfactory explanation of the hierarchy problem as it merely removes one disparity in scales by introducing another, specifically that between the weak scale and the compactification scale: $M_w \gg 1/L$. However by confining all but the gravitational sector to the brane the model demonstrated that the size of extra compact dimensions may be much larger than previously supposed and is mainly restricted by the current limit on the scale at which the Newtonian inverse-square law is known to hold true.

1.3.2 Randall-Sundrum (RS) Braneworlds

In 1999 Randall and Sundrum proposed a novel solution to the hierarchy problem [26] whereby our 4-dimensional universe is confined to a brane in a bulk spacetime with negative curvature. Their model utilises a non-factorisable five-dimensional geometry, in which the 4-dimensional metric of the visible universe is dependent

on the location of the brane in the higher-dimensional bulk. The extra dimension is compactified and $\mathbb{Z}_2$ symmetric with a negative tension brane (on which our universe resides) and a hidden positive tension brane located at the orbifold fixed points. In this scenario it can be seen that mass hierarchies in our visible universe are exponentially generated from fundamental mass scales all of order ${}^{(4)}M_P$ owing to the curvature of the bulk and the separation of the branes in the higher dimension.

In a subsequent paper [27] Randall and Sundrum extended this setup and, discarding the hidden brane of their first model, demonstrated that Newtonian gravity can be consistent with the presence of non-compact extra dimensions if the geometry of the bulk spacetime forces the zero mode of the five-dimensional graviton to be bound to the brane. Having such a mode ensures four-dimensional Newtonian gravity is recovered on the brane, while the contribution from the continuum of Kaluza-Klein states generates a correction to the force law that is potentially observable in short-distance gravitational experiments.

It is this second Randall-Sundrum model that is perhaps the most geometrically appealing form of the braneworld model and forms the foundation upon which a significant part of this thesis is based. Consequently a full discussion of the Randall-Sundrum models is conducted in chapter 2.

1.3.3 Dvali, Gabadadze and Porrati (DGP) Braneworlds

Shortly after Randall and Sundrum showed that extra dimensions could be compatible with Newtonian gravity in a warped spacetime, Dvali et al. demonstrated that such a situation was also possible with infinite flat extra dimensions [28]. They examined the competition between the bulk five-dimensional curvature scalar, ${}^{(5)}R$, and the corresponding intrinsic curvature scalar on the brane, ${}^{(4)}R$, in an action of the form

$$S = \frac{1}{16\pi {}^{(5)}G_N}\int \sqrt{-{}^{(5)}g}\,{}^{(5)}R d^5x + \frac{1}{16\pi {}^{(4)}G_N}\int \sqrt{-{}^{(4)}g}\,{}^{(4)}R d^4x\,, \tag{1.9}$$

where ${}^{(5)}g_{MN}(x) = {}^{(5)}g_{MN}(x^\alpha, y)$ is the five-dimensional bulk metric for which ${}^{(5)}R$ is the Ricci scalar and ${}^{(4)}g_{\mu\nu}(x) = {}^{(5)}g_{\mu\nu}(x^\alpha, 0)$ is the induced metric on the brane (located at $y = 0$) with corresponding 4-d Ricci scalar, ${}^{(4)}R$. Analysis of the grav-

itational potential on the brane found by considering small perturbations from a five-dimensional Minkowski bulk produces the $1/r$ form of the Newtonian potential at small distances, with a leading-order correction corresponding to logarithmic repulsion. However, in the DGP case the tensor structure of the graviton propagator is found to correspond to a massless five-dimensional graviton (or equivalently a massive 4-dimensional one),

$$\frac{1}{2}\eta^{\mu\alpha}\eta^{\nu\beta} + \frac{1}{2}\eta^{\mu\beta}\eta^{\nu\alpha} - \frac{1}{3}\eta^{\mu\nu}\eta^{\alpha\beta}\,, \tag{1.10}$$

instead of the desired massless four-dimensional propagator,

$$\frac{1}{2}\eta^{\mu\alpha}\eta^{\nu\beta} + \frac{1}{2}\eta^{\mu\beta}\eta^{\nu\alpha} - \frac{1}{2}\eta^{\mu\nu}\eta^{\alpha\beta}\,. \tag{1.11}$$

While this difference may seem slight, it is critical in reproducing the results of 4-dimensional gravity as a 5-dimensional graviton has an extra polarisation state, manifested as an additional four-dimensional scalar field, which must be included in the 4-d effective theory. Therefore having a graviton propagator with the structure of (1.10) is equivalent to having a scalar-tensor theory of gravity from the four-dimensional perspective, which yields an additional attractive force. This additional force causes the DGP model to predict anomalous results for experimental tests of general relativity. In particular the gravitational bending of light by the sun is found to be only 3/4 its correct value [29].

1.4 Summary and Overview

The notion of confinement of non-gravitational physics to lower-dimensional hypersurfaces holds particular importance in string theory where open strings, representing the matter and gauge particle sector, are attached at each end to objects known as D-branes. Braneworld models, such as those outlined in this chapter, present an instructive phenomenological realisation of string theory ideas and have consequently been the source of a great deal of research over the last decade. While three of the most common classes of braneworld model have been outlined here, it should be noted that numerous other brane configurations have been explored in the literature [30–33]. As the braneworld concept has matured it has developed into an

interesting possible resolution of a number of longstanding problems in mathematical physics, most notably the hierarchy problem and the consistent incorporation of extra dimensions. Many extensive review articles have been written [34–37], the contents of which have been drawn upon while preparing the theoretical background presented in chapters 2 and 4.

In the course of extended debate with physicists and mathematicians it is easy to lose the sense of wonder felt upon first realisation that the universe might have more dimensions than the three we readily perceive. If incontrovertible evidence of extra dimensions were to be found through experiment it would be a truly revolutionary discovery. One of the most exciting aspects of braneworld theory is that it does not exclude such discoveries being made in the relatively near future. Given the possible lowering of the fundamental scale of gravity down to levels achievable in the Large Hadron Collider, there is a chance that production of microscopic black holes in ground-based experiment may be within present technical capability. The prospect of witnessing quantum gravity effects has never been so close.

***

To outline the content of this thesis: in chapter 2 a review of the Randall-Sundrum models will be conducted. Subsequent attempts to find descriptions of astrophysical objects, such as black holes, within this framework will be outlined and the limitations of the resulting expressions will be discussed. Chapter 3 presents a new approach to the search for a braneworld black hole. Although the braneworld black hole metric remains elusive, by embedding a four-dimensional brane containing perfect fluid in a number of bulk spacetimes, a fully consistent system describing objects with interpretation as braneworld "stars" is obtained.

In the absence of an analytic braneworld black hole metric the calculation of observable signatures of astrophysical objects within the Randall-Sundrum framework is somewhat restricted. However, progress can be made within the ADD model, a scenario which may be considered equivalent to a Randall-Sundrum braneworld when the brane tension, black hole mass and bulk curvature are all small. It is possible to derive the field equations for particles propagating in higher-dimensional black hole backgrounds and compute the Hawking radiation spectrum both on the

brane and in the bulk. Chapter 4 outlines the theory behind this calculation and defines the quantities used to characterise Hawking radiation spectra from higher-dimensional black holes. Chapter 5 contains a new calculation of the emission of particles from a higher-dimensional rotating black hole onto the brane, while chapter 6 is concerned with emission of scalars into the bulk. Chapter 7 fills a gap existing in the literature by examining the emission of gravitons from a higher-dimensional Schwarzschild black hole into the bulk. Finally, in chapter 8 conclusions are drawn.

Chapter 2

Randall-Sundrum Braneworlds

When developing their first braneworld model Randall and Sundrum were motivated by resolving the hierarchy problem. The ADD model had recently offered an explanation using large extra dimensions that eliminated one disparity in scales by creating another. To avoid this rather unsatisfactory feature they considered a brane configuration motivated by a new $S^1/\mathbb{Z}_2$ compactification of M-theory [38,39] combined with a non-factorisable warped geometry.

2.1 The Randall-Sundrum Two Brane Model (RS1)

In the first Randall-Sundrum model [26] two four-dimensional branes are embedded in a five-dimensional anti-de Sitter (adS) bulk. The extra dimension, denoted by the coordinate ϕ with range $-\pi \leq \phi \leq \pi$, is compactified with radius r_c and taken to be $\mathbb{Z}_2$ symmetric in the hypersurface $\phi = 0$. A negative tension brane, on which the Standard Model is confined, and a positive tension brane are located at the orbifold fixed points in the extra dimension, $\phi = \pi, 0$ respectively. The action for such a configuration is given by

$$S = \int \sqrt{-{}^{(5)}g} \left(\frac{{}^{(5)}R}{2\kappa_5} - \Lambda_5 \right) d^5x + \int \sqrt{-{}^{(vis)}g} \left(\mathcal{L}_{vis} - \lambda_{vis} \right) \delta(\phi - \pi)\, d^5x + \int \sqrt{-{}^{(hid)}g} \left(\mathcal{L}_{hid} - \lambda_{hid} \right) \delta(\phi)\, d^5x \,, \qquad (2.1)$$

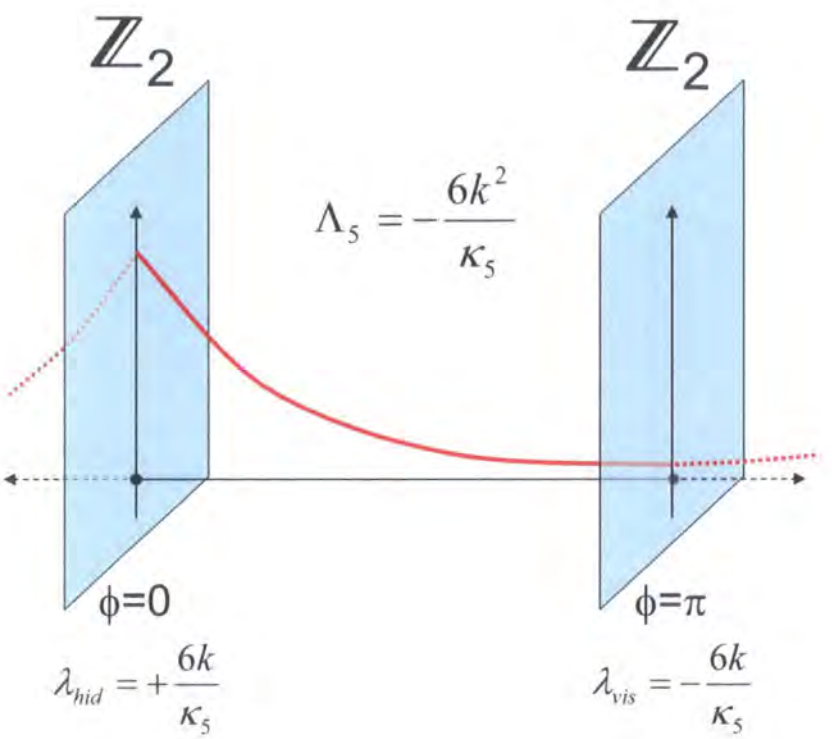

Figure 2.1: A schematic of the RS1 model illustrating the location of the branes and the form of the warp factor.

where $\kappa_5 = 8\pi {}^{(5)}G_N$ and Λ_5 is the negative bulk cosmological constant. The metrics on the hidden and visible branes are induced from the bulk metric by

$$ {}^{(hid)}g_{\mu\nu} = {}^{(5)}g_{\mu\nu}(x^\alpha, \phi = 0)\,, \qquad \text{and} \qquad {}^{(vis)}g_{\mu\nu} = {}^{(5)}g_{\mu\nu}(x^\alpha, \phi = \pi)\,, \tag{2.2} $$

and the details of the 3-brane Lagrangians, $\mathcal{L}_{hid}$ and $\mathcal{L}_{vis}$, are unimportant beyond their vacuum energies, λ_{hid} and λ_{vis}, which have been separated out.

If it is assumed that a non-factorisable solution to the above configuration exists that respects four-dimensional Poincaré invariance in the coordinates on the branes, x^α, then the bulk metric in Gaussian normal coordinates, $X^A = (x^\alpha, \phi)$ based on the brane at $\phi = 0$ is given by

$$ ds^2 = e^{-2kr_c|\phi|}\eta_{\mu\nu}dx^\mu dx^\nu + r_c^2 d\phi^2\,, \tag{2.3} $$

where k is the adS curvature of the bulk. In order for this to be a solution to the five-dimensional Einstein equations, a very specific balancing of cosmological constants

in the bulk and on the brane must be imposed

$$\Lambda_5 = -\frac{6k^2}{\kappa_5}, \qquad \lambda_{hid} = -\lambda_{vis} = \frac{6k}{\kappa_5}. \tag{2.4}$$

In the coordinates of equation (2.3) all slicings of constant ϕ have metrics proportional to the Minkowski standard vacuum. They are related to one another by a "warp" factor which takes its maximum value of unity at the hidden brane and decays exponentially towards a minimum on the Standard Model brane at $\phi = \pi$. Figure 2.1 illustrates the configuration of branes and this variation of the warp factor in RS1.

2.1.1 The Physics of RS1

By considering massless fluctuations about the classical solution (2.3) it is possible to relate the fundamental five-dimensional parameters ${}^{(5)}G_N, r_c$ and k to those that would be experienced by a brane observer witnessing the effective four-dimensional theory. The perturbed four-dimensional metric is written, ${}^{(4)}\bar{g}_{\mu\nu}(x) = \eta_{\mu\nu} + h_{\mu\nu}$ so that the bulk line-element takes the form

$$ds^2 = e^{-2kr_c|\phi|}\,{}^{(4)}\bar{g}_{\mu\nu}(x)dx^\mu dx^\nu + r_c^2 d\phi^2, \tag{2.5}$$

where it has been assumed that some mechanism stabilises the inter-brane distance so that fluctuations in the brane separation can be neglected [40–42]. The effective Newton's constant ${}^{(4)}G_N$ is recovered by substituting the form of the metric (2.5) into the expression for the five-dimensional action and picking out the component proportional to the four-dimensional curvature scalar ${}^{(4)}\bar{R}$ that is constructed from the perturbed four-dimensional metric ${}^{(4)}\bar{g}_{\mu\nu}$

$$S_{eff} = \int d^4x \int_{-\pi}^{\pi} r_c\, e^{-2kr_c|\phi|} \sqrt{-{}^{(4)}\bar{g}}\, \frac{{}^{(4)}\bar{R}}{2\kappa_5} + \dots . \tag{2.6}$$

Integrating out the extra dimension ϕ yields the relation between four and five-dimensional gravitational couplings

$${}^{(5)}G_N = \frac{{}^{(4)}G_N}{k}\left(1 - e^{-2kr_c\pi}\right), \tag{2.7}$$

or, using equation (1.7) in natural units, between Planck masses,

$${}^{(4)}M_P^2 = \frac{{}^{(5)}M_P^3}{k}\left(1 - e^{-2kr_c\pi}\right). \tag{2.8}$$

Next consider the action for a Standard Model particle on the visible brane. A scalar field, H, would have action

$$S_{vis} = \int d^4x \sqrt{-{}^{(vis)}g} \left[{}^{(vis)}g^{\mu\nu} \nabla_\mu H^\dagger \nabla_\nu H - \lambda(|H|^2 - m_0^2)^2 \right] + \dots \,, \tag{2.9}$$

but owing to the presence of the warp factor and the location of the brane at $\phi = \pi$, the metric on the visible brane is not equal to the "fundamental" metric appearing in the effective Einstein action, ${}^{(4)}\bar{g}_{\mu\nu}$, but related by ${}^{(4)}g_{\mu\nu} = e^{-2kr_c\pi}\, {}^{(4)}\bar{g}_{\mu\nu}$. Making this replacement in the scalar action yields

$$S_{vis} = \int d^4x \sqrt{-{}^{(4)}\bar{g}} e^{-4kr_c\pi} \left[{}^{(4)}\bar{g}^{\mu\nu} e^{2kr_c\pi} \nabla_\mu H^\dagger \nabla_\nu H - \lambda(|H|^2 - m_0^2)^2 \right] + \dots \,, \tag{2.10}$$

which must then be renormalised, $H \to e^{kr_c\pi} H$, to extract the physical masses measured by an observer on the brane when making measurements within the effective theory which has metric ${}^{(4)}\bar{g}_{\mu\nu}$,

$$S_{eff} = \int d^4x \sqrt{-{}^{(4)}\bar{g}} \left[{}^{(4)}\bar{g}^{\mu\nu} \nabla_\mu H^\dagger \nabla_\nu H - \lambda(|H|^2 - e^{-2kr_c\pi} m_0^2)^2 \right] + \dots \,. \tag{2.11}$$

So within the first Randall-Sundrum model fundamental masses, m_0, are related to observed masses, m, in the effective four-dimensional theory by

$$m \equiv e^{-kr_c\pi} m_0 \,. \tag{2.12}$$

Equations (2.8) and (2.12) now afford an explanation to the hierarchy problem.

Suppose there is only one fundamental scale in nature, taken to be around the order of the observed Planck scale ${}^{(4)}M_P \sim 10^{19}$ GeV. If this is true then both the fundamental Planck scale ${}^{(5)}M_P$ and the fundamental masses of Standard Model particles m_0 must also be of this magnitude. However, the observed masses of particles may be significantly lower owing to the exponential relation in equation (2.12). In particular, if $kr_c \approx 10$ then equation (2.12) generates observable masses of around 1 TeV from fundamental masses of order ${}^{(4)}M_P$. Furthermore, if $e^{-kr_c\pi}$ really is of order 10^{-16} then equation (2.8) becomes

$${}^{(4)}M_P^2 \approx \frac{{}^{(5)}M_P^3}{k} \,, \tag{2.13}$$

so clearly no dramatic hierarchy is required between the fundamental parameters of the five-dimensional theory: ${}^{(5)}M_P$, k, $\mu_c = 1/r_c$ and m_0. To generate TeV scale

particle masses from a theory with all parameters at the scale ${}^{(4)}M_P$ requires a hierarchy of at worst $k/\mu_c \approx 10$.

Finally, a change of viewpoint to that of a visible-brane-based observer shows that it is even possible to consider the TeV scale fundamental and the Planck scale derived from the system geometry. By making the coordinate transformation $x^\mu \rightarrow e^{kr_c\pi}x^\mu$ the warp factor on the visible brane becomes unity, while that on the hidden brane takes the value $e^{2kr_c\pi}$. Now no rescaling of Standard Model fields is required so the fundamental masses are all equal to the observed masses in the TeV range. The extremely weak gravitational coupling, ${}^{(4)}G_N$, is due to the magnitude of the graviton wavefunction (the warp factor) being $\approx 10^{32}$ times smaller on the visible brane than it is on the hidden one. The suggestion that physics may be consistent with a fundamental scale around 1 TeV is extraordinary as it raises the possibility that radically new phenomenology may be accessible in the next generation of ground-based collider experiments.

2.2 The Randall-Sundrum One Brane Model (RS2)

In their second braneworld model [27] Randall and Sundrum dispensed with the brane at $\phi = \pi$ and with it their solution to the hierarchy problem. What they gained was a braneworld model using a warped extra dimension of infinite extent that produces a viable four-dimensional effective theory of gravity. To achieve this they begin with the RS1 model and reverse the roles of the hidden and visible branes so that the Standard Model is confined to the positive tension brane at $\phi = 0$. They then remove the negative tension brane at $\phi = \pi$ from the system by sending the compactification radius of the extra dimension $r_c \rightarrow \infty$. This then leaves a single, positive tension brane residing in a five-dimensional adS bulk which is $\mathbb{Z}_2$ symmetric in the brane. The bulk metric for this model is given by

$$ds^2 = e^{-2k|y|}\eta_{\mu\nu}dx^\mu dx^\nu + dy^2\,. \tag{2.14}$$

where $y = r_c\,\phi$, in terms of the RS1 compactified coordinate ϕ. The brane resides at $y = 0$ and y now takes the range $0 \leq y < \infty$. The problem of stabilising the inter-brane separation no longer exists as it becomes desirable for the second brane

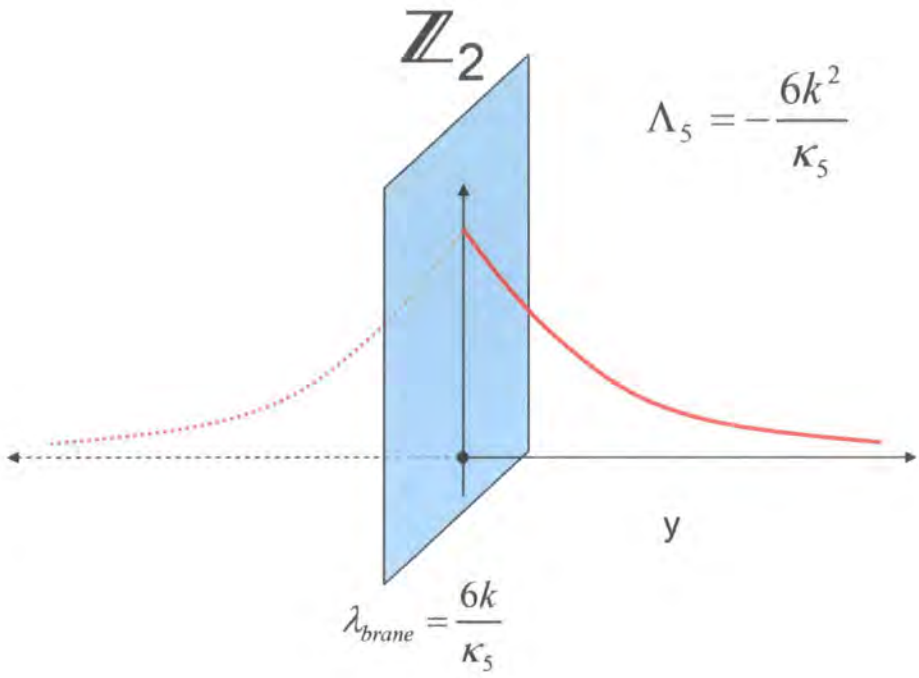

Figure 2.2: A schematic of the RS2 model illustrating the decay of the warp factor into the bulk.

to escape to infinity. The RS2 setup can be visualised as in figure 2.2 where again the extra-dimensional dependence of the warp factor is illustrated. The fine tuning between bulk and brane cosmological constants

$$\Lambda_5 = -\frac{6k^2}{\kappa_5}, \qquad \lambda_{brane} = \frac{6k}{\kappa_5} \equiv \rho_{RS}, \tag{2.15}$$

still remains and serves to exactly cancel the effect of the bulk negative energy density on the brane so that the induced metric is Minkowski. No mechanism by which this fine tuning may be realised is suggested in the model, it is simply a constraint that must be imposed. If the fine tuning is relaxed so that the brane cosmological constant is less than the critical value, ρ_{RS}, then the induced metric becomes that of four-dimensional anti-de Sitter spacetime. Conversely, if the brane energy density exceeds ρ_{RS} then a constant positive curvature brane is recovered.

2.2.1 Gravity in RS2

The most interesting feature of RS2 is its gravitational phenomenology. According to the conventional large extra dimension scenario there was no way in which four-dimensional gravity could be reproduced on a brane unless the extra dimensions were compactified on a large (in comparison to the Planck length) yet sufficiently small scale (to avoid conflict with Newton's law). Randall and Sundrum demonstrated that if the extra dimension is warped then it may be infinite in extent and still consistent with known gravitational law.

To find the effective four-dimensional gravitational field it is again necessary to consider fluctuations about the classical solution to Einstein's equations (2.14). However, since the extra dimension is now infinite in extent, it is no longer possible to neglect the massive Kaluza-Klein modes as there will be no energy gap between the zero mode and the lowest mode with mass. The infinite nature of the extra dimension imposes a continuous Kaluza-Klein spectrum and the resulting gravitational force is due to the combined effect of exchange of all of these graviton modes. To see this consider generalised linear fluctuations of the metric of the form

$$^{(5)}g_{\mu\nu} = e^{-2k|y|}\eta_{\mu\nu} + h_{\mu\nu}(x,y)\,. \tag{2.16}$$

Suppressing Lorentz indices, the metric perturbation is then assumed to be separable in its dependence on bulk and brane coordinates: $h(x,y) = h_m(y)e^{ip\cdot x}$, with $p^2 = -m^2$ and m being the mass of the Kaluza-Klein mode on the brane. Working in the Randall-Sundrum gauge defined by: $h_{yy} = h_{\mu y} = \partial_\mu h^\mu{}_\nu = h^\mu{}_\mu = 0$, evaluation of the linearised Einstein equations expanded about (2.14) yields the equation of motion for the extra-dimensional component of the tensor fluctuations

$$-\frac{1}{2}\partial_y^2 h_m(y) + \left[2k^2 - \frac{m^2}{2}e^{2k|y|} - 2k\delta(y)\right] h_m(y) = 0\,. \tag{2.17}$$

This must be satisfied along with the boundary condition that $h_m(y)$ is an even function owing to the $\mathbb{Z}_2$ symmetry in the brane. The transformations

$$z \equiv sgn(y)\frac{e^{k|y|}-1}{k}, \qquad h_m(y) = e^{-\frac{k|y|}{2}}\hat{h}_m(z)\,, \tag{2.18}$$

allow the equation of motion to be converted into Schrodinger-like form

$$-\frac{1}{2}\partial_z^2\hat{h}_m(z) + V(z)\hat{h}_m(z) = \frac{m^2}{2}\hat{h}_m(z)\,, \tag{2.19}$$

where the potential is given by

$$V(z) = \frac{15k^2}{8(k|z|+1)^2} - \frac{3k\delta(z)}{2}. \tag{2.20}$$

Much of the physics of RS2 can be interpreted through this potential. Firstly the δ-function supports a single normalisable bound state mode, the massless zero mode, corresponding to the usual four-dimensional graviton. The zero mode has wavefunction

$$\hat{h}_0(z) = \frac{1}{k(k|z|+1)^{\frac{3}{2}}}, \tag{2.21}$$

which is peaked on the brane and decays rapidly into the bulk. The presence of a massless zero mode bound to the brane ensures four-dimensional gravity is reproduced to leading order. The remaining massive Kaluza-Klein modes form a continuum and asymptote to plane waves as the potential decays into the bulk. In the region of the brane the massive mode wavefunctions are strongly suppressed indicating that the Kaluza-Klein modes couple only weakly to low-energy states on the brane. An analysis of the Newtonian potential experienced on the brane due to a particle of mass M reveals it is of the form

$$\phi = \frac{{}^{(4)}G_N M}{r}\left(1 + \frac{2}{3k^2r^2}\right), \tag{2.22}$$

where the short scale correction is due to the combined effect of the continuum of suppressed massive Kaluza-Klein modes.

It should be noted that although Randall and Sundrum's original analysis, as followed in the above discussion, produces a qualitatively correct picture of the effective gravity on the brane, the specific result (2.22) has been taken from the more complete analysis performed by Garriga and Tanaka [43]. They considered the effect of placing an isolated point mass on the brane and then calculating the weak gravitational field that it produces. Since both the brane energy density and the point mass are sources in Einstein's equations they interact with one another, resulting in the brane bending in the fifth dimension [44, 45]. Garriga and Tanaka also showed that the effect of this brane bending is to contribute a term to the metric perturbation that exactly converts the factor of $\frac{1}{3}$ featuring in the massless 5-d graviton propagator (see equation (1.10)) to the factor of $\frac{1}{2}$ that is required in the corresponding four-dimensional case. Since it accurately reproduces both the Newtonian

force law and correct four-dimensional structure of the graviton propagator in the low-energy limit, the Randall-Sundrum single brane model has become something of a paradigm of extra-dimensional model building.

2.3 Black Holes in RS2

As mentioned in the introduction, it is critical that a realistic model incorporating extra dimensions reproduces the standard strong-gravity results of cosmology and astrophysics. The braneworld generalisation of the Friedmann-Robertson-Walker universe is an extensively studied subject [46–57]. Owing to the high degree of symmetry required of a cosmology the five-dimensional problem was found to be fully integrable [52]. The general cosmological braneworld can be completely understood as a four-dimensional hypersurface following a time-dependent trajectory through a five-dimensional adS bulk containing a black hole. The most pressing question in braneworld astrophysics has been no less a source of investigation than its counterpart in cosmology. However, almost a decade later, the braneworld black hole remains undescribed.

2.3.1 The Black String

It was noticed that the form of the Randall-Sundrum metric (2.14) permits convenient generalisation [58]. It is possible to replace the Minkowski component with any four-dimensional metric that is Ricci flat and the resulting 5-d metric is still a solution to the higher-dimensional Einstein equations with negative cosmological constant. This presents an obvious candidate for a braneworld black hole. Chamblin et al. [59] replaced the Minkowski metric with that describing a 4-d Schwarzschild geometry

$$ds^2 = \frac{1}{k^2u^2}\left[-U(r)dt^2 + \frac{dr^2}{U(r)} + r^2d\Omega_2^2 + du^2\right], \tag{2.23}$$

where $U(r) = 1 - \frac{2M}{r}$, $d\Omega_2^2$ is the metric on a 2-sphere and the coordinate u is related to the RS coordinate y by $ku = e^{k|y|}$. By taking this brane-based approach they guaranteed that the correct description of a four-dimensional black hole is found on the brane. However, from a five-dimensional bulk perspective this metric can

be considered as the foliation of the 5-d spacetime by Schwarzschild slices with magnitude scaled by the warp factor. From the higher-dimensional viewpoint it is clear that the Schwarzschild singularity is not localised on the brane, but projects out along the extra dimension. This candidate braneworld black hole is a slice of an infinite five-dimensional black string.

To reproduce the results of four-dimensional general relativity the gravitational collapse of uncharged, non-rotating matter confined to the brane should ultimately settle down to a final state which is stable and without naked singularity. Unfortunately for the black string, neither of these results hold.

While the Ricci scalar and square of the Ricci tensor are finite everywhere in the spacetime (2.23), the square of the Riemann tensor

$$R_{ABCD}R^{ABCD} = k^4\left(40 + \frac{48M^2u^4}{r^6}\right), \tag{2.24}$$

diverges for every finite value of u at the black string singularity $r = 0$, in addition to the adS horizon $u = \infty$. The latter divergence is only encountered when the adS horizon is approached along certain geodesics (eg. along the axis of the string), however Chamblin et al. showed that components of the Riemann tensor diverge in a frame parallelly propagated along any timelike geodesic that reaches the adS horizon, so the singularity will be visible from the brane.

It was originally conjectured that Gregory-Laflamme instabilities [60] near the adS horizon would cause the black string to pinch off forming a stable extended object referred to as a "black cigar". Subsequent analysis demonstrated [61] that it decays into an accumulation of "mini black holes" towards the adS horizon. According to either result it is clear that the black string solution's status as the endpoint of gravitational collapse is questionable.

2.3.2 A General Covariant Approach

With the failure of the simplest method, a more general brane-based approach to finding the black hole metric was developed. Shiromizu et al. [54] derived the relation between the 5-d bulk Einstein equations and the effective equations induced on a four-dimensional brane for arbitrary bulk and brane geometries.

By using the equations of Gauss

$$ {}^{(4)}R^{A}{}_{BCD} = {}^{(5)}R^{E}{}_{FGH}h_{E}{}^{A}h_{B}{}^{F}h_{C}{}^{G}h_{D}{}^{H} + K^{A}{}_{C}K_{BD} - K^{A}{}_{D}K_{BC}\,, \tag{2.25} $$

and Codazzi

$$ D_{B}K_{A}{}^{B} - D_{A}K_{B}{}^{B} = {}^{(5)}R_{EF}n^{F}h_{A}{}^{E}\,, \tag{2.26} $$

where $h_{AB} = {}^{(5)}g_{AB} - n_{A}n_{B}$ is the induced metric, n^{A} is the vector normal to the brane and $K_{AB} = h_{A}{}^{E}h_{B}{}^{F}\nabla_{E}n_{F}$ is the extrinsic curvature, the five-dimensional Einstein equations

$$ {}^{(5)}G_{AB} \equiv {}^{(5)}R_{AB} - \frac{1}{2}{}^{(5)}R^{(5)}g_{AB} = \kappa_{5}{}^{(5)}T_{AB}\,, \tag{2.27} $$

project onto the brane as

$$ \begin{aligned} {}^{(4)}G_{\mu\nu} = \frac{2\kappa_{5}}{3}\left({}^{(5)}T_{AB}h_{\mu}{}^{A}h_{\nu}{}^{B} + \left[{}^{(5)}T_{AB}n^{A}n^{B} - \frac{1}{4}{}^{(5)}T\right]h_{\mu\nu}\right) + \\ KK_{\mu\nu} - K_{\mu}{}^{\alpha}K_{\alpha\nu} + \frac{1}{2}\left(K^{\alpha\beta}K_{\alpha\beta} - K^{2}\right)h_{\mu\nu} - \mathcal{E}_{\mu\nu}\,. \end{aligned} \tag{2.28} $$

In the above ${}^{(5)}T_{AB}$ is the 5-d energy-momentum tensor and ${}^{(5)}T = {}^{(5)}T_{A}{}^{A}$ (likewise for K), also $\mathcal{E}_{\mu\nu} = {}^{(5)}C_{ABCD}n^{C}n^{D}h_{\mu}{}^{A}h_{\nu}{}^{B}$ is the projection of the bulk Weyl curvature orthogonal to n^{A}. Note that in the notation adopted the induced metric, h_{AB}, can be written as either a four or five-dimensional tensor with corresponding greek or roman indices. It can also be used to project five-dimensional quantities onto the brane thereby converting roman indices to greek. With the braneworld scenario in mind the 5-d energy-momentum tensor is written as

$$ {}^{(5)}T_{AB} = T^{bulk}_{AB} - \Lambda_{5}{}^{(5)}g_{AB} + \tilde{T}_{AB}\delta(y)\,, \tag{2.29} $$

where the δ-function enforces confinement of brane energy-momentum, $\tilde{T}_{AB}$, to a hypersurface located at $y = 0$. From Einstein's equations it is clear that the presence of a discontinuous source of energy-momentum in the spacetime causes the geometry to possess a corresponding discontinuous feature. The nature of this discontinuity is encoded in Israel's junction conditions [62], which can be found by integrating Einstein's equations along a path which just crosses the brane, picking out only the singular components of the geometry and energy-momentum

$$ [h_{AB}]^{+}_{-} = 0\,, \tag{2.30} $$

$$ [K_{AB}]^{+}_{-} = \kappa_{5}\left(\tilde{T}_{AB} - \frac{1}{3}h_{AB}\tilde{T}\right)\,, \tag{2.31} $$

where $[X]^+_- \equiv \lim_{y\to 0^+} X - \lim_{y\to 0^-} X = X^+ - X^-$. Fixing the $\mathbb{Z}_2$ symmetry of the bulk imposes a strict constraint on the geometry either side of the brane. Specifically, as an observer passes through the brane they measure quantities of exactly the same magnitude, but with the direction of the normal reversed. Consequently

$$K^+_{AB} = -K^-_{AB} = \frac{\kappa_5}{2}\left(\tilde{T}_{AB} - \frac{1}{3}h_{AB}\tilde{T}\right), \tag{2.32}$$

and it is therefore possible to work with quantities on the + side of the brane only, allowing $\pm$ labels to be omitted. Substituting equations (2.29) and (2.32) into (2.28) yields the induced Einstein equation

$${}^{(4)}G_{\mu\nu} = -\frac{\kappa_5}{2}\Lambda_5 h_{\mu\nu} + \frac{2\kappa_5}{3}\mathcal{F}_{\mu\nu}(T^{bulk}) + \kappa_5^2\Pi_{\mu\nu}(\tilde{T}) - \mathcal{E}_{\mu\nu}, \tag{2.33}$$

where

$$\mathcal{F}_{\mu\nu}(T^{bulk}) = T^{bulk}_{AB}h_\mu{}^A h_\nu{}^B + h_{\mu\nu}\left(T^{bulk}_{AB}n^A n^B - \frac{T^{bulk}}{4}\right), \tag{2.34}$$

and

$$\Pi_{\mu\nu}(\tilde{T}) = \frac{1}{12}\tilde{T}\tilde{T}_{\mu\nu} - \frac{1}{24}\tilde{T}^2 h_{\mu\nu} - \frac{1}{4}\tilde{T}_\mu{}^\alpha\tilde{T}_{\nu\alpha} + \frac{1}{8}\tilde{T}^{\alpha\beta}\tilde{T}_{\alpha\beta}h_{\mu\nu}. \tag{2.35}$$

As in the original Randall-Sundrum case, it is common to make a distinction between the self-energy of the brane and the energy-momentum arising from Standard Model matter fields

$$\tilde{T}_{\mu\nu} = T^{SM}_{\mu\nu} - \lambda_{brane}\, h_{\mu\nu}. \tag{2.36}$$

With this separation the Einstein equations can be written in their final form

$${}^{(4)}G_{\mu\nu} = \kappa_4\left(T^{SM}_{\mu\nu} - \Lambda_4 h_{\mu\nu}\right) + \frac{2\kappa_5}{3}\mathcal{F}_{\mu\nu}(T^{bulk}) + \kappa_5^2\Pi_{\mu\nu}(T^{SM}) - \mathcal{E}_{\mu\nu}, \tag{2.37}$$

where

$${}^{(4)}G_N = \frac{\kappa_4}{8\pi} = \frac{4\pi\,{}^{(5)}G_N^2\lambda_{brane}}{3} \qquad \text{and} \qquad \Lambda_4 = \frac{3\Lambda_5}{\kappa_5\,\lambda_{brane}} + \frac{\lambda_{brane}}{2}. \tag{2.38}$$

In the general covariant approach to determining the braneworld metric there are essentially three independent modifications to the standard four-dimensional Einstein equations:

- $\mathcal{F}_{\mu\nu}(T^{bulk})$ – arising from any energy-momentum present in the bulk beyond pure cosmological constant.

- $\Pi_{\mu\nu}(T^{SM})$ – a consequence of extrinsic curvature terms resulting from the brane embedding.

- $\mathcal{E}_{\mu\nu}$ – the projected Weyl term inherited from the geometry of the bulk space-time.

It is possible to show that the first of these corrections vanishes if ordinary energy-momentum conservation is required on the brane. From equations (2.26), (2.27) and (2.32) the divergence of the Standard Model energy-momentum tensor may be expressed as

$$\nabla^{\nu} T^{SM}_{\mu\nu} = 2h_{\mu}{}^{A} n^{B} T^{bulk}_{AB} \,. \tag{2.39}$$

In general, energy-momentum is exchanged between bulk and brane fields violating 4-d conservation. To make the interaction between the brane and the bulk purely gravitational it is necessary to impose $T^{bulk}_{AB} = 0$, which then removes the term $\mathcal{F}_{\mu\nu}\left(T^{bulk}\right)$ from the projected Einstein equations.

It is instructive to see where the RS2 model fits into this covariant framework. For a pure adS background the bulk Weyl term, $\mathcal{E}_{\mu\nu}$, vanishes. Also the brane energy-momentum is taken to be zero beyond its cosmological constant so $T^{SM}_{\mu\nu} = 0$, $\Rightarrow \Pi_{\mu\nu}(T^{SM}) = 0$. Finally the bulk and brane cosmological constants are tuned so that the metric on the brane is Minkowski. From equation (2.38) the condition for this is $\lambda^2_{brane} = -6\Lambda_5/\kappa_5$ which is satisfied by the RS2 cosmological constants in (2.15).

Within the covariant formalism the vacuum outside a braneworld black hole or star will satisfy the induced field equations

$$^{(4)}R_{\mu\nu} = -\mathcal{E}_{\mu\nu} \,. \tag{2.40}$$

In order to solve this equation some assumption must be made about the form of $\mathcal{E}_{\mu\nu}$. A first possibility is to set $\mathcal{E}_{\mu\nu} = 0$ and seek solutions that correspond to exact 4-d gravity. This was the approach taken by Chamblin et al. [59] and led to the black string geometry and its undesirable features. The second option is to assume some non-zero form for $\mathcal{E}_{\mu\nu}$ and seek brane solutions of static black hole exteriors with 5-d corrections. This would seem the most realistic approach

given that the four-dimensional effective potential (2.22) was found to contain short-distance corrections caused by the 5-d Kaluza-Klein modes. Indeed, such solutions have been found [63–67] but they all face a common problem. The bulk metric corresponding to the particular choice of $\mathcal{E}_{\mu\nu}$ has either not been found or is without physical interpretation.

2.3.3 A Bulk-Based Perspective

Since the development of the covariant brane-based formalism other analytic approaches have been pursued [68–73] without complete success and attempts to solve the system numerically [74–77] have been plagued with issues of sensitivity. A persistent problem with brane-based methods is that assumptions must be made regarding the geometry of the bulk that either introduce physically undesirable features or render the background spacetime uninterpretable. An obvious way around this is to adopt a bulk-based perspective. From the outset, the required features of the extra-dimensional spacetime are specified, and then a brane with energy-momentum is introduced in such a way that the 5-d Einstein equations remain satisfied without the bulk being perturbed. This task is no more than explicitly solving the Israel equations (2.30) and (2.31) in a fixed background. It is a procedure that was successfully applied to brane cosmology [50] and was hoped might transfer to braneworld black holes.

Unfortunately it has so far proven unsuccessful. The problem with this method is that although the bulk remains well behaved, the Israel equations are sufficiently restrictive that they specify the trajectory of the brane and its energy-momentum content completely, up to a small number of integration constants. In their appendix Chamblin et al. [59] demonstrate that it is not possible to intersect the 5-d Schwarzschild-adS black hole with a static, pure vacuum domain wall. However, a time-dependent trajectory with more general matter distribution has never been explored.

Chapter 3

Black Holes and Braneworld Stars

Motivated by a desire to find the braneworld black hole metric, the problem of embedding time-dependent branes containing perfect fluid in a variety of standard five-dimensional backgrounds has now been addressed [1]. To conform with the RS2 model a solution is sought in asymptotically adS spacetime that is $\mathbb{Z}_2$ symmetric in the brane.

To describe a braneworld black hole a fully consistent bulk-brane-black-hole gravitational system must preserve the SO(3) symmetry on the brane that is present in our desired 4-d Schwarzschild-like induced metric. The brane trajectory and its matter content must satisfy the Israel junction conditions (2.30)–(2.31) that allow a gravitating domain wall to be inserted into a spacetime without perturbing the background geometry. The formalism for achieving such a setup is outlined in the next section.

3.1 The General Brane Equations

Analysis of a general braneshape embedded in a 5-d SO(4) symmetric spacetime is most conveniently performed in a coordinate system which makes this symmetry explicit. In such a system the 5-dimensional line-element takes the form

$$ds^2 = -U(r)\,d\tau^2 + \frac{1}{U(r)}\,dr^2 + r^2(d\chi^2 + \sin^2\chi\,d\Omega_2^2)\,, \tag{3.1}$$

where $U(r)$ is a general function of the global radial coordinate and $d\Omega_2^2$ is the line element on a unit 2-sphere. To specify the brane position a constraint is imposed

between the coordinate functions: $\chi = \chi(\tau, r)$. This is the most general embedding that preserves the desired SO(3) symmetry on the brane. If a general 5-vector is described by the coordinate functions $x^A = (\tau, r, \chi, \theta, \phi)$, then a new basis may be constructed in terms of the unnormalised brane tangent vectors and unit normal:

$$\begin{aligned} T^A &= (1, 0, \dot{\chi}, 0, 0) \\ R^A &= (0, 1, \chi', 0, 0) \\ \Theta^A &= (0, 0, 0, 1, 0) \\ \Phi^A &= (0, 0, 0, 0, 1) \\ n_A &= n(-\dot{\chi}, -\chi', 1, 0, 0)\,. \end{aligned} \tag{3.2}$$

In the above, overdot and prime denote partial differentiation with respect to τ and r, respectively, and $\frac{1}{n^2} = \left(-\frac{\dot{\chi}^2}{U} + U\chi'^2 + \frac{1}{r^2}\right)$. The tensor $h_{AB} = {}^{(5)}g_{AB} - n_A n_B$ projects vectors onto the wall, and its tangential components define the induced metric on the brane. In the aforementioned basis, it can be evaluated as

$$h_{AB} = \begin{pmatrix} -U + r^2\dot{\chi}^2 & r^2\dot{\chi}\chi' & & & & \\ r^2\dot{\chi}\chi' & \frac{1}{U} + r^2\chi'^2 & & & & \\ & & r^2\sin^2\chi & & & \\ & & & r^2\sin^2\chi\sin^2\theta & & \\ & & & & 0 & \end{pmatrix}.$$

It should be noted that in the present convention the non-zero four-dimensional component of the above tensor representing the metric induced on the brane may be referred to with greek indices as $h_{\mu\nu}$.

The physical manifestation of the brane is as a hypersurface containing energy-momentum. It is described by the tensor $\tilde{T}_{AB}$ which includes contributions from both Standard Model fields and brane vacuum energy. For simplicity its brane-projected form is taken to be

$$\tilde{T}_{\mu\nu} = [\rho(\tau, r) + p(\tau, r)]\, h_{\mu\sigma} h_{\nu\rho}\, u^\sigma u^\rho + p(\tau, r)\, h_{\mu\nu}\,, \tag{3.3}$$

which describes an isotropic distribution of perfect fluid with $\rho(\tau, r)$ and $p(\tau, r)$ the fluid energy density and pressure, respectively. Note that in writing down the brane

energy-momentum no distinction is made between the component from Standard Model fields and that due to vacuum energy. The vector u^μ is the fluid's 4-velocity on the brane, chosen to satisfy the normalisation condition $u^\mu u^\nu h_{\mu\nu} = -1$. In the tangent vector basis (T, R, Θ, Φ) the fluid's 4-velocity is chosen to be

$$u^\mu = \frac{1}{\sqrt{-h_{TT}}}(1,0,0,0)\,. \tag{3.4}$$

The ansatz (3.4) allows the brane energy-momentum tensor to be rewritten as

$$\tilde{T}_{\mu\nu} = -(\rho + p)\frac{h_{\mu T}h_{\nu T}}{h_{TT}} + p\,h_{\mu\nu}\,. \tag{3.5}$$

For later convenience, the energy density and pressure of the fluid will be related by an "equation of state" $p(\tau, r) = w(\tau, r)\rho(\tau, r)$, and the quantity

$$v(\tau, r) \equiv 2 + 3w(\tau, r)\,, \tag{3.6}$$

is defined for use in subsequent calculation. In the context defined above w is unusual as an equation of state since it is an arbitrary function of both r and τ so does not restrict the pressure in any way.

As mentioned in §2.3.2, it is possible to embed an energy-momentum-containing brane into a fixed bulk spacetime without perturbing the geometry providing Israel's junction conditions [62] are satisfied

$$[K_{\mu\nu} - Kh_{\mu\nu}]^+_- = \kappa_5\tilde{T}_{\mu\nu}\,, \tag{3.7}$$

where $K_{\mu\nu} = h_\mu{}^A h_\nu{}^B \nabla_A n_B$ is the extrinsic curvature of the brane, and $\kappa_5 = 8\pi^{(5)}G_N$. As in equation (2.32), under imposition of the $\mathbb{Z}_2$ reflection symmetry in the wall these conditions become

$$K_{\mu\nu} = \frac{\kappa_5}{2}\left(\tilde{T}_{\mu\nu} - \frac{1}{3}h_{\mu\nu}\tilde{T}\right)\,. \tag{3.8}$$

If the brane is then taken to contain the perfect fluid of equation (3.5) with equation of state (3.6) then the Israel conditions become

$$K_{\mu\nu} = \frac{\kappa_5}{6}\rho\left[h_{\mu\nu} - (1+v)\frac{h_{\mu T}h_{\nu T}}{h_{TT}}\right]\,, \tag{3.9}$$

or in component form,

$$K_{TT} = -n\left(\ddot{\chi} + Ur\chi'\dot{\chi}^2 - \frac{1}{2}UU'\chi'\right) = -\frac{\kappa_5}{6}\rho v\left(-U + r^2\dot{\chi}^2\right), \tag{3.10}$$

$$K_{RR} = -n\left(\chi'' + \frac{2\chi'}{r} + \frac{U'\chi'}{2U} + Ur\chi'^3\right) = \frac{\kappa_5}{6}\rho\left[\frac{1}{U} + r^2\chi'^2 + \frac{(1+v)\,r^4\dot{\chi}^2\chi'^2}{U - r^2\dot{\chi}^2}\right], \tag{3.11}$$

$$K_{TR} = -n\left(\dot{\chi}' + \frac{\dot{\chi}}{r} + Ur\chi'^2\dot{\chi} - \frac{U'\dot{\chi}}{2U}\right) = -\frac{\kappa_5}{6}\rho v r^2\dot{\chi}\chi', \tag{3.12}$$

$$K_{\Theta\Theta} = -n\left(Ur\chi'\sin^2\chi - \sin\chi\cos\chi\right) = \frac{\kappa_5}{6}\rho r^2\sin^2\chi\,. \tag{3.13}$$

A detailed derivation of the above extrinsic curvature components can be found in appendix A.1. Two further equations may be obtained by ensuring consistency of τ and r derivatives of (3.13) with the remaining Israel equations

$$\dot{\chi}\left(1 + \frac{1}{2}U'r - U + \frac{\kappa_5\rho}{6n}(1+v)r^2\cot\chi\right) = -\frac{\kappa_5\dot{\rho}}{6n}r^2, \tag{3.14}$$

$$\chi'\left(1 + \frac{1}{2}U'r - U + \frac{\kappa_5\rho}{6n}(1+v)\frac{r^4\dot{\chi}^2\cot\chi}{-U + r^2\dot{\chi}^2}\right) = -\frac{\kappa_5\rho'}{6n}r^2. \tag{3.15}$$

In summary, a 4-dimensional brane containing perfect fluid may be defined by its energy density, $\rho(\tau, r)$, equation of state, $p(\tau, r) = w(\tau, r)\rho(\tau, r)$, and the shape of its embedding, $\chi(\tau, r)$, in a 5-dimensional spacetime. When the bulk spacetime is spherically-symmetric and defined by a single function $U(r)$ then the embedding is consistent with Einstein's equations providing the set of functions $\rho(\tau, r)$, $w(\tau, r)$ and $\chi(\tau, r)$ simultaneously satisfying (3.10)-(3.15) may be found. This task may be simplified by defining a new function $\alpha = r\cos\chi$ and using equation (3.13) to eliminate the quantity $\kappa_5\rho/6n$. Equations (3.10)-(3.15) are then rewritten as

- $$\frac{r^2\ddot{\alpha}}{U} - (\alpha' r - \alpha)\left(\frac{1}{2}U'r - U\right) + \alpha + \frac{(1+v)}{U}\left[U(\alpha' r - \alpha) + \alpha\right]\left(-U + \frac{r^2\dot{\alpha}^2}{r^2 - \alpha^2}\right) = 0, \tag{3.16}$$

- $$Ur^2\alpha'' + (\alpha' r - \alpha)\left(\frac{1}{2}U'r - U\right) - \alpha + (1+v)\frac{\left[U(\alpha' r - \alpha) + \alpha\right]Ur^2\dot{\alpha}^2(\alpha' r - \alpha)^2}{(r^2 - \alpha^2)\left(r^2\dot{\alpha}^2 - U(r^2 - \alpha^2)\right)} = 0, \tag{3.17}$$

- $$r\dot{\alpha}' - \frac{1}{2}\frac{U'r}{U}\dot{\alpha} + (1+v)(U(\alpha' r - \alpha) + \alpha)\frac{\dot{\alpha}(\alpha' r - \alpha)}{(r^2 - \alpha^2)} = 0\,, \tag{3.18}$$

- $$U(\alpha' r - \alpha) + \alpha = \frac{\kappa_5}{6}\rho r\left(-\frac{r^2\dot{\alpha}^2}{U} + U(\alpha' r - \alpha)^2 + r^2 - \alpha^2\right)^{\frac{1}{2}}\,, \tag{3.19}$$

- $$\frac{\dot{\rho} r}{\rho} = r\dot{\alpha}\left(\frac{1 + \frac{1}{2}U'r - U}{U(\alpha' r - \alpha) + \alpha} + (1+v)\frac{\alpha}{r^2 - \alpha^2}\right), \tag{3.20}$$

- $$\frac{\rho' r}{\rho} = (\alpha' r - \alpha)\left(\frac{1 + \frac{1}{2}U'r - U}{U(\alpha' r - \alpha) + \alpha} + \frac{(1+v)}{(r^2 - \alpha^2)}\frac{r^2\dot{\alpha}^2\alpha}{(r^2\dot{\alpha}^2 - U(r^2 - \alpha^2))}\right). \tag{3.21}$$

3.2 The Time-Dependent Brane

The solution of the full time-dependent problem, equations (3.16)-(3.21), is an extremely complicated task. It is demonstrated in appendix A.2 that consistency of the third order mixed derivatives, found by further differentiation of equations (3.16)-(3.18), allows the equation of state to be expressed entirely in terms of the braneshape and its first derivatives

$$1 + v = \frac{(r^2 - \alpha^2)(\frac{1}{2}U''r^2 - U'r + U - 1)}{(U(\alpha' r - \alpha) + \alpha)[(\alpha' r - \alpha)(\frac{1}{2}U'r - U) + \alpha - \frac{r^2\dot{\alpha}^2(\alpha' r - \alpha)(\frac{1}{2}U'r - U)}{(r^2 - \alpha^2)(-U + \frac{r^2\dot{\alpha}^2}{r^2 - \alpha^2})}]}\,. \tag{3.22}$$

It is then possible to substitute for $(1+v)$ using this expression in each of equations (3.16)-(3.18), (3.20) and (3.21) to recover partial differential equations for α which may, in principle, be integrated to give the braneshape. From equations (3.20) and (3.21) the energy density may then be determined to obtain the complete set of functions $\rho(\tau, r)$, $w(\tau, r)$ and $\chi(\tau, r)$ specifying the system. However, in order to progress analytically it is necessary to make some simplifying assumptions.

3.2.1 A Class of Time-Dependent Solutions

Inspection of the brane equations reveals an obvious simplification that results from setting $v = -1$. This corresponds to demanding $w = -1$ in the brane equation of state, but does not restrict our analysis to pure vacuum branes since the energy density and pressure both remain r- and τ-dependent. Under this restriction equations

(3.16)-(3.21) become

- $r^2\ddot{\alpha} - U(\alpha' r - \alpha)\left(\frac{1}{2}U' r - U\right) + U\alpha = 0\,,$ (3.23)
- $Ur^2\alpha'' + (\alpha' r - \alpha)\left(\frac{1}{2}U' r - U\right) - \alpha = 0\,,$ (3.24)
- $r\dot{\alpha}' - \frac{1}{2}\frac{U' r}{U}\dot{\alpha} = 0\,,$ (3.25)
- $U(\alpha' r - \alpha) + \alpha = \frac{\kappa_5}{6}\rho r\left(-\frac{r^2\dot{\alpha}^2}{U} + U(\alpha' r - \alpha)^2 + r^2 - \alpha^2\right)^{\frac{1}{2}}\,,$ (3.26)
- $\frac{\dot{\rho}}{\rho} = \dot{\alpha}\left(\frac{1 + \frac{1}{2}U' r - U}{U(\alpha' r - \alpha) + \alpha}\right)\,,$ (3.27)
- $\frac{\rho' r}{\rho} = (\alpha' r - \alpha)\left(\frac{1 + \frac{1}{2}U' r - U}{U(\alpha' r - \alpha) + \alpha}\right)\,.$ (3.28)

Equations (3.27) and (3.28) can then be integrated to determine the energy density

$$\rho = \frac{\rho_0}{r^2}\left[U(\alpha' r - \alpha) + \alpha\right]\,, \tag{3.29}$$

which may, in principle, be a (τ, r)-dependent quantity. In addition, (3.25) is immediately integrable yielding

$$\alpha(\tau, r) = f(\tau)\sqrt{U(r)} + g(r)\,, \tag{3.30}$$

where $f(\tau)$ and $g(r)$ are, at present, arbitrary functions. If the above form of $\alpha(\tau, r)$ is substituted into (3.24) then

$$\sqrt{U}\left(\frac{1}{2}U'' r^2 - U' r + U - 1\right) f(\tau) + Ur^2 g'' + (g' r - g)\left(\frac{1}{2}U' r - U\right) - g = 0\,. \tag{3.31}$$

The only way for this equation to be satisfied for all τ, with $f(\tau) \neq 0$, is for the factor preceding $f(\tau)$ to vanish:

$$\frac{1}{2}U'' r^2 - U' r + U - 1 = 0\,, \tag{3.32}$$

which has solution

$$U(r) = 1 + Ar + Br^2\,, \tag{3.33}$$

for constants A and B. Thus a brane with equation of state $w = -1$ may only be embedded in a bulk with the above form for the metric function. Apart from Minkowski spacetime, the only known case with physical interpretation is that of a

5-dimensional (anti) de Sitter spacetime, obtained by setting $A = 0$; nevertheless in order to describe the most complete set of analytic time-dependent solutions both A and B will be retained in the analysis.

Further information about the braneshape may be determined by inserting the solution for $\alpha(\tau, r)$ into the sum of equations (3.23)-(3.24): $\ddot{\alpha} + U^2\alpha'' = 0$, to obtain

$$\ddot{f}(\tau) + f(\tau)\left(\frac{UU''}{2} - \frac{U'^2}{4U}\right) + U\sqrt{U}\, g'' = 0\,. \tag{3.34}$$

If it is assumed the brane trajectory oscillates in time with constant frequency λ so that

$$f(\tau) = C_1 \cos(\lambda\tau) + C_2 \sin(\lambda\tau)\,, \tag{3.35}$$

then equation (3.34) will be satisfied if the following two constraints hold independently

$$\frac{UU''}{2} - \frac{U'^2}{4U} - \lambda^2 = 0 \qquad \text{and} \qquad g'' = 0\,. \tag{3.36}$$

By using the solution for the metric function (3.33), the first of the constraints leads to the result $\lambda^2 = B - A^2/4$, and the second to $g(r) = g_1 r + g_0$. The latter, when inserted into equation (3.31) after the coefficient of $f(\tau)$ has been set equal to zero, yields the relation $g_1 = g_0 A/2$.

Finally, the energy density constant ρ_0 may be determined by demanding the solution satisfies (3.26). If the form of ρ given in equation (3.29) is substituted into (3.26) then

$$U(\alpha' r - \alpha)^2 - \alpha^2 + \left(1 - \frac{\dot{\alpha}^2}{U} - \frac{36}{\kappa_5^2 \rho_0^2}\right) r^2 = 0\,, \tag{3.37}$$

which leads to

$$\frac{36}{\kappa_5^2 \rho_0^2} = 1 - \dot{f}^2 - \left(B - \frac{A^2}{4}\right)(f^2 - g_0^2)\,. \tag{3.38}$$

Substitution of the oscillatory ansatz for $f(\tau)$ into the above equation yields

$$\rho_0 = \frac{6}{\kappa_5 \sqrt{1 + \left(B - \frac{A^2}{4}\right)(g_0^2 - C_1^2 - C_2^2)}}\,. \tag{3.39}$$

To summarise, a fully consistent family of time-dependent brane embeddings in a 5-dimensional spherically-symmetric bulk spacetime, specified by the single metric

component $U(r) = 1 + Ar + Br^2$, are determined by the functions:

- Brane shape: $$r\cos\chi(\tau, r) = f(\tau)\sqrt{U(r)} + g_0\left(1 + \frac{Ar}{2}\right), \tag{3.40}$$
- Energy density: $$\rho(\tau, r) = -\frac{3A\left[g_0 + f(\tau)\sqrt{U(r)}\right] + 6g_0Br}{r\kappa_5\sqrt{1 + \left(B - \frac{A^2}{4}\right)(g_0^2 - C_1^2 - C_2^2)}}, \tag{3.41}$$
- Pressure: $$p(\tau, r) = -\rho(\tau, r), \tag{3.42}$$

where

$$f(\tau) = C_1\cos\left(\sqrt{B - \frac{A^2}{4}}\tau\right) + C_2\sin\left(\sqrt{B - \frac{A^2}{4}}\tau\right),$$

and A, B, C_1, C_2 and g_0 are all arbitrary real constants.

It is apparent that the energy-momentum tensor on the brane, although characterised by an equation of state with $w = -1$, can be both τ- and r-dependent, providing $A \neq 0$. If $A = 0$ all coordinate dependence is removed from the brane energy density, leaving the constant

$$\rho = -\frac{6g_0B}{\kappa_5\sqrt{1 + B(g_0^2 - C_1^2 - C_2^2)}}. \tag{3.43}$$

With $A = 0$ the bulk metric may be interpreted as that of a 5-d maximally symmetric spacetime. Furthermore, the choice of parameters $C_1 = 1/k$, $C_2 = 0$, $B = k^2$ and $g_0 = -1/k$ corresponds to the specific case of a pure tension brane with self-energy

$$\rho = \rho_{RS} = \frac{6k}{\kappa_5}, \tag{3.44}$$

following the trajectory

$$\alpha(\tau, r) = r\cos\chi(\tau, r) = \frac{1}{k}\sqrt{1 + k^2r^2}\,\cos(k\tau) - \frac{1}{k}, \tag{3.45}$$

in a bulk spacetime that is pure anti-de Sitter, with curvature k. This is exactly the Randall-Sundrum brane in global coordinates. To demonstrate this it is necessary to employ the transformation between global adS and Randall-Sundrum horospherical coordinates:

$$\begin{aligned} ku &= \left[\sqrt{1 + k^2r^2}\cos k\tau - kr\cos\chi\right]^{-1}, \\ kt &= (ku)\sqrt{1 + k^2r^2}\,\sin k\tau, \\ k|\mathbf{x}| &= (ku)\,kr\sin\chi, \end{aligned} \tag{3.46}$$

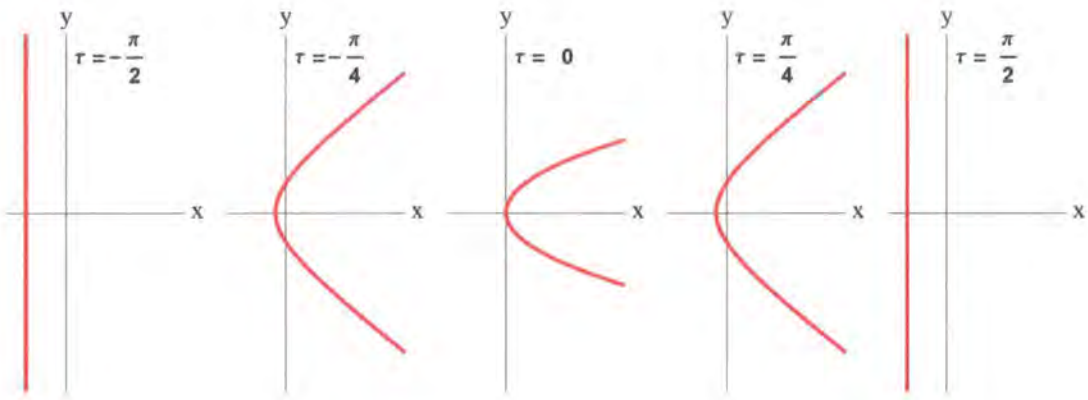

Figure 3.1: A cartoon illustrating the time dependence of the Randall-Sundrum brane trajectory, equation (3.45), when expressed in global coordinates.

in which the RS metric, equation (2.14), is

$$ds^2 = \frac{1}{k^2u^2}\left[-dt^2 + du^2 + d\mathbf{x}^2\right] , \tag{3.47}$$

and the trajectory in equation (3.45) corresponds to $ku = 1$. The wall trajectory in global coordinates appears oscillatory: a fact that motivated the choice of ansatz for $f(\tau)$ in equation (3.35). The brane originates at the adS boundary, progressing in towards the origin when it closes off the entire adS boundary, before returning from where it came. The reason for this oscillatory behaviour, illustrated in figure 3.1, is that the spherical coordinates are the universal covering space of adS, and so the 'wall' is actually an infinite family of walls, each in the local patch covered by the horospherical coordinates.

Although a family of analytic time-dependent brane trajectories satisfying the Israel conditions have been outlined in this section, their use in describing the braneworld black hole metric is limited owing to the restriction imposed on the form of the bulk metric function by equation (3.33). In order to incorporate a singularity into the bulk-brane system it is necessary to permit a more general equation of state. If analytic progress is to be made in solving equations (3.16)-(3.21) then an alternative simplification is required.

3.3 The Static Brane

The brane equations may also be considerably simplified if the system is taken to be time-independent. Then $\dot{\chi} = \dot{\alpha} = 0$ and $\dot{\rho} = 0$. The remaining conditions (excluding (3.18) which is now trivially satisfied) become:

- $$v = -(\alpha' r - \alpha)\left(\frac{\frac{1}{2}U' r}{U(\alpha' r - \alpha) + \alpha}\right), \tag{3.48}$$
- $$U r^2 \alpha'' + (\alpha' r - \alpha)\left(\frac{1}{2}U' r - U\right) - \alpha = 0, \tag{3.49}$$
- $$U(\alpha' r - \alpha) + \alpha = \frac{\kappa_5}{6}\rho r \left[U(\alpha' r - \alpha)^2 + r^2 - \alpha^2\right]^{\frac{1}{2}}, \tag{3.50}$$
- $$\frac{\rho' r}{\rho} = (\alpha' r - \alpha)\left(\frac{1 + \frac{1}{2}U' r - U}{U(\alpha' r - \alpha) + \alpha}\right). \tag{3.51}$$

Once again the brane energy density can be found by integrating restriction (3.51) to give:

$$\rho(r) = \frac{\rho_0}{r^2}\left[U(\alpha' r - \alpha) + \alpha\right], \tag{3.52}$$

where ρ_0 is an integration constant. Substituting for $\rho(r)$ in (3.50) yields

$$U(\alpha' r - \alpha)^2 - \alpha^2 + \left(1 - \frac{36}{\kappa_5^2 \rho_0^2}\right) r^2 = 0. \tag{3.53}$$

In fact, equations (3.49) and (3.53) governing the brane trajectory can be solved exactly by transforming to the modified radial variable

$$\tilde{r} = \int \frac{dr}{r\sqrt{U}}. \tag{3.54}$$

Expressed in these terms the time-independent brane equations admit the fully-consistent solution:

- Brane shape: $$\cos\chi(r) = a e^{\tilde{r}} + b e^{-\tilde{r}}, \tag{3.55}$$
- Energy density: $$\rho(r) = \frac{\rho_0}{r}\left[\sqrt{U}\left(a e^{\tilde{r}} - b e^{-\tilde{r}}\right) + a e^{\tilde{r}} + b e^{-\tilde{r}}\right], \tag{3.56}$$
- Pressure: $$p(r) = -\frac{2}{3}\rho(r) - \frac{\rho_0 U'}{6\sqrt{U}}\left(a e^{\tilde{r}} - b e^{-\tilde{r}}\right), \tag{3.57}$$

where

$$4ab = 1 - \frac{36}{\kappa_5^2 \rho_0^2}.$$

Finally, the induced metric on the brane can be written as

$$ds^2 = -U d\tau^2 + \frac{36}{\kappa_5^2 \rho_0^2} \frac{r^2 dr^2}{U(r^2 - \alpha^2)} + (r^2 - \alpha^2)\, d\Omega_2^2 . \tag{3.58}$$

It should be noted that the constants a and b featuring in equation (3.55) encode exactly the same information as the integration constant ρ_0, and the arbitrary zero point of the modified radial variable $\tilde{r}$ from the integration in (3.54).

3.4 Static Braneworld "Stars"

The static brane equations have been shown to admit an implicit exact solution in terms of the radial variable $\tilde{r}$, which depends on an integral of the bulk Newtonian potential $U(r)$. Although this is an exact solution, the properties of the brane depend on the specific relation between $\tilde{r}$ and r. Once this is determined for a given background, equations (3.55) - (3.57) represent a consistent static, spherically symmetric distribution of isotropic perfect fluid on the brane. This is the brane equivalent of the Tolman-Oppenheimer-Volkoff system describing the interior of a star in astrophysics. In the static case there exists a variety of background spacetimes with physical interpretation in which a brane may be embedded. This results in a correspondingly varied set of energy density and pressure distributions, some of which may correspond to a static braneworld star. In order to determine which of these solutions represent physically interesting configurations it is necessary to undertake a systematic examination of the permissible energy density and pressure profiles.

The simplest possible bulk spacetime with physical significance is the vacuum: $U = 1$. In this case $\tilde{r} = \ln r$, and $\alpha(r) = ar^2 + b$. Introducing the polar coordinates

$$x^* = r\cos\chi\,, \qquad y^* = r\sin\chi\,, \tag{3.59}$$

brings the brane trajectories to the form

$$\left(x^* - \frac{1}{2a}\right)^2 + y^{*2} = \frac{1 - 4ab}{4a^2}\,, \tag{3.60}$$

with $x^* = b$ in the particular case $a = 0$. These solutions are of limited physical importance as they have constant energy and pressure: $\rho = 2a\rho_0$, $p = -2\rho/3$. A

shift of the x^* coordinate by $1/2a$ reveals that they correspond to an Einstein static universe,

$$ds^2 = -d\tau^2 + R_0^2 d\Omega_3^2 \tag{3.61}$$

where $R_0^2 = (1 - 4ab)/4a^2$.

A more general family of bulk spacetimes can be considered by making the choice $U(r) = 1 + Cr^n$ for the bulk metric function, where C and n are arbitrary constants. It is then possible to find $\tilde{r}$ as a function of r by straightforward analytic integration:

$$\tilde{r} = \frac{1}{n} \ln \left| \frac{\sqrt{U} - 1}{\sqrt{U} + 1} \right| , \tag{3.62}$$

allowing α to be written in the general form:

$$\alpha(r) = \left[A \left| \sqrt{U} - 1 \right|^{\frac{2}{n}} + B \left(\sqrt{U} + 1 \right)^{\frac{2}{n}} \right] , \tag{3.63}$$

with A and B convenient redefinitions of the integration constants a and b appearing in the general solution (3.55).

These solutions (3.63), in conjunction with the choice for the bulk metric function $U(r) = 1 + Cr^n$, describe different brane configurations in a variety of spherically symmetric bulk backgrounds. Two such backgrounds of immediate physical significance correspond to $n = \pm 2$, – pure adS spacetime, and the Schwarzschild solution in five dimensions.

3.4.1 A 5-Dimensional Anti-de Sitter Bulk

In the case of a 5-dimensional bulk filled with negative cosmological constant, the bulk metric function may be written as $U(r) = 1 + k^2 r^2$, where k is the inverse adS radius. The shape of the brane, $\alpha(r)$, is then given by the expression:

$$\alpha(r) \equiv r \cos \chi(r) = A \left(\sqrt{U} - 1 \right) + B \left(\sqrt{U} + 1 \right) , \tag{3.64}$$

where, in terms of (3.55), $\tilde{r}$ has been set to zero at infinity, $A = a/k$, and $B = b/k$. Using the planar coordinates (3.59), the above trajectory may be written as

$$(1 - \beta) \left(x^* + \frac{(A - B)}{1 - \beta} \right)^2 - \beta y^{*2} = \frac{(A + B)^2 \, (1 - 4ABk^2)}{(1 - \beta)} , \tag{3.65}$$

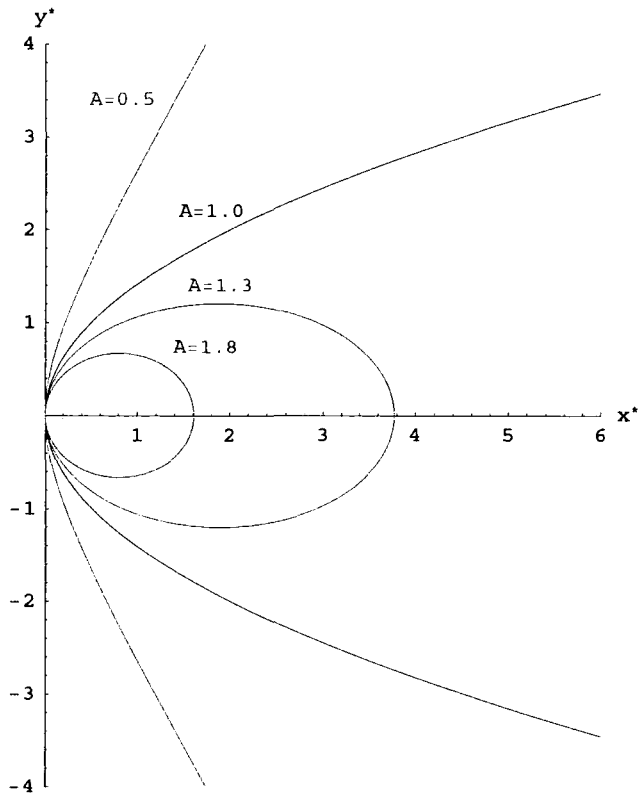

Figure 3.2: A selection of branes of varying coefficient A, for the case $B = 0, k = 1$ in a 5-dimensional anti-de Sitter bulk.

where $\beta = k^2(A+B)^2$. When projected in the (x^*, y^*) plane these brane trajectories can be thought of as conic sections classified by the parameter β. For $\beta > 1$, the brane is an ellipse, $\beta = 1$, a parabola, $\beta < 1$, an hyperbola, and when $\beta = 0$ the projection of the brane is a straight line. In Figure 3.2, the resulting brane configurations for some indicative values of the integration parameters A and B are displayed. For simplicity, k has been set to 1, and $B = 0$. As A varies, the shape of the brane changes gradually covering the three main cases outlined above. The physical significance of β becomes apparent from computation of the energy density according to (3.56):

$$\rho = k^2\rho_0(A - B) = \frac{6k}{\kappa_5}\frac{k(A-B)}{\sqrt{1-\beta+k^2(A-B)^2}}. \tag{3.66}$$

This reveals that the energy density is constant throughout the brane and for $A > B$ it remains positive. Then for $\beta = 1$, the energy density has precisely the Randall-Sundrum critical value $\rho_{RS} = 6k/\kappa_5$, while for β less (greater) than unity the branes

are sub- (super-) critical. Turning to the equation of state on the brane, equations (3.48) and (3.6) imply

$$p(r) = -\rho + \frac{(A+B)k^2\rho_0}{3\sqrt{U}} = \frac{6k}{\kappa_5}\frac{k}{\sqrt{1-\beta+k^2(A-B)^2}}\left(\frac{(A+B)}{3\sqrt{U}} - (A-B)\right). \tag{3.67}$$

It should be noted that a static trajectory may not be obtained for a critical or super-critical brane composed of pure cosmological constant ($w = -1$). Such a solution requires $A + B = 0$, which necessarily corresponds to $\beta = 0$ and thus a sub-critical, or Karch-Randall brane [33]. For $\beta \neq 0$, a varying tension is required to support the braneshape – a feature that will be manifested in the braneworld as a surplus pressure.

Finally, the induced metric on the brane can be evaluated

$$\begin{aligned} ds^2 &= -U(r)\,d\tau^2 + \frac{36}{\kappa_5^2\rho_0^2}\frac{r^2dr^2}{U(r)(r^2-\alpha^2)} + \left(r^2-\alpha^2(r)\right)d\Omega_2^2 \\ &= -U(r(\hat{r}))\,d\tau^2 + \frac{36}{\kappa_5^2\rho_0^2}\frac{d\hat{r}^2}{U(r(\hat{r}))\left(1-\frac{\alpha\alpha'}{r}\right)^2} + \hat{r}^2d\Omega_2^2 \\ &= -U\left(r(\hat{r})\right)\,d\tau^2 + \frac{d\hat{r}^2}{1-\lambda\hat{r}^2/3} + \hat{r}^2d\Omega_2^2, \end{aligned} \tag{3.68}$$

where $\lambda/3 = -k^2 + \rho^2\kappa_5^2/36$ is the effective cosmological constant on the brane and the general time-independent result

$$U(r)\left(1-\frac{\alpha\alpha'}{r}\right)^2 = \frac{36}{\kappa_5^2\rho_0^2}\left[U - \frac{\kappa_5^2\rho^2}{36}r^2 + \frac{\kappa_5^2\rho_0^2}{36}\frac{\alpha^2}{r^2}(1-U+U\alpha'^2)\right], \tag{3.69}$$

found by combining equations (3.52) and (3.53), has been used in the particular case $U(r) = 1 + k^2r^2$ and $\alpha(r)$ given by (3.64). In equation (3.68) the coordinate $\hat{r} = r\sin\chi$ has been defined. Its physical interpretation is of a brane radial coordinate as it sets the scale of the two-sphere line element $d\Omega_2^2$ in the induced metric. Clearly, the spatial part of the metric takes the form of a constant curvature space, being flat, anti-de Sitter or de Sitter depending on whether the brane is critical, sub- or super-critical respectively. However, since the relation between r and $\hat{r}$ is in general convoluted, the brane has a non-trivial Newtonian potential. This is because unless $A = -B$, the surplus pressure on the brane described above acts as a source and results in a spacetime that is not asymptotically flat. To see this explicitly consider

a critical brane

$$ds_c^2 = -\frac{k^2\left(A^2+B^2+\hat{r}^2/2\right)^2}{(A-B)^2}\,d\tau^2 + d\hat{r}^2 + \hat{r}^2\,d\Omega_2^2\,. \tag{3.70}$$

This spacetime is clearly not asymptotically flat, and can be shown to result from the source

$$\tilde{T}^\tau_\tau = 0\,, \qquad \tilde{T}^r_r = \tilde{T}^\theta_\theta = \tilde{T}^\varphi_\varphi = \frac{4}{\kappa_5(2A^2+2B^2+\hat{r}^2)}\,, \tag{3.71}$$

which corresponds to the actual pressure discrepancy on the brane: $p + 6k/\kappa_5$. Similar results hold for the case of sub- or super-critical branes for which $\tilde{T}^\tau_\tau = \lambda \neq 0$.

Therefore these particular trajectories have excess pressure on the brane, which results in metrics that do not asymptote exact Randall-Sundrum or Karch-Randall branes. However, if $|kA|$ and $|kB|$ are large enough, the metric can be flat (or asymptotically (a)dS) over many orders of magnitude before the effect of the pressure is significant.

3.4.2 A 5-Dimensional Schwarzschild Bulk

The cosmological constant may now be removed from the 5-dimensional bulk and a point mass inserted to establish a spherically symmetric Schwarzschild background. This is accomplished by setting $n = -2$ and $C = -\mu$ so that the metric function becomes $U(r) = 1 - \mu/r^2$, where μ is related to the actual mass of the black hole by $M_{BH} = 3\pi^2\mu/\kappa_5$. Then, equation (3.63), that describes the shape of the brane, takes the form

$$\alpha(r) = r\cos\chi(r) = r^2\left[A\left(\sqrt{U}-1\right) + B\left(\sqrt{U}+1\right)\right], \tag{3.72}$$

where now $A = -b/\sqrt{\mu}$, $B = a/\sqrt{\mu}$, and $\tilde{r} = 0$ at the horizon. By construction, these trajectories are strictly valid only outside the black hole event horizon since the definition of the $\tilde{r}$ coordinate involves a branch cut there. It would be possible to redefine $\tilde{r}$ inside the horizon, although since interest is focused on the exterior solution this will not be performed here.

Following the same analysis as before, the functions ρ and p are now found to be

$$\rho(r) = \rho_0\left[B(\sqrt{U}+1)^2 - A(\sqrt{U}-1)^2\right], \tag{3.73}$$

$$p(r) = -\rho(r) + \frac{\rho_0}{3\sqrt{U}}\left[B(\sqrt{U}+1)^2(2\sqrt{U}-1) - A(\sqrt{U}-1)^2(2\sqrt{U}+1)\right], \tag{3.74}$$

where $\rho_0 = \frac{6}{\kappa_5\sqrt{1+4AB\mu}}$. Clearly ρ is not constant for these branes, in contrast to the adS case, and it is now necessary to consider what may be thought of as a physically sensible brane energy and trajectory. If the above solutions are to correspond to realistic astrophysical objects such as stars or black holes then ρ must necessarily be positive and ideally possess a distribution representing a localised accumulation of energy density. When viewed in terms of a coordinate that a brane-based observer would perceive as "radial" it is desired that the brane energy density increases towards the centre of the brane. This is not quite equivalent to ρ being a decreasing function of r since, as discussed in §3.4.1, the brane radial coordinate is in fact $r\sin\chi$, therefore each trajectory must be examined in turn.

To examine the shape of the brane, equation (3.72) is squared to obtain:

$$4AB\,r^2 + 2(B-A)r\cos\chi - \cos^2\chi = \mu(A+B)^2\,. \tag{3.75}$$

The solutions of the above equation are hyperbolae in the $(\cos\chi, r)$-plane, which leads to the following parametric solution in polar coordinates:

$$r = \sqrt{\mu}\cosh\lambda\,, \tag{3.76}$$

$$\chi = \mathrm{Arccos}\left(\sqrt{\mu}(Be^{\lambda} - Ae^{-\lambda})\right)\,. \tag{3.77}$$

Constraints must be imposed on the range of the parameter λ since $|\cos\chi| \leq 1$, and only solutions with positive ρ are sought.

Subject to these restrictions it is possible to classify the qualitatively different families of trajectory allowed. First of all, note that the brane can only touch the event horizon providing

$$0 < B - A \leq 1/\sqrt{\mu}\,, \tag{3.78}$$

the first inequality arising from positivity of energy. Computing the derivative $\frac{d\chi}{dr}$ from (3.76) and (3.77) shows that unless $B = -A$, $\frac{d\chi}{dr} \to \infty$ at the horizon, so the brane touches the horizon at a tangent. However, if $B = -A$, then the brane may actually pass through the horizon, and coincide with the central singularity.

From (3.75), it is clear that the general shape of a trajectory is primarily determined by the quantity AB. There are three distinct cases to consider:

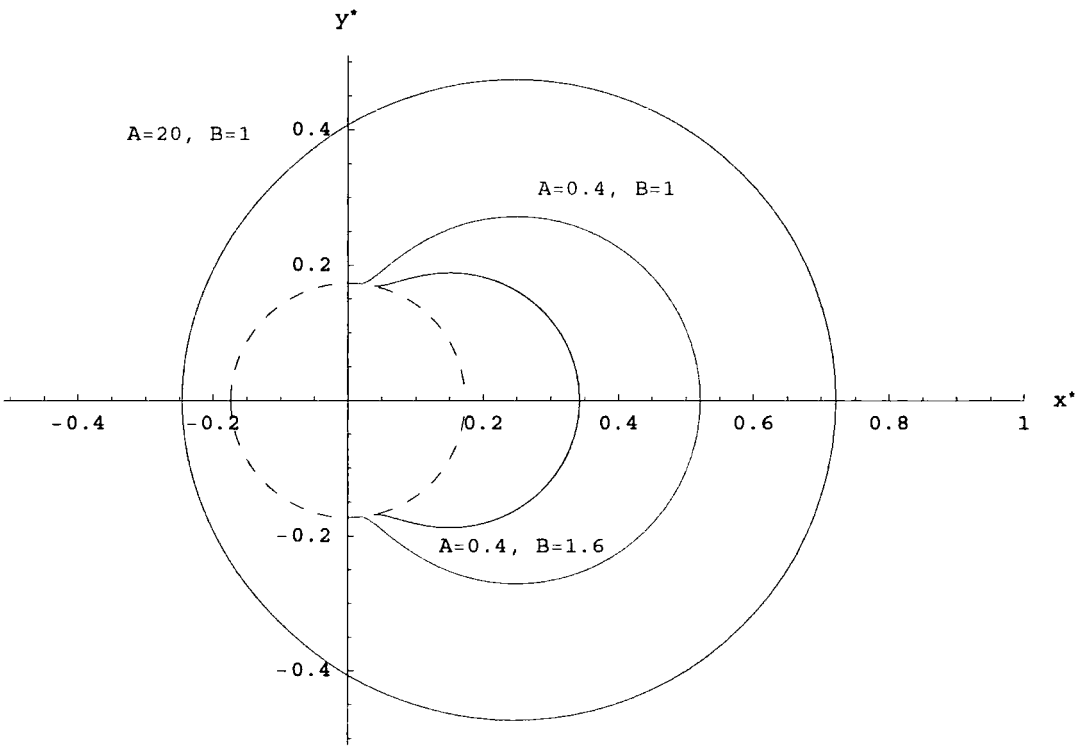

Figure 3.3: A selection of branes for the case $AB > 0$, in a 5-dimensional Schwarzschild bulk of fixed mass parameter $\mu = 0.03$. The dashed line denotes the corresponding horizon radius.

- $AB > 0$. In this case (3.77) implies that either the brane completely encloses or touches and terminates on the event horizon, depending on the value of $B - A$ in comparison to the critical value $1/\sqrt{\mu}$. If the brane touches the horizon then it does so on the right of the (x^*, y^*)-plane since positivity of energy requires $B > A$. The brane then exists to the right of such points of contact since, from equation (3.72), $\cos\chi$ is then an increasing function of r. Figure 3.3 shows a sample set of brane trajectories in this class.

  For $B > A > 0$, the energy density (3.73) remains positive throughout the brane. From equation (3.51), it can be seen that this corresponds to ρ being an increasing function of r, hence these branes have an energy surplus at the point farthest from the event horizon. The branes terminating on the horizon have the appearance of the inside of a bubble, with the event horizon defining its boundary and its energy density concentrated at the centre, $\hat{r} = 0$.

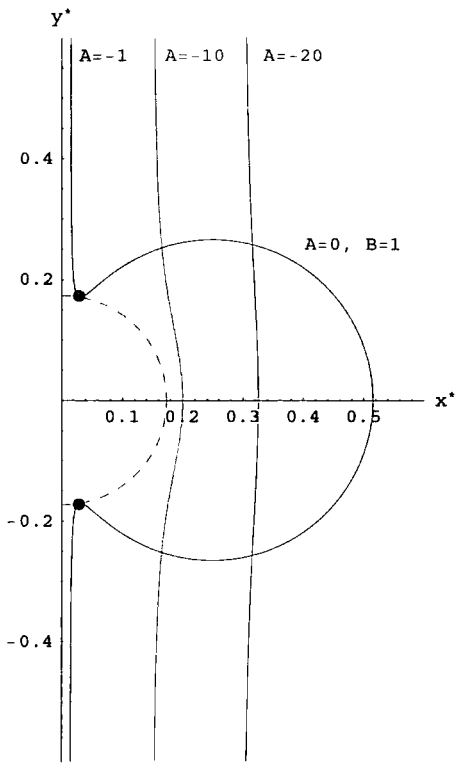

Figure 3.4: A selection of branes for the case $AB = 0$, in a 5-dimensional Schwarzschild bulk of fixed mass parameter $\mu = 0.03$. The case $A = 0, B = 1$ is shown together with a set of branes with $B = 0$ and variable A. The dashed line again denotes the event horizon.

However, the pressure (3.74) increases away from the bubble centre becoming infinite on contact with the event horizon, thus rendering the bubble boundary singular.

- $AB = 0$. If $A = 0$, then (3.72) will only correspond to a brane outside the horizon if $|\cos\chi| = rB\,(1 + \sqrt{U}) \leq 1$. This leads to the bound $B \leq 1/\sqrt{\mu}$ while positivity of energy demands that $B > 0$. Examination of (3.72) then shows that these trajectories begin tangent to the horizon, curving outwards into the bulk, before returning to the event horizon once again. The indicative case ($A = 0$, $B = 1$) is shown in figure 3.4. The energy density and pressure of these trajectories are similar to those of branes with $AB > 0$ terminating on the horizon, and they also correspond to bubbles with a singular pressure boundary.

On the other hand, if $B = 0$ the trajectories asymptote $r\cos\chi = -\mu A/2$ at infinity, remaining approximately straight until the vicinity of the horizon at which point they bend away from the black hole. Those branes which make contact with the horizon are equivalent to the planar solutions first considered in [71]. If $-A < 1/\sqrt{\mu}$, then they become tangent to the horizon at the same point as the trajectory found by swapping B and $-A$ (as illustrated by the two blue lines in figure 3.4). If $-A > 1/\sqrt{\mu}$, the trajectories manage to bend sufficiently far that they avoid the event horizon altogether. In the limiting case $A = -1/\sqrt{\mu}$ the brane just skims the horizon. Figure 3.4 also demonstrates a number of these brane trajectories with $B = 0$ and variable A.

The energy and pressure of brane trajectories with $B = 0$ have a particularly simple form:

$$\rho = \frac{-6A}{\kappa_5}\left(\sqrt{U} - 1\right)^2, \qquad p = -\frac{\rho}{3}\frac{(\sqrt{U} - 1)}{\sqrt{U}}. \tag{3.79}$$

For $A < 0$, these branes have ρ positive and uniformly decreasing as r increases. If $|A| \leq 1/\sqrt{\mu}$, the energy density decreases away from the horizon, however the pressure still diverges there. If $|A| > 1/\sqrt{\mu}$, the brane never touches the horizon and the pressure remains finite everywhere. Moreover, the energy density decreases away from the central region $\hat{r} = 0$, and hence these trajectories correspond to asymptotically empty branes with localised positive mass sources.

- $AB < 0$. From positivity of energy A must be negative, and the brane lies exclusively on the right hand side of the (x^*, y^*)-plane. As in the case $AB > 0$, the brane is either a single arc which touches the horizon, or a closed loop. A selection of these branes are depicted in figure 3.5.

  For arc branes with $B - |A| > 0$, the energy density increases away from the horizon and reaches its maximum value at the centre of the brane ($\hat{r} = 0$), again creating a bubble with diverging pressure at its boundary. The same singular pressure behaviour is exhibited by the arc branes with $B - |A| < 0$, although in this case, the energy initially decreases away from the horizon, before increasing again to form an energy source around $\hat{r} = 0$. In

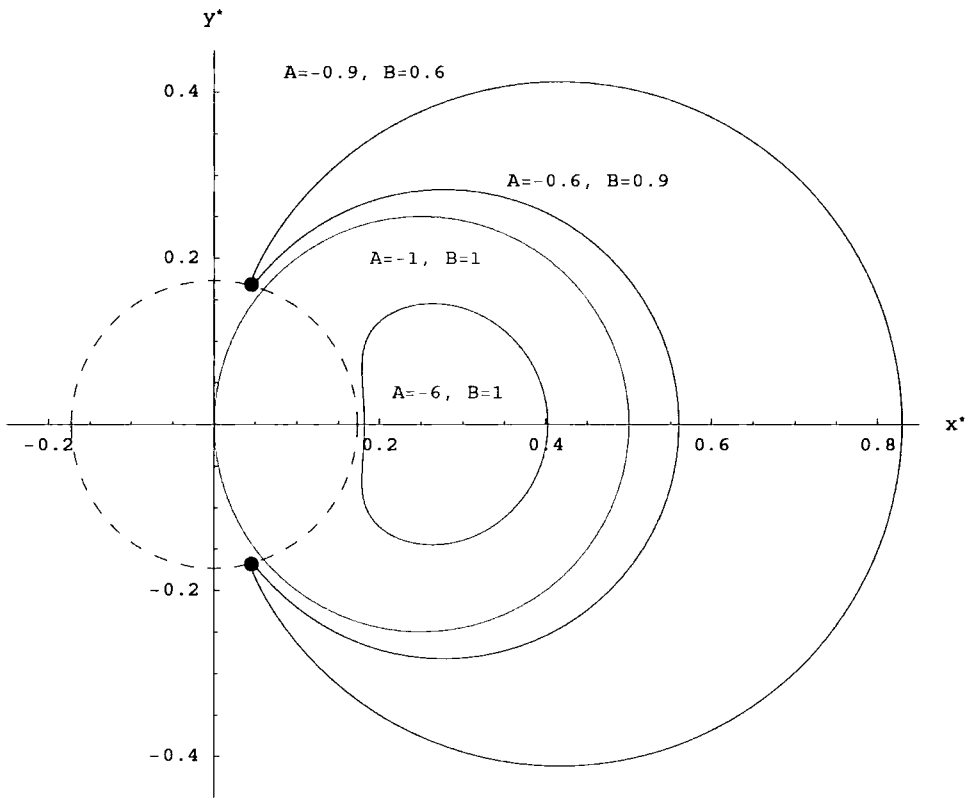

Figure 3.5: A selection of branes for the case $AB < 0$, in a 5-dimensional Schwarzschild bulk of fixed mass parameter $\mu = 0.03$. The dashed line denotes again the corresponding horizon radius.

the case of closed loops that do not touch the horizon the pressure singularity is avoided, and the energy density profile resembles one of the two described above depending on the particular value of $B - |A|$ in that case.

In the cases described above the brane may touch the horizon but never cross it. However, if the integration constants are arranged so that $A = -B$ then the brane equation may be written as

$$y^{*2} + \left(x^* - \frac{1}{4B}\right)^2 = \frac{1}{16B^2}. \tag{3.80}$$

This situation is unique in that the brane extends beyond the black hole horizon and even intersects the point mass located at $x^* = y^* = 0$. For this trajectory the singularity problem associated with crossing the horizon is removed by the choice $A = -B$. The energy density is uniformly increasing with r for $B > 0$, and acquires

its maximum value at the point farthest from the black hole. This type of brane is also shown in figure 3.5 – the solid purple line indicating the sole trajectory which crosses the horizon.

Having derived these brane trajectories, it is important to draw attention to those which may be considered most physically relevant. It should be noted that from the definition of the brane extrinsic curvature the normal, defined in (3.2), points out of the spacetime being kept in the $\mathbb{Z}_2$ symmetric identification. This means that, in figures 3.3-3.5, for a trajectory which escapes to infinity it is the right-hand side of the bulk spacetime which is being kept, and for closed branes it is the interior of the bubble.

Focusing on the asymptotically flat $B = 0$ trajectories, it is possible to show that these have precisely the energy-momentum expected of a Tolman-Oppenheimer-Volkoff (TOV) star solution. From (3.79) both the energy density and pressure are peaked around $\hat{r} = r \sin\chi = 0$. Moving away from the central region the energy falls off as $1/r^4$ and the pressure as $1/r^6$ (with $\hat{r} \propto r$ for large r). Plotting the energy and pressure for the brane shows that this does indeed correspond to a localised matter source, with the peak energy density dependent on the minimal distance from the horizon. The central energy and pressure can be readily calculated from this minimal radius, $r_m = \mu|A|/2 + 1/2|A|$:

$$\rho_c = \frac{24|A|}{\kappa_5(1+\mu A^2)^2}, \qquad p_c = \frac{16|A|}{\kappa_5(\mu A^2-1)(1+\mu A^2)^2}, \tag{3.81}$$

which shows that the central pressure diverges as $\mu A^2 \to 1$. However, for $|A| = 1/\sqrt{\mu}$ the trajectory just touches the event horizon of the black hole, which is the source of this divergent pressure. This is analogous to the divergence of central pressure in the four-dimensional TOV system, which is indicative of the existence of a Chandrasekhar limit for the mass of the star.

Some examples of the solutions to the brane TOV equations are given in figure 3.6. In the left hand plot the brane intersects the horizon at $\hat{r} = 0.17$, at which point the pressure becomes singular but the energy density remains finite. As the brane trajectory is displaced further from the horizon, the pressure of matter on the brane decreases, being barely distinguishable from the axis in the right-hand plot. Also as μA^2 increases, the spread of the matter on the brane increases slightly. In

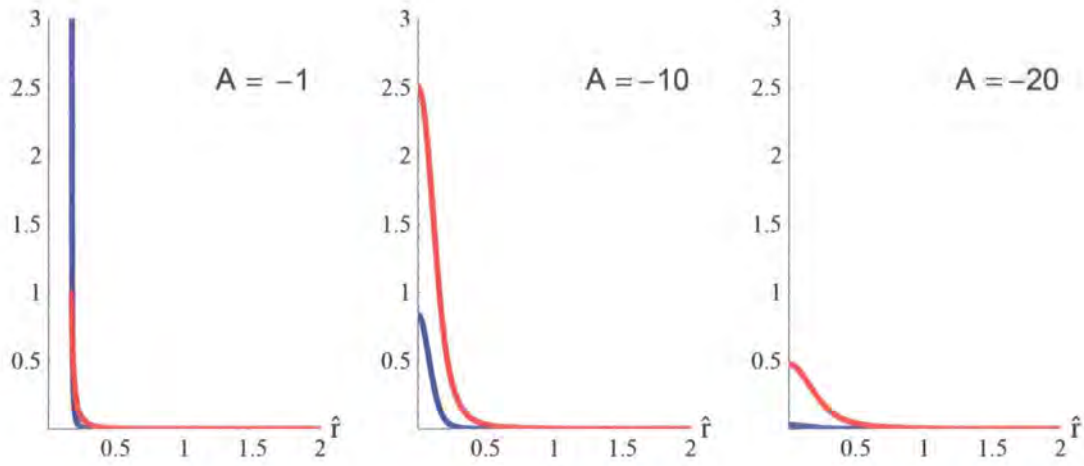

Figure 3.6: The energy density (red) and pressure (blue) of brane stars in a pure Schwarzschild bulk as a function of the brane radial coordinate $\hat{r}$. The black hole mass is fixed at $\mu = 0.03$ and the vertical scale has been normalised in units of the Randall-Sundrum energy density, ρ_{RS}. The figures correspond to those trajectories that extend to infinity in figure 3.4.

these spacetimes, there is no actual black hole in the bulk, since it is the bulk to the right of the brane that is retained. Rather, it is the combination of the bulk Weyl curvature and the brane bending which produces the fully coupled gravitational solution.

By working in dimensionless units, $\xi = r/\sqrt{\mu}$ and $b = -A\sqrt{\mu}$, it is possible to extract more information about the dependence of the energy on the bulk Weyl mass parameter, μ, and the 'impact parameter' A (or b). For instance, the energy density on the brane scales as $b/\sqrt{\mu}$, and the spread of the star as b. The total mass of the star may be calculated using the induced metric (3.58) as

$$\begin{aligned} M_s &= 4\pi \frac{6}{\kappa_5 \rho_0} \int_{r_m}^{\infty} \rho \frac{\sqrt{r^2-\alpha^2}}{\sqrt{U}} r\, dr \\ &= \frac{24\pi\mu}{\kappa_5} \left[b \int_{\xi_m}^{\infty} \left(\sqrt{U}-1\right)^2 \frac{\sqrt{1-\xi^2 b^2 \left(\sqrt{U}-1\right)^2}}{\sqrt{U}} \xi^2\, d\xi \right] \\ &= \frac{24\pi\mu}{\kappa_5} F(b) \end{aligned} \tag{3.82}$$

where $F(b) \to$ constant of $O(1)$ from above very rapidly. In other words, the total mass of the star is directly proportional to the bulk mass parameter. The central singularity in the pressure results from either reducing b to bring the brane into contact with the horizon, or increasing μ to expand the horizon onto the brane. In either case, the total mass and the concentration of the matter increases. There is however no overall upper bound on the mass of the star, as it is always possible to obtain a non-singular solution for any μ by making b large enough. The limit on mass is therefore not a true Chandrasekhar limit, but more a statement about an upper bound on the concentration of matter. The real reason there is no absolute upper bound is because, unlike the RS system with an adS bulk, gravity on the braneworld is not localised, nor is it four-dimensional. This is also seen in the induced metric on the brane (3.58), which in the case of a Schwarzschild bulk has no convenient expression in terms of the radial coordinate $\hat{r}^2 = r^2 - \alpha^2$. However, for the one solution which tends to infinity $\alpha \to \mu|A|/2$, which implies that the asymptotic metric is in fact the projection of the 5-dimensional Schwarzschild metric on the brane.

In summary, the pure Schwarzschild spacetime has a diverse set of brane trajectories, most of which are closed, however, there is a class of asymptotically flat branes which have a localised source satisfying the dominant energy condition (DEC) (except where pressure singularities occur) and hence with the interpretation of an isolated gravitating star.

3.5 Braneworld Stars: A Schwarzschild-adS Bulk

Since the Randall Sundrum model is a brane in adS spacetime, it is instructive to examine the case of a static brane embedded in a 5-dimensional Schwarzschild-anti-de Sitter (SadS) spacetime. It is anticipated that any consistent brane trajectories in SadS have the potential to correspond to brane stars or black holes. It should be emphasised that these solutions will be not just brane solutions, but fully consistent brane and bulk solutions, since the Israel equations for the brane have been solved in a known bulk background.

In the Randall-Sundrum scenario the empty brane solution does not have zero energy-momentum, but a background constant energy and tension: $\tilde{T}_{\mu\nu} = \lambda_{brane} h_{\mu\nu}$, where $\lambda_{brane} = \rho_{RS}$ for the critical RS brane, and $\lambda_{brane} < \rho_{RS}$ for the subcritical Karch-Randall brane. Therefore, computed values of ρ and p in the brane energy-momentum tensor (3.5) will include this background brane energy-momentum. According to [54], the brane gravitational field couples to the differential energy-momentum

$$\mathcal{T}_{\mu\nu} = \tilde{T}_{\mu\nu} - \frac{\rho_b}{\kappa_5} h_{\mu\nu}\,, \tag{3.83}$$

where ρ_b is the background brane tension. For critical branes, $\mathcal{T}_{\mu\nu}$ will correspond to the additional matter on the brane sourcing the spherically symmetric gravitational field, however, sub- and super-critical branes will have an additional gravitational effect from the imbalance of bulk and brane cosmological constants. In order to ensure consistency with those brane trajectories already described in a pure adS bulk, from equation (3.5) the background brane tension will be identified as

$$\rho_b = \frac{6k(a-b)}{\kappa_5\sqrt{1-4ab}}\,, \tag{3.84}$$

In five-dimensional Schwarzschild-adS spacetime the metric function $U(r)$ is given by

$$U(r) = 1 + k^2 r^2 - \frac{\mu}{r^2}\,, \tag{3.85}$$

and is not covered by the general metric ansatz studied in section §3.4. The function $\tilde{r}$ does have an exact analytic expression

$$\tilde{r}(r) = \frac{1}{kr_+}\,\text{Elliptic F}\left[\text{Arcsin}\left(\frac{r}{r_-}\right), \frac{r_-^2}{r_+^2}\right]\,, \tag{3.86}$$

although it is of limited use owing to the presence of the Elliptic function and the imaginary value of r_-. In the above, r_+ (the black hole horizon) and r_- are defined by the expressions

$$r_+^2 = \frac{-1+\sqrt{1+4k^2\mu}}{2k^2}\,, \qquad r_-^2 = \frac{-1-\sqrt{1+4k^2\mu}}{2k^2}\,. \tag{3.87}$$

An alternative analytic approach is to find a series solution for the shape of the brane $\alpha(r)$ by making the change of variable $\lambda = r^2$. Then equation (3.49) may be written as

$$2\alpha''\lambda^2\left(k^2\lambda^2+\lambda-\mu\right) + \alpha'\lambda\left(k^2\lambda^2+\mu\right) - \mu\alpha = 0\,, \tag{3.88}$$

where prime now denotes differentiation with respect to λ. If a series solution of the form

$$\alpha(\lambda) = \sum_{n=0}^{\infty} a_n \lambda^{n+\gamma}, \tag{3.89}$$

is sought, then (3.88) becomes

$$\sum_{n=2}^{\infty} k^2(n+\gamma-2)\left(n+\gamma-\frac{5}{2}\right)a_{n-2}\lambda^{n+\gamma} + \sum_{n=1}^{\infty}(n+\gamma-1)(n+\gamma-2)a_{n-1}\lambda^{n+\gamma} - \sum_{n=0}^{\infty}\mu(n+\gamma-1)\left(n+\gamma-\frac{1}{2}\right)a_n\lambda^{n+\gamma} = 0. \tag{3.90}$$

Equating powers of λ yields relations between coefficients of the series expansion

$$\begin{aligned} n &= 0 \quad & \mu(\gamma-1)\left(\gamma-\frac{1}{2}\right)a_0 = 0, \\ n &= 1 \quad & \gamma(\gamma-1)a_0 - \mu\gamma\left(\gamma+\frac{1}{2}\right)a_1 = 0, \\ n &\geq 2 \quad & k^2(n+\gamma-2)\left(n+\gamma-\frac{5}{2}\right)a_{n-2} + (n+\gamma-1)(n+\gamma-2)a_{n-1} - \\ & & \mu(n+\gamma-1)\left(n+\gamma-\frac{1}{2}\right)a_n = 0. \end{aligned} \tag{3.91}$$

From the above relations all possible series coefficients may be computed in terms of the lowest order coefficient for each of the independent solutions corresponding to $\gamma = 1/2, 1$. This leads to the general solution for the braneshape

$$\alpha(\xi) = a_0\xi^2\left[1+\frac{1}{\sigma}\frac{\xi^4}{10}+\frac{1}{\sigma^2}\left[\frac{2\xi^6}{35}+\frac{\xi^8}{24}\right]+O\left(\frac{1}{\sigma^3}\right)\right] + b_0\xi\left[1-\frac{1}{\sigma}\frac{\xi^2}{2}-\frac{1}{\sigma^2}\left[\frac{\xi^4}{8}+\frac{\xi^6}{10}\right]-\frac{1}{\sigma^3}\left[\frac{\xi^6}{16}+\frac{3\xi^8}{28}+\frac{7\xi^{10}}{150}\right]+O\left(\frac{1}{\sigma^4}\right)\right], \tag{3.92}$$

where the dimensionless variable $\xi = kr$ and parameter $\sigma = \mu k^2$ have been introduced (for convenience the symbols a_0 and b_0 have been used to denote the arbitrary integration constant when the solution is expressed in terms of dimensionless variables, but it should be noted that their dimensionality has then changed to preserve consistency). From this expression the form of the pressure and energy density may be derived through equations (3.48) and (3.52) respectively. It is clear that if a solution is sought in the limit $\sigma = \mu k^2 \gg 1$ then the infinite series may be truncated and a finite term expression used to describe a Schwarszschild-adS brane to the required accuracy. Unfortunately, the analysis presented in appendix A.3 demonstrates that

a limit may be placed on the radius of convergence of the series solution that tends to the radius of the Schwarzschild-adS black hole horizon when the large σ limit is taken. In order to describe branes in this background it is necessary to resort to numerical solution through equation (3.86). Before proceeding, it is instructive to first deduce some general properties of SadS brane trajectories based in part on what has been learned from the study of Schwarzschild and anti-de Sitter embeddings separately.

For large enough r, the geometry will be dominated by the cosmological constant so any brane trajectories found should asymptote to a pure adS solution. Also, if $\mu k^2 \ll 1$, so that the black hole is much smaller than the adS scale, then in the vicinity of the horizon the trajectory should be well approximated by one of the Schwarzschild branes already described. Owing to these two facts it is reasonable to expect that, for small mass black holes at least, the brane trajectories ought to be well approximated by some combination of Schwarzschild and adS branes already analysed.

For ease of comparison with the asymptotic pure adS limit, in the subsequent analysis the $\tilde{r}$-coordinate is zeroed at infinity. Then, the range of $\tilde{r}$ in SadS turns out to be finite, and to decrease sharply with increasing μ (for example, if $\mu = 0.01$, $r_+ \simeq 0.1$ and $\tilde{r}_+ \simeq -3.7$, whereas if $\mu = 10^5$, $r_+ \simeq 10$ and $\tilde{r}_+ \simeq -0.13$). This suggests that trajectories in large mass SadS black hole spacetimes are in some respect more finely tuned than their small mass counterparts.

The focus of this study is those branes which have a matter distribution that may be interpreted as an isolated gravitating source. The key requirements of such an object are a localised energy excess at the centre of the brane which decays rapidly with increasing brane radial coordinate. To satisfy this then, unless the brane is a closed bubble, the energy density ρ must be a decreasing function of r. From (3.51) it can be seen that in SadS

$$\rho' = \frac{2\mu\rho_0}{r^3}(\cos\chi)', \tag{3.93}$$

so ρ will be a decreasing function of r providing $\cos\chi$ is also. However, from (3.56), ρ is asymptotically dominated by $\rho_0\sqrt{U}(ae^{\tilde{r}} - be^{-\tilde{r}})/r \propto (\cos\chi)'$, hence any positive energy brane trajectory will have $(\cos\chi)' > 0$ as r tends to infinity, and hence ρ

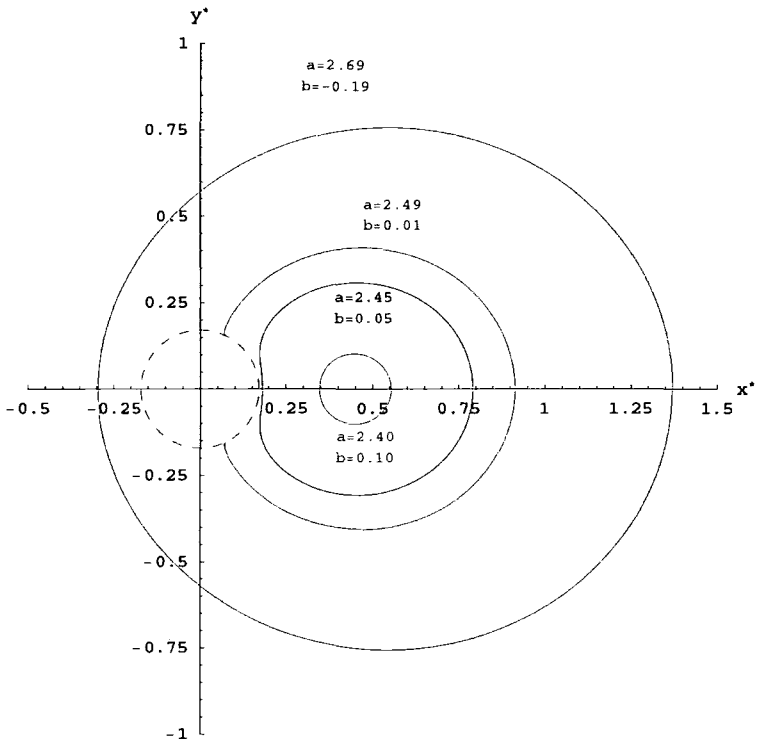

Figure 3.7: A sample of supercritical brane trajectories with $a + b > 1$ in a 5-dimensional Schwarzschild-anti-de Sitter background of fixed parameters $k = 1$ and $\mu = 0.03$. The dashed line denotes again the horizon.

will slowly increase towards infinity also. Consequently there will be a region at large r that is under-dense in comparison with the "background" energy density at infinity. However, this under-density will prove to be extremely marginal, and many trajectories have, as their main feature, interior energies significantly in excess of their background value.

As in the case of a pure adS background, the SadS trajectories can be classified according to whether they asymptote the adS boundary at non-zero χ, at $\chi = 0$, or close off and do not reach the boundary at all. These correspond to subcritical ($a + b > 1$), critical ($a + b = 1$), or supercritical branes ($a + b < 1$) respectively.

3.5.1 Supercritical Branes

It is possible to show that all closed trajectories must be supercritical. Clearly if a trajectory is not closed, it is not supercritical since if a brane asymptotes the adS

boundary then in that asymptotic regime it must have $|\cos\chi| \simeq |a+b| \leq 1$ from the pure adS results. Now suppose that the brane has a finite extent. In that case the brane must satisfy $\cos\chi = 1$ at some value $\tilde{r}_1 < 0$. If the brane is closed it should also satisfy $\cos\chi = \cos\chi_0$ at some other value $\tilde{r}_0 < \tilde{r}_1$, where $\chi_0 = 0$ if the bubble lies entirely on the right-hand side of the black hole and $\chi_0 = \pi$ if the bubble encloses the black hole. The only other possibility for a finite brane is to terminate on the horizon and, in that case, $\tilde{r}_0 = \tilde{r}_H$ if $\chi_0 \in (0, \pi)$. Applying these conditions the constants a and b may be evaluated as

$$a = \frac{e^{\tilde{r}_1} - e^{\tilde{r}_0}\cos\chi_0}{e^{2\tilde{r}_1} - e^{2\tilde{r}_0}}, \qquad b = e^{\tilde{r}_1+\tilde{r}_0}\frac{(e^{\tilde{r}_1}\cos\chi_0 - e^{\tilde{r}_0})}{e^{2\tilde{r}_1} - e^{2\tilde{r}_0}}. \tag{3.94}$$

From the above it may be seen that, since $\tilde{r}_0 < \tilde{r}_1 < 0$, $a+b$ is a decreasing function of $\tilde{r}_1$; therefore, since $a+b = 1$ for $\tilde{r}_1 = 0$, $a+b > 1$ for a closed bubble with $\tilde{r}_1 < 0$.

In figure 3.7, a sample of supercritical brane trajectories are depicted for fixed background parameters $k = 1$, $\mu = 0.03$, and various values of the constants a and b that feature in the general solution (3.55). The branes exhibit the features discussed above and form either closed loops or arcs terminating on the horizon. The latter characteristic is determined by whether a and b satisfy the constraint $|\cos\chi| \simeq |ae^{\tilde{r}_+} + be^{-\tilde{r}_+}| \leq 1$ near the horizon. For the arcs terminating on the horizon the energy density remains positive and increases towards the centre of the brane. However, as in the Schwarzschild case, the pressure becomes singular at the horizon. For branes forming a closed loop entirely to the right-hand side of the horizon a similar behaviour is found to that encountered in the Schwarzschild background: the energy density is maximised at the most distant point on the brane and decreases towards the vicinity of the horizon. A uniformly increasing behaviour for the energy density is found in the case of brane trajectories that enclose the black hole horizon: ρ reaches its maximum positive value at the point located farthest from the black hole, although care must be taken over the choice of a and b to ensure that ρ remains positive throughout the trajectory.

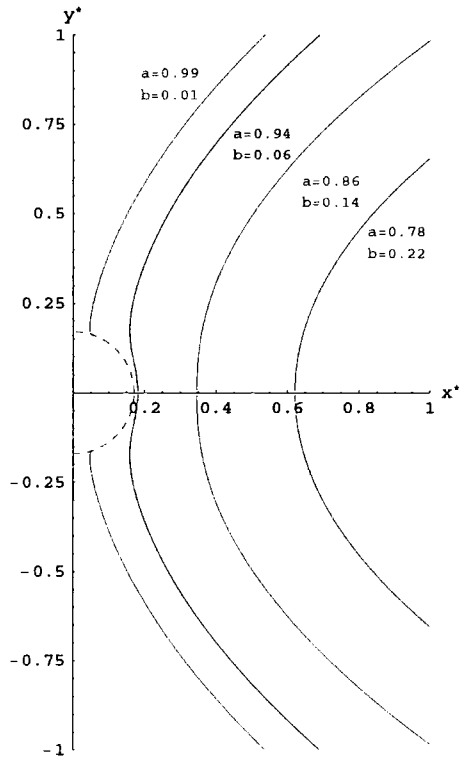

Figure 3.8: A sample of critical brane trajectories with $a+b=1$ in a 5-dimensional Schwarzschild-anti-de Sitter background of fixed parameters $k=1$ and $\mu=0.03$. The dashed line again denotes the black hole horizon.

3.5.2 Critical Branes

Critical branes are defined by the condition $a+b=1$, asymptoting the adS boundary at exactly $\chi=0$. The branes are open, and may or may not touch the black hole horizon depending on the exact values of the parameters a and b. To determine when this occurs the trajectories may be described in terms of a single parameter by writing $a=(1+c)/2$ and $b=(1-c)/2$. Then, if

$$c < |\tanh \tilde{r}_+/2|\,, \tag{3.95}$$

the trajectory remains on the right-hand side of the horizon: after reaching a point of closest proximity, the brane bends to avoid the horizon and eventually escape to infinity. If c saturates or exceeds the above bound, the brane terminates on the horizon. A sample of critical trajectories in a SadS background is shown in figure 3.8.

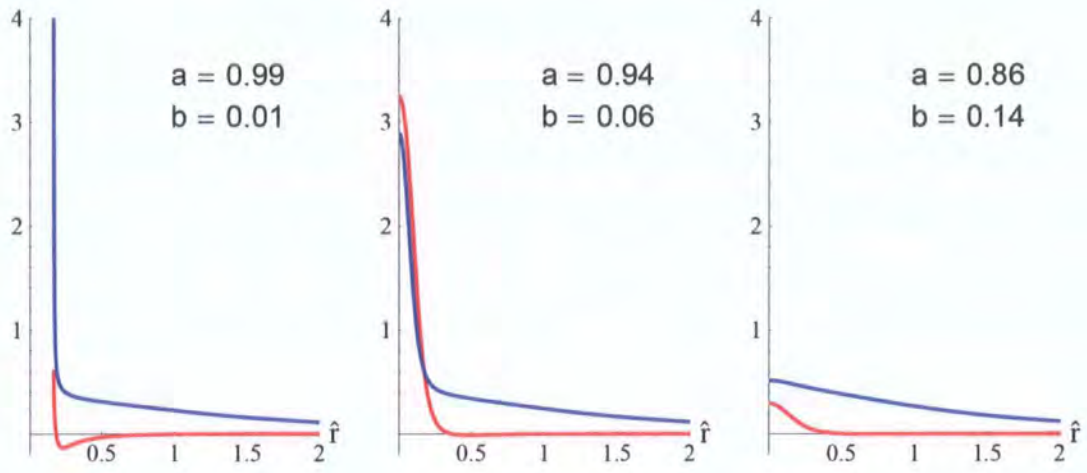

Figure 3.9: The differential energy density (red) and pressure (blue) of brane stars in a Schwarzschild-adS bulk as a function of the brane radial coordinate $\hat{r}$. The black hole mass is fixed at $\mu = 0.03$ and the adS scale $k = 1$. The vertical scale has been normalised in units of ρ_{RS}. The profiles correspond to three of the trajectories presented in figure 3.8.

The behaviour of the energy density and pressure on critical branes is strongly dependent on the proximity of the brane to the black hole. Branes that originate from the horizon and extend to infinity have their energy density positive, providing they intersect the horizon at $\chi_0 < \pi/2$, i.e. $c < |\coth \tilde{r}_+|$. The horizon is then a local energy maximum if $c < |\tanh \tilde{r}_+|$, with the energy initially decreasing, undershooting the Randall-Sundrum value before increasing again towards the asymptotic critical value. If $c > |\tanh \tilde{r}_+|$, then the energy monotonically increases out to infinity. As might be expected, the pressure diverges at the black hole boundary.

According to figure 3.8, as the value of the c parameter decreases, the brane shifts away from the black hole. For branes that avoid the horizon the energy density is again positive with its maximum in the central region. It falls off rapidly, undershooting the background value slightly to form the under-dense region already discussed before tending to the critical value. The pressure also reaches its maximum value at the centre, but is uniformly decreasing with r at a much slower rate, consistent with the pressure excess observed for the pure adS branes. Apart from

this pressure excess, the other main difference with pure Schwarzschild trajectories, is that whether branes satisfy the differential dominant energy condition (DEC) at their centre depends crucially on the choice of c.

The term "differential DEC" refers to the DEC for the differential energy-momentum $\mathcal{T}_{\mu\nu}$, and thus the energy-momentum tensor for an observer on the brane. In pure Schwarzschild, the DEC is satisfied except for branes which skirt extremely close to the horizon, where the local Weyl curvature causes the pressure to diverge. This phenomenon is also observed for the SadS branes passing close to the horizon, however, as c is decreased (or b increased) the central energy dominates the pressure for only a finite range of b before once again dropping below the pressure. This is because further from the horizon the adS curvature becomes more significant and for pure adS branes the effect of this curvature is to induce a pressure excess. Many of these features are illustrated in figure 3.9 where the differential energy density and pressure profiles of three of the trajectories in figure 3.8 are presented. There is clear localisation of both energy density and pressure at the centre of the brane, corresponding to the distribution of a positive mass source, and in the middle figure the DEC is satisfied in the central region.

3.5.3 Subcritical Branes

This family of branes with $a + b < 1$ are similar in many respects to critical branes. They correspond to open trajectories that asymptote the adS boundary, although at nonzero χ. The same bound as before, whether $|\cos\chi| \simeq |ae^{\tilde{r}_+} + be^{-\tilde{r}_+}| \leq 1$, determines if the brane terminates on the event horizon or remains to the right of it. As the subcritical brane trajectories look similar to those presented in figure 3.8, apart from the angle of approach to the adS boundary, it is not necessary to present another graph detailing their appearance. As might be expected, the energy density and pressure profile in this case is also similar to that already studied. Once again, for a large family of parameters a and b, solutions with a positive energy excess at the centre of the brane may be readily found.

One special subcritical trajectory highlighted in the pure adS case was the Karch-

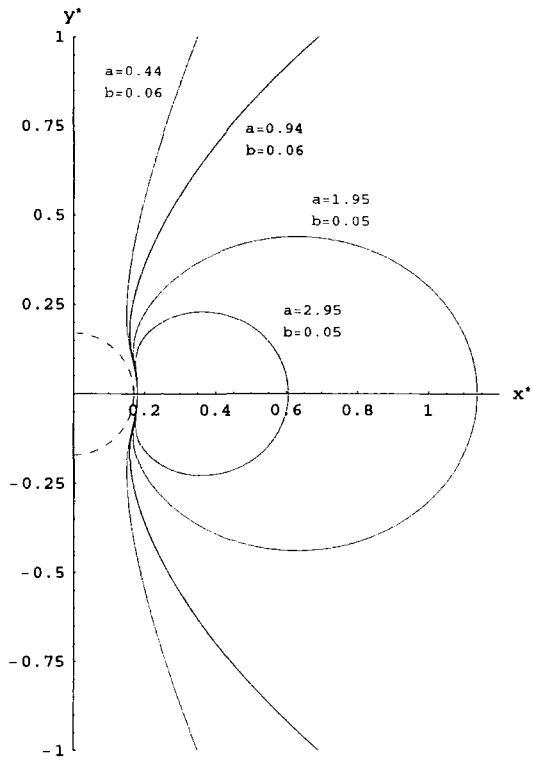

Figure 3.10: A mixture of sub-, super- and critical brane trajectories in a 5-dimensional Schwarzschild-anti-de Sitter background of fixed parameters $k = 1$ and $\mu = 0.03$.

Randall brane, $a + b = 0$. This can be extended to the SadS case obtaining

$$\cos\chi = 2a\sinh\tilde{r}\,. \tag{3.96}$$

However, since $a > 0$ for a positive energy trajectory, this has $(\cos\chi)' > 0$ so the energy density is always increasing with r. Therefore, regardless of whether these trajectories terminate on the horizon, they always correspond to energy deficits on the brane, and hence negative mass sources from the point of view of a brane observer.

Finally, it is important to see if the Schwarzschild trajectory that was non-singular on the horizon, intersecting perpendicularly and extending to the origin, has a Sch-adS generalisation. This corresponded to $ae^{\tilde{r}_+} = be^{-\tilde{r}_+}$ (note that the condition $A = B$ for Schwarzschild was for the $\tilde{r}$ coordinate zeroed at the horizon).

Extending this concept to SadS gives the trajectory

$$\cos\chi = 2ae^{\tilde{r}_+}\cosh(\tilde{r} - \tilde{r}_+)\,. \tag{3.97}$$

These can be super- sub- or precisely critical, depending on the magnitude of a, however, all of these branes have $(\cos\chi)' > 0$, so contain energy deficits on the brane.

The brane trajectories found in this section and depicted in figures 3.7 and 3.8 have obvious similarities with those presented in the previous sections. As expected, trajectories in a bulk containing both a mass and a negative cosmological constant are hybrid constructions, exhibiting a mixture of the features and characteristics that appear with a pure adS or Schwarzschild background. As an example, figure 3.10 presents one possible SadS generalisation of figure 3.2, exhibiting all three possible forms that branes may take in a spacetime that is asymptotically adS. The parameters a and b in this particular case have been chosen so that the branes remain to the right of the horizon, bending away to avoid contact in the central region. Finally, it should be noted that the study of SadS backgrounds with larger mass parameter μ leads to similar families of trajectories. As mentioned earlier, an increase in the value of μ causes the range of the $\tilde{r}$-coordinate to reduce, requiring an increased accuracy in the numerical analysis involved in plotting the corresponding trajectories. Beyond this increase in numerical sensitivity, the study of large mass SadS backgrounds yields the same characteristics for permitted brane trajectories.

3.6 Summary

In this chapter fully consistent gravitational systems involving a brane containing perfect fluid embedded in a variety of five-dimensional spherically symmetric bulk spacetimes have been presented. A time-dependent family of brane trajectories was found with equation of state $p(\tau, r) = -\rho(\tau, r)$, however the background spacetimes in which these could be embedded excluded the possibility of a black hole occurring in the bulk. In the hope of finding a consistent braneworld black hole solution within the RS2 model a time-independent scenario was then investigated. Static branes embedded in pure five-dimensional adS and Schwarzschild bulks were first

analysed separately, before considering the more general Schwarzschild-adS case in full.

The static slicing of a known spherically symmetric bulk was found to be completely integrable, with the solution conveniently written in terms of an implicit function of the bulk radial variable. All possible trajectories for a brane containing a perfect fluid matter source, corresponding to braneworld Tolman-Oppenheimer-Volkoff solutions, have been classified. A number of these solutions have pressure and energy density distributions that permit the interpretation of braneworld stars. However, the part of the bulk spacetime retained under the $\mathbb{Z}_2$ symmetric identification does not, in general, include the singularity or even the black hole horizon. The induced metrics on the brane are non-singular everywhere and therefore cannot correspond to the desired braneworld black hole.

Almost all branes embedded in asymptotically adS space were found to contain excess pressure at large radius. The only possible case that produces a well-behaved asymptotic limit is the subcritical Karch-Randall brane. Unfortunately reconciling a subcritical choice of brane cosmological constant with a positive mass distribution on the brane proved to be impossible. It is interesting to note that the original RS2 model is not plagued by this problem of excess pressure. Its appearance is related to the fact that the brane trajectories analysed here are static in global coordinates. As noted in §3.2, the RS2 brane trajectory is actually a time-dependent slicing of adS in global coordinates. This suggests that removal of the pressure excess may only be achieved through solution of the complete time-dependent system of equations (3.16)-(3.21).

So a static solution with all the features of a braneworld star has also proved elusive. However, it is important to note that in the course of investigation much progress has been made towards finding the exact braneworld star and black hole solutions through the development of an analytical strategy for finding complete solutions to the brane Tolman-Oppenheimer-Volkoff problem, as well as a systematic scheme for classifying such solutions according to their distribution of energy-momentum.

Chapter 4

Hawking Radiation in Large Extra Dimensions

One of the most exciting features of braneworld models is the possible lowering of the fundamental scale of gravity to levels achievable in next generation particle colliders. High-energy scattering experiments involving collisions with trans-Planckian centre-of-mass energy, $\sqrt{s} \gg {}^{(4+n)}M_P$, have potential to produce miniature black holes [78, 79]. Such low-mass black holes will be characterised by a relatively large temperature T_H and extremely short lifetime, decaying rapidly via Hawking radiation into all kinematically permitted elementary particles. In order to correctly identify a collider-produced black hole it is important to determine its characteristic emission spectrum of Hawking radiation.

4.1 Black Hole Creation in High-Energy Collisions

Black hole creation is a fundamentally quantum gravity process. However, in a similar manner to conventional quantum theory, if the produced black hole has a mass that is several times the fundamental Planck mass then, on quantum gravity scales, the black hole may be considered a macroscopic object and a semi-classical approach adopted.

Intuitively, a black hole with mass $M_{BH} = \sqrt{s} \gg {}^{(4+n)}M_P$ and corresponding horizon radius, r_H, will be created in the collision between two highly-energetic particles with centre-of-mass energy $\sqrt{s}$ if the impact parameter of their collision $b \leq r_H$. Owing to the complexity of the collision process, a detailed relativistic study including the effects of gravitational radiation [80–84] and the formation of a closed-trapped surface around the colliding particles [85–93] must be performed to reliably improve these intuitive bounds. Fortunately an analytic expression accurately reproducing the upper bound on the impact parameter for $n \geq 1$ may be derived by assuming a black hole will form if particles approach within [94, 95]

$$b_{\max} = 2\left[\frac{\mu}{1+\left(\frac{n+2}{2}\right)^2}\right]^{\frac{1}{n+1}}, \tag{4.1}$$

where μ is related to the mass of the black hole in a manner that will be outlined in §4.3. A corresponding lower bound on the centre-of-mass energy retained by the black hole seems to suggest it is a decreasing function of the number of extra dimensions present [85, 87]. This result is significant since if only a small fraction of the energy available in particle collision is retained by the black hole then the semi-classical assumption employed in subsequent analysis may not apply to black holes created in the next generation of particle accelerators.

4.2 Black Hole Evolution

Hawking demonstrated that when general relativity and quantum mechanics are combined black holes may evaporate the energy they contain into a spectrum of fundamental particles [96]. This Hawking radiation may be understood through the creation of virtual particle/anti-particle pairs at the horizon. If a positive-energy particle escapes to infinity, while its negative-energy partner falls into the black hole then the net effect is that the black hole loses mass and emits radiation. The infalling particle may have negative energy, as viewed from infinity, since the asymptotically timelike Killing vector becomes spacelike inside the horizon.

The existence of Hawking radiation suggests that the lifetime of an isolated black

hole must be finite. In (4+n)-dimensions the lifetime can be approximated as [97]

$$\tau \sim \frac{1}{^{(4+n)}M_P}\left(\frac{M_{BH}}{^{(4+n)}M_P}\right)^{\frac{n+3}{n+1}}. \tag{4.2}$$

Within extra-dimensional models $^{(4+n)}M_P \sim 1$ TeV so a black hole of minimum mass $M_{BH} \sim 5$ TeV may be safely considered macroscopic [98, 99]. Substituting this bound into equation (4.2) yields extremely small predictions for the lifetime of a microscopic black hole. For example, if $n = 2$, collider black holes evaporate within the vanishingly small period $\tau \sim 1 \times 10^{-26}$ s.

Despite the fleeting nature of its existence, the lifetime of a trans-Planckian black hole may be divided into four phases [98, 99]:

- The balding phase: All quantum numbers possessed by the colliding particles are shed, except for charge, angular momentum and mass. The black hole emits mainly gravitational radiation and the asymmetry present in the violent production process is reduced.

- The spin-down phase: Any remaining angular momentum about an axis perpendicular to the plane in which the particles collided is lost through Hawking radiation. Such angular momentum arises where the original collision occurs with non-zero impact parameter.

- The Schwarzschild phase: Having shed all its angular momentum the black hole is reduced to a static, spherically symmetric state which continues to lose its remaining mass through Hawking radiation.

- The Planck phase: As the mass of the black hole approaches $^{(4+n)}M_P$ quantum gravity effects dominate and the semi-classical approximation breaks down.

Particles emerging from a black hole do so into a spacetime with significant curvature. This curvature presents a gravitational potential energy barrier, impeding propagation to infinity and causing some particles to be reflected back towards the singularity. The spectrum of Hawking radiation witnessed by observers at infinity will therefore depend upon the specific structure of the spacetime outside the black hole at the moment the particle is emitted.

Within the Randall-Sundrum models no analytic braneworld black hole metric exists so it is difficult to perform a realistic calculation of the emission spectrum during any of the four phases of a black hole's lifetime. However, closed-form solutions describing both static and rotating black holes exist in asymptotically flat spacetime of arbitrary dimension [100]. Under certain assumptions these metrics present an ideal starting point for calculation within the ADD model where extra spatial dimensions are compactified but with large radius. If the black hole is of sufficiently low mass that its horizon radius is much smaller than the compactification scale of the extra dimensions, then the black hole will appear to be a higher-dimensional object submerged in an extra-dimensional spacetime of effectively infinite extent.

4.3 The Myers-Perry Black Hole

In 1986 Myers and Perry [100] discovered a solution to Einstein's equations representing a rotating point source in arbitrary-dimensional, asymptotically flat spacetime. In the four-dimensional Kerr solution [101] there is only one possible plane of rotation, but as the dimensionality increases the number of independent planes in which rotation may occur (and hence the number of parameters required to specify the motion of the black hole) increases also. In (4+n)-dimensional spacetime up to $[(n+3)/2]$ angular momentum parameters must be specified. However, black holes that are created in collisions between particles confined to an infinitely thin four-dimensional brane may only have non-zero impact parameter along the brane, and thus acquire only one non-zero angular momentum parameter about an axis in the brane. Consequently the (4+n)-dimensional black hole metric relevant to the study of microscopic black hole evaporation in collider experiments is that with only a single angular momentum parameter

$$ds^2 = -\left(1 - \frac{\mu}{\Sigma r^{n-1}}\right)dt^2 - \frac{2a\mu \sin^2\theta}{\Sigma r^{n-1}}\, dt\, d\varphi + \frac{\Sigma}{\Delta}\, dr^2 + \Sigma\, d\theta^2 + \left(r^2 + a^2 + \frac{a^2 \mu \sin^2\theta}{\Sigma r^{n-1}}\right) \sin^2\theta\, d\varphi^2 + r^2 \cos^2\theta\, d\Omega_n^2\,, \qquad (4.3)$$

where

$$\Delta = r^2 + a^2 - \frac{\mu}{r^{n-1}}\,, \qquad \Sigma = r^2 + a^2 \cos^2\theta\,, \qquad (4.4)$$

and $d\Omega_n^2(\theta_1, \theta_2, \ldots, \theta_{n-1}, \phi)$ is the line-element on a unit n-sphere. The mass, angular momentum and temperature of such a black hole are given by

$$M_{BH} = \frac{(n+2)A_{n+2}}{16\pi^{(4+n)}G_N}\mu\,, \qquad J = \frac{2}{n+2}M_{BH}\,a\,, \qquad T_H = \frac{(n+1)+(n-1)a_*^2}{4\pi(1+a_*^2)r_H}\,, \tag{4.5}$$

where the area of a $(n+2)$-dimensional unit sphere, A_{n+2}, and the horizon radius r_H (defined by $\Delta(r_H) = 0$) are given by

$$A_{n+2} = \frac{2\pi^{(n+3)/2}}{\Gamma[\frac{n+3}{2}]}\,, \qquad r_H = \left[\frac{\mu}{1+a_*^2}\right]^{\frac{1}{n+1}}\,, \tag{4.6}$$

and the definition $a_* = a/r_H$ has been made.

Since the creation of the black hole depends crucially on the value of the impact parameter between the two highly-energetic particles, and that in turn defines the angular momentum of the black hole, an upper bound can be imposed on the angular momentum parameter, a, by demanding that the black hole is created during the collision. As already discussed, the maximum impact parameter value leading to creation of a black hole is given in equation (4.1). If the black hole is assumed to be formed when two massless particles of equal energy $M_{BH}/2$ collide with impact parameter b then in the centre-of-mass frame the angular momentum of the particles before collision is $J = bM_{BH}/2$. Taking this to be equal to the angular momentum of the resultant black hole then, using the definition of the horizon radius r_H and the second of equations (4.5), the maximum value the black hole angular momentum parameter may take is [94]

$$a_*^{\max} = \frac{n+2}{2}\,. \tag{4.7}$$

Without the restriction imposed by equation (4.7) the black-hole angular momentum parameter would be unbounded for $n > 1$, contrary to the cases $n = 0$ and $n = 1$, where a maximum value of a exists so that a real solution for the black-hole horizon is guaranteed.

The Myers-Perry metric, equation (4.3), is a good approximation to the space-time experienced by particles escaping from a microscopic black hole providing two key assumptions are satisfied. The first is that the energy contained in the field of the escaping particle is sufficiently small in comparison to the mass of the black hole that the background metric is unperturbed by the emission. This will be true during

the early stages of evaporation for black holes with mass $\gtrsim 5$ TeV – significantly larger than the rest masses of all known particles. As the decay proceeds the black hole mass will decrease to the point where the energy of an emitted particle is a significant fraction of the mass of the black hole, at which point the back-reaction on the black hole metric must be taken into account. However, when M_{BH} has reduced to ≈ 1 TeV the black hole will pass into the Planck phase where the semi-classical analysis breaks down and a quantum theory of gravity is required for calculation. The second assumption is that the emission process is quasi-stationary so that as each particle is emitted the black hole has time to reach equilibrium at its new temperature before further energy is lost. This assumption does not hold in the balding phase where the black hole rapidly loses the hair inherited from the particle collision. Both assumptions are only valid in the spin down and Schwarzschild phases, so attention will be focused on these parts of the black hole lifetime in the subsequent analysis.

4.4 The Role of the Brane

Up to now the role of the brane has been neglected in the discussion of higher-dimensional black hole evaporation. In order for equation (4.3) to represent the spacetime into which Hawking radiation emerges it is essential that the tension of the brane is much smaller than the black hole mass so that the Myers-Perry background is unperturbed. The dominant effect of the brane is in restricting the region of spactime into which particles may be emitted.

One of the major features of braneworld models is that Standard Model particles are confined to the brane while gravity and possibly scalar fields may propagate in the bulk. This must also be true of particles emitted via Hawking radiation. While all known scalar, fermion, gauge boson and graviton degrees of freedom may, in principle, be detected in the emission spectra on the brane, there will also be a missing energy signal comprising graviton and scalar modes that have escaped our directly visible universe, being emitted into the bulk.

In order to account for all the energy of a black hole lost in Hawking radiation it

is therefore necessary to consider the equations of motion of particles propagating both on the brane and in the bulk separately. To achieve this, bulk calculations are made using the full metric (4.3) whereas brane calculations are performed projecting the metric onto the four-dimensional submanifold found by restricting all additional angular coordinates $\{\theta_i = \pi/2, \phi = 0\}$. The induced metric is then identical to (4.3), but with the term proportional to $d\Omega_n^2$ omitted.

4.5 Calculation of the Hawking Radiation Spectrum

The energy radiated by a black hole into a particular degree of freedom may be calculated by considering the asymptotic form of the vacuum expectation value of the energy-momentum tensor for that particle species in the background created by the black hole. Since the concepts of "vacuum" and "particle" are observer-dependent in quantum field theories on curved spacetimes, it is important to define the components of such a calculation with great care [102].

There are many standard vacua defined in the literature in curved backgrounds, the most common of which are:

- The Hartle-Hawking vacuum – defined to be a vacuum state that respects all spacetime symmetries and is regular everywhere, in particular on the past and future event horizons $\mathcal{H}^{\pm}$.
- The Boulware vacuum – is free from particle flux at both past and future null infinity $\mathcal{I}^{\pm}$. An observer with such a vacuum state would see no particles entering the black hole or escaping to infinity.
- The Unruh vacuum – exhibits no incoming radiation from past null infinity $\mathcal{I}^{-}$, but modes emanating from the white hole region of the analytically continued spacetime $\mathcal{H}^{-}$ are thermally populated.

Applying these concepts to the specific case of the four-dimensional Kerr background (with metric given by the $n = 0$ case of equation (4.3)) it is possible to show that, in

the sense defined above, no "true" Hartle-Hawking or Boulware vacuum states exist [103, 104]. However, the vacuum relevant for calculation of the Hawking radiation spectrum is the Unruh vacuum, for which no complications arise in construction.

To illustrate the procedure, consider the case of a massless scalar field in the background of a rotating four-dimensional black hole. The field satisfies the corresponding curved-spacetime Klein-Gordon equation

$$\nabla_\mu \nabla^\mu \Phi = \frac{1}{\sqrt{-g}} \partial_\mu (\sqrt{-g} g^{\mu\nu} \partial_\nu \Phi) = 0 \,. \tag{4.8}$$

This equation can be shown to be separable [105], employing basis functions of the form

$$u_{\omega\ell m}(x) \sim \frac{1}{\sqrt{r^2 + a^2}} e^{-i\omega t + im\varphi} S_{\omega\ell m}(\cos\theta) R_{\omega\ell m}(r) \,, \tag{4.9}$$

where $S_{\omega\ell m}(\cos\theta)$ are the four-dimensional spheroidal harmonics. The radial component $R_{\omega\ell m}(r)$ satisfies a Schrodinger-like ordinary differential equation

$$\left(\frac{d^2}{dr_*^2} - V_{\omega\ell m} \right) R_{\omega\ell m} = 0 \,, \tag{4.10}$$

when written in terms of the 'tortoise' coordinate, defined by $dr_*/dr = (r^2 + a^2)/\Delta$. In the asymptotic regions close to the horizon ($r_* \to -\infty$) and out at infinity ($r_* \to \infty$) the potential takes the constant values

$$V_{\omega\ell m} \sim \begin{cases} -k^2 & \text{as } r_* \to -\infty \\ -\omega^2 & \text{as } r_* \to \infty \,. \end{cases} \qquad \text{where } k = \omega - m\Omega = \omega - \tfrac{ma}{r_H^2 + a^2}$$

In order to ensure that a ground state with the desired properties of an Unruh vacuum is obtained it is convenient to work in a basis of solutions to the scalar field equation that is tailored to the Cauchy surface $\mathcal{I}^- \cup \mathcal{H}^-$, upon which boundary conditions are to be applied. Modes that would have emanated from the white hole region $\mathcal{H}^-$ are commonly referred to as "up" modes, while those corresponding to unit particle flux from $\mathcal{I}^-$ are known as "in" modes. Given the asymptotic forms of the potential, a basis of solutions to the radial equation (4.10) that is tailored to the surfaces $\mathcal{H}^-$ and $\mathcal{I}^-$ take the asymptotic forms

$$\begin{aligned} R^{up}_{\omega\ell m}(r) &\sim \begin{cases} e^{ikr_*} + A^{up} e^{-ikr_*} & r_* \to -\infty \\ B^{up} e^{i\omega r_*} & r_* \to \infty \end{cases} \\ R^{in}_{\omega\ell m}(r) &\sim \begin{cases} B^{in} e^{-ikr_*} & r_* \to -\infty \\ e^{-i\omega r_*} + A^{in} e^{i\omega r_*} & r_* \to \infty \,. \end{cases} \end{aligned} \tag{4.11}$$

Continuing the Schrodinger equation analogy, it is possible to think of the coefficient A^{up} as a reflection coefficient for a particle propagating away from the black hole and B^{up} to be the corresponding transmission coefficient. Similar interpretations may be employed for the coefficients A^{in} and B^{in} when applied to a particle propagating towards the horizon. Wronskian relations between the "up" and "in" solutions impose a number of restrictions that allow the "up" parameters, relevant in describing a particle propagating away from the horizon, to be recast in terms of "in" parameters that refer to the inverse problem of a particle incident on the black hole. In particular

$$1 - |A^{in}|^2 = \frac{k}{\omega}|B^{in}|^2 \tag{4.12}$$

$$1 - |A^{up}|^2 = \frac{\omega}{k}|B^{up}|^2 \tag{4.13}$$

$$\omega (B^{up})^* A^{in} = -kB^{in} (A^{up})^* \tag{4.14}$$

$$\omega B^{up} = kB^{in}. \tag{4.15}$$

The above relations (4.12) and (4.13) demonstrate an interesting feature of radiation from a rotating black hole. For $\omega > 0$, $k < 0$ both $|A^{in}|^2$ and $|A^{up}|^2$ exceed unity, indicating that the amplitude of the reflected wave is greater than that of the incident one. This amplification of the reflected wave is a phenomenon known as superradiance [106].

Using the "up" and "in" radial solutions of equation (4.11) in (4.9) to construct a basis of solutions to the field equation, it is then straightforward (although care must be taken for modes with $k < 0$ [104]) to quantise the scalar field and define the past Unruh vacuum, $|U^-\rangle$, as the state which is annihilated by all operators creating a particle incident from $\mathcal{I}^-$ and which contains a thermal population of particles from $\mathcal{H}^-$. Using this vacuum state it is then possible to calculate the (past Unruh-) vacuum expectation value of the renormalised scalar field energy-momentum tensor at future null infinity. Integrating the $\{rt\}$-component of this vacuum expectation value over a two sphere at spatial infinity yields

$$\langle U^-|T^{rt}|U^-\rangle_{ren} = \sum_{\ell,m} \int_{\omega=0}^{\infty} \frac{\omega}{\exp(k/T_H) - 1} \frac{\omega |B^{up}|^2}{k} \frac{d\omega}{2\pi}, \tag{4.16}$$

which represents a flux of energy away from the black hole, corresponding to Hawking

radiation. This expression can be simplified slightly by changing perspective to that of a particle incident on the black hole. Using equations (4.15) and (4.12)

$$\frac{\omega}{k}|B^{up}|^2 = 1 - |A^{in}|^2 \equiv |\mathcal{A}_{0\ell m}|^2 , \tag{4.17}$$

where $|\mathcal{A}_{0\ell m}|^2$ is the absorption probability for a scalar particle incident on the Kerr black hole. The absorption probability for a particle with spin s is formally defined as the ratio of the incoming particle flux at the horizon, $\mathcal{F}^{(H)}_{s,in}$, to that at infinity, $\mathcal{F}^{(\infty)}_{s,in}$

$$|\mathcal{A}_{s\ell m}|^2 = \frac{\mathcal{F}^{(H)}_{s,in}}{\mathcal{F}^{(\infty)}_{s,in}} . \tag{4.18}$$

The preceding analysis has also been performed for emission of fermions [107] and gauge bosons [108] from the Kerr black hole and yields very similar expressions. More specific comment on the derivation of the absorption probability for particles with non-zero spin is left for the next chapter where particle emission on the brane is considered in detail. Overall, the power spectrum due to emission of an individual degree of freedom with spin s from a four-dimensional rotating black hole may be written as [109]

$$\frac{d^2E^{(s)}}{dtd\omega} = \frac{1}{2\pi}\sum_{\ell,m}\frac{\omega|\mathcal{A}_{s\ell m}|^2}{\exp(k/T_H) \pm 1} , \tag{4.19}$$

where the nature of the $\pm$ factor in the denominator is determined by the spin of the emitted particle: "+" for fermions and "−" for bosons.

The discussion leading to equation (4.19) focused exclusively on particle emission in the four-dimensional Kerr background, however, extending the argument to the projected Myers-Perry background of the induced on-brane metric is straightforward. The only deviation arises in the form of the radial equation that must be solved to extract the absorption coefficient $|\mathcal{A}_{s\ell m}|^2$. This calculation is the subject of the next chapter.

In addition to Hawking radiation on the brane, it would be interesting to know the fraction of energy lost to the bulk. To find the spectrum of radiation into the bulk spacetime it is necessary to perform a higher-dimensional field theoretical calculation analogous to that outlined above. This is yet to be accomplished for an arbitrary number of spatial dimensions, although the specific case of a five-dimensional spacetime has been addressed [110]. The result of that study is an

identical expression to equation (4.19), except that summation occurs over the mode structure relevant to the spheroidal harmonics in four spatial dimensions. Given this result, it will be assumed here that the bulk Hawking radiation spectrum in a $(4 + n)$-dimensional spacetime may be calculated according to equation (4.19) but with summation over the mode structure relevant to the $(3 + n)$-dimensional spheroidal harmonics. The emission of bulk scalar fields is studied in chapter 6.

Before proceeding with direct analytic calculation it is worth pausing to consider the characteristic features that might be expected of the Hawking radiation spectra.

4.6 Features of the Spectrum

In four dimensions the contribution from a single degree of freedom to the energy emission spectrum of a perfect blackbody at temperature T takes the form

$$\frac{d^2E^{(BB)}}{dtd\omega} = \frac{1}{2\pi^2}\frac{\omega^3}{\exp(\omega/T) \pm 1}. \tag{4.20}$$

It is apparent from comparing equations (4.20) and (4.19) that, while there is a clear resemblance, the spectrum of radiation from a black hole differs from that of a true blackbody in a number of ways. In particular, the presence of k rather than simply ω in the exponential is closely tied to the phenomenon of superradiance that occurs for modes co-rotating with the black hole. As previously mentioned, this is defined as the reflection probability of a wave incident on the gravitational barrier exceeding unity, or equivalently the absorption probability being negative. Superradiance occurs when $k = \omega - ma/(r_H^2 + a^2) < 0$, so should be visible in plots of the absorption probability both on the brane and in the bulk, but only for modes with $m > 0$ and over a finite range of ω.

The absorption probability is dependent on properties both of the particle being emitted, such as its spin, energy of emission and the partial wave under consideration, and also of the surrounding spacetime, including the number of extra dimensions and rotation rate of the black hole. The latter two dependencies are of particular interest if the evaporation of black holes is to be observed at future colliders. The ω-dependence of $|\mathcal{A}_{s\ell m}|^2$ contributes further to the deviation between

spectra of black holes and black bodies. Despite these differences there are two particular limits in which the forms of the spectra more closely coincide.

4.6.1 The Low-Energy Limit

The gravitational potential barrier typically increases with increasing value of the principal angular momentum quantum number ℓ. Consequently, at very low energy, the absorption probability for the lowest modes tend to dominate over all others by several orders of magnitude. For scalar particles, since the $\ell = 0$ mode requires $m = 0$, the on-brane low-energy spectrum may be written as

$$\frac{d^2E^{(0)}}{dtd\omega} \approx \frac{1}{2\pi}\frac{\omega\,|\mathcal{A}_{000}|^2}{\exp(\omega/T_H)-1} = \sigma_0^{(0)}(\omega)\,\frac{d^2E^{(BB)}}{dtd\omega}\,, \tag{4.21}$$

where

$$\sigma_0^{(0)}(\omega) = \frac{\pi}{\omega^2}|\mathcal{A}_{000}|^2 \tag{4.22}$$

encodes the residual deviation of the black hole spectrum from that of a standard four-dimensional blackbody with temperature T_H, and is consequently termed the "graybody factor". It represents the outgoing transmission cross-section of the lowest partial wave in the gravitational background. The definition may be extended to general modes

$$\sigma_{\ell m}^{(s)}(\omega) = \frac{\pi}{\omega^2}|\mathcal{A}_{s\ell m}|^2\,, \tag{4.23}$$

and partial cross-sections may be calculated by summing over desired vales of m and ℓ. For example, the low-energy cross-section for particles with non-zero spin is determined by summing over the values of m corresponding to the lowest principle quantum number for that species ℓ_0

$$\sigma_{\ell_0}^{(s)}(\omega) = \frac{\pi}{\omega^2}\sum_m |\mathcal{A}_{s\ell_0 m}|^2\,. \tag{4.24}$$

Studies of on-brane radiation during the Schwarzschild phase have discovered that the value of the graybody factor in the low-energy limit tends to different values depending on the spin of the particle emitted [111]. In particular, it has been found that for scalar particles it always reduces to the brane-projected area of the horizon, $4\pi r_H^2$. For emission in the bulk, a corresponding higher-dimensional low-energy

cross-section may be defined as [112]

$$\sigma^{(s)}_{\ell_0,n}(\omega) = \frac{2^{n+1}\pi^{\frac{n+1}{2}}}{\omega^{n+2}}\Gamma\left(\frac{n+3}{2}\right)\sum_m |\mathcal{A}_{s\ell_0 m,n}|^2 \,. \tag{4.25}$$

In the Schwarzschild phase this quantity was found to reduce to the full area of the higher-dimensional black hole in the limit of emission of extreme low-energy scalar particles. It would be interesting to see if these results also hold in the spin-down phase.

4.6.2 The High-Energy Limit

At very high energy $k \simeq \omega$ for all modes and the Hawking radiation spectrum on the brane can be written

$$\frac{d^2E^{(s)}}{dtd\omega} \approx \frac{1}{2\pi}\sum_{\ell,m}\frac{\omega|\mathcal{A}_{s\ell m}|^2}{\exp(\omega/T_H)\pm 1} = \sigma^{(s)}_{tot}(\omega)\frac{d^2E^{(BB)}}{dtd\omega}\,, \tag{4.26}$$

where

$$\sigma^{(s)}_{tot}(\omega) = \sum_{\ell,m}\sigma^{(s)}_{\ell m} = \frac{\pi}{\omega^2}\sum_{\ell,m}|\mathcal{A}_{s\ell m}|^2\,, \tag{4.27}$$

is the total cross-section, found by summing over individual cross-sections for each mode. Particles emitted with extremely high energy should experience negligible effect from the gravitational potential barrier. In this limit the total cross-section should tend towards a high-energy asymptotic value, known as the geometrical optics limit, which is the same for all particle species.

Owing to the relations between infalling and outgoing particle parameters in the field theory calculation of the radiation spectrum, the geometrical optics limit may be calculated from purely classical arguments as the cross-sectional area corresponding to the minimum impact parameter that permits an incoming relativistic particle to escape to infinity. This calculation is conducted for brane-confined particles in the analysis of the next chapter.

As in the low-energy limit, a corresponding higher-dimensional analog of the total cross-section may be defined as

$$\sigma^{(s)}_{tot,n}(\omega) = \frac{2^{n+1}\pi^{\frac{n+1}{2}}}{\omega^{n+2}}\Gamma\left(\frac{n+3}{2}\right)\sum_{\{J\}}|\mathcal{A}_{s\{J\},n}|^2\,, \tag{4.28}$$

where $\{J\}$ represents the set of quantum numbers indexing all possible higher-dimensional spheroidal harmonic states. This should also tend to a geometrical optics limit, although it will differ from the on-brane value owing to the larger number of directions from which a particle may approach the black hole in a higher-dimensional space.

Having defined the absorption probabilities, energy emission rate and asymptotic cross-sections for Hawking radiation both on the brane and in the bulk, it is now possible to analyse the spin-down phase of a collider-manufactured black hole in terms of these physical quantities.

Chapter 5

Brane Emission in the Spin-Down Phase

While the Schwarzschild phase of the lifetime of a microscopic black hole has been studied extensively using both analytic [113, 114] and numerical techniques [111], owing to the increased complexity of the gravitational background, the spin-down phase has been the subject of less attention. As was mentioned in chapter 4, collider-manufactured black holes are highly likely to have finite angular momentum immediately after creation as a result of the non-zero impact parameter between colliding parent particles. Consequently, the emission of Hawking radiation during this period of rotation is an important component of the total energy lost by the black hole that may either be available for detection on the brane or must be accounted for if lost to the bulk.

This chapter considers the spectrum of Hawking radiation from degrees of freedom emitted by the black hole onto the brane. A number of recent studies have addressed this topic mainly through numerical analysis [115–121] or by focusing on a spacetime of specific dimensionality [94, 122]. In the following sections a well-known matching technique is employed to solve the field equations in the projected background and derive analytic expressions for the on-brane Hawking radiation spectra from a black hole with angular momentum [2, 3].

5.1 The Field Equations

As mentioned in the previous chapter, the gravitational background on the brane from a collider-produced black hole in a $(4+n)$-dimensional bulk is given by the projected Myers-Perry solution

$$ds^2 = -\left(1 - \frac{\mu}{\Sigma r^{n-1}}\right)dt^2 - \frac{2a\mu \sin^2\theta}{\Sigma r^{n-1}}\, dt\, d\varphi + \frac{\Sigma}{\Delta}\, dr^2 + \Sigma\, d\theta^2 + \left(r^2 + a^2 + \frac{a^2 \mu \sin^2\theta}{\Sigma r^{n-1}}\right) \sin^2\theta\, d\varphi^2 \,, \tag{5.1}$$

where

$$\Delta = r^2 + a^2 - \frac{\mu}{r^{n-1}} \,, \qquad \Sigma = r^2 + a^2 \cos^2\theta \,, \tag{5.2}$$

The mass, angular momentum and temperature of the black hole were given in equation (4.5).

Although the above background is very similar to the standard four-dimensional Kerr spacetime, it contains an explicit dependence on the number of additional spacelike dimensions n. The potentially observable deviations of the Hawking radiation spectra from that predicted in ordinary 4-d general relativity may be traced back to this dependence.

To study the propagation of fields in the above background it is necessary to derive their equations of motion. For simplicity it is assumed that particles couple only minimally to the gravitational background and have no other interactions so that they satisfy the corresponding free equations.

The exact forms of these equations of motion for particles with spin s can be found by employing the Newman-Penrose formalism [123, 124] which permits the study of multi-component fields propagating in a curved background. In the case of particles propagating in the brane-induced background of a rotating higher-dimensional black hole (5.1) this task has already been performed [37, 94], so is not repeated here. To outline the result: if the factorised ansatz for the field

$$\Psi_s(t, r, \theta, \varphi) = e^{-i\omega t}\, e^{im\varphi}\, R_s(r)\, S^m_{s,\ell}(\theta) \,, \tag{5.3}$$

is assumed, where $S^m_{s,\ell}(\theta)$ are the spin-weighted spheroidal harmonics [125–130], then the free equations of motion for particles with spin $s = 0$, $\frac{1}{2}$ and 1 may be combined

to form the following "master" equation [119], satisfied by the radial part of all radiative components of the field,

$$\Delta^{-s}\frac{d}{dr}\left(\Delta^{s+1}\frac{dR_s}{dr}\right)+\left[\frac{K^2-isK\Delta'}{\Delta}+4is\omega r+s\left(\Delta''-2\right)\delta_{s,|s|}-\Lambda_{s\ell}\right]R_s=0\,, \tag{5.4}$$

where

$$K=(r^2+a^2)\,\omega-am\,,\qquad \Lambda_{s\ell}=\lambda_{s\ell}+a^2\omega^2-2am\omega\,. \tag{5.5}$$

In the above, $\lambda_{s\ell}$ is the angular eigenvalue appearing in the equation satisfied by the spheroidal harmonics

$$\frac{1}{\sin\theta}\frac{d}{d\theta}\left(\sin\theta\frac{dS^m_{s,\ell}}{d\theta}\right)+ \left(a^2\omega^2\cos^2\theta-2a\omega s\cos\theta-\frac{(m+s\cos\theta)^2}{\sin^2\theta}+\lambda_{s\ell}+s\right)S^m_{s,\ell}=0\,. \tag{5.6}$$

From equation (5.4), it is clear that the radial parts of the radiative components with $s=|s|$ and $s=-|s|$ satisfy different equations, owing to the presence of the $\delta_{s,|s|}$ term. This can be overcome by redefining

$$R_{+|s|}\equiv\Delta^{-|s|}\,P_{+|s|}\,,\qquad R_{-|s|}\equiv P_{-|s|}\,. \tag{5.7}$$

In terms of these new functions, the radial master equation on the brane takes the simplified form

$$\Delta^{|s|}\frac{d}{dr}\left(\Delta^{1-|s|}\frac{dP_s}{dr}\right)+\left(\frac{K^2-isK\Delta'}{\Delta}+4is\omega r-\tilde{\Lambda}_{s\ell}\right)P_s(r)=0\,, \tag{5.8}$$

where the Δ''-term has been removed, and $\tilde{\Lambda}_{s\ell}=\Lambda_{|s|\ell}+2|s|$. It is not possible to express the angular eigenvalue $\lambda_{|s|\ell}$ in closed form, however it can be written as a power series in $a\omega$ [125, 127, 131, 132] as

$$\lambda_{|s|\ell}=-|s|(|s|+1)+\sum_k f_k\,(a\omega)^k\,. \tag{5.9}$$

For the purpose of calculation in this chapter, terms to fourth order have been retained and the corresponding coefficients may be written [132]

$$f_0=\ell(\ell+1)\,, \tag{5.10}$$

$$f_1 = -\frac{2ms^2}{\ell(\ell+1)}\,, \tag{5.11}$$

$$f_2 = h(\ell+1) - h(\ell) - 1\,, \tag{5.12}$$

$$f_3 = \frac{2h(\ell)ms^2}{\ell^2(\ell-1)(\ell+1)} - \frac{2h(\ell+1)ms^2}{\ell(\ell+1)^2(\ell+2)}\,, \tag{5.13}$$

$$f_4 = \left(\frac{4h(\ell+1)m^2}{\ell^2(\ell+1)^4(\ell+2)^2} - \frac{4h(\ell)m^2}{\ell^4(\ell-1)^2(\ell+1)^2}\right)s^4 - \frac{(\ell+2)h(\ell+1)h(\ell+2)}{2(\ell+1)(2\ell+3)} + \frac{h^2(\ell+1)}{2(\ell+1)} + \frac{h(\ell)h(\ell+1)}{2\ell(\ell+1)} - \frac{h^2(\ell)}{2\ell} + \frac{(\ell-1)h(\ell-1)h(\ell)}{2\ell(2\ell-1)}\,. \tag{5.14}$$

where

$$h(\ell) = \frac{(\ell^2 - \frac{1}{4}(\alpha+\beta)^2)(\ell^2 - s^2)(\ell^2 - \frac{1}{4}(\alpha-\beta)^2)}{2\ell^3(\ell-\frac{1}{2})(\ell+\frac{1}{2})}\,, \tag{5.15}$$

$$\frac{1}{2}(\alpha+\beta) = \max(|m|,|s|) \qquad \frac{1}{2}(\alpha-\beta) = \frac{ms}{\max(|m|,|s|)}\,. \tag{5.16}$$

The absorption probability $|\mathcal{A}_{s\ell m}|^2$ for propagation of fields in the on-brane background around a rotating black hole may be calculated by solving equation (5.8) and then computing the ratio of the total inward flux at the horizon to that at infinity, equation (4.18). Once $|\mathcal{A}_{s\ell m}|^2$ has been determined it is possible to calculate the Hawking radiation spectrum, equation (4.19), and the cross-sections (4.24) and (4.27).

5.2 Analytic Solution of the Field Equations

Even in the case of a standard four-dimensional rotating black hole there is no known exact analytic solution to the radial master equation that is valid throughout the entire radial regime. To proceed it is necessary to adopt a well-known approximate method whereby the radial equation is first solved in two asymptotic regimes: close to the black hole horizon ($r \simeq r_H$), and very far away from it ($r \gg r_H$). These two solutions are then stretched and matched at an intermediate zone to create a smooth analytical solution extending over all r. In the following analysis a unified formalism is developed encompassing all brane-localised particles by treating their spin s as an arbitrary parameter.

5.2.1 The Near-Horizon Solution

Focusing first on the near-horizon regime, if the change of variable

$$r \to f(r) = \frac{\Delta(r)}{r^2 + a^2} \;\Rightarrow\; \frac{df}{dr} = (1-f)\, r\, \frac{A(r)}{r^2 + a^2}\,, \tag{5.17}$$

is employed, where the function $A(r)$ is defined by $A(r) \equiv (n+1) + (n-1)\, a^2/r^2$, then equation (5.8) takes the near-horizon ($r \simeq r_H$) form

$$f\,(1-f)\,\frac{d^2 P_s}{df^2} + (1 - |s| - B_*\, f)\,\frac{dP_s}{df} + \left[\frac{K_*^2 - isK_*\Delta'_*}{A_*^2\, f(1-f)} + \frac{(4is\omega_* - \tilde{\Lambda}_{s\ell})(1+a_*^2)}{A_*^2\,(1-f)}\right] P_s(r) = 0\,, \tag{5.18}$$

where the following definitions have been made

$$\begin{aligned} \omega_* &= \omega r_H\,, & a_* &= a/r_H\,, \\ A_* &= (n+1) + (n-1)\, a_*^2\,, & K_* &= (1+a_*^2)\,\omega_* - a_* m\,, \\ B_* &\equiv 1 - |s| + \frac{2|s| + n\,(1+a_*^2)}{A_*} - \frac{4a_*^2}{A_*^2}\,, & \Delta'_* &= \left.\frac{\partial \Delta}{\partial r}\right|_{r_H} = A_*\,. \end{aligned} \tag{5.19}$$

By making the field redefinition $P_s(f) = f^{\alpha}(1-f)^{\beta} F(f)$, equation (5.18) takes the form of a hypergeometric equation [133]

$$f\,(1-f)\,\frac{d^2 F}{df^2} + \left[c - (1+a+b)\, f\right]\frac{dF}{df} - ab\, F = 0\,, \tag{5.20}$$

with

$$a = \alpha + \beta + B_* - 1\,, \qquad b = \alpha + \beta\,, \qquad c = 1 - |s| + 2\alpha\,. \tag{5.21}$$

The power coefficients α and β can be determined by solving the second-order algebraic equations

$$\alpha^2 - |s|\,\alpha + \frac{K_*^2}{A_*^2} - \frac{isK_*}{A_*} = 0\,, \tag{5.22}$$

and

$$\beta^2 + \beta\,(B_* + |s| - 2) + \frac{K_*^2}{A_*^2} - \frac{isK_*}{A_*} + \frac{(4is\omega_* - \tilde{\Lambda}_{s\ell})\,(1+a_*^2)}{A_*^2} = 0\,, \tag{5.23}$$

that follow from demanding that the coefficient of $F(f)$ is indeed $-ab$. These restrictions have solutions

$$\alpha_{\pm} = \frac{|s|}{2} \pm \left(\frac{iK_*}{A_*} + \frac{s}{2}\right)\,, \tag{5.24}$$

and

$$\beta_{\pm} = \frac{1}{2}\Bigg[(2-|s|-B_*) \pm \sqrt{(B_*+|s|-2)^2 - \frac{4K_*^2 - 4isK_*A_*}{A_*^2} - \frac{4(4is\omega_* - \tilde{\Lambda}_{s\ell})\,(1+a_*^2)}{A_*^2}}\Bigg]. \tag{5.25}$$

The general solution of the master equation near the horizon is then given by

$$P_{NH}(f) = A_- f^{\alpha}\,(1-f)^{\beta}\,F(a,b,c;f) + A_+ f^{-\alpha}\,(1-f)^{\beta}\,F(a-c+1,b-c+1,2-c;f)\,. \tag{5.26}$$

where $A_{\pm}$ are arbitrary constants. Since the choice has been made to express the absorption probability purely in terms of the "in" modes, according to equation (4.17), it is appropriate to impose the boundary condition that no outgoing modes may exist near the black hole horizon. To ensure this, the near-horizon solution (5.26) can be expanded in the limit $r \to r_H$ (equivalently $f(r) \to 0$). The result depends on which value of α is selected from equation (5.24). The choice $\alpha = \alpha_+$ yields

$$P_{NH}(f) \simeq A_-\, f^{\frac{|s|+s}{2}}\, f^{i\frac{K_*}{A_*}} + A_+\, f^{-\frac{|s|+s}{2}}\, f^{-i\frac{K_*}{A_*}}\,, \tag{5.27}$$

while $\alpha = \alpha_-$ gives

$$P_{NH}(f) \simeq A_- f^{\frac{|s|-s}{2}}\, f^{-i\frac{K_*}{A_*}} + A_+ f^{-\frac{|s|-s}{2}}\, f^{i\frac{K_*}{A_*}}\,. \tag{5.28}$$

Introducing the tortoise-like coordinate

$$y = r_H(1+a_*^2)\frac{\ln(f)}{A_*}\,, \tag{5.29}$$

the factors $f^{\pm i\frac{K_*}{A_*}}$ reduce to $e^{\pm iky}$, with

$$k \equiv \omega - m\Omega = \omega - \frac{ma}{r_H^2 + a^2} \tag{5.30}$$

describing an outgoing and incoming free wave, respectively. It should be noted that, although the coordinate y is not identical to the canonical tortoise coordinate, defined by $dr_*/dr = (r^2+a^2)/\Delta(r)$, it is true that

$$\frac{dy}{dr} = \left(\frac{A}{A_*}\right)\frac{(r_H^2+a^2)^2}{(r^2+a^2)^2}\left(\frac{r_H}{r}\right)^{n-2}\frac{dr_*}{dr}\,, \tag{5.31}$$

so in the limit $r \to r_H$ the two coordinates converge and the near-horizon asymptotic solution assumes, as found previously [116, 117], the free-wave form in terms of the standard tortoise coordinate. In order that the field is neither singular nor identically zero at the horizon, the correct boundary condition in the vicinity of r_H for a field with spin s is [134]

$$R_s \sim \Delta^{-s} e^{-ikr_\star} . \tag{5.32}$$

In the present context this translates to

$$P_{+|s|} \sim e^{-iky} = f^{-i\frac{K_\star}{A_\star}} , \qquad P_{-|s|} \sim f^{|s|} e^{-iky} = f^{|s|} f^{-i\frac{K_\star}{A_\star}} . \tag{5.33}$$

So the boundary condition of no outgoing waves near the horizon requires the selection $\alpha = \alpha_-$ and $A_+ = 0$. There is one further criterion that must be applied. In order that the hypergeometric function $F(a, b, c; f)$ may converge it is necessary that $Re(c - a - b) > 0$. Imposing this leads to the choice $\beta = \beta_-$, bringing the near-horizon solution to the final form

$$P_{NH}(f) = A_- f^\alpha (1 - f)^\beta F(a, b, c; f) . \tag{5.34}$$

For the purpose of matching the near-horizon and far-field solutions at an intermediate region it is necessary to stretch the near-horizon solution to values of the radial coordinate that are much larger than the horizon radius. This may be achieved by first changing the argument of the hypergeometric function from f to $1 - f$ using the identity [133]

$$F(a, b, c; f) = \frac{\Gamma(c)\,\Gamma(c - a - b)}{\Gamma(c - a)\,\Gamma(c - b)} F(a, b, a + b - c + 1; 1 - f) + \tag{5.35}$$

$$(1 - f)^{c-a-b} \frac{\Gamma(c)\,\Gamma(a + b - c)}{\Gamma(a)\,\Gamma(b)} F(c - a, c - b, c - a - b + 1; 1 - f) .$$

The function $f(r)$ may be alternatively written as

$$f(r) = 1 - \frac{\mu}{r^{n-1}} \frac{1}{r^2 + a^2} = 1 - \left(\frac{r_H}{r}\right)^{n-1} \frac{(1 + a_*^2)}{(r/r_H)^2 + a_*^2} , \tag{5.36}$$

where the defining equation of the horizon, $\Delta(r_H) = 0$, has been used to eliminate μ. In the limit $r \gg r_H$, and for $n \geq 0$, the above expression tends to unity.

Using the above result, the argument of the "stretched" hypergeometric function goes to zero in the limit of large r and the corresponding "stretched" near-horizon solution takes the form

$$P_{NH}(f) \simeq A_-\,(1-f)^{\beta}\,\frac{\Gamma(c)\,\Gamma(c-a-b)}{\Gamma(c-a)\,\Gamma(c-b)} + A_-\,(1-f)^{-\beta+2-B_*-|s|}\,\frac{\Gamma(c)\,\Gamma(a+b-c)}{\Gamma(a)\,\Gamma(b)}\,. \tag{5.37}$$

For $r \gg r_H$, the quantity $(1-f)$ can be accurately approximated by

$$1-f \simeq (1+a_*^2)\,\left(\frac{r_H}{r}\right)^{n+1}\,, \tag{5.38}$$

bringing the stretched near-horizon solution to the final power-law form

$$P_{NH}(r) \simeq A_1\,r^{-(n+1)\beta} + A_2\,r^{(n+1)(\beta+|s|+B_*-2)}\,, \tag{5.39}$$

with

$$A_1 = A_-\left[(1+a_*^2)\,r_H^{n+1}\right]^{\beta}\frac{\Gamma(c)\Gamma(c-a-b)}{\Gamma(c-a)\Gamma(c-b)}\,, \tag{5.40}$$

$$A_2 = A_-\left[(1+a_*^2)\,r_H^{n+1}\right]^{-(\beta+|s|+B_*-2)}\frac{\Gamma(c)\Gamma(a+b-c)}{\Gamma(a)\Gamma(b)}\,. \tag{5.41}$$

Before addressing the form of the far-field solution it is worth noting that all near-horizon results in this section smoothly reduce to those known to be valid in the Schwarzschild phase by taking the limit $a \to 0$ [113,114].

5.2.2 The Far-Field Solution

In the far-field limit $r \gg r_H$ the radial master equation (5.8) may be expanded as

$$\frac{d^2P_s}{dr^2} + \frac{2(1-|s|)}{r}\frac{dP_s}{dr} + \left(\omega^2 + \frac{2is\omega}{r} - \frac{\lambda_{|s|\ell}+2|s|+a^2\omega^2}{r^2}\right)P_s = 0\,, \tag{5.42}$$

where in each term only the dominant component in the expansion in powers of $1/r$ has been retained. By making the redefinition $P_s = e^{-i\omega r}r^{\frac{1}{2}(2|s|-1+Z)}\tilde{P}_s$, where

$$Z = \sqrt{(2|s|-1)^2 + 4(\lambda_{|s|\ell}+2|s|+a^2\omega^2)}\,, \tag{5.43}$$

the far-field master equation (5.42) is transformed to a confluent hypergeometric equation

$$z\frac{d^2\tilde{P}_s}{dz^2} + (b-z)\frac{d\tilde{P}_s}{dz} - a\tilde{P}_s = 0\,, \tag{5.44}$$

which has as its independent solutions the Kummer functions $M(a,b,z)$ and $U(a,b,z)$ [133]. Overall, the solution to the master equation in the far-field limit may be written as

$$P_{FF}(r) = e^{-i\omega r} r^{\frac{1}{2}(2|s|-1+Z)} \times \left[B_1 M\left(\frac{1}{2} - s + \frac{Z}{2}, 1+Z, 2i\omega r\right) + B_2 U\left(\frac{1}{2} - s + \frac{Z}{2}, 1+Z, 2i\omega r\right)\right] . \tag{5.45}$$

As in the near-horizon case, the above solution may also be extrapolated beyond its region of validity, on this occasion towards small values of the radial coordinate. This is achieved by taking the limit $r \longrightarrow 0$ in (5.45), yielding [133]

$$P_{FF}(r) \simeq B_1 r^{\frac{1}{2}(2|s|-1+Z)} + B_2 r^{\frac{1}{2}(2|s|-1-Z)} \frac{\Gamma(Z)}{\Gamma(\frac{1}{2} - s + \frac{Z}{2})} (2i\omega)^{-Z} . \tag{5.46}$$

It is apparent that the far-field solution also adopts a power-law form upon extrapolation. This feature may be used to construct a complete radial solution by matching the two expressions (5.39) and (5.46) at an intermediate value of r. On first inspection there is no obvious way to achieve this matching, however, if the limits $\omega r_H = \omega_* \ll 1$ and $a/r_H = a_* \ll 1$ are taken, in which case

$$B_* \simeq 2 - |s| + \frac{2|s|-1}{n+1} , \tag{5.47}$$

$$\beta \simeq \frac{1}{2(n+1)} \left(1 - 2|s| - \sqrt{(2|s|-1)^2 + 4\tilde{\Lambda}_{s\ell}}\right) , \tag{5.48}$$

then the stretched near-horizon solution (5.39) takes the form

$$P_{NH}(r) = A_1 r^{\frac{1}{2}\left(2|s|-1+\sqrt{(2|s|-1)^2+4\tilde{\Lambda}_{s\ell}}\right)} + A_2 r^{\frac{1}{2}\left(2|s|-1-\sqrt{(2|s|-1)^2+4\tilde{\Lambda}_{s\ell}}\right)} . \tag{5.49}$$

From the definitions (5.5) and (5.43) for $\Lambda_{s\ell}$ and Z respectively, the low-$a\omega$ limits

$$\tilde{\Lambda}_{s\ell} \approx \lambda_{s\ell} + 2|s| \tag{5.50}$$

$$Z \approx \sqrt{(2|s|-1)^2 + 4(\lambda_{s\ell} + 2|s|)} \tag{5.51}$$

may be found. Providing this limit is adhered to, the powers of r in the two stretched solutions (5.46) and (5.49) match exactly. It should be emphasised that in order to achieve a higher level of accuracy in the analysis, no expansion is performed in the arguments of the gamma functions and terms to order $(a\omega)^4$ are retained in the expansion of the eigenvalues. A smooth solution valid over the entire radial regime

is then obtained if the relevant coefficients corresponding to matching powers of r between the two solutions are identified. This requires

$$B \equiv \frac{B_1}{B_2} = \frac{\Gamma(Z)}{\Gamma(\frac{1}{2} - s + \frac{Z}{2})} (2i\omega)^{-Z} \frac{A_1}{A_2}, \tag{5.52}$$

where A_1/A_2 follows from equations (5.40) and (5.41)

$$\frac{A_1}{A_2} = \frac{\Gamma(c-a-b)\Gamma(a)\Gamma(b)}{\Gamma(c-a)\Gamma(c-b)\Gamma(a+b-c)} \left[(1+a_*^2)\, r_H^{n+1}\right]^{2\beta+|s|+B_*-2}. \tag{5.53}$$

Having found a solution to the radial master equation that is exactly valid in the near-horizon and far-field limits and smoothly connects the two regions, it is now possible to calculate the absorption probabilities of low-energy particles ($\omega_* \ll 1$) with general spin s incident on a slowly rotating ($a_* \ll 1$) black hole.

5.3 Calculation of the Absorption Probability

The absorption probability $|\mathcal{A}_{s\ell m}|^2$ is defined, as in equation (4.18), as the ratio of the incoming particle flux at the horizon to that at infinity

$$|\mathcal{A}_{s\ell m}|^2 = \frac{\mathcal{F}^{(H)}_{s,in}}{\mathcal{F}^{(\infty)}_{s,in}}. \tag{5.54}$$

Where it is possible to write the $r \to \infty$ limit of the solution to the field equation as a sum of incoming and outgoing spherical waves of the form

$$R_s(r) \simeq A^{(in)}_{s\ell m} \frac{e^{-i\omega r}}{r^\nu} + A^{(out)}_{s\ell m} \frac{e^{i\omega r}}{r^\nu}, \tag{5.55}$$

for some constant ν, then a reflection coefficient $\mathcal{R}_{s\ell m} = A^{(out)}_{s\ell m}/A^{(in)}_{s\ell m}$ may be defined, in terms of which the absorption probability can be written

$$|\mathcal{A}_{s\ell m}|^2 = 1 - |\mathcal{R}_{s\ell m}|^2 = 1 - \left| \frac{A^{(out)}_{s\ell m}}{A^{(in)}_{s\ell m}} \right|^2. \tag{5.56}$$

To see if this is possible for the solution to the field equation derived in the previous section it is necessary to expand the far-field solution (5.45) to the extreme far-field limit by taking the $z \to \infty$ limit of the Kummer functions $M(a,b,z)$ and

$U(a,b,z)$ [133]. Performing this expansion yields

$$P_{FF}(r) \simeq \frac{B_2}{(2i\omega)^{\frac{1}{2}-s+\frac{Z}{2}}}\left(\frac{B_1\, e^{i\pi\left(\frac{1}{2}-s+\frac{Z}{2}\right)}\Gamma(1+Z)}{\Gamma\left(\frac{1}{2}+s+\frac{Z}{2}\right)}+1\right)\frac{e^{-i\omega r}}{r^{1-s-|s|}}+ \\ \frac{B_2}{(2i\omega)^{\frac{1}{2}+s+\frac{Z}{2}}}\frac{B\,\Gamma(1+Z)}{\Gamma\left(\frac{1}{2}-s+\frac{Z}{2}\right)}\frac{e^{i\omega r}}{r^{1+s-|s|}} \tag{5.57}$$

$$\equiv Y_s^{(in)}\frac{e^{-i\omega r}}{r^{1-s-|s|}}+Y_s^{(out)}\frac{e^{i\omega r}}{r^{1+s-|s|}}\,, \tag{5.58}$$

where the second equality defines the coefficients $Y_s^{(in)}$ and $Y_s^{(out)}$. It is clear from the above that, while the solution may be expanded asymptotically as incoming and outgoing waves, the radial dependence of the two modes does not match for general s, so the absorption probabilities for different particle species must be calculated separately.

5.3.1 Scalars

For scalar particles with $s = 0$ the extreme far-field expansion reduces to

$$P_{FF}(r) \simeq Y_0^{(in)}\frac{e^{-i\omega r}}{r}+Y_0^{(out)}\frac{e^{i\omega r}}{r}\,. \tag{5.59}$$

In this case the powers of r in the inward and outwardly propagating waves do indeed match and the absorption probability may be found using equation (5.56)

$$|\mathcal{A}_{0\ell m}|^2 = 1-\left|\frac{Y_0^{(out)}}{Y_0^{(in)}}\right|^2\,. \tag{5.60}$$

5.3.2 Fermions

For $s = \pm 1/2$ the components of the asymptotic solution do not match, being

$$P^{FF}_{+\frac{1}{2}}(r) \simeq Y^{(in)}_{+\frac{1}{2}}e^{-i\omega r}+Y^{(out)}_{+\frac{1}{2}}\frac{e^{i\omega r}}{r}\,, \qquad P^{FF}_{-\frac{1}{2}}(r) \simeq Y^{(in)}_{-\frac{1}{2}}\frac{e^{-i\omega r}}{r}+Y^{(out)}_{-\frac{1}{2}}e^{i\omega r}\,. \tag{5.61}$$

The flux of fermions emitted by the black hole follows formally by integrating the radial component of the conserved current over solid angle. However, as in the 4-dimensional case [107, 124, 135–137], it is possible to show using the radial master equation that the relation

$$\frac{d}{dr}\left(|P_{\frac{1}{2}}|^2-|P_{-\frac{1}{2}}|^2\right)=0 \tag{5.62}$$

holds and hence the quantity $\mathcal{F}_{\frac{1}{2}} \propto |P_{\frac{1}{2}}|^2 - |P_{-\frac{1}{2}}|^2$ is conserved for arbitrary values of r. Since particle number is conserved, the sum of the flux in at the horizon and out at infinity must equal the total flux in at infinity, consequently

$$|\mathcal{A}_{\frac{1}{2}\ell m}|^2 = \frac{\mathcal{F}^{(H)}_{\frac{1}{2},in}}{\mathcal{F}^{(\infty)}_{\frac{1}{2},in}} = 1 - \frac{\mathcal{F}^{(\infty)}_{\frac{1}{2},out}}{\mathcal{F}^{(\infty)}_{\frac{1}{2},in}} . \tag{5.63}$$

Substituting for the form of the flux, $\mathcal{F}_{\frac{1}{2}}$, and accounting for the difference in sign between fluxes in opposite directions, the absorption probability may be written as

$$\begin{aligned} |\mathcal{A}_{\frac{1}{2}\ell m}|^2 &= 1 - \frac{\left|P^{(\infty)}_{\frac{1}{2},out}\right|^2 - \left|P^{(\infty)}_{-\frac{1}{2},out}\right|^2}{\left|P^{(\infty)}_{-\frac{1}{2},in}\right|^2 - \left|P^{(\infty)}_{\frac{1}{2},in}\right|^2} \\ &= 1 - \left|\frac{Y^{(out)}_{-\frac{1}{2}}}{Y^{(in)}_{+\frac{1}{2}}}\right|^2 , \end{aligned} \tag{5.64}$$

where the explicit far-field form of the radial solution (5.61) has been used in the second equality. Then from the definition of $Y^{(out)}_s$ in equation (5.58) it is apparent that the $s = \pm 1/2$ components are related by

$$Y^{(out)}_{-\frac{1}{2}} = \frac{2i\omega}{\sqrt{\lambda_{\frac{1}{2}\ell} + 1 + a^2\omega^2}} Y^{(out)}_{+\frac{1}{2}} , \tag{5.65}$$

and using this equation the absorption probability may be written entirely in terms of the $s = +1/2$ component as

$$|\mathcal{A}_{\frac{1}{2}\ell m}|^2 = 1 - \frac{4\omega^2}{\lambda_{\frac{1}{2}\ell} + 1 + a^2\omega^2} \left|\frac{Y^{(out)}_{\frac{1}{2}}}{Y^{(in)}_{\frac{1}{2}}}\right|^2 . \tag{5.66}$$

5.3.3 Gauge Bosons

Again, the $s = \pm 1$ components have non-matching powers of r in their asymptotic expansions so it is not possible to use equation (5.56) to calculate the absorption probability. There is also no conserved particle current permitting an analogous calculation to that of the fermion case. To proceed a technique may be followed in which the radial master equation is transformed, through a radial function redefinition and use of the tortoise coordinate r_*, to an alternative form with real,

short-range potential [138]. Then, the asymptotic solution at infinity for the gauge field is given in terms of the new radial function by the expression [108, 138]

$$X_{\ell m\omega} \sim e^{-i\omega r_*} + A^{(in)}_{\ell m\omega}\, e^{i\omega r_*}\,, \tag{5.67}$$

representing a sum of outgoing and incoming plane waves with constant amplitudes. From this the absorption probability may easily follow according to equation (5.56)

$$|\mathcal{A}_{1\ell m}|^2 = 1 - |A^{(in)}_{\ell m\omega}|^2\,. \tag{5.68}$$

A full analysis [108, 138] relates the amplitude $A^{(in)}_{\ell m\omega}$ in equation (5.67) to the coefficients $Y_s^{(in,out)}$ appearing in equation (5.58), leading to the result

$$|A_{1\ell m}|^2 = 1 - \frac{16\omega^4}{B^2_{\ell m\omega}} \left| \frac{Y_1^{(out)}}{Y_1^{(in)}} \right|^2\,, \tag{5.69}$$

where the constant $B_{\ell m\omega}$ is defined as the coefficient appearing in the differential equation [124]

$$\Delta\, D_0^\dagger D_0^\dagger P_{+1} = B_{\ell m\omega}\, P_{-1}\,, \qquad \left(D_0^\dagger = \partial_r + iK/\Delta\right) \tag{5.70}$$

or, equivalently, as the constant of proportionality relating

$$Y_{-1}^{(out)} = -\frac{4\omega^2}{B_{\ell m\omega}}\, Y_1^{(out)} \tag{5.71}$$

when the asymptotic solution (5.58) is substituted in equation (5.70). By using the explicit expressions of $Y_{\pm 1}^{(out)}$ from equation (5.58) the $s = \pm 1$ components of $Y_s^{(out)}$ are related by

$$Y_{-1}^{(out)} = -\frac{4\omega^2}{\lambda_{1\ell} + 2 + a^2\omega^2} Y_{+1}^{(out)}\,, \tag{5.72}$$

which leads to $B_{\ell m\omega} = \lambda_{1\ell} + 2 + a^2\omega^2$, and gives the final expression for the absorption probability for brane-localised fields with spin 1

$$|A_{1\ell m}|^2 = 1 - \frac{16\omega^4}{(\lambda_{1\ell} + 2 + a^2\omega^2)^2} \left| \frac{Y_1^{(out)}}{Y_1^{(in)}} \right|^2\,. \tag{5.73}$$

Curiously enough, although no conserved particle current exists, an identical result to that given above is recovered by assuming such a current does in fact exist. By examining the energy flux through the horizon, the radial photon number flux may

be shown to be proportional to $\mathcal{F}_1 = |P_1|^2 - |P_{-1}|^2$ [139]. If this quantity is assumed to be conserved then, following the argument for fermions

$$|\mathcal{A}_{1\ell m}|^2 = 1 - \left| \frac{Y_{-1}^{(out)}}{Y_{+1}^{(in)}} \right|^2 . \tag{5.74}$$

Substituting for $Y_{-1}^{(out)}$ using equation (5.72) in the above expression then recovers the result (5.73).

To summarise, the absorption probabilities for particles with spin $s = 0, \frac{1}{2}, 1$ given in equations (5.60), (5.66) and (5.73) respectively, may be written in terms of the single expression

$$|\mathcal{A}_{s\ell m}|^2 = 1 - \left(\frac{4\omega^2}{\lambda_{s\ell} + 2s + a^2\omega^2} \right)^{2s} \left| \frac{Y_s^{(out)}}{Y_s^{(in)}} \right|^2 . \tag{5.75}$$

5.4 Plotting the Absorption Probability

Since it is the absorption probability that largely characterises the Hawking radiation spectra, it is worth examining in detail its dependence on the spacetime properties, n and a, and also those of the emitted particle, ω and (s, ℓ, m).

5.4.1 Dependence on Particle Properties

Figures 5.1–5.3 illustrate the absorption probabilities of the modes corresponding to the three lowest principal angular momentum quantum numbers ℓ for scalars, fermions and brane gauge bosons, respectively. In this case the black hole has rotation parameter $a_* = 0.4$ and exists in a spacetime with $n = 6$ extra dimensions. It is clear that for each species of particle $|\mathcal{A}_{s\ell m}|^2$ is suppressed with increasing ℓ and also suppressed with increasing m for fixed ℓ. It is also apparent that a general trend exists whereby the absorption probability for the lowest mode decreases with increasing s. This trend persists for the second lowest mode and beyond although it becomes somewhat obscured at higher ℓ, owing to the increasing number of modes and differing mode structures of different particle species.

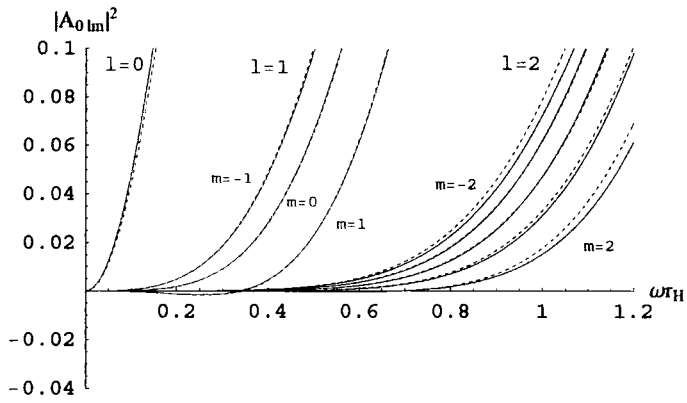

Figure 5.1: Absorption probability $|\mathcal{A}_{0\ell m}|^2$ for brane scalar particles, for $n = 6$, $a_* = 0.4$ and the modes $\ell = 0$ (red), 1 (green) and 2 (blue). The solid lines represent the analytic solution, while the dashed lines follow from numerical calculation.

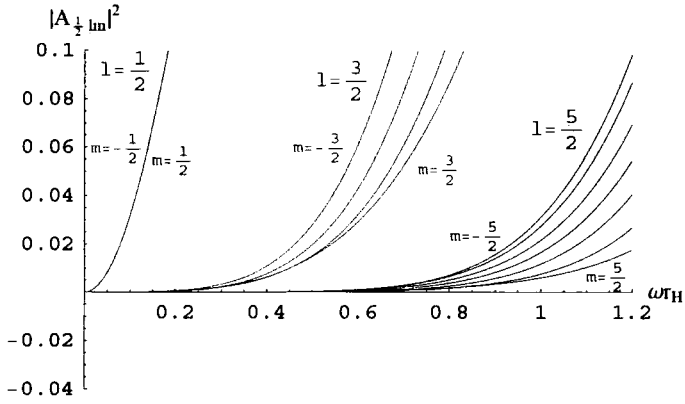

Figure 5.2: Absorption probability $|\mathcal{A}_{\frac{1}{2}\ell m}|^2$ for brane fermions, for $n = 6$, $a_* = 0.4$ and the modes $\ell = \frac{1}{2}$ (red), $\frac{3}{2}$ (green) and $\frac{5}{2}$ (blue).

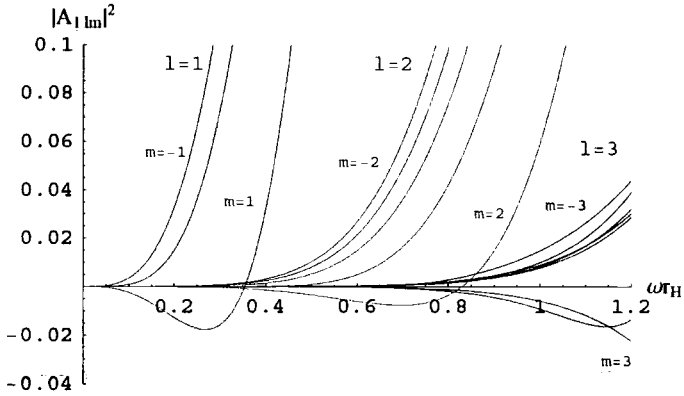

Figure 5.3: Absorption probability $|\mathcal{A}_{1\ell m}|^2$ for brane gauge bosons, for $n = 6$, $a_* = 0.4$ and the modes $\ell = 1$ (red), 2 (green) and 3 (blue).

In general, absorption probabilities increase as the energy of the emitted particle ω increases. This is to be expected as higher-energy particles will feel less effect from the gravitational potential barrier impeding their propagation to infinity. However, modes with positive values of m have absorption coefficients which initially decrease, becoming negative over a finite range of ω, before increasing again. This is the phenomenon of superradiance that was described previously and is exhibited in figure 5.1 and more clearly in 5.3. In figure 5.1 two sets of lines are depicted: the solid lines are the analytical results derived in the previous section, while the dotted lines follow from a numerical study that was performed to reproduce the results appearing in [116, 117][1]. To ensure the highest possible level of accuracy in the numerical solution this study included the exact numerical eigenvalues of the spheroidal harmonics. There is excellent agreement between the two sets of values, particularly in the low-ω_* limit. Significant deviation is only exhibited for the $\ell = 2$ modes at energies $\omega_* \approx 0.9$.

5.4.2 Dependence on Spacetime Properties

Since the lowest-order modes are dominant at low energy for all particle species, it is the behaviour of these modes that will be used to describe the dependence of the absorption probability on the spacetime parameters a_* and n.

Figures 5.4–5.6 illustrate the effect on $|\mathcal{A}_{s\ell m}|^2$ of increasing a_* for the lowest modes with $s = 0$, $1/2$ and 1 respectively. It is apparent that, in almost all cases, the low-energy absorption probability is enhanced with increasing angular momentum of the black hole. The only circumstance in which this does not hold is for superradiant modes where $|\mathcal{A}_{s\ell m}|^2$ becomes increasingly negative as a_* increases. While this behaviour is only illustrated in the left-hand plot of figure 5.6 for gauge bosons, it is also found to be true of superradiant scalar modes.

For fermions and gauge bosons the low-energy, low-angular momentum analytic expression may be extended to higher values of ω_* and a_* and still used to draw

[1]Thanks are extended to Chris Harris for providing the basis of the code and numerical values of the eigenvalues used in this study.

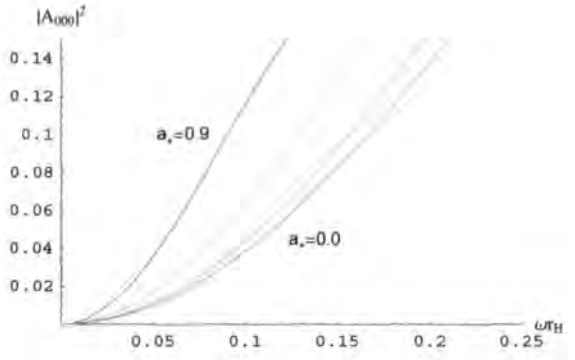

Figure 5.4: Absorption probability $|\mathcal{A}_{000}|^2$ for brane scalar particles, for $n = 6$ and $a_* = 0$ (red), 0.3 (green), 0.6 (light blue) and 0.9 (dark blue).

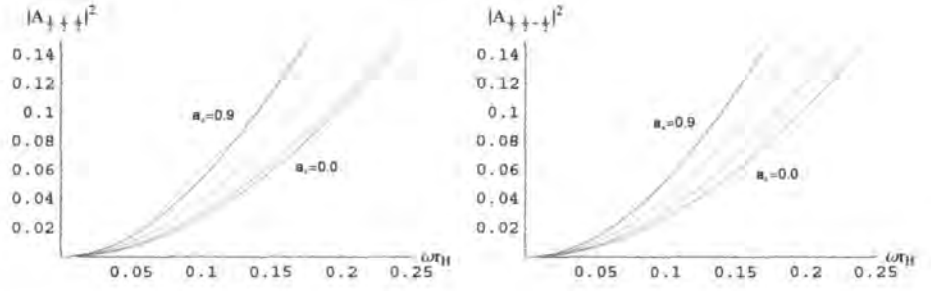

Figure 5.5: Absorption probability $|\mathcal{A}_{\frac{1}{2}\frac{1}{2}m}|^2$ for brane fermions with $m = +1/2$ (left) and -1/2 (right) and the same parameter values as figure 5.4.

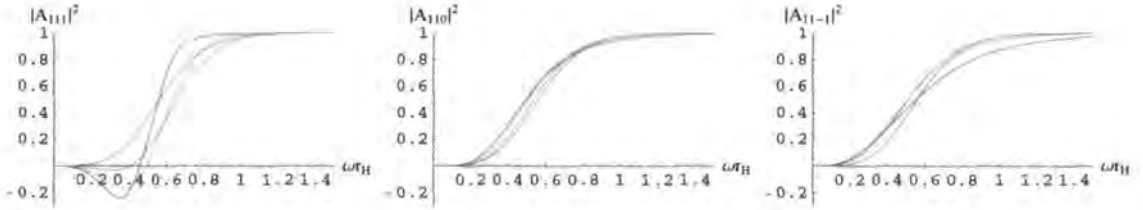

Figure 5.6: Absorption probability $|\mathcal{A}_{11m}|^2$ for brane gauge bosons with $n = 6$, $m = +1$ (left), 0 (centre) and -1 (right) and $a_* = 0$ (red), 0.5 (green), 1 (light blue) and 1.5 (dark blue), extended to higher energy.

reliable conclusions about the behaviour of the absorption probability. Figure 5.6 has been extended to larger ω_* and considers values of a_* up to 1.5 to illustrate this. Examination of the behaviour of the lowest gauge boson modes reveals that, for modes with $m \leq 0$, what is initially an enhancement with a_* at low-energy becomes a suppression as ω_* increases beyond the strict range of validity of the analytic expressions. Similarly, while increasing a_* enhances the superradiant effect of modes with $m > 0$ at low energy, at higher energy increased rotation of the black hole increases the absorption probability. Comparison of these features with the corresponding numerical results [115] reveals a good quantitative agreement in the low-energy and low-angular momentum regime. Outside this limit the qualitative agreement is favourable for $m = \pm 1$, although the analytic expression tends to underestimate the magnitude of the superradiance for larger values of a_*. For $m = 0$ the numerical results predict monotonic increase of the absorption probability with a_* over the full range of ω, while this holds true for the analytic expression only for $\omega < 0.6$. The corresponding expression for fermions may also be extended to high energy, revealing similar behaviour. Modes with $m > 0$ have absorption probabilities that are monotonically increasing throughout the range of energy $0 < \omega_* < 1.5$, while modes with $m < 0$ are enhanced with a_* at low energy, but suppressed with a_* in the high-energy limit. Comparison with existing numerical results [119] reveals that again, the analytical results are quantitatively accurate in the low-ω and low-a_* limit and qualitatively correct for both $m = \pm 1/2$. The high-energy extension of the scalar case is less reliable since, outside the low-ω_* limit, the gamma functions featuring in equation (5.53) exhibit singular behaviour for some parameter values, rendering the absorption probabilities unphysical.

Figures 5.7–5.9 depict the dependence of $|\mathcal{A}_{s\ell m}|^2$ on the number of extra dimensions n for all three particle species. In general, the low-energy absorption probabilities are enhanced with increasing number of extra dimensions. However, there are several exceptions to this, in particular the gauge boson modes with $m < 0$, for which the situation is reversed. Additionally, the behaviour of superradiant modes differs depending on the value of s. The low-energy absorption probability increases with n for superradiant gauge bosons, but becomes more negative for superradiant

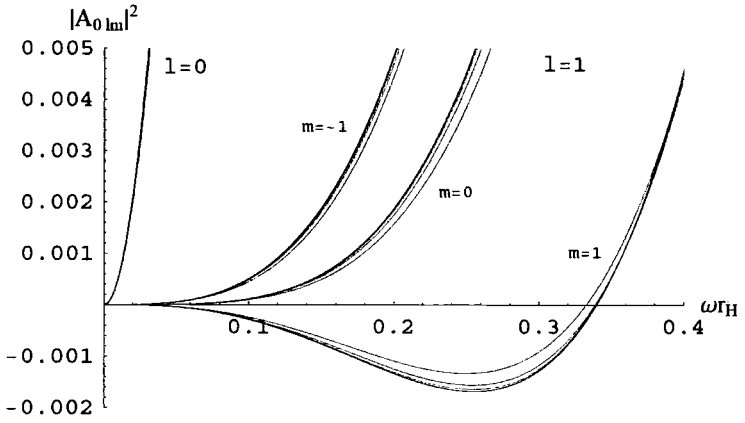

Figure 5.7: Absorption probability $|\mathcal{A}_{0\ell m}|^2$ for brane scalar particles, for $\ell = 0, 1$, $a_* = 0.4$ and $n = 3$ (red), 5 (green), 7 (light blue) and 9 (dark blue).

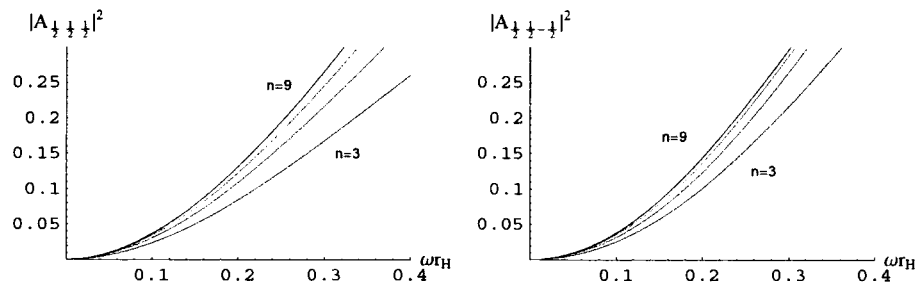

Figure 5.8: Absorption probability $|\mathcal{A}_{\frac{1}{2}\frac{1}{2}m}|^2$ for brane fermions with $m = +1/2$ (left) and -1/2 (right), $a_* = 0.4$ and $n = 3$ (red), 5 (green), 7 (light blue) and 9 (dark blue).

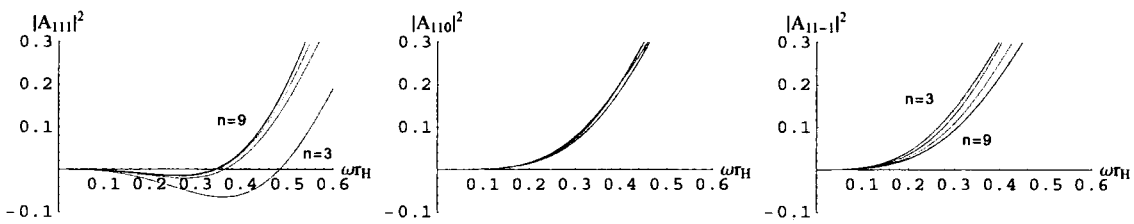

Figure 5.9: Absorption probability $|\mathcal{A}_{11m}|^2$ for brane gauge bosons with $m = +1$ (left), 0 (centre) and -1 (right) and $a_* = 0.4$, $n = 3$ (red), 5 (green), 7 (light blue) and 9 (dark blue).

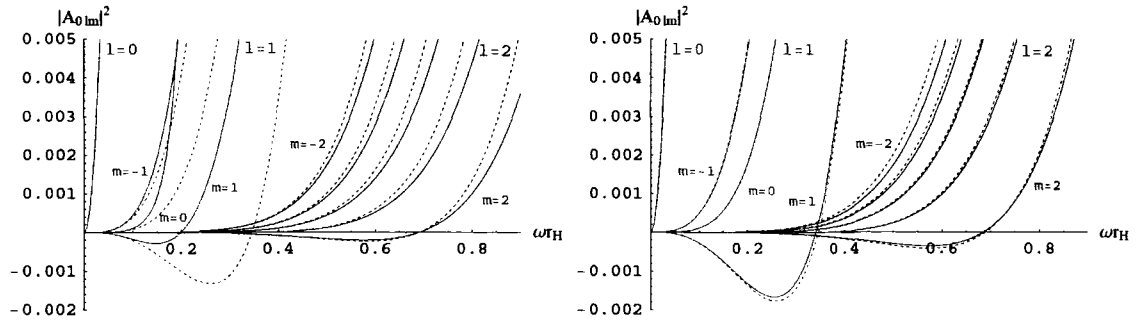

Figure 5.10: Absorption probability $|\mathcal{A}_{0\ell m}|^2$ of brane scalar particles, for $\ell = 0$ (red), 1 (green), 2 (blue), $a_* = 0.4$ and $n = 2$ (left) and $n = 6$ (right). The solid lines correspond to the analytic solution, while the dashed lines are the result of an exact numerical analysis.

scalars.

Finally, it should be noted that the accuracies of a number of approximations made in the course of the analysis are n-dependent. In particular, as n increases the assumed behavior of $f(r)$ at infinity in equation (5.38) improves and terms that were neglected during the matching of the asymptotic solutions, such as K_*/A_*, become even more suppressed. Figure 5.10 compares the accuracy of the $n = 2$ absorption probabilities for the lowest scalar modes with the corresponding case for $n = 6$. In both plots the analytic and numerical solutions are depicted. It is clear that increasing n improves the accuracy of the analytic solution over a wider range of energy.

5.5 An Improved Scalar Analysis

In general, there is significant disagreement between the analytic scalar absorption probability and the numerical results, even at low energy, for modes with $\ell = 1$ and low n. The error arises from the attempt to maintain a unified formalism for emission of particles with differing spin. In the case of scalar fields it is possible to improve upon the result derived in the previous section by returning to the far-field

radial equation (5.42), which takes the form

$$\frac{d^2P_0}{dr^2} + \frac{2}{r}\frac{dP_0}{dr} + \left(\omega^2 - \frac{\lambda_{0\ell} + a^2\omega^2}{r^2}\right) P_0(r) = 0\,. \tag{5.76}$$

In the analysis of §5.2 this was solved by transformation to a confluent hypergeometric equation and had as its solution equation (5.45), written in terms of the Kummer functions. It is also possible to transform equation (5.76) into a Bessel equation for $\tilde{P}_0(r)$ by making the substitution $P_0(r) = \frac{1}{\sqrt{r}}\tilde{P}_0(r)$. Its solution then takes the form

$$P_{FF}(r) = \frac{B_1^{sca}}{\sqrt{r}} J_\nu(\omega r) + \frac{B_2^{sca}}{\sqrt{r}} Y_\nu(\omega r)\,, \tag{5.77}$$

where J_ν and Y_ν are the Bessel functions of the first and second kind, respectively, with $\nu = \sqrt{\lambda_{0\ell} + a^2\omega^2 + 1/4}$, and $B_{1,2}^{sca}$ integration constants. Repeating the analysis of §5.2 for this new far-field solution, it is necessary to stretch the Bessel functions to the near-horizon regime. Using the standard identities for Bessel functions as the argument $z \to 0$ [133],

$$J_\nu(z) \approx \frac{1}{\Gamma(\nu+1)}\left(\frac{z}{2}\right)^\nu, \tag{5.78}$$

$$Y_\nu(z) \approx -\frac{1}{\pi}\Gamma(\nu)\left(\frac{z}{2}\right)^{-\nu}, \tag{5.79}$$

the stretched far-field solution becomes

$$P_{FF}(r) \simeq \frac{B_1^{sca}\left(\frac{\omega r}{2}\right)^{\sqrt{\lambda_{0\ell}+a^2\omega^2+1/4}}}{\sqrt{r}\,\Gamma\left(\sqrt{\lambda_{0\ell}+a^2\omega^2+1/4}+1\right)} - \frac{B_2^{sca}}{\pi\sqrt{r}}\Gamma\left(\sqrt{\lambda_{0\ell}+a^2\omega^2+1/4}\right)\left(\frac{\omega r}{2}\right)^{-\sqrt{\lambda_{0\ell}+a^2\omega^2+1/4}}. \tag{5.80}$$

Again, the stretched far-field solution takes a power-law form which may be matched to the stretched near-horizon expression (5.49) providing the low-energy and low-angular momentum limits are taken. Performing the matching leads to a restriction analogous to equation (5.52), given by

$$B_{sca} \equiv \frac{B_1^{sca}}{B_2^{sca}} = -\frac{1}{\pi}\left(\frac{2}{\omega r_H\left(1+a_*^2\right)^{\frac{1}{n+1}}}\right)^{2\ell+1} \sqrt{\lambda_{0\ell}+a^2\omega^2+1/4}\ \times \tag{5.81}$$

$$\frac{\Gamma^2\left(\sqrt{\lambda_{0\ell}+a^2\omega^2+1/4}\right)\Gamma(\alpha+\beta+B_*-1)\,\Gamma(\alpha+\beta)\,\Gamma(2-2\beta-B_*)}{\Gamma(2\beta+B_*-2)\,\Gamma(2+\alpha-\beta-B_*)\,\Gamma(1+\alpha-\beta)}\,.$$

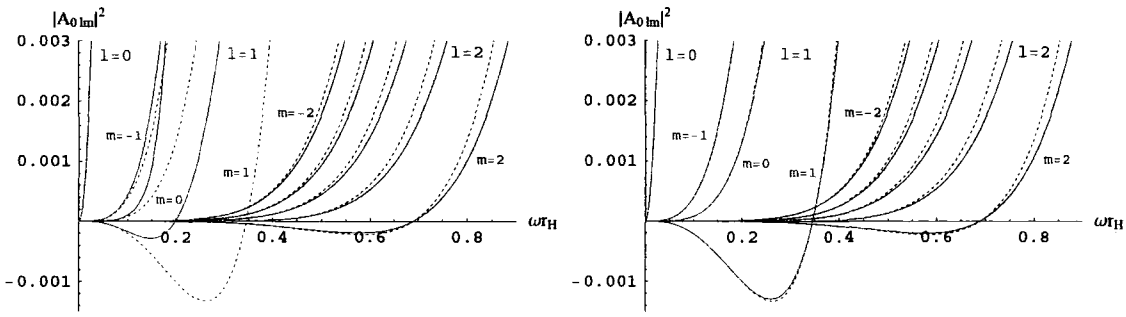

Figure 5.11: Absorption probability $|\mathcal{A}_{0\ell m}|^2$ of brane scalar particles, for $\ell = 0$ (red), 1 (green), 2 (blue), $a_* = 0.4$, $n = 2$ using the far-field Kummer function solution (left) and Bessel function solution (right). The solid lines correspond to the analytic solution, while the dashed lines are the result of an exact numerical analysis.

In the asymptotic far-field limit $r \to \infty$ the Bessel functions may be approximated using the standard $z \to \infty$ relations [133]

$$J_\nu(z) \to \sqrt{\frac{2}{\pi z}} \cos\left(z - \frac{\nu\pi}{2} - \frac{\pi}{4}\right), \tag{5.82}$$

$$Y_\nu(z) \to \sqrt{\frac{2}{\pi z}} \sin\left(z - \frac{\nu\pi}{2} - \frac{\pi}{4}\right). \tag{5.83}$$

This leads to

$$\begin{aligned} P_{FF}(r) &\simeq \frac{1}{\sqrt{2\pi\omega}} \left[\frac{(B_1 + iB_2)}{r} e^{-i\left(\omega r - \frac{\pi\nu}{2} - \frac{\pi}{4}\right)} + \frac{(B_1 - iB_2)}{r} e^{i\left(\omega r - \frac{\pi\nu}{2} - \frac{\pi}{4}\right)} \right] \\ &= A_{sca}^{(in)} \frac{e^{-i\omega r}}{r} + A_{sca}^{(out)} \frac{e^{i\omega r}}{r}. \end{aligned} \tag{5.84}$$

Since the incoming and outgoing spherical wave components have the same radial dependence, the absorption probability may be calculated using equation (5.56) as

$$\begin{aligned} |\mathcal{A}_{0\ell m}|^2 &= 1 - \left| \frac{A_{sca}^{(out)}}{A_{sca}^{(in)}} \right|^2 = 1 - \left| \frac{B_1^{sca} - iB_2^{sca}}{B_1^{sca} + iB_2^{sca}} \right|^2 \\ &= 1 - \left| \frac{B_{sca} - i}{B_{sca} + i} \right|^2 = \frac{2i\left(B_{sca}^* - B_{sca}\right)}{B_{sca}B_{sca}^* + i\left(B_{sca}^* - B_{sca}\right) + 1}. \end{aligned} \tag{5.85}$$

To illustrate the improvement in accuracy that is achieved by using Bessel instead of Kummer functions in the far-field solution, figure 5.11 presents both methods for $n = 2$ and $a_* = 0.4$. In the remainder of this chapter the Bessel function solution will be used to plot scalar quantities.

5.6 The Low-Energy Limit

By expanding the analytic expressions (5.75) and (5.85) for the absorption probabilities one may obtain simplified, compact expressions that reveal more clearly the low-energy asymptotic behaviours of the individual particle species as well as characteristic differences in the extreme low-energy values of the corresponding absorption cross-sections.

5.6.1 Scalars

Beginning with scalar particles, according to equation (5.81), in the limit $\omega \to 0$, $B_{sca} \sim \omega^{-(2\ell+1)}$ and, therefore, $B_{sca}B^*_{sca} \gg i(B^*_{sca} - B_{sca}) \gg 1$. Then, equation (5.85) simplifies to

$$|\mathcal{A}_{0\ell m}|^2 \simeq \frac{2i(B^*_{sca} - B_{sca})}{B_{sca}B^*_{sca}} = 2i\left(\frac{1}{B_{sca}} - \frac{1}{B^*_{sca}}\right). \tag{5.86}$$

Substituting for B_{sca} using equation (5.81), and the fact that α is purely imaginary, yields

$$\begin{aligned} |\mathcal{A}_{0\ell m}|^2 \;=\; & \frac{-2i\pi\,(\omega r_H/2)^{2\ell+1}}{(\ell+\frac{1}{2})\,\Gamma^2(\ell+\frac{1}{2})}\,\frac{\Gamma(2\beta+B_*-2)}{(1+a_*^2)^{-\frac{2\ell+1}{n+1}}\,\Gamma(2-2\beta-B_*)} \;\times \\ & \frac{1}{\Gamma(\alpha+\beta+B_*-1)\,\Gamma(-\alpha+\beta+B_*-1)\,\Gamma(\alpha+\beta)\,\Gamma(-\alpha+\beta)} \;\times \\ & \Big[\Gamma(2+\alpha-\beta-B_*)\,\Gamma(-\alpha+\beta+B_*-1)\,\Gamma(1+\alpha-\beta)\,\Gamma(-\alpha+\beta) - \\ & \Gamma(2-\alpha-\beta-B_*)\,\Gamma(\alpha+\beta+B_*-1)\,\Gamma(1-\alpha-\beta)\,\Gamma(\alpha+\beta)\Big] \\ =\; & \Sigma_1 \times \Sigma_2 \times \Sigma_3\,, \end{aligned} \tag{5.87}$$

where Σ_1, Σ_2 and Σ_3 are defined by the quantities on each of the three lines above. Focusing attention first on Σ_3, and using the gamma function relation $\Gamma(z)\Gamma(1-z) = \pi/\sin\pi z$ [133], this can be written as

$$\Sigma_3 = \frac{-\pi^2\,\sin(2\pi\alpha)\,\sin\pi(2\beta+B_*)}{\sin\pi(\alpha+\beta+B_*)\,\sin\pi(-\alpha+\beta+B_*)\,\sin\pi(\alpha+\beta)\,\sin\pi(-\alpha+\beta)}. \tag{5.88}$$

From the factor $\omega^{2\ell+1}$ in equation (5.87), it is clear that the expression for the absorption probability in the very low-energy regime is dominated by the lowest

partial waves, a property that is in accordance with the results presented in section 5.4. Then, assuming that m is small and $a_* < 1$, the limit $\omega \to 0$ is equivalent to $\alpha \to 0$. Expanding terms in Σ_2 and Σ_3 to linear order in α gives

$$\Sigma_2 = \frac{1}{\Gamma(\beta + B_* - 1)^2\,\Gamma(\beta)^2}\,, \qquad \Sigma_3 = -\frac{2\pi^3\alpha\,\sin\pi(2\beta + B_*)}{\sin^2\pi(\beta + B_*)\,\sin^2\pi\beta}\,. \tag{5.89}$$

The additional gamma function relation $\Gamma(z)\Gamma(-z) = -\pi/z\sin\pi z$ allows the overall expression for the low-energy limit of the scalar absorption probability to be written as

$$|\mathcal{A}_{0\ell m}|^2 = \frac{4\pi\,(\omega r_H/2)^{2\ell+1}\,K_*\,\sin^2\pi(2\beta + B_*)\,\Gamma^2(2\beta + B_* - 2)\,\Gamma^2(1-\beta)\,(2 - B_* - 2\beta)}{A_*\,(1+a_*^2)^{-\frac{2\ell+1}{n+1}}\,(\ell + \frac{1}{2})\,\Gamma^2(\ell + \frac{1}{2})\,\Gamma^2(\beta + B_* - 1)\,\sin^2\pi(\beta + B_*)}\,. \tag{5.90}$$

By using the expression for β in equation (5.25), one may easily conclude that the quantity $(2 - B_* - 2\beta)$ is always positive, while the same also holds for $A_* \equiv (n+1)+(n-1)a_*^2$, for all values of a_* and $n > 0$. Therefore, the overall sign of $|\mathcal{A}_{0\ell m}|^2$ is determined by the sign of K_*, or equivalently of $\omega - ma/(r_H^2 + a^2) = \omega - m\Omega$. A negative sign for the latter quantity arises only where $m > 0$, and denotes the occurrence of superradiance. A superradiant domain therefore exists in the low-energy regime and extends over the range of values $0 < \omega < \omega_s \equiv m\,\Omega$. For $a_* < 1$, the larger the value of a_*, the larger the rotational velocity Ω of the black hole, and the more extended the superradiant regime becomes. This is in agreement with the behaviour described in section 5.4.

From equation (5.90), the low-ω behaviour of the absorption probability for a partial wave with general ℓ is governed by a factor of $\omega^{2\ell+2}$ (including the ω-dependence of K_*). The on-brane cross-section is derived from the absorption probability, via equation (4.22), through division by ω^2 and is therefore proportional to $\omega^{2\ell}$. Consequently, only the cross-section for the lowest mode $\ell = 0$ reduces to a non-vanishing asymptotic value as $\omega \to 0$. Focusing attention on this lowest mode, in order to simplify equation (5.90) further, it is also necessary to expand the expression of β in the limit $\omega \to 0$. In this limit $\beta = -(|s| + \ell)/(n+1) + \mathcal{O}(\omega_*^2, a_*^2, a_*\omega_*)$, so for $s = \ell = 0$, $\beta \simeq 0$, which allows the extreme low-energy absorption probability for

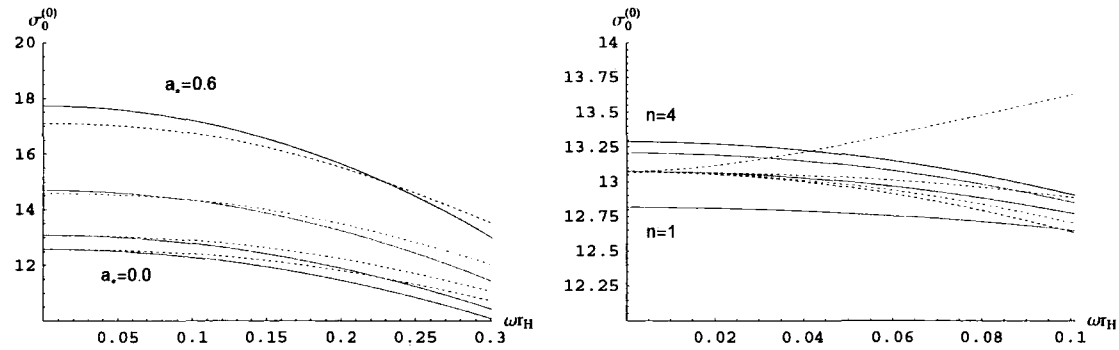

Figure 5.12: Low-energy cross-section $\sigma_0^{(0)}$ (in units of r_H^2) for brane scalar particles. The left-hand figure depicts $n = 2$ and $a_* = 0$ (red), 0.2 (green), 0.4 (light blue) and 0.6 (dark blue) while the right-hand figure is for $a_* = 0.2$ and $n = 1$ (red), 2 (green), 3 (light blue) and 4 (dark blue) In each case the solid lines denote the analytic approximation while the dotted lines represent the exact numerical result.

scalar particles to be written

$$|\mathcal{A}_{000}|^2 = \frac{4\,(\omega r_H)^2\,(1+a_*^2)}{A_*\,(1+a_*^2)^{-1/(n+1)}\,(2-B_*)} + \ldots . \tag{5.91}$$

The corresponding absorption cross-section for the dominant partial wave is then

$$\sigma_0^{(0)} = \frac{\pi}{\omega^2}\,|\mathcal{A}_{000}|^2 = 4\pi\,(r_H^2+a^2)\,\frac{(1+a_*^2)^{\frac{1}{n+1}}}{[(n+1)+(n-1)\,a_*^2]\,(2-B_*)} + \ldots . \tag{5.92}$$

In the case of scalar particles propagating in a Schwarzschild-like brane-projected line-element, the low-energy asymptotic value of the absorption cross-section resulting from the lowest partial wave was shown to be equal to the projected 4-d horizon area of the higher-dimensional black hole, $4\pi r_H^2$, regardless of the number of extra dimensions [111, 113]. It would be instructive to determine whether a similar relation holds in the case of an axially-symmetric brane background. According to equation (5.92), $\sigma_0^{(0)}$ is indeed proportional to the projected 4-d horizon area of the higher-dimensional rotating black hole $A_H = 4\pi(r_H^2 + a^2)$, however, the relation involves a multiplicative factor which is both a_* and n-dependent. In the left-hand plot of figure 5.12, both the analytic and exact numerical versions of $\sigma_0^{(0)}$ are illustrated for fixed n and a_* between 0 and 0.6. The numerical results reveal that the asymptotic low-energy cross-section is indeed equal to the horizon area of the black

hole, regardless of the number of extra dimensions. For small values of a_*, the multiplicative factor appearing in equation (5.92) is very close to unity and the analytic expression closely reproduces the exact numerical one. As a_* increases though, the range of validity of the approximation is exceeded and a deviation appears. At fixed a_*, the right-hand image in 5.12 reveals that the analytic low-energy cross-section is enhanced with increasing n, whereas the numerical result retains the constant value A_H. For $n \leq 1$ the analytic expression is smaller than the exact result, whereas for $n \geq 2$ the opposite is true. For $n \geq 2$ the magnitude of the deviation is an increasing function of a_*.

From the above results it may be concluded that the behaviour of the lowest mode of a scalar particle, whereby its partial cross-section equals the on-brane area of the black-hole horizon in the low-energy regime, generalises to rotating black holes. This feature has been found before in the particular case of a 5-dimensional bulk [122], but was yet to be demonstrated for the general $(4 + n)$-dimensional case. As was found with a spherically-symmetric brane line-element, the result is independent of the number of additional transverse spacelike dimensions.

5.6.2 Fermions and Gauge Bosons

In a similar manner the low-energy properties of the absorption probabilities and cross-sections for fermions and gauge bosons may be determined by expanding equation (5.75) in the limit $\omega \to 0$. In this limit equation (5.43) reduces to $Z \simeq 2\ell + 1$ and then, from the expression of B_1/B_2 in (5.52), it is found that

$$\frac{B_1}{B_2} \simeq \frac{\Gamma(2\ell+1)}{\Gamma(1+\ell-s)} (2i\omega)^{-(2\ell+1)} \left.\frac{A_1}{A_2}\right|_{\omega=0} \equiv M_{s\ell m} (2i\omega)^{-(2\ell+1)}, \tag{5.93}$$

with $M_{s\ell m}$ a complex constant independent of the energy ω. Examining first the fermions, if $s = 1/2$ then equation (5.66) becomes

$$\begin{aligned} |\mathcal{A}_{\frac{1}{2}\ell m}|^2 &\simeq 1 - \left| \frac{M_{\frac{1}{2}\ell m}\,\Gamma(2\ell+2)}{M_{\frac{1}{2}\ell m}\Gamma(2\ell+2)\, e^{i\pi(\ell+1/2)} + \Gamma(\ell+3/2)\,(2i\omega)^{2\ell+1}} \right|^2 \\ &\simeq \frac{(2\omega)^{2\ell+1}\,\Gamma(\ell+3/2)}{\Gamma(2\ell+2)} \left(\frac{1}{M_{\frac{1}{2}\ell m}} + \frac{1}{M^*_{\frac{1}{2}\ell m}} \right) + \ldots . \end{aligned} \tag{5.94}$$

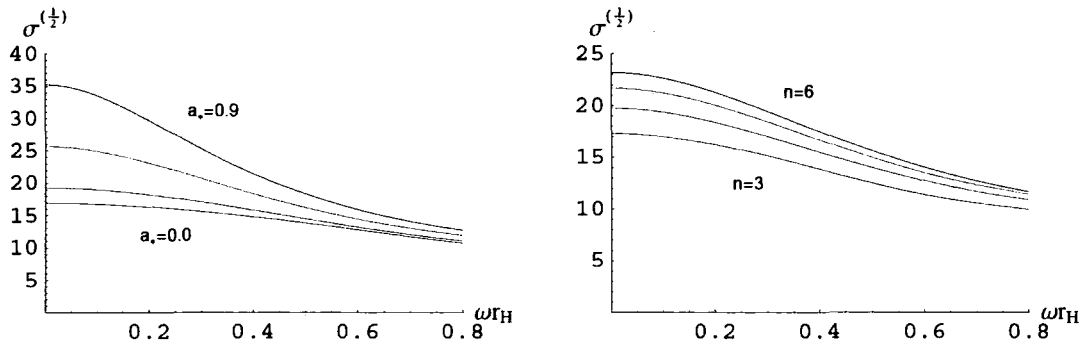

Figure 5.13: Total absorption cross-section for spinor fields in units of r_H^2. The left-hand figure is for $n = 6$ and $a_* = 0$ (red), 0.3 (green), 0.6 (light blue) and 0.9 (dark blue). The right-hand figure is for $a_* = 0.5$ and $n = 3$ (red), 4 (green), 5 (light blue) and 6 (dark blue).

Corresponding absorption cross-sections for individual modes may be defined as $\sigma^{(\frac{1}{2})}_{\ell m} = \pi\,|\mathcal{A}_{\frac{1}{2}\ell m}|^2/\omega^2$ and take the form

$$\sigma^{(\frac{1}{2})}_{\ell m} = \frac{2^{2\ell+1}\pi\,\omega^{2\ell-1}\,\Gamma(\ell+3/2)}{\Gamma(2\ell+2)}\left(\frac{1}{M_{\frac{1}{2}\ell m}}+\frac{1}{M^*_{\frac{1}{2}\ell m}}\right)+\ldots. \tag{5.95}$$

From the above result it is clear that, in a similar manner to the non-rotating higher-dimensional black hole [111,113], the absorption cross-section of the lowest fermionic mode, with $\ell = 1/2$, assumes a non-zero asymptotic value, specifically

$$\sigma^{(\frac{1}{2})}_{\frac{1}{2}m} = 2\pi\left(\frac{1}{M_{\frac{1}{2}\frac{1}{2}m}}+\frac{1}{M^*_{\frac{1}{2}\frac{1}{2}m}}\right), \tag{5.96}$$

while all higher fermionic partial waves, with $\ell > 1/2$, have zero absorption cross-section as $\omega \to 0$. The quantity $M_{\frac{1}{2}\frac{1}{2}m}$ depends both on the number of extra dimensions n and on the angular momentum parameter a_* of the black hole. In figure 5.13 the dependence of the low-energy cross-section, found by summing over ℓ and m, on both a_* and n is depicted. It may be observed that the asymptotic value of the absorption cross-section for fermions in the low-energy regime is enhanced in terms of both parameters of the gravitational background.

For gauge fields, with $s = 1$, equation (5.73) leads to a similar result for the

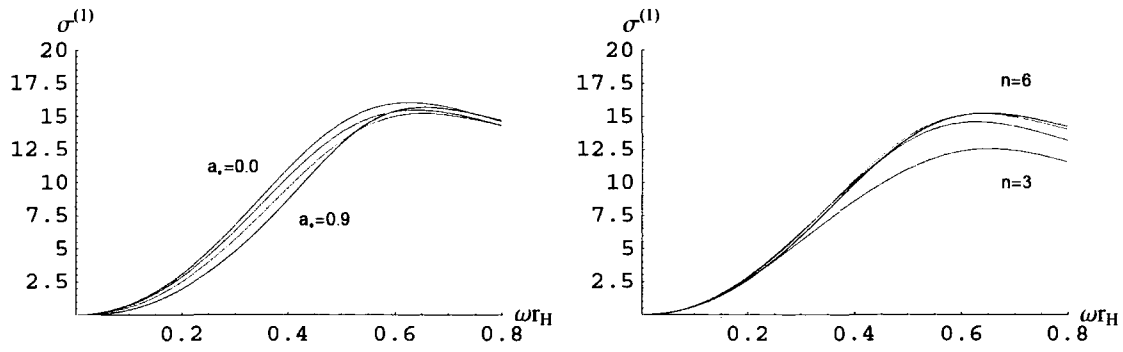

Figure 5.14: Total absorption cross-section for gauge bosons in units of r_H^2. The left-hand figure is for $n = 6$ and $a_* = 0$ (red), 0.3 (green), 0.6 (light blue) and 0.9 (dark blue). The right-hand figure is for $a_* = 0.5$ and $n = 3$ (red), 4 (green), 5 (light blue) and 6 (dark blue).

absorption probability, namely

$$|A_{1\ell m}|^2 \simeq 1 - \left| \frac{M_{1\ell m}\,\Gamma(2\ell+2)}{M_{1\ell m}\Gamma(2\ell+2)\,e^{i\pi\ell} + \Gamma(\ell+2)\,(2i\omega)^{2\ell+1}} \right|^2$$
$$\simeq \frac{(2\omega)^{2\ell+1}\,\Gamma(\ell+2)}{\Gamma(2\ell+2)}\,\frac{i(M^*_{1\ell m} - M_{1\ell m})}{|M_{1\ell m}|^2} + \ldots . \qquad (5.97)$$

The corresponding absorption cross-section has the form

$$\sigma_{1\ell m} = \frac{2^{2\ell+1}\pi\,\omega^{2\ell-1}\,\Gamma(\ell+2)}{\Gamma(2\ell+2)}\,\frac{i(M^*_{1\ell m} - M_{1\ell m})}{|M_{1\ell m}|^2} + \ldots . \qquad (5.98)$$

In this case all gauge field modes, including the lowest with $\ell = 1$, have zero asymptotic low-energy cross-section. Again, this is in agreement with the corresponding results derived for the non-rotating case [111,113]. The dependence of $\sigma^{(1)}$, summed over ℓ and m, on a_* and n is shown in figure 5.14. In this case, while an increase in n results in an enhancement of the cross-section, increasing a_* causes suppression.

5.7 The High-Energy Limit

In this section a comprehensive study is conducted of the high-energy asymptotic limit of the total absorption cross-section for fields existing in the brane-induced background of a $(4+n)$-dimensional rotating black hole. The asymptotic limit has been studied previously for a Schwarzschild black hole, both in the four-dimensional

[140–145] and $(4 + n)$-dimensional case [79, 111]. For a rotating black hole, the corresponding analysis has been performed only in the 4-d [146] and 5-d [122] cases – the general $(4 + n)$-dimensional situation has yet to be considered. As will be seen, in an analogous manner to the higher-dimensional Schwarzschild-like brane background, the number of transverse dimensions, although inaccessible to brane-localised fields, affects the high-energy limit of the cross-section. For fermions and gauge bosons the analytic expressions derived in this chapter may be extended to successfully describe the intermediate and high-energy regimes of the absorption probability and calculate a value of the high-energy cross-section. The corresponding extension for scalar fields is less accurate, so the results of an exact numerical analysis are presented instead.

5.7.1 The High-Energy Cross-Section

As discussed in §4.6.2 the total absorption cross-section $\sigma_{tot}^{(s)} = \sum_{\ell,m} \sigma_{\ell m}^{(s)}$ of extremely high-energy particles tends towards a constant value that is independent of particle species. Although each individual partial cross-section $\sigma_{\ell m}^{(s)}$ asymptotes to zero in the high-energy regime, the superposition of an infinite number of partial waves, each reaching its maximum value at a larger value of ω as ℓ increases, results in the total cross-section oscillating towards this constant high-energy value.

Figure 5.15 illustrates the features described above for the case of scalar particles with $n = 2$ and $a_* = 0.3$. Exact numerical results are presented for the partial cross-sections $\sigma_{\ell}^{(0)} = \sum_m \sigma_{\ell m}^{(0)}$ for the modes $\ell = 0$ to 5, as well as the total value $\sigma_{tot}^{(0)}$ found through summation over ℓ. The oscillatory emergence of a constant high-energy value for the total cross-section is clear.

Figure 5.16 compares the total cross-sections of different particle species. The characteristic low-energy behaviours described in the previous section are apparent, as is the fact that $\sigma_{tot}^{(s)}$ tends towards the same high-energy value, regardless of the type of particle under consideration.

In the course of the analysis, the high-energy limit of $\sigma_{tot}^{(s)}$ has been studied for a range of values of n and a_* and the results are displayed in table 5.1. It should be noted that, while for low values of n and a_* summation over a relatively small

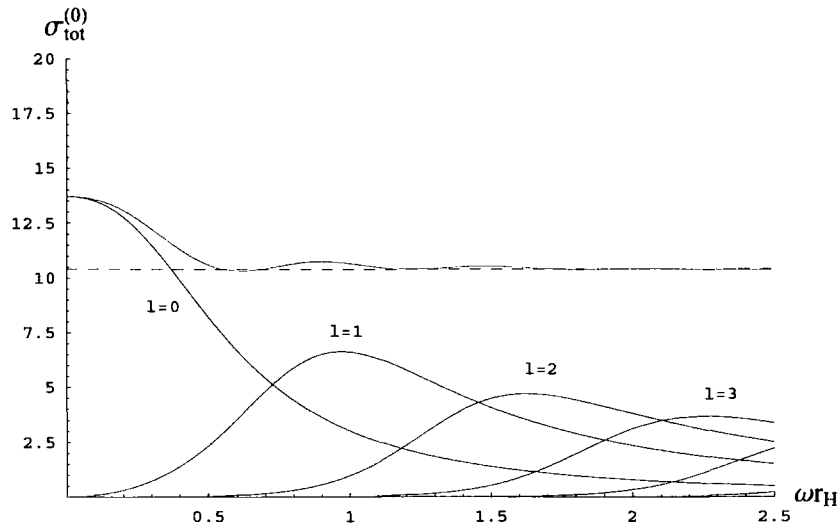

Figure 5.15: Partial absorption cross-sections $\sigma_\ell^{(0)}$, for the modes $\ell = 0, 1, 2, 3, 4$ (blue curves), and the total absorption cross-section $\sigma_{tot}^{(0)}$ (red curve) for $n = 2$ and $a_* = 0.3$, both in units of r_H^2. The dashed line denotes the value obtained by using the geometrical optics limit (5.105).

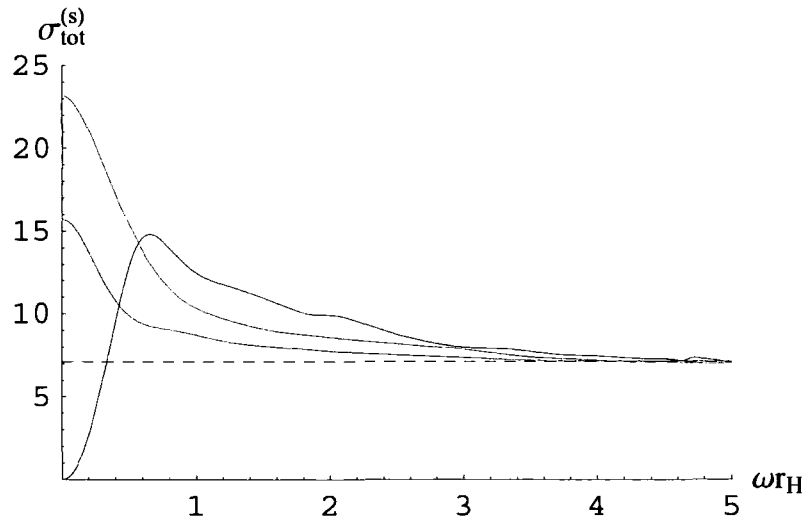

Figure 5.16: Total absorption cross-sections $\sigma_{tot}^{(s)}$, for scalars (red), fermions (green) and gauge bosons (blue) for $n = 6$ and $a_* = 0.5$, in units of r_H^2. All species tend to the same high-energy geometrical optics value (5.105) denoted by the dashed line.

$a_*\backslash n$	1	2	3	4	5	6
0.0	12.6	9.6	8.2	7.3	6.7	6.2
0.3	13.6	10.4	8.6	7.6	7.0	6.5
0.5	15.7	11.5	9.5	8.4	7.6	7.1
0.7	18.7	13.2	10.7	9.4	8.5	7.9
1.0	25.1	16.6	13.2	11.4	10.3	9.5
1.5	40.7	24.1	18.6	15.8	14.0	12.9
2.0	62.8	33.6	25.2	21.1	18.7	17.2

Table 5.1: High-energy asymptotic values of the total absorption cross-section $\sigma_{tot}^{(s)}$, in units of r_H^2, as a function of n and a_*.

number of partial waves is necessary to recover the high-energy value, as either a_* or n increases the number of modes that must be taken into account increases also. In addition the asymptotic value of $\sigma_{tot}^{(s)}$ emerges at ever larger values of ω, which lengthens the computation time considerably.

From the entries of table 5.1 the strong dependence of the high-energy absorption cross-section on both the number of extra dimensions and the angular momentum of the black hole may be observed. As in the non-rotating case [111], $\sigma_{tot}^{(s)}$ is strongly suppressed as n increases. On the other hand, an increase in the value of a_* results in an enhancement. As would be expected, for $a_* = 0$ the values of $\sigma_{tot}^{(s)}$ match those obtained for a scalar particle in a Schwarzschild-like projected brane background [111]. It should also be noted that a feature which seemed to hold for scalars in the 5-dimensional case [122], that the high-energy limit of $\sigma_{tot}^{(s)}$ is close to the low-energy value, appears to be unique to that particular spacetime dimension. This is evident in figures 5.15 and 5.16, or can be seen by comparing the entries of table 5.1 with the horizon area $A_H = 4\pi(r_H^2 + a^2)$ that corresponds to the low-energy value $\sigma_0^{(0)}$.

5.7.2 The Geometrical Optics Limit

For a non-rotating black hole, the geometrical optics limit has been successfully used to explain the high-energy asymptotic value of the absorption cross-section $\sigma_{tot}^{(s)}$ both

in the pure 4-dimensional [140–142, 145] and $(4+n)$-dimensional [79, 111] cases. In the higher-dimensional situation the analysis demonstrated that, for particles living on the brane, the Schwarzschild black hole behaves as a perfect absorber of radius

$$r_c = r_H \left(\frac{n+3}{2}\right)^{\frac{1}{n+1}} \sqrt{\frac{n+3}{n+1}}\,. \tag{5.99}$$

The geometrical optics cross-section is then given by the target area, $\sigma_g = \pi r_c^2$. For all n, the values following from this expression are in perfect agreement with the results of a numerical analysis [111], and are displayed in the first row of table 5.1.

Here, a similar study will be performed in an axially-symmetric black-hole brane background to investigate the potential connection between the analytic values that follow from this analysis and the exact numerical ones appearing in table 5.1, for $a_* \neq 0$. To achieve this, a method described in [146] is closely followed. Although the formalism there was developed for the case of a pure 4-dimensional Kerr black hole, it also applies exactly to the case of a brane-projected rotating black hole, the only difference appearing in the expression of the metric function $\Delta(r)$. For brevity, only the basic assumptions and final equation describing the particle's trajectory will be presented here.

The line-element (5.1), in which the brane-localised particles propagate, is invariant under translations of the form $t \to t + \Delta t$ and $\phi \to \phi + \Delta\phi$. The corresponding Killing vectors $\xi^\mu_{(t)} = \delta^\mu_t$ and $\xi^\mu_{(\varphi)} = \delta^\mu_\varphi$ then lead to the conserved conjugate momenta $p_t \equiv -E$ and $p_\phi \equiv -L_z$. The brane metric also possesses a Killing tensor $\xi_{\mu\nu}$, that leads to an additional conserved quantity $\mathcal{Q} = \xi_{\mu\nu}\, p^\mu p^\nu - (Ea + L_z)^2$. Combining the above, the equation of motion of a particle with rest mass m, i.e. $p_\mu\, p^\mu = -m^2$, takes the form [146]

$$\Sigma \frac{dr}{d\lambda} = \pm \mathcal{R}^{1/2}\,, \quad \mathcal{R} = \left[E(r^2+a^2) + L_z a\right]^2 - \Delta\left[m^2 r^2 + (L_z + aE)^2 + \mathcal{Q}\right]\,, \tag{5.100}$$

where λ is the affine parameter of the trajectory. The conserved quantity $\mathcal{Q}$ takes the explicit form $\mathcal{Q} = L^2 - L_z^2 - a^2(E^2 - m^2)\cos^2\theta_\infty$, where θ_∞ is the value of the azimuthal angle as the particle approaches the black hole from infinity, and L the total angular momentum of the particle.

A particle approaching a rotating black hole from infinity, may do so by following

a number of possible trajectories. Here attention will be focused on the cases of a massless particle with its trajectory either transverse ($\theta_\infty = \pi/2$) or parallel ($\theta_\infty = 0, \pi$) to the rotation axis. Starting with the transverse case it is found that, for motion strictly on the equatorial plane, $\cos\theta_\infty = 0$ and $L = L_z$. Then, $\mathcal{Q} = 0$, and equation (5.100) takes the form

$$\left(\Sigma \frac{dr}{d\lambda}\right)^2 = E^2 \left[b^2(a^2 - \Delta) + 2b\frac{a\mu}{r^{n-1}} + (r^2 + a^2)^2 - a^2\Delta\right]. \tag{5.101}$$

In the above the definition $b \equiv L/E$ has been made, where $b > 0$ is the impact parameter of the particle. For the above equation to be consistent, its right-hand side, or equivalently the expression inside the square brackets, must be positive-definite. Since the particle approaches the black hole from large r, attention will be focused on the radial regime outside the ergosphere, where the coefficient of b^2, $(a^2 - \Delta)$, can be shown to be negative. Then the constraint on the values of b takes the form $b_2 < b < b_1$, where $b_{1,2}$ are the roots of the expression which follows from setting the right-hand side of equation (5.101) equal to zero. However, it may easily be seen that $b_2 < 0$, therefore the classically permissible regime is defined by the constraint $0 < b < b_1$. Particles with impact parameters in this range can access all values of the radial coordinate, and thus reach the black-hole horizon where they may be absorbed. According to the geometrical optics argument, the closest distance a particle may approach the black hole without being captured is

$$r_c = \min(b_1) = \min\left(\frac{a\mu + r^{n+1}\sqrt{a^2 + r^2 - \frac{\mu}{r^{n-1}}}}{r^{n+1} - \mu}\right). \tag{5.102}$$

As a consistency check it is noticed that, for $a = 0$, the above expression reduces to $r_c = \min\left(r/\sqrt{1 - \frac{\mu}{r^{n+1}}}\right)$, which is identical to the result (5.99) for a non-rotating brane black-hole background derived in [79,111]. By further setting $n = 0$, the purely 4-dimensional Schwarzschild case [140–142] is also recovered, with $r_c = 3\sqrt{3}\, r_H/2$.

For general n and a, an analytic expression for the minimum distance referred to in equation (5.102) is difficult to find. Nevertheless, a simple numerical analysis may lead to the value of r_c in units of r_H, after using equation (4.6) to eliminate the mass parameter μ. Then, through the relation $\sigma_g = \pi r_c^2$, the corresponding absorption cross-section may be found; its values, for a variety of n and a_*, are displayed in table

$a_*\backslash n$	1	2	3	4	5	6
0.0	12.6	9.6	8.2	7.3	6.6	6.2
0.3	17.9	12.8	10.4	9.0	8.1	7.4
0.5	23.5	15.9	12.6	10.7	9.5	8.7
0.7	31.0	20.0	15.4	12.9	11.4	10.3
1.0	46.0	27.6	20.6	17.0	14.8	13.4
1.5	81.9	44.3	31.7	25.6	22.2	19.9
2.0	131.6	65.4	45.3	36.3	31.3	28.2

$a_*\backslash n$	1	2	3	4	5	6
0.0	12.6	9.6	8.2	7.3	6.6	6.2
0.3	10.0	8.2	7.3	6.6	6.2	5.9
0.5	9.5	8.1	7.3	6.8	6.4	6.1
0.7	9.5	8.4	7.7	7.3	6.9	6.7
1.0	10.5	9.6	9.0	8.6	8.4	8.1
1.5	13.4	13.2	12.7	12.3	12.1	11.9
2.0	19.2	18.5	18.1	17.8	17.5	17.4

Table 5.2: Geometrical optics value of the absorption cross-section σ_g, in units of r_H^2, for particles moving in the equatorial plane of the axially-symmetric brane black hole (5.1), for $a > 0$ (upper table) and $a < 0$ (lower table).

5.2. The two sub-tables correspond to the two possible orientations of the particle's angular momentum L: as it approaches the black hole from infinity moving in the equatorial plane, its angular momentum and that of the black-hole can be either parallel ($aL > 0$) or anti-parallel ($aL < 0$). It has been assumed here that $L > 0$ always, and then the sign choices $a > 0$ and $a < 0$ correspond to the first and second sub-tables of table 5.2, respectively. For $a < 0$, the sign of the first term in the numerator of (5.102) is reversed, leading to a lower value of r_c and consequently of the cross-section.

It is also possible to analyse the case of a zero-mass particle approaching from

$a_*\backslash n$	1	2	3	4	5	6
0.0	12.6	9.6	8.2	7.3	6.6	6.2
0.3	13.7	10.4	8.7	7.8	7.1	6.6
0.5	15.7	11.6	9.7	8.6	7.9	7.3
0.7	18.7	13.5	11.2	9.8	9.0	8.4
1.0	25.1	17.2	14.0	12.3	11.3	10.5
1.5	40.9	25.7	20.5	18.0	16.5	15.4
2.0	62.8	36.5	28.9	25.3	23.3	22.0

Table 5.3: Geometrical optics absorption cross-section σ_g, in units of r_H^2, for particles moving parallel to the rotation axis of the axially-symmetric brane black hole (5.1).

infinity along an orbit that is parallel to the black hole's rotation axis. This corresponds to $\cos^2\theta_\infty = 1$ and $L_z = 0$. In this case

$$\left(\Sigma\frac{dr}{d\lambda}\right)^2 = E^2(r^2+a^2)^2 - \Delta L^2. \tag{5.103}$$

Defining, as before, $b \equiv L/E$, one may easily conclude that the above equation is only consistent providing

$$b < \left(\frac{r^2+a^2}{\sqrt{\Delta}}\right). \tag{5.104}$$

The above leads to the minimum distance of the particle's approach avoiding capture by the black hole being

$$r_c = \min\left(\frac{r^2+a^2}{\sqrt{a^2+r^2-\frac{\mu}{r^{n-1}}}}\right). \tag{5.105}$$

For $a = 0$ this result also reduces to the Schwarzschild case (5.99), as it must since in the absence of rotation all directions of the particle's orbit are equivalent. Using equation (5.105), the values of the corresponding absorption cross-section σ_g, in units of r_H^2, are given in table 5.3.

Having derived these geometrical optics values, it is now possible to compare them to the exact numerical ones derived from a full analysis of the high-energy scalar field absorption cross-section. It is important to realise that the values displayed in tables 5.2 and 5.3 correspond to trajectories with a specific azimuthal

angle, while the numerical values of table 5.1 represent quantities integrated over all possible angles of incidence. Nevertheless, it is informative to determine if any relationship exists between the various results.

A direct comparison of the entries of tables 5.1 and 5.2 reveals that the numerical cross-section is smaller than that corresponding to a trajectory in the equatorial plane with $aL > 0$, but larger than the one with $aL < 0$. On the other hand, by comparing the entries of tables 5.1 and 5.3, a near-perfect agreement is realised for low values of a_* or n. The same agreement can be seen graphically in figures 5.15 and 5.16, where the dashed black lines represent the appropriate values from table 5.3. It may therefore be concluded that, in the low n or a_* limit at least, particle trajectories running parallel to the rotation axis of the black hole lead to an absorption cross-section that is almost identical to the high-energy asymptotic value of the total cross-section. As either n or a_* increases a deviation between the two values arises, however the values in table 5.3 still provide a good approximation to the exact result that avoids resorting to the numerically intensive task of accounting for contributions of all possible particle trajectories.

5.8 Energy Emission Rates

To complete the study of Hawking radiation on the brane from a higher-dimensional rotating black hole, the analytic expressions for the absorption probabilities can be used to compute the energy emission spectra of the various particle species and determine their dependencies on the topological parameters of the spacetime. Figure 5.17 illustrates these dependencies for the specific cases of gauge boson emission at constant n and variable a_* (left-hand plot), and fermion emission at constant a_* and variable n (right-hand plot). In each case emission is enhanced by increasing the relevant spacetime parameter. This is in accordance with results derived for static black holes [111, 113, 114] and also in numerical studies of the rotating case [115–117, 119]. Since these dependencies are found to hold true for all particle species, only two plots are presented to avoid repetition.

A comparison of the different particle species is illustrated in figure 5.18. In the

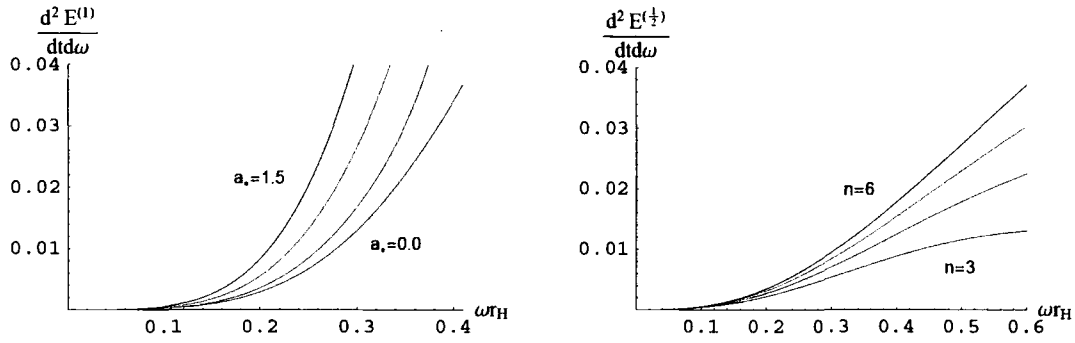

Figure 5.17: Low-energy emission rates of particles on the brane. The left-hand figure is for emission of gauge bosons with $n = 6$ and $a_* = 0$ (red), 0.5 (green), 1 (light blue) and 1.5 (dark blue). The right-hand plot is for fermions with $a_* = 0.5$ and $n = 3$, (red), 4 (green), 5 (light blue) and 6 (dark blue).

extreme low-energy regime scalar particles dominate, followed by fermions and then gauge bosons. However, as the energy of the emitted particle increases the black hole preferentially radiates energy in the form of gauge bosons. The exact same behaviour was found in the non-rotating case for $n = 6$ [111, 113, 114], although it should be noted that the relative magnitude of particle species is n-dependent. This n-dependence for fixed a_* is unchanged from the non-rotating case so will not be discussed further here. At fixed n, the pattern of behaviour is unchanged by increasing a_* – the competition for dominance is merely shifted to smaller ω_* as the spectra of all fields is enhanced.

5.9 Summary

The spectrum of Hawking radiation from a higher-dimensional rotating black hole has been studied analytically by solving the field equations of particles propagating in the brane-induced black hole background using an extension of a well-known solution matching technique. This permitted calculation of an analytic expression for the absorption probability of particles $|\mathcal{A}_{s\ell m}|^2$ that is valid in the limits of low particle energy and slow black hole rotation. A single formalism was presented to account for all types of particle, however comparison of scalar absorption probabilities with

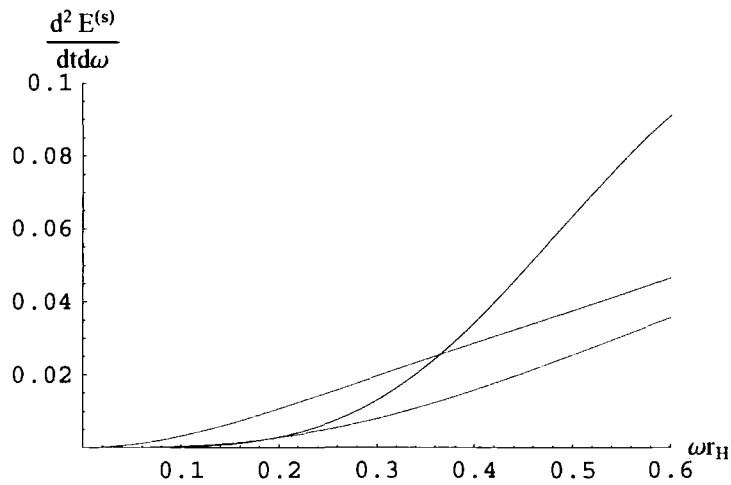

Figure 5.18: Comparison of the energy emission rates of scalars (red), fermions (green) and gauge bosons (blue) on the brane with $n = 6$ and $a_* = 0.1$.

the results of an exact numerical analysis revealed that a significant improvement could be achieved by using Bessel rather than Kummer functions to describe the far-field radial behaviour of the scalar field.

Investigation of the properties of the absorption probabilities revealed that, in all cases, the lowest partial mode is dominant at low energy, and this mode is suppressed with increasing spin s. In general, $|\mathcal{A}_{s\ell m}|^2$ is enhanced with increasing rotation of the black hole a_* and also with the number of extra dimensions n, although this behaviour is complicated by phenomena such as superradiance.

The extreme low-energy limit of both the absorption probabilities and cross-sections was investigated by expanding the analytic expressions in the limit $\omega \to 0$. It was discovered that the low-energy cross-section for scalars tends to the brane-projected area of the higher-dimensional rotating black hole $A_H = 4\pi(r_H^2 + a^2)$, a result that generalises a well-known feature of emission from static black holes. The cross-section for fermions tends to a n- and a_*-dependent quantity, the form of which was derived, and the corresponding quantity for bosons tends to zero.

The high-energy limit of the cross-section was also investigated, revealing that it reaches a constant value independent of the particle's spin. A classical analysis, evaluating the minimum impact parameter that permits a particle following a geodesic in the black hole spacetime to escape to infinity, predicted a range of

theoretical "geometrical optics" cross-sections, depending on the orientation of the particle's approach to the black hole. It was found that the value assuming the particle approaches parallel to the axis of rotation very closely matches the high-energy asymptotic limit of the cross-section, both in its dependence on a_* and n.

Finally the Hawking radiation spectra were investigated using the analytic expressions for the absorption probabilities previously derived. The spectra of all particles was found to be enhanced with both a_* and n, while the dominance of a particular species depended largely on the energy range being examined and the number of extra dimensions transverse to the brane.

Chapter 6

Bulk Emission of Scalars in the Spin-Down Phase

Although not directly detectable by brane-based observers, the emission of particles into the bulk by evaporating black holes is of great interest as it is an important component in determining the proportion of the black hole's total energy that is available for detection on the brane.

Under the assumptions of extra-dimensional models, only gravitons and scalar fields propagate in the bulk. Owing to the relative simplicity of the field equation, the emission of scalars into the bulk has been studied previously from a Schwarzschild black hole [113] and for the rotating case in five-dimensions [110]. In this chapter the emission of scalar modes into the full spacetime surrounding a $(4+n)$-dimensional rotating black hole is studied [4].

6.1 The Field Equation

The gravitational background into which scalar particles emerge when emitted into the bulk is that of the full Myers-Perry metric with a single angular momentum parameter

$$ds^2 = -\left(1 - \frac{\mu}{\Sigma r^{n-1}}\right)dt^2 - \frac{2a\mu\sin^2\theta}{\Sigma r^{n-1}}\,dt\,d\varphi + \frac{\Sigma}{\Delta}\,dr^2 + \Sigma\,d\theta^2 + \left(r^2 + a^2 + \frac{a^2\mu\sin^2\theta}{\Sigma r^{n-1}}\right)\sin^2\theta\,d\varphi^2 + r^2\cos^2\theta\,d\Omega_n^2\,, \qquad (6.1)$$

where

$$\Delta = r^2 + a^2 - \frac{\mu}{r^{n-1}}\,, \qquad \Sigma = r^2 + a^2\,\cos^2\theta\,. \tag{6.2}$$

As in the case of brane-emission the particles are assumed to couple only minimally to the background and be free from any other interactions so that they satisfy the higher-dimensional free equation of motion

$$\nabla_M \nabla^M \Phi = \frac{1}{\sqrt{-g}}\,\partial_M(\sqrt{-g}g^{MN}\partial_N\Phi) = 0\,, \tag{6.3}$$

where

$$\sqrt{-g} = \Sigma \sin\theta\, r^n \cos^n\theta \prod_{i=1}^{n-1} \sin^i\theta_i\,. \tag{6.4}$$

The above field equation can be separated by assuming the factorised ansatz

$$\Phi = e^{-i\omega t}e^{im\varphi}R(r)\,S(\theta)\,Y_{jn}(\theta_1,\ldots,\theta_{n-1},\phi)\,, \tag{6.5}$$

where $Y_{jn}(\theta_1,\ldots,\theta_{n-1},\phi)$ are the hyperspherical harmonics on the n-sphere that satisfy [147]

$$\sum_{k=1}^{n-1} \frac{1}{\prod_{i=1}^{n-1}\sin^i\theta_i}\,\partial_{\theta_k}\left[\left(\prod_{i=1}^{n-1}\sin^i\theta_i\right)\frac{\partial_{\theta_k}Y_{jn}}{\prod_{i>k}^{n-1}\sin^2\theta_i}\right] + \frac{\partial_{\phi\phi}Y_{jn}}{\prod_{i=1}^{n-1}\sin^2\theta_i} + j(j+n-1)\,Y_{jn} = 0\,. \tag{6.6}$$

The functions $R(r)$ and $S(\theta)$ are then found as the solutions to the decoupled equations

$$\frac{1}{r^n}\,\partial_r\left(r^n\Delta\,\partial_r R\right) + \left(\frac{K^2}{\Delta} - \frac{j(j+n-1)a^2}{r^2} - \Lambda_{j\ell m}\right)R = 0\,, \tag{6.7}$$

$$\frac{1}{\sin\theta\cos^n\theta}\,\partial_\theta\left(\sin\theta\cos^n\theta\partial_\theta S\right) + \left(\omega^2a^2\cos^2\theta - \frac{m^2}{\sin^2\theta} - \frac{j(j+n-1)}{\cos^2\theta} + E_{j\ell m}\right)S = 0\,, \tag{6.8}$$

that first appeared in the literature in [148]. In the above,

$$\Lambda_{j\ell m} = E_{j\ell m} + a^2\omega^2 - 2am\omega\,. \tag{6.9}$$

The angular eigenvalue $E_{j\ell m}(a\omega)$ provides a link between the angular and radial equation and, as was the case with on-brane emission, its value cannot be written in closed analytic form, but may be expressed as a power series in $a\omega$ [149, 150]. For the purpose of this analysis, which will be valid only in the low-ω and low-a limit,

it suffices to retain terms in this expansion to 5th order[1]

$$E_{j\ell m} = \ell(\ell+n+1) + (a\omega)^2\left[\frac{1+2m^2-2j(j-1)-2\ell(\ell+1)-2n(\ell+j)-n^2}{(2\ell+n-1)(2\ell+n+3)}\right] +$$
$$(a\omega)^4\left[\frac{(\ell-j-|m|)(\ell+j+n-|m|-1)}{16(2\ell+n-1)^2(2\ell+n-3)}\left[(\ell-j-|m|-2)(\ell+j-|m|+n-3)-\right.\right.$$
$$\left.\frac{4(2\ell+n-3)(1+2m^2-2j(j-1)-2\ell(\ell+1)-2n(\ell+j)-n^2)}{(2\ell+n-1)(2\ell+n+3)}\right]-$$
$$\frac{(\ell-j-|m|+2)(\ell+j+n-|m|+1)}{16(2\ell+n+3)^2(2\ell+n+5)}\left[(\ell-j-|m|+4)(\ell+j-|m|+n+3)+\right.$$
$$\left.\left.\frac{4(2\ell+n+5)(1+2m^2-2j(j-1)-2\ell(\ell+1)-2n(\ell+j)-n^2)}{(2\ell+n-1)(2\ell+n+3)}\right]\right]+\cdots . \quad (6.10)$$

In order for the power series to converge in the limit $a\omega \to 0$ by terminating at finite order, a number of restrictions must be imposed on the allowed values of the integer parameters (j,ℓ,m) specifying the emission mode: in general, m may take any integer value and j and ℓ any positive or zero integer value providing [149]

$$\ell \geq j+|m| \qquad \text{and} \qquad \frac{\ell-(j+|m|)}{2} \in \{0,\mathbb{Z}^+\}\,. \quad (6.11)$$

By using the power series form of the angular eigenvalues it is possible to solve the radial equation (6.7) analytically using the method of the previous chapter. The solution for the radial function $R(r)$ will permit calculation of the absorption probability $|\mathcal{A}_{j\ell m}|^2$ for the propagation of a massless scalar field in the bulk. Exactly as in the on-brane case, this will then allow calculation of the corresponding cross-sections and Hawking radiation emission rates of the black hole.

[1]Equation (6.10) for the eigenvalues $E_{j\ell m}$ is based on the analysis of [149] but disagrees slightly with the version given there as the sign of the second order term is reversed. This is necessary so that, in the limit $j,n \to 0$, the expression for $E_{j\ell m}$ correctly reproduces the on-brane eigenvalues that have appeared in the literature previously [127,132].

6.2 Analytic Solution of the Field Equation

6.2.1 The Near-Horizon Regime

In the near-horizon limit equation (6.7) may be brought to hypergeometric form by employing the same transformations as in §5.2.1. Changing variable $r \to f(r) = \Delta(r)/(r^2+a^2)$ yields

$$f\,(1-f)\,\frac{d^2R}{df^2} + (1 - D_*\,f)\,\frac{dR}{df} + \left[\,\frac{K_*^2}{A_*^2\,f(1-f)} - \frac{(j(j+n-1)a_*^2 + \Lambda_{j\ell m})\;(1+a_*^2)}{A_*^2\,(1-f)}\,\right] R = 0\,, \tag{6.12}$$

where

$$D_* \equiv 1 - \frac{4a_*^2}{A_*^2}\,, \tag{6.13}$$

and A_* and K_* retain their definitions from equation (5.19). Following the same arguments as in §5.2.1 equation (6.12) has solution in terms of the hypergeometric function F

$$R_{NH}(f) = A_-\,f^{\alpha}\,(1-f)^{\beta}\,F(a,b,c;f) + A_+\,f^{-\alpha}\,(1-f)^{\beta}\,F(a-c+1,b-c+1,2-c;f)\,, \tag{6.14}$$

where

$$a = \alpha + \beta + D_* - 1\,, \qquad b = \alpha + \beta\,, \qquad c = 1 + 2\alpha\,, \tag{6.15}$$

and the power coefficients α and β are defined by

$$\alpha = \pm\frac{iK_*}{A_*}\,, \tag{6.16}$$

$$\beta = \frac{1}{2}\left[\,(2 - D_*) \pm \sqrt{(D_*-2)^2 - 4\left[\frac{K_*^2 - (j(j+n-1)a_*^2 + \Lambda_{j\ell m})\,(1+a_*^2)}{A_*^2}\right]}\,\right]. \tag{6.17}$$

To impose the boundary condition of no ingoing modes at the horizon, the near-horizon solution may be expanded in the limit $r \to r_H$ to give

$$R_{NH}(f) \simeq A_-\,f^{\pm iK_*/A_*} + A_+\,f^{\mp iK_*/A_*} = A_-\,e^{\pm iky} + A_+\,e^{\mp iky}\,, \tag{6.18}$$

where the tortoise-like coordinate y and quantity k are defined in equations (5.29) and (5.30) respectively. In this case it is possible to set either $A_- = 0$ or $A_+ = 0$, depending on the choice for α. The two options are equivalent, so to be consistent with the notation of the previous chapter the choice $\alpha = \alpha_-$ is made, which imposes $A_+ = 0$. Then, requiring that the hypergeometric function converges restricts the choice of power coefficient $\beta = \beta_-$ so that the near-horizon solution may be written as

$$R_{NH}(f) = A_- f^{\alpha} (1-f)^{\beta} F(a,b,c;f)\,, \tag{6.19}$$

using the newly defined quantities in equations (6.15)–(6.17).

The near-horizon solution may be stretched towards the far-field regime by using the identity (5.35) and the approximation for $1-f$ in equation (5.38) to yield

$$R_{NH}(r) \simeq A_1\, r^{-(n+1)\beta} + A_2\, r^{(n+1)(\beta+D_*-2)}\,, \tag{6.20}$$

with A_1 and A_2 defined as

$$\begin{aligned} A_1 &= A_- \left[(1+a_*^2)\, r_H^{n+1}\right]^{\beta} \frac{\Gamma(c)\Gamma(c-a-b)}{\Gamma(c-a)\Gamma(c-b)}\,, \\ A_2 &= A_- \left[(1+a_*^2)\, r_H^{n+1}\right]^{-(\beta+D_*-2)} \frac{\Gamma(c)\Gamma(a+b-c)}{\Gamma(a)\Gamma(b)}\,. \end{aligned} \tag{6.21}$$

6.2.2 The Far-Field Regime

Following the "improved" method of §5.5, the substitution $R(r) = r^{-\left(\frac{n+1}{2}\right)} \tilde{R}(r)$ brings equation (6.7) into the form of a Bessel equation [133], in terms of $z = \omega r$,

$$\frac{d^2\tilde{R}}{dz^2} + \frac{1}{z}\frac{d\tilde{R}}{dz} + \left(1 - \frac{E_{j\ell m} + a^2\omega^2 + \left(\frac{n+1}{2}\right)^2}{z^2}\right)\tilde{R} = 0\,. \tag{6.22}$$

The solution in the far-field regime may be written as

$$R_{FF}(r) = \frac{B_1}{r^{\frac{n+1}{2}}} J_{\nu}(\omega r) + \frac{B_2}{r^{\frac{n+1}{2}}} Y_{\nu}(\omega r)\,, \tag{6.23}$$

with J_ν and Y_ν Bessel functions of the first and second kind and

$$\nu = \sqrt{E_{j\ell m} + a^2\omega^2 + \left(\frac{n+1}{2}\right)^2}\,. \tag{6.24}$$

The far-field solution may be stretched to small r by expanding the Bessel functions using (5.78) and (5.79)

$$R_{FF}(r) \simeq \frac{B_1 \left(\frac{\omega r}{2}\right)^{\nu}}{r^{\frac{n+1}{2}}\,\Gamma(\nu+1)} - \frac{B_2}{\pi\, r^{\frac{n+1}{2}}} \frac{\Gamma(\nu)}{\left(\frac{\omega r}{2}\right)^{\nu}}. \tag{6.25}$$

Then, taking the small a_* and ω_* limit in the power coefficients of r – so that terms of order $(\omega_*^2, a_*^2, a_*\omega_*)$ or higher may be ignored – exact matching between the two asymptotic solutions (6.20) and (6.25) may be achieved since

$$\begin{aligned} -(n+1)\,\beta &\simeq \ell + \mathcal{O}(\omega_*^2, a_*^2, a_*\omega_*)\,, \\ (n+1)\,(\beta + D_* - 2) &\simeq -(\ell + n + 1) + \mathcal{O}(\omega_*^2, a_*^2, a_*\omega_*)\,, \\ \nu &\simeq \ell + \frac{n+1}{2} + \mathcal{O}(a_*^2\omega_*^2)\,. \end{aligned} \tag{6.26}$$

As in the previous chapter, to ensure greatest possible accuracy no expansion is performed in the arguments of the gamma functions and terms to order $(a\omega)^4$ are retained in the expansion of the eigenvalues. Then, the matching of the two asymptotic solutions leads to the constraint

$$\begin{aligned} B \equiv \frac{B_1}{B_2} = -\frac{1}{\pi}\left(\frac{2}{\omega r_H\,(1+a_*^2)^{\frac{1}{n+1}}}\right)^{2\ell+n+1} \sqrt{E_{j\ell m} + a^2\omega^2 + \left(\frac{n+1}{2}\right)^2} \\ \times \frac{\Gamma^2\left(\sqrt{E_{j\ell m} + a^2\omega^2 + \left(\frac{n+1}{2}\right)^2}\right)\Gamma(\alpha+\beta+D_*-1)\,\Gamma(\alpha+\beta)\,\Gamma(2-2\beta-D_*)}{\Gamma(2\beta+D_*-2)\,\Gamma(2+\alpha-\beta-D_*)\,\Gamma(1+\alpha-\beta)}. \end{aligned} \tag{6.27}$$

The above relation guarantees the existence of a smooth, analytic solution for the radial part of the wavefunction for all r, valid in the low-energy and low-rotation limit.

6.3 The Absorption Probability

The absorption probability may be calculated by examining the extreme far-field limit of the solution to the radial equation. Using the Bessel function identities (5.82) and (5.83) the $r \to \infty$ limit of the far-field solution takes on the form of

incoming and outgoing plane waves

$$R_{FF}(r) \simeq \frac{1}{r^{\frac{n+2}{2}}\sqrt{2\pi\omega}}\left[(B_1+iB_2)\,e^{-i\left(\omega r-\frac{\pi}{2}\nu-\frac{\pi}{4}\right)}+(B_1-iB_2)\,e^{i\left(\omega r-\frac{\pi}{2}\nu-\frac{\pi}{4}\right)}\right]$$
$$= A_{in}^{(\infty)}\frac{e^{-i\omega r}}{r^{\frac{n+2}{2}}}+A_{out}^{(\infty)}\frac{e^{i\omega r}}{r^{\frac{n+2}{2}}}. \qquad (6.28)$$

Since the powers of r multiplying the incoming and outgoing components are identical, equation (5.56) may be used to calculate the absorption probability

$$|\mathcal{A}_{j\ell m}|^2 = 1-\left|\frac{A_{out}^{(\infty)}}{A_{in}^{(\infty)}}\right|^2 = 1-\left|\frac{B_1-iB_2}{B_1+iB_2}\right|^2 = \frac{2i\,(B^*-B)}{BB^*+i\,(B^*-B)+1}. \qquad (6.29)$$

6.3.1 A Numerical Check

To test the accuracy of the above analytic expression it is possible to follow the method of [95] and construct a numerical solution to the radial equation (6.7) using the `NDSolve` routine in Mathematica. It should be noted that the solution will not be exact as the low-order expansion of the angular eigenvalues (6.10) will be used in place of the exact values that would follow from numerical analysis of equation (6.8) also. However, in the low-$(a\omega)$ limit this numerical solution will serve as a good approximation to the true value, against which the analytic expression may be tested.

The boundary condition of no incoming waves at the horizon may be applied in the numerical routine by imposing, in the limit $r \to r_H$,

$$R(r) = 1\,, \qquad \frac{dR}{dr} = -\frac{ik}{f(r)}\,. \qquad (6.30)$$

This holds owing to the form of the very near-horizon solution written in terms of the tortoise-like coordinate in equation (6.18). Once the field equation has been solved numerically, the absorption probability may be extracted from the far-field limit of the solution. From equation (6.28) it is possible to define at infinity

$$B_+ = \frac{1}{2}e^{i\omega r}\left[r^{\frac{n+2}{2}}R+\frac{i}{\omega}\frac{d}{dr}\left(r^{\frac{n+2}{2}}R\right)\right] = \frac{1}{\sqrt{2\pi\omega}}(B_1+iB_2)e^{i\frac{\pi}{4}(2\nu+1)}, \qquad (6.31)$$
$$B_- = \frac{1}{2}e^{-i\omega r}\left[r^{\frac{n+2}{2}}R-\frac{i}{\omega}\frac{d}{dr}\left(r^{\frac{n+2}{2}}R\right)\right] = \frac{1}{\sqrt{2\pi\omega}}(B_1-iB_2)e^{-i\frac{\pi}{4}(2\nu+1)},$$

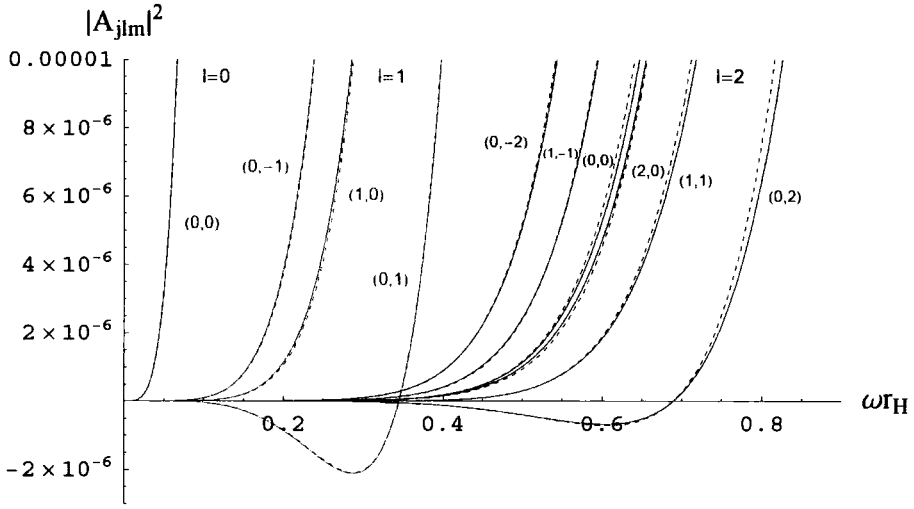

Figure 6.1: Absorption probabilities $|\mathcal{A}_{j\ell m}|^2$ for bulk scalar fields with $n = 2$, $a_* = 0.4$ and $\ell = 0$ (red), 1 (green) and 2 (blue), with individual modes labelled by the indices (j, m). Solid lines correspond to the analytic result (6.29), while dashed lines follow from numerical analysis.

and then the absorption probability can be extracted from the numerical radial solution using these quantities as

$$|\mathcal{A}_{j\ell m}|^2 = 1 - \left|\frac{B-i}{B+i}\right|^2 = 1 - \left|\frac{B_-}{B_+}\right|^2 . \tag{6.32}$$

6.3.2 Plotting the Absorption Probability

In figure 6.1 the absorption probability is plotted for the lowest partial waves with $n = 2$, $a_* = 0.4$, and values of j, ℓ, m obeying the restrictions (6.11). As in the on-brane case, the dominance of the first partial wave $j = \ell = m = 0$ is observed, and the suppression of $|\mathcal{A}_{j\ell m}|^2$ with increasing values of the angular momentum numbers is evident also. Superradiance can again be seen for modes with positive m. Figure 6.1 depicts both the value of $|\mathcal{A}_{j\ell m}|^2$ that follows from the analytic result (6.29) (solid lines), as well as that obtained by integrating the radial equation (6.7) numerically (dashed lines). As in the case of fields propagating on the brane, the approximate analytic method leads to values that are in excellent agreement with the numerical results, not only in the low-energy regime but beyond this also.

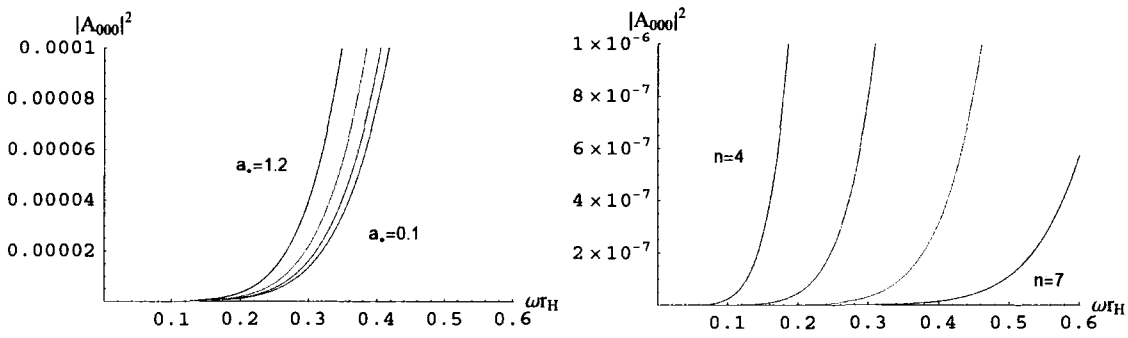

Figure 6.2: Absorption probabilities for the bulk scalar mode $j = \ell = m = 0$. The left-hand figure has variable a_*: $n = 4$ and $a_* = 0.1$ (red), 0.4 (green), 0.7 (light blue) and 1.2 (dark blue). The right-hand plot has variable n: $a_* = 0.5$ and $n = 4$ (red), 5 (green), 6 (light blue) and 7 (dark blue).

Focusing on the dominant first partial wave, figure 6.2 demonstrates the dependence of the absorption probability on the rotation parameter a_* and the number of extra dimensions n. From the left-hand plot it is clear that an increase in the rotation of the black hole causes an enhancement in the value of $|\mathcal{A}_{j\ell m}|^2$ in the low- and intermediate-energy regimes. The right-hand plot shows that the absorption probability is strongly suppressed as n increases. The latter behaviour was also found for bulk scalar fields propagating in the background of a spherically-symmetric higher-dimensional black hole [111].

An interesting question is how the absorption probabilities for brane and bulk scalar fields in a rotating black-hole background compare. By examining the results presented in this section and the previous chapter, it may be concluded that the absorption probabilities for both types of scalar field are enhanced as the black hole rotation parameter increases. In contrast to this, the value of the absorption probability increases with n for brane scalars, while it decreases for bulk scalar fields. Important conclusions may also be drawn by directly comparing figure 6.1 with the corresponding figure for on-brane emission 5.11: for the same values of n and a_*, the absorption probability for brane scalar fields is consistently larger than that for bulk scalars by almost 3 orders of magnitude, both for superradiant and non-superradiant modes. The same observation was made in the 5-dimensional case [122] – here, it

has been demonstrated that this behaviour persists for higher values of n.

6.4 The Low-Energy Limit

In the extreme low-energy limit a compact analytic expression for the absorption probability may be derived by following a similar procedure to that of §5.6. In the higher-dimensional case, as $\omega \to 0$, $B \propto 1/\omega^{2\ell+n+1}$, therefore

$$|\mathcal{A}_{j\ell m}|^2 \simeq 2i\left(\frac{1}{B} - \frac{1}{B^*}\right) . \tag{6.33}$$

Substituting for B from equation (6.27) it is found

$$\begin{aligned} |\mathcal{A}_{j\ell m}|^2 \;=\; & \frac{-2i\pi\,(\omega r_H/2)^{2\ell+n+1}}{(\ell+\frac{n+1}{2})\,\Gamma^2(\ell+\frac{n+1}{2})}\frac{\Gamma(2\beta+D_*-2)}{(1+a_*^2)^{-\frac{2\ell+n+1}{n+1}}\,\Gamma(2-2\beta-D_*)}\times \\ & \left[\frac{\Gamma(2+\alpha-\beta-D_*)\,\Gamma(1+\alpha-\beta)}{\Gamma(\alpha+\beta+D_*-1)\,\Gamma(\alpha+\beta)} - \frac{\Gamma(2-\alpha-\beta-D_*)\,\Gamma(1-\alpha-\beta)}{\Gamma(-\alpha+\beta+D_*-1)\,\Gamma(-\alpha+\beta)}\right] . \end{aligned} \tag{6.34}$$

Focusing attention on the dominant mode $j = \ell = m = 0$, and performing an analysis similar to that in §5.6, the extreme low-energy absorption probability may be written

$$|\mathcal{A}_{000}|^2 = \frac{4\pi(1+a_*^2)^2(\omega r_H)^{n+2}}{A_*\,2^n(n+1)\Gamma^2\left(\frac{n+1}{2}\right)(2-D_*)} + \ldots . \tag{6.35}$$

The above result allows computation of the higher-dimensional absorption cross-section $\sigma^{(0)}_{0,n}$ for the dominant bulk scalar mode in the asymptotic low-energy regime. The cross-section for a scalar partial wave indexed by the values (j,ℓ,m) may be written as

$$\begin{aligned} \sigma^{(0)}_{j\ell m}(\omega) \;&=\; \frac{2^{n+1}\pi^{\frac{n+1}{2}}}{\omega^{n+2}}\Gamma\left(\frac{n+3}{2}\right) N_j\,|\mathcal{A}_{j\ell m}|^2 \\ &=\; \frac{2^n}{\pi}\Gamma^2\left(\frac{n+3}{2}\right)\frac{A_H}{(\omega r_H)^{n+2}}\,\frac{N_j}{(1+a_*^2)}\,|\mathcal{A}_{j\ell m}|^2 , \end{aligned} \tag{6.36}$$

where

$$N_j = \frac{(2j+n-1)(j+n-2)!}{j!\,(n-1)!} , \qquad A_H = \frac{2\pi^{\frac{n+3}{2}} r_H^n\,(r_H^2+a^2)}{\Gamma\left(\frac{n+3}{2}\right)} \tag{6.37}$$

are the multiplicity of the jth partial wave in the expansion of the wave function over the hyperspherical harmonics on the n-sphere, and the horizon area of the

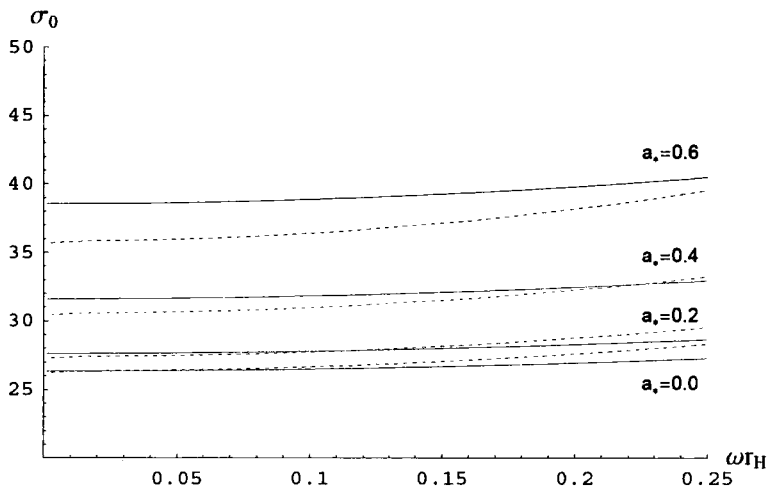

Figure 6.3: Absorption cross-section for the bulk scalar mode $j = \ell = m = 0$, for $n = 2$ and various values of a_*.

$(4+n)$-dimensional rotating black hole, respectively. Substituting for the low-energy absorption probability (6.35) in the above recovers the low-energy cross-section as

$$\sigma_0^{(0)}(\omega) \simeq \frac{(n+1)(1+a_*^2)A_H}{A_*(2-D_*)} + \dots . \tag{6.38}$$

For $a_* \to 0$ this reduces to A_H, a behaviour that was found in the analysis of a static black hole [111]. For $a_* \neq 0$, the numerical results (dashed lines) presented in figure 6.3 confirm that, here also, the low-energy limit of the cross-section tends to the full higher-dimensional area of the corresponding rotating black hole. The solid lines demonstrate the agreement of the analytic results with the numerical ones for small values of a_*, and the deviation that occurs as the rotation parameter is increased.

6.5 The Energy Emission Rate

Having found the absorption probability it is now possible to compute the rate of energy emission of massless scalar fields in the bulk. This is given by the expression

$$\frac{d^2E}{dtd\omega} = \frac{1}{2\pi} \sum_{j,\ell,m} \frac{\omega}{\exp\left[k/T_{\rm H}\right] - 1} N_j \left|\mathcal{A}_{j\ell m}\right|^2 . \tag{6.39}$$

The above differs from the 4-dimensional expression (4.19) in the presence of an additional sum over the new angular momentum number j, and from the 5-dimensional

one [110] in the introduction of the multiplicity of states N_j (6.37) following from expansion of the wavefunction over the n-dimensional sphere.

A useful check of the validity of the above emission rate is to take the non-rotating limit. In this circumstance equation (6.39) should reduce to the well-known result for bulk scalar emission from a $(4+n)$-dimensional Schwarzschild black hole [111, 113]

$$\frac{d^2E}{dtd\omega} = \frac{1}{2\pi}\sum_{\ell}\frac{\omega}{\exp\left[\omega/T_{\rm H}\right]-1}N_\ell\left|\mathcal{A}_\ell\right|^2\,, \tag{6.40}$$

where N_ℓ is the degeneracy of the ℓth mode of the harmonics on the $(n+2)$-sphere

$$N_\ell = \frac{(2\ell+n+1)(\ell+n)!}{\ell!\,(n+1)!}\,. \tag{6.41}$$

In the limit $a \to 0$, then $k=\omega$, and the absorption probability becomes independent of both m and j, retaining a dependence only on the principal quantum number ℓ. Equation (6.39) then matches (6.40) providing the following relation holds

$$\sum_{j,m} N_j = \sum_{j=0}^{\ell}(\ell-j+1)\,\frac{(2j+n-1)(j+n-2)!}{j!\,(n-1)!} \equiv N_\ell\,. \tag{6.42}$$

The first equality in the above equation holds since, according to the restrictions (6.11) imposed on the quantum numbers, for each value of (j,ℓ) m may take $\ell-j+1$ values and for each value of ℓ, j may take the values $0 \le j \le \ell$. In order to prove equation (6.42), the factor $2j+n-1$ is rewritten as $(j+n-1)+j$ and the sum is then split into two parts. Replacing the index j by $i-n+1$ in the first sum and by $i-n+2$ in the second, the middle part of equation (6.42) takes the form

$$\sum_{i=n-1}^{\ell+n-1}(\ell+n-1-i+1)\,C(i,n-1) + \sum_{i=n-1}^{\ell+n-2}(\ell+n-2-i+1)\,C(i,n-1)\,, \tag{6.43}$$

where $C(s,r)$ is the combination function, $C(s,r) = \frac{s!}{r!(s-r)!}$. By using the identity

$$\sum_{i=r}^{s}(s-i+1)\,C(i,r) = C(s+2,r+2)\,, \tag{6.44}$$

the first sum in equation (6.43) reduces to $C(\ell+n+1,n+1)$, and the second to $C(\ell+n,n+1)$. The sum of these two combination functions is equal to N_ℓ.

By using equation (6.39) the energy emission rate of bulk scalar fields from a higher-dimensional rotating black hole is plotted in figure 6.4 and its dependence on

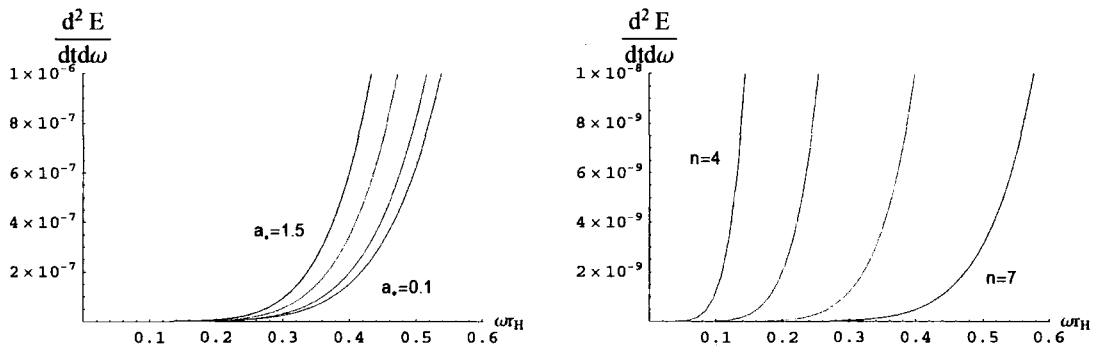

Figure 6.4: Energy emission rates for bulk scalar fields. The left-hand figure has variable a_*: $n = 5$ and $a_* = 0.1$ (red), 0.5 (green), 1.0 (light blue) and 1.5 (dark blue). The right-hand plot has variable n: $a_* = 0.5$ and $n = 4$ (red), 5 (green), 6 (light blue) and 7 (dark blue).

the angular momentum parameter and number of extra dimensions is illustrated. The profile exhibited by the absorption probability is also observed here: the emission rate is enhanced with a_* in the low-energy regime, as was the case for brane particles, but is suppressed in terms of n. Drawing experience from previous studies, the enhancement resulting from increased black hole rotation is expected to persist over the entire range of energy – on the other hand it is likely, given the similarity of the results with those for bulk scalar fields in a non-rotating background [111], that the low-energy suppression with n will be replaced by a strong enhancement at the high-energy regime.

Finally, it is important to address the question of the brane-to-bulk ratio of the rate of scalar field energy emission from a higher-dimensional rotating black hole. The answer to this question will define the amount of energy spent by the black hole in the observable brane channel. The comparison of bulk and brane absorption probabilities discussed in the previous section has given a clear signal as to which emission is dominant, however the final comparison should involve the total emission rates where the different multiplicities of states have been taken into account. By using equations (6.39) and (4.19), the brane-to-bulk ratio for scalar fields emitted by a rotating black hole is depicted in figure 6.5. It may easily be observed that increasing n greatly increases this ratio, suggesting the brane channel is more highly

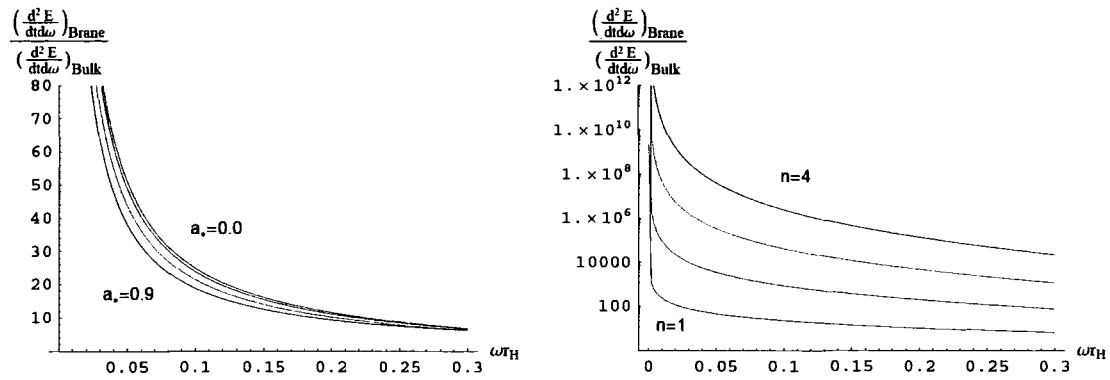

Figure 6.5: Brane-to-bulk ratio of the energy emission rates for scalar fields. The left-hand figure illustrates the dependence on a_* for $n = 1$ and $a_* = 0$ (red), 0.3 (green), 0.6 (light blue) and 0.9 (dark blue). The right-hand plot demonstrates the dependence on n for $a_* = 0.5$ and $n = 1$ (red), 2 (green), 3 (light blue) and 4 (dark blue).

favoured in higher-dimensional spacetimes. Increasing a_* suppresses the ratio in the low-energy limit, although the effect is slight. It should be noted that in all cases the ratio of the brane to bulk emission rate always remains above unity, rendering the brane channel dominant. This result, along with the strong n-dependence, was also found in the study of radiation from a Schwarzschild black hole [111].

6.6 Summary

In this chapter the emission of scalar particles from a higher-dimensional rotating black hole into the bulk spacetime has been investigated. The method used for brane scalar particles in the previous chapter has been extended to the full bulk spacetime to derive an analytic solution to the radial part of the field equation. This was then used to calculate absorption probabilities, cross-sections and finally the energy emission rate. A numerical analysis of the radial equation has also been performed and found to be in good agreement with the analytic expressions.

Many of the same dependencies on model parameters were found as in the case of on-brane emission. The notable exception to this is that the absorption probability, and consequently the energy emission rate, decreases with increasing number of

extra dimensions n for emission in the bulk. While this is in contrast to the on-brane behaviour, a similar trend was found in emission from a static black hole [111]. Comparison of bulk and brane absorption probabilities revealed that, for a given mode, emission on the brane is favoured by approximately three orders of magnitude.

An analysis of the bulk scalar rate of energy emission revealed its behaviour is largely inherited from the absorption probability, showing an increase with a_*, but decrease with n. Calculation of this rate permitted determination of the fraction of the black hole's total scalar energy emission that is potentially detectable on the brane, taking into account the differing multiplicity of states between brane and bulk particle modes. In the low-energy limit the brane-to-bulk ratio is consistently above unity, tending rapidly to infinity as the emitted particle's energy approached zero. An increase in the number of extra dimensions brings a dramatic increase in the ratio, as also found in studies of the Schwarzschild case, while increasing angular momentum of the black hole introduces a very mild suppression.

The quantities presented here are all valid in the low-ω_*, low-a_* limit and so cannot be used to integrate over ω and determine the total energy emission rate into a given mode. Also, when deciding how much of the black hole's total energy is available on the brane for detection, no mention has yet been made of energy lost in the form of bulk gravitons. Owing to the higher degree of complexity involved in deriving the appropriate field equations for gravitons, this is a topic that has only recently been studied for a higher-dimensional Schwarzschild black hole [5].

Chapter 7

Bulk Graviton Emission in the Schwarzschild Phase

Gravitational perturbations of a $D = 4+n$-dimensional static black hole with metric [151]

$$ds^2 = -h(r)\,dt^2 + \frac{dr^2}{h(r)} + r^2 d\Omega_{2+n}^2\,, \qquad h(r) = 1 - \frac{\mu}{r^{n+1}}\,, \tag{7.1}$$

(which follows from taking the limit $a \to 0$ of the Myers-Perry solution (4.3)) may be decomposed into a symmetric traceless tensor, a vector and a scalar component [152]. Owing to the $SO(2+n)$ symmetry of the above metric, these perturbations can be further expanded in terms of the spin-weighted spherical harmonics on the S^{2+n} unit sphere. Using this decomposition and employing a gauge-invariant formalism [153] the graviton field equations $\delta R_{AB} = 0$ are completely separable and the radial components may be written in terms of a number of gauge-invariant variables [154]. For each species of gravitational perturbation it is possible to define a "master variable" Φ in terms of the gauge-invariant variables so that the radial equations for all three types of gravitational perturbation may be written as a Schrodinger-like equation

$$h\frac{d}{dr}\left(h\frac{d\Phi}{dr}\right) + (\omega^2 - V)\,\Phi = 0\,. \tag{7.2}$$

The form of the potential V varies depending on the type of perturbation. For tensor and vector-like perturbations

$$V_{T,V} = \frac{h(r)}{r^2}\left[\ell(\ell+n+1) + \frac{n(n+2)}{4} - \frac{k(n+2)^2}{4}\left(\frac{r_H}{r}\right)^{n+1}\right], \tag{7.3}$$

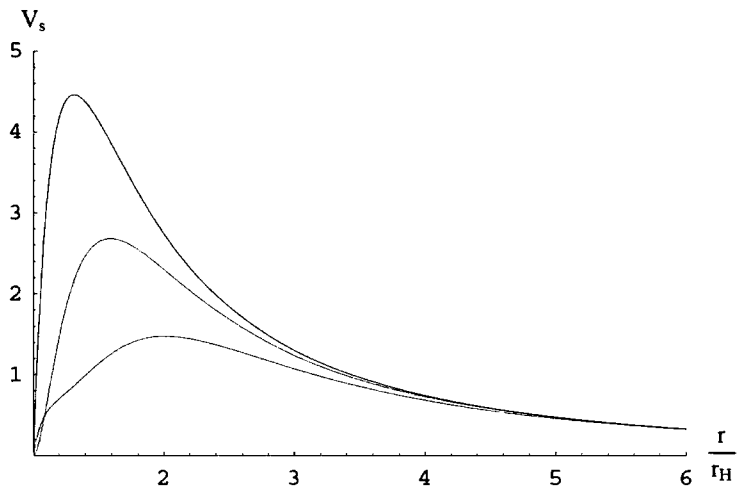

Figure 7.1: Comparison of the potentials experienced by scalar (red), vector (green) and tensor (blue) gravitational perturbations for $n = 2$ and $\ell = 2$.

with $k = -1$ and $k = 3$ respectively, and ℓ being the angular momentum quantum number of the mode in the expansion of the field over the spherical harmonics. For scalar gravitational perturbations the form of the potential is rather more complicated

$$V_S = \frac{h(r)}{r^2} \frac{q(1-h)^3 + p(1-h)^2 + w(1-h) + z}{4\left[2m + (n+2)(n+3)(1-h)\right]^2} . \tag{7.4}$$

In the above $m \equiv \ell(\ell + n + 1) - n - 2$, and

$$\begin{aligned} q &\equiv (n+2)^4(n+3)^2 , \qquad z \equiv 16m^3 + 4m^2(n+2)(n+4) , \\ p &\equiv (n+2)(n+3)\left[4m\left(2n^2+5n+6\right) + n(n+2)(n+3)(n-2)\right] , \\ w &\equiv -12m\,(n+2)\left[m(n-2) + n(n+2)(n+3)\right] . \end{aligned} \tag{7.5}$$

For illustration, the potentials experienced by each of the three types of gravitational perturbation are shown in figure 7.1 for the case $n = 2$, $\ell = 2$.

7.1 Solving the Field Equations

Equation (7.2) has no known analytic solution over the entire range of the radial coordinate for any of the potentials (7.3)-(7.4). In order to proceed it is possible to

once again adopt the approximate method that has been used to solve the radial equations in the previous two chapters.

Concentrating first on derivation of the near-horizon solution, it is possible to treat tensor and vector perturbations together, owing to the similarity in the form of their potentials (7.3). The more complicated scalar potential (7.4) must be considered separately. Employing the change of variable $r \to h(r)$ allows equations (7.2)-(7.3) for tensors and vectors to be rewritten in the near-horizon region in the form

$$h\,(1-h)\,\frac{d^2\Phi}{dh^2} + \left[1 - \frac{(2n+3)}{(n+1)}\,h\right]\frac{d\Phi}{dh} + \left[\frac{(\omega r_H)^2}{(n+1)^2 h(1-h)} - \frac{\tilde{A}}{(1-h)} + \frac{k(n+2)^2}{4(n+1)^2}\right]\Phi = 0\,, \quad (7.6)$$

where again $k = -1$ for tensors and $k = 3$ for vectors, and the quantity

$$\tilde{A} \equiv \frac{\ell(\ell+n+1)}{(n+1)^2} + \frac{n(n+2)}{4(n+1)^2}\,, \quad (7.7)$$

has been defined for convenience.

The above equation takes the form of a hypergeometric equation (5.20) if the field redefinition $\Phi(h) = h^\alpha(1-h)^\beta F(h)$ is made and the constants a, b and c are identified as

$$a = \alpha + \beta + \frac{(n+2)}{2(n+1)} + G\,, \qquad b = \alpha + \beta + \frac{(n+2)}{2(n+1)} - G\,, \qquad c = 1 + 2\alpha\,, \quad (7.8)$$

where G is an arbitrary constant. Furthermore, demanding that the coefficient of $F(h)$ in the transformed equation be exactly $-ab$ yields three additional constraints that determine the remaining unknown constants, α, β and G

$$\alpha_\pm = \pm\frac{i\omega r_H}{n+1}\,, \quad (7.9)$$

$$\beta_\pm = \frac{-1 \pm \sqrt{(2\ell+n+1)^2 - 4\omega^2 r_H^2}}{2(n+1)}\,, \quad (7.10)$$

$$G^{(T,V)} = \frac{(1+k)(n+2)}{4(n+1)}\,. \quad (7.11)$$

Then, the general solution of the transformed radial equation (7.6) may be written as

$$\Phi_{NH}(h) = A_- h^\alpha\,(1-h)^\beta\,F(a,b,c;h) + A_+\,h^{-\alpha}\,(1-h)^\beta\,F(a-c+1, b-c+1, 2-c; h)\,, \quad (7.12)$$

where $A_{\pm}$ are arbitrary integration constants. Once again, the boundary condition of no outgoing waves immediately outside the black-hole horizon may be ensured by expanding the solution in the limit $r \to r_H$, or equivalently $h \to 0$, in which case

$$\Phi_{NH}(h) \simeq A_- \, h^{\alpha} + A_+ \, h^{-\alpha} = A_- \, e^{\pm i\omega y} + A_+ \, e^{\mp i\omega y} \,, \tag{7.13}$$

where, in the last part of the above equation, the tortoise-like coordinate in the Schwarzschild spacetime

$$\frac{dy}{dr} = \frac{r_H^{n+2}}{h(r)\, r^{n+2}} \,, \tag{7.14}$$

has been used. The asymptotic near-horizon solution is written in terms of both incoming and outgoing plane waves since very close to the horizon, as illustrated in figure 7.1, the potential V for all types of gravitational perturbation vanishes. As in the bulk scalar case, performing the interchange $\alpha_+ \leftrightarrow \alpha_-$ simply interchanges the integration constants $A_- \leftrightarrow A_+$ in equation (7.12), therefore the sign of α can be chosen arbitrarily; to be consistent with the conventions of previous chapters the choice $\alpha = \alpha_-$ has been made. The aforementioned boundary condition then forces the outgoing wave to be discarded by setting $A_+ = 0$. The sign in the expression for β is again fixed by imposing the convergence condition of the hypergeometric function, $\mathrm{Re}\,(c - a - b) = -\frac{1}{n+1} - 2\beta > 0$, which demands the choice $\beta = \beta_-$ be made. This brings the near-horizon solution to its final form

$$\Phi_{NH}(h) = A_- h^{\alpha} \, (1-h)^{\beta} \, F(a, b, c; h) \,. \tag{7.15}$$

In the case of scalar gravitational perturbations, by employing the same change of variable, the corresponding near-horizon field equation can be brought to the form

$$h\,(1-h)\,\frac{d^2\Phi}{dh^2} + \left[1 - \frac{(2n+3)}{(n+1)}\,h\right]\frac{d\Phi}{dh} + \left[\frac{(\omega r_H)^2}{(n+1)^2 h(1-h)} - \frac{\tilde{A}}{(1-h)} - C\right]\Phi = 0 \,, \tag{7.16}$$

where $\tilde{A}$ was defined in equation (7.7) and the quantity C is

$$C \equiv \frac{q(1-h)^2 + \tilde{p}(1-h) + \tilde{w}}{4(n+1)^2[2m + (n+2)(n+3)(1-h)]^2} \,, \tag{7.17}$$

with

$$\tilde{p} = p - \frac{z(n+2)^2(n+3)^2}{4m^2}, \tag{7.18}$$

$$\tilde{w} = w - \frac{z(n+2)(n+3)}{m}. \tag{7.19}$$

In this form, equation (7.16) has poles at $h = 0$ and $h = 1$ (or, at $r = r_H$ and $r = \infty$, respectively) while the quantity C takes on a constant value in both limits.

In order to transform this equation to hypergeometric form using the same field redefinition as in the vector and tensor case, it is important that the third term in the part of equation (7.16), proportional to Φ, is a constant. Since this equation is valid in the near-horizon regime, the most obvious choice of constant is that which arises by taking the limit $h \to 0$ in the expression for C (7.17)

$$C_0 = \frac{q + \tilde{p} + \tilde{w}}{4(n+1)^2[2m + (n+2)(n+3)]^2}. \tag{7.20}$$

The method then proceeds exactly as before, with the hypergeometric indices (a, b, c) given by equations (7.8), and the powers (α, β) by (7.9)–(7.10). The only difference arises in the constant G that, in the case of scalar perturbations, takes the value

$$G^{(S)} = \sqrt{\frac{(n+2)^2}{4(n+1)^2} - C_0}. \tag{7.21}$$

By applying the same boundary condition, the general solution for scalar perturbations in the near-horizon regime is also given by equation (7.15), with $\alpha = \alpha_-$ and $\beta = \beta_-$.

Next, the solution in the far-field regime is constructed. In the limit $r \gg r_H$, $h \to 1$, and the radial equation for all types of gravitational perturbations takes the simplified form

$$\frac{d^2\Phi}{dr^2} + \left(\omega^2 - \frac{(n+1)^2\tilde{A}}{r^2}\right)\Phi = 0, \tag{7.22}$$

where $\tilde{A}$ was defined in equation (7.7). By setting $\Phi = \sqrt{r}\,R$, the new radial function R is found to satisfy a Bessel differential equation

$$\frac{d^2R(z)}{dz^2} + \frac{1}{z}\frac{dR(z)}{dz} + \left(1 - \frac{\nu^2}{z^2}\right)R(z) = 0, \tag{7.23}$$

with $z = \omega r$ and $\nu = \ell + (n+1)/2$. Therefore, the general analytic solution to the field equation for all species of graviton in the far-field limit can be written as

$$\Phi_{FF}(r) = B_1 \sqrt{r}\, J_{\ell+\frac{n+1}{2}}(\omega r) + B_2 \sqrt{r}\, Y_{\ell+\frac{n+1}{2}}(\omega r)\,, \tag{7.24}$$

where J_ν and Y_ν are Bessel functions of the first and second kind, respectively, and $B_{1,2}$ are arbitrary integration constants.

To construct the complete radial solution it is necessary to stretch the near-horizon solution (7.15) towards large values of r, and the far-field solution (7.24) towards the origin. The near-horizon solution may be stretched by using the hypergeometric function identity (5.35) in equation (7.15), before taking the limit $r \gg r_H$, or $h \to 1$. This then yields

$$\Phi_{NH}(r) \simeq A_- \left(\frac{r_H}{r}\right)^{\beta(n+1)} \frac{\Gamma(c)\,\Gamma(c-a-b)}{\Gamma(c-a)\,\Gamma(c-b)} + A_- \left(\frac{r_H}{r}\right)^{-1-\beta(n+1)} \frac{\Gamma(c)\,\Gamma(a+b-c)}{\Gamma(a)\,\Gamma(b)}\,. \tag{7.25}$$

Turning next to the far-field solution, it may be expanded in the opposite limit, $r \to 0$, by using the standard formulae, (5.78) and (5.79), for the Bessel functions as the argument $z \to 0$ in equation (7.24) to obtain

$$\Phi_{FF}(r) \simeq B_1 \left(\frac{\omega}{2}\right)^{\ell+\frac{n+1}{2}} \frac{r^{\ell+\frac{n}{2}+1}}{\Gamma\left(\ell+\frac{n+3}{2}\right)} - \frac{B_2}{\pi}\left(\frac{2}{\omega}\right)^{\ell+\frac{n+1}{2}} \frac{\Gamma\left(\ell+\frac{n+1}{2}\right)}{r^{\ell+\frac{n}{2}}}\,. \tag{7.26}$$

To ensure the stretched forms of the two asymptotic solutions match it is necessary to take the low-energy limit $\omega r_H \ll 1$ in the expression of β, equation (7.10). At first-order approximation, the ωr_H-term may be ignored, in which case $\beta(n+1) \to -(\ell + n/2 + 1)$ and the powers of r in equations (7.25) and (7.26) become identical. A smooth matching is then achieved, and a complete solution is constructed, providing the following relations between the near-horizon and far-field integration constants hold

$$\frac{B_1}{A_-} = \left(\frac{2}{\omega r_H}\right)^{\ell+\frac{n+1}{2}} \frac{\Gamma\left(\ell+\frac{n+3}{2}\right)\,\Gamma(c)\,\Gamma(c-a-b)}{\Gamma(c-a)\,\Gamma(c-b)\,\sqrt{r_H}}\,, \tag{7.27}$$

$$\frac{B_2}{A_-} = -\pi\left(\frac{\omega r_H}{2}\right)^{\ell+\frac{n+1}{2}} \frac{\Gamma(c)\,\Gamma(a+b-c)}{\Gamma\left(\ell+\frac{n+1}{2}\right)\,\Gamma(a)\,\Gamma(b)\,\sqrt{r_H}}\,. \tag{7.28}$$

This completes the derivation of a low-energy analytical solution to the field equations for all types of gravitational perturbations propagating in a $(4+n)$-dimensional

Schwarzschild black-hole background. With these solutions it is now possible to calculate the corresponding absorption probabilities.

7.2 The Absorption Probability

In the limit $r \to \infty$ the effective potentials for all types of gravitational perturbation again vanish due to the asymptotically flat nature of the metric. In this regime the general solution is described by incoming and outgoing plane waves, the form of which can be found by approximating the Bessel functions using equations (5.82) and (5.83). Equation (7.24) becomes

$$\Phi_{FF}(r) \simeq \frac{1}{\sqrt{2\pi\omega}} \left\{ (B_1 - iB_2)\, e^{i\left(\omega r - \frac{\pi}{2}\nu - \frac{\pi}{4}\right)} + (B_1 + iB_2)\, e^{-i\left(\omega r - \frac{\pi}{2}\nu - \frac{\pi}{4}\right)} \right\} + \ldots , \tag{7.29}$$

where as before $\nu = \ell + (n+1)/2$. Since the incoming and outgoing wave components decay at the same rate, the absorption probability may be evaluated using equation (5.56)

$$|\mathcal{A}_\ell|^2 = 1 - |\mathcal{R}_\ell|^2 = 1 - \left| \frac{A_\ell^{(out)}}{A_\ell^{(in)}} \right|^2 = 1 - \left| \frac{B - i}{B + i} \right|^2 , \tag{7.30}$$

where $A_\ell^{(in)}$ and $A_\ell^{(out)}$ are the incoming and outgoing wave amplitudes evaluated at infinity and B is defined as

$$B \equiv \frac{B_1}{B_2} = -\left(\frac{2}{\omega r_H}\right)^{2\ell+n+1} \frac{\Gamma\left(\ell + \frac{n+3}{2}\right)\, \Gamma\left(\ell + \frac{n+1}{2}\right)\, \Gamma(a)\, \Gamma(b)\, \Gamma(c-a-b)}{\pi\, \Gamma(c-a)\, \Gamma(c-b)\, \Gamma(a+b-c)} . \tag{7.31}$$

The above two equations define the low-energy analytic absorption coefficient associated with the propagation of gravitons in the higher-dimensional black hole background given in equation (7.1). Individual solutions for scalar, vector and tensor components of the gravitational perturbations follow upon substituting the corresponding values for the hypergeometric indices (a, b, c) found in the previous section.

As in previous chapters, a compact low-energy expression for the absorption probability may be derived for gravitons. For convenience the hypergeometric indices are rewritten as

$$a = \alpha + \beta + G_1 , \qquad b = \alpha + \beta + G_2 , \qquad c = 1 + 2\alpha , \tag{7.32}$$

where

$$G_1 \equiv \frac{n+2}{2(n+1)} + G\,, \qquad G_2 \equiv \frac{n+2}{2(n+1)} - G\,. \tag{7.33}$$

As G takes a different value for each type of perturbation under consideration, $G_{1,2}$ will also. Since $B \sim 1/(\omega r_H)^{2\ell+n+1}$, then in the extreme low-energy limit $BB^* \gg i(B^* - B) \gg 1$. Therefore, by keeping only the dominant term in the denominator

$$|\mathcal{A}_\ell|^2 = 2i\left(\frac{1}{B} - \frac{1}{B^*}\right) = K(\omega r_H, \beta)\,\left[Z(\alpha,\beta) - Z^*(\alpha,\beta)\right]\,, \tag{7.34}$$

where

$$K(\omega r_H, \beta) \equiv -\left(\frac{\omega r_H}{2}\right)^{2\ell+n+1} \frac{2i\pi\,\left(\ell + \frac{n+1}{2}\right)}{\Gamma\left(\ell + \frac{n+3}{2}\right)^2}\,\frac{\Gamma(-1+2\beta+G_1+G_2)}{\Gamma(1-2\beta-G_1-G_2)} \tag{7.35}$$

and

$$Z(\alpha,\beta) \equiv \frac{\Gamma(1+\alpha-\beta-G_1)\,\Gamma(1+\alpha-\beta-G_2)}{\Gamma(\alpha+\beta+G_1)\,\Gamma(\alpha+\beta+G_2)}\,. \tag{7.36}$$

Using the Gamma-function identity

$$\Gamma(x)\,\Gamma(1-x) = -x\,\Gamma(-x)\,\Gamma(x) = \frac{\pi}{\sin(\pi x)}\,, \tag{7.37}$$

the definitions of $G_{1,2}$ (7.33) and keeping only the dominant term

$$\beta^{(0)} \equiv -\frac{(2\ell+n+2)}{2(n+1)}\,, \tag{7.38}$$

in the expansion of β (equation (7.10)), then $K(\omega r_H, \beta)$ may be written in the limit $\omega r_H \ll 1$ as

$$K(\omega r_H, \beta) = \left(\frac{\omega r_H}{2}\right)^{2\ell+n+1} \frac{i\pi^2\,(n+1)}{\Gamma\left(\ell+\frac{n+3}{2}\right)^2\,\Gamma\left(1+\frac{2\ell}{n+1}\right)^2\,\sin\left[\pi(2\beta^{(0)}+G_1+G_2)\right]}\,. \tag{7.39}$$

Considering next the expression for $Z(\alpha,\beta)$, the only complex quantity appearing is α, which is purely imaginary, therefore $Z^*(\alpha,\beta) = Z(-\alpha,\beta)$. By using the same Gamma-function identity as above, it is possible to write

$$Z - Z^* = \frac{\pi^2}{|\Gamma(\alpha+\beta+G_1)|^2\,|\Gamma(\alpha+\beta+G_2)|^2} \times \tag{7.40}$$

$$\frac{\sin\left[\pi(\alpha+\beta+G_1)\right]\,\sin\left[\pi(\alpha+\beta+G_2)\right] - \sin\left[\pi(\alpha-\beta-G_1)\right]\,\sin\left[\pi(\alpha-\beta-G_2)\right]}{|\sin\left[\pi(\alpha+\beta+G_1)\right]|^2\,|\sin\left[\pi(\alpha+\beta+G_2)\right]|^2}\,.$$

Finally, expanding in the limit $\omega r_H \ll 1$, or equivalently $\alpha \to 0$

$$Z - Z^* = \frac{2\alpha}{\pi} \sin\left[\pi(2\beta^{(0)} + G_1 + G_2)\right] \Gamma(1 - \beta^{(0)} - G_1)^2 \Gamma(1 - \beta^{(0)} - G_2)^2 . \quad (7.41)$$

By combining equations (7.39) and (7.41), the asymptotic low-energy absorption probability may be written in the relatively compact analytic form

$$|\mathcal{A}_\ell|^2 = 4\pi \left(\frac{\omega r_H}{2}\right)^{2\ell+n+2} \frac{\Gamma\left(1 + \frac{\ell}{n+1} - G\right)^2 \Gamma\left(1 + \frac{\ell}{n+1} + G\right)^2}{\Gamma\left(\ell + \frac{n+3}{2}\right)^2 \Gamma\left(1 + \frac{2\ell}{n+1}\right)^2} . \quad (7.42)$$

In the above the zero-order approximation for $\beta \simeq \beta^{(0)}$ has been used again and also the definitions (7.33) to recover the dependence on the parameter G. According to equation (7.11), the value of G is zero for tensor perturbations and $\frac{n+2}{n+1}$ for vector ones, while for scalar gravitons its value is given in equation (7.21). In the case of tensor perturbations it can be shown that the above result reduces to that of the absorption probability for a scalar field propagating in the bulk [113]. This result could have been anticipated by examining the equation satisfied by tensor gravitational perturbations in the bulk more closely: starting from equation (7.2) and setting $\Phi^{(T)}(r) = \sqrt{r^{n+2}}\,\Phi(r)$, the new radial function $\Phi(r)$ is found to satisfy the equation of a scalar field (equation (10) in [113]) propagating in the static, higher-dimensional black-hole background (7.1).

From equation (7.42), it is clear that the absorption probability depends on both the angular momentum quantum number ℓ and number of extra dimensions n, through the arguments of the Gamma functions as well as the power of ωr_H. As either ℓ or n increases, the power of ωr_H increases too which, for $\omega r_H \ll 1$, causes a suppression in the value of $|\mathcal{A}_\ell|^2$. As the behaviour of the remaining factor is less clear table 7.1 displays the explicit value of $|\mathcal{A}_\ell|^2$ for all three types of gravitational perturbation, as follows from the simplified expression (7.42), for the indicative values $n = 2, 4, 6$ and $\ell = 2, 3, 4$. From these entries, one may easily conclude that, as either ℓ or n increases, the value of $|\mathcal{A}_\ell|^2$ for all types of gravitational perturbation in the asymptotic low-energy regime is significantly suppressed. It should be noted also that, for the same values of ℓ and n, $|\mathcal{A}_\ell|^2$ assumes a different value for each type of perturbation. From table 7.1 it appears that the tensor perturbations are suppressed by orders of magnitude in comparison to the other two, while the relative

n	ℓ	p	$\lvert\mathcal{A}_\ell^{(\mathrm{T})}\rvert^2$	$\lvert\mathcal{A}_\ell^{(\mathrm{V})}\rvert^2$	$\lvert\mathcal{A}_\ell^{(\mathrm{S})}\rvert^2$
$n=2$	$\ell=2$	8	$1.7\cdot10^{-4}$	$7.4\cdot10^{-3}$	$2.7\cdot10^{-3}$
	$\ell=3$	10	$1.1\cdot10^{-6}$	$1.6\cdot10^{-5}$	$1.8\cdot10^{-5}$
	$\ell=4$	12	$4.6\cdot10^{-9}$	$3.7\cdot10^{-8}$	$5.5\cdot10^{-8}$
$n=4$	$\ell=2$	10	$3.2\cdot10^{-6}$	$2.2\cdot10^{-4}$	$3.4\cdot10^{-5}$
	$\ell=3$	12	$1.9\cdot10^{-8}$	$4.2\cdot10^{-7}$	$3.1\cdot10^{-7}$
	$\ell=4$	14	$8.1\cdot10^{-11}$	$9.5\cdot10^{-10}$	$1.3\cdot10^{-9}$
$n=6$	$\ell=2$	12	$3.1\cdot10^{-8}$	$3.2\cdot10^{-6}$	$2.2\cdot10^{-7}$
	$\ell=3$	14	$1.5\cdot10^{-10}$	$4.7\cdot10^{-9}$	$1.9\cdot10^{-9}$
	$\ell=4$	16	$5.4\cdot10^{-13}$	$8.9\cdot10^{-12}$	$8.4\cdot10^{-12}$

Table 7.1: Dependence of the absorption probability for tensor, vector and scalar gravitational perturbations in the bulk on n and ℓ, in the asymptotic regime $\omega r_H \to 0$. Entries represent coefficients of $(\omega r_H)^p$, eg. for tensor perturbations with $\ell = 2$, $n = 2$ the absorption probability should read $|\mathcal{A}_\ell^{(T)}|^2 = 1.7\cdot10^{-4}\,(\omega r_H)^8$.

magnitude of vectors and scalars strongly depends on the particular values of ℓ and n chosen. As tensor perturbations have the same absorption probability as bulk scalar fields, it would be interesting to determine whether gravitons dominate over scalar fields during the emission of Hawking radiation in the bulk.

In deriving the absorption probability for gravitational perturbations in the bulk the low-energy assumption was made only once – during the matching of the two asymptotic solutions in the intermediate zone. Nevertheless, that was sufficient to restrict the validity of the solution to values of the energy parameter ωr_H well below unity. The simplified analytical result (7.42) emerged after a series of expansions in the arguments of the Gamma functions appearing in equations (7.31) and consequently its validity is rather more restricted. Table 7.2 offers a comparison of the values of the absorption coefficient derived by using the two analytical expressions, equations (7.30)-(7.31) and (7.42), as ωr_H ranges from 0.001 to 0.5. It may easily be seen that, for very low values of ωr_H, the agreement between the two expressions

ωr_H	$\lvert\mathcal{A}_\ell^{(T)}\rvert^2$ (simplified expression)	$\lvert\mathcal{A}_\ell^{(T)}\rvert^2$ (exact expression)
0.001	1.6997×10^{-28}	1.6997×10^{-28}
0.01	1.6997×10^{-20}	1.6999×10^{-20}
0.1	1.6697×10^{-12}	1.7112×10^{-12}
0.3	1.1152×10^{-8}	1.1839×10^{-8}
0.5	6.6396×10^{-7}	7.8001×10^{-7}

Table 7.2: Deviation between the values of the absorption probability for tensor gravitational perturbations given by the simplified and complete analytical expressions for $n = 2$, $\ell = 2$ and different values of $\omega r_H < 1$.

is remarkable; however, as ωr_H reaches 0.5, the values deviate by as much as 15%.

In the final stages of preparation of these results for publication [5] a number of additional papers appeared in the literature [155–157] that also study emission of bulk gravitons in a higher-dimensional Schwarzschild background. The results for vector and tensor perturbations in [156] are in excellent agreement with those presented here, however, in contradiction to that just derived, it is claimed that scalar gravitational perturbations cannot be treated analytically and a numerical result is provided instead. Examination of this numerical expression found it to disagree significantly with the analytical result derived above for scalars[1], so a numerical analysis of the problem was required to independently check the extent to which the absorption coefficients (7.30)-(7.31) may be deemed accurate.

7.2.1 A Numerical Check

As in the previous chapter, the field equation (7.2) may be solved numerically for all types of perturbation using the `NDSolve` routine in Mathematica. In this case, the boundary condition of no incoming waves at the horizon may be applied by imposing

$$\Phi(r) = 1\,, \qquad \frac{d\Phi}{dr} = -\frac{i\omega}{h(r)}\,, \tag{7.43}$$

[1]Thanks are extended to Julien Grain and Aurelien Barrau for drawing attention to this.

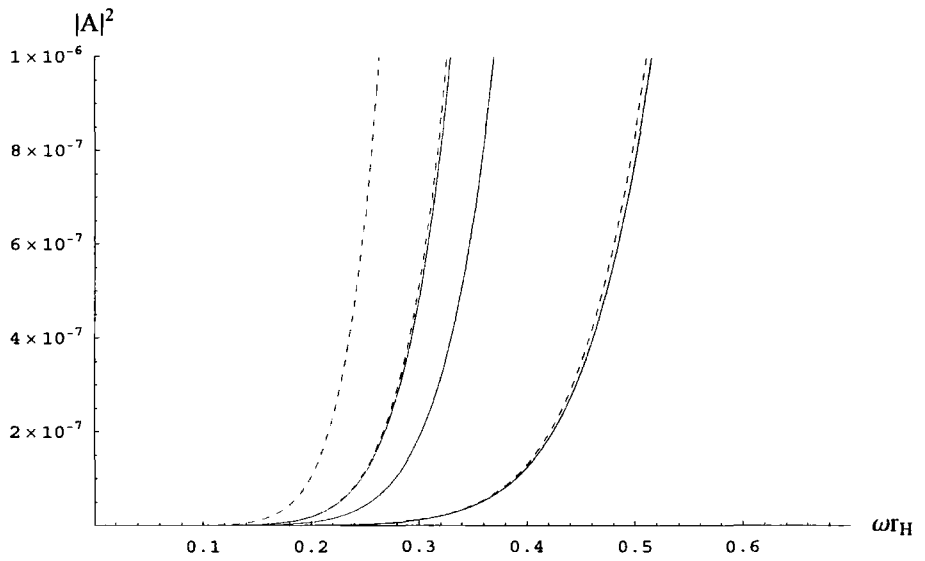

Figure 7.2: Comparison of the analytic (solid lines) and numerically (dashed lines) derived absorption probabilities for scalar (red), vector (green) and tensor (blue) gravitational perturbations for $n = 2$, $\ell = 2$.

in the limit $r \to r_H$. Once the field equation has been solved numerically it is possible to define at infinity

$$B_+ = \frac{1}{2}e^{i\omega r}\left[\Phi + \frac{i}{\omega}\frac{d\Phi}{dr}\right] = \frac{1}{\sqrt{2\pi\omega}}(B_1 + iB_2)e^{i\frac{\pi}{4}(2\ell+n+2)},$$
$$B_- = \frac{1}{2}e^{-i\omega r}\left[\Phi - \frac{i}{\omega}\frac{d\Phi}{dr}\right] = \frac{1}{\sqrt{2\pi\omega}}(B_1 - iB_2)e^{-i\frac{\pi}{4}(2\ell+n+2)}, \tag{7.44}$$

and then the absorption probability can be written in terms of these quantities

$$|\mathcal{A}_\ell|^2 = 1 - \left|\frac{B-i}{B+i}\right|^2 = 1 - \left|\frac{B_-}{B_+}\right|^2. \tag{7.45}$$

A comparison of the analytic and numerically derived absorption coefficients, plotted as a function of the dimensionless energy parameter ωr_H, for all types of perturbation in the case $n = 2$, $\ell = 2$ is shown in figure 7.2. It is clear from this single instance that, while the expressions for the tensor and vector perturbations are in excellent agreement with the numerical result at low energy, the scalar case displays significant deviation. In fact, the analytical results predict that scalars should be subdominant to vectors for the lowest mode, $\ell = 2$, while the corresponding numerical results predict the exact opposite. It is clearly necessary to improve the analytic scalar result significantly.

7.3 Gravitational Scalars Revisited

Given the accuracy with which the vector and tensor absorption coefficients are described, the error must lie in an assumption made uniquely for the scalar case. In the far-field regime the solutions for all types of perturbation are necessarily identical since the potentials tend to zero at large r in all cases. Therefore the problem must arise in the near-horizon limit.

Reexamining the near-horizon limit reveals that, in the scalar case alone, a choice had to be made so that the equation of motion could be cast into hypergeometric form. In general, any equation of the form

$$h(1-h)\frac{d^2\Phi}{dh^2} + \left[1 - \frac{(2n+3)}{(n+1)}h\right]\frac{d\Phi}{dh} + \left[\frac{(\omega r_H)^2}{(n+1)^2 h(1-h)} - \frac{\mathscr{A}}{(1-h)} - \mathscr{C}\right]\Phi = 0\,, \tag{7.46}$$

for arbitrary constants $\mathscr{A}$ and $\mathscr{C}$, may be converted into hypergeometric form with indices as in equation (7.8), by employing the transformation $\Phi(h) = h^{\alpha}(1-h)^{\beta}F(h)$, where

$$\alpha = \alpha_- = -\frac{i\omega r_H}{n+1}\,, \tag{7.47}$$

$$\beta = \beta_- = \frac{-1 - \sqrt{1 + 4\left[(n+1)^2\mathscr{A} - (\omega r_H)^2\right]}}{2(n+1)}\,, \tag{7.48}$$

$$G = \sqrt{\frac{(n+2)^2}{4(n+1)^2} - \mathscr{C}}\,, \tag{7.49}$$

and α_- and β_- have been chosen to be consistent with the discussion in §7.1. In the previous scalar analysis the parameter choices $\mathscr{A} = \tilde{A}$ (as in equation (7.7)) and $\mathscr{C} = C_0$ (equation (7.20)) were made. However, changing the variable in (7.46) back to the original radial coordinate r reveals that an arbitrary choice of $\mathscr{A}$ and $\mathscr{C}$ corresponds to starting from an original Schrodinger-like equation of the form (7.2) but with potential

$$V = \frac{(n+1)^2 h(r)}{r^2}\left[\mathscr{A} + (1-h)\mathscr{C}\right]\,. \tag{7.50}$$

So choosing $\tilde{A}$ and C_0 as the arbitrary constants required for the hypergeometric analysis is equivalent to starting out with a different form of potential in the original

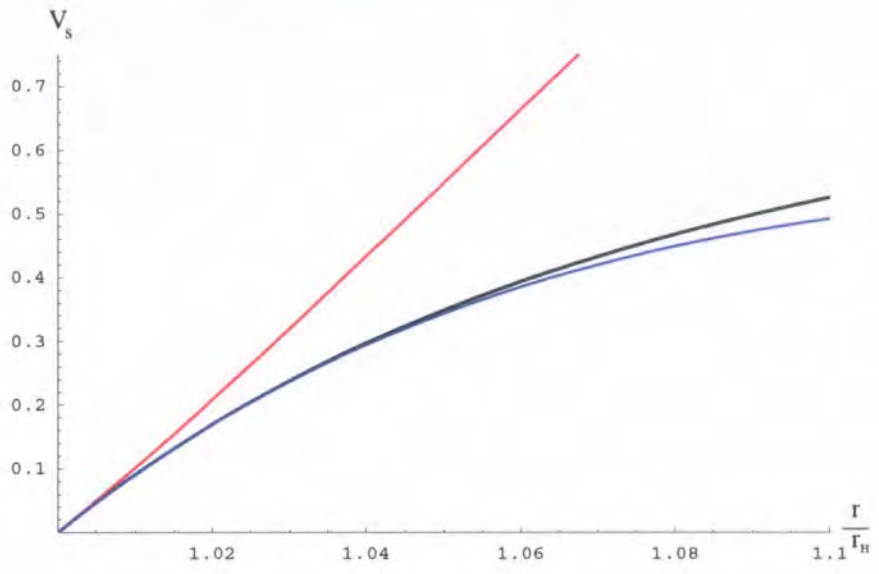

Figure 7.3: Comparison of the true near-horizon scalar potential, equation (7.4), (black) with the original approximation (7.51) (red) and the optimal version ((7.50) using (7.52) and (7.53)) (blue) for $n = 2$, $\ell = 2$.

Schrodinger-like equation. Specifically, the assumed potential that has been used in the analysis of §7.1 with this choice of constants may be written as

$$V = \frac{h(r)}{4r^2}\left[\frac{zh}{4m^2} + \frac{(1-h)(q+p+w+z)}{[2m+(n+2)(n+3)]^2}\right], \tag{7.51}$$

while the true potential is that of equation (7.4). Figure 7.3 shows a comparison of this approximation to the true scalar potential in the case $n = 2$, $\ell = 2$ and $r_H = 1$. In the extreme near-horizon limit the approximation is good: for $n = 2$, $\ell = 2$ the deviation is only 2% at $r = 1.002\, r_H$. However, the two expressions rapidly diverge away from the horizon: by $r = 1.02\, r_H$ the error is 23%. To improve the calculation a better approximation to the true scalar potential is clearly required.

The most accurate possible near-horizon expression that still permits use of the hypergeometric transformation can be found by expanding (7.4) to quadratic order in h. If the expansion is then written in the form (7.50), the best possible choice of $\mathscr{A}$ and $\mathscr{C}$ may be determined by inspection. Performing this calculation recovers

the optimal coefficients

$$A_{opt} = \frac{(n+2)(n+3)(q+p+w+z)}{2(n+1)^2\big(2m+(n+2)(n+3)\big)^3} + \frac{z-2q-p}{4(n+1)^2\big(2m+(n+2)(n+3)\big)^2}, \tag{7.52}$$

$$C_{opt} = \frac{3q+2p+w}{4(n+1)^2\big(2m+(n+2)(n+3)\big)^2} - \frac{(n+2)(n+3)(q+p+w+z)}{2(n+1)^2\big(2m+(n+2)(n+3)\big)^3}. \tag{7.53}$$

For comparison, the improved potential (7.50), using the above choice of coefficients, is also displayed in figure 7.3. The increased accuracy this choice offers is instantly apparent. In particular, at $r = 1.02\,r_H$ the deviation from the true value is only 0.2%, while at $r = 1.002\,r_H$ it is 0.002%. It is now possible to repeat the analysis of §7.1 in full using the new values of β and G to obtain an enhanced solution to the gravitational scalar field equation valid over the entire radial regime. However, performing this calculation reveals the improvement has come at a price.

When stretching the near and far-field solutions to an intermediate region, (7.25) and (7.26), exact matching of the powers of r was only possible because in the low-energy limit $\beta(n+1) \to -(\ell + n/2 + 1)$. In that case the powers of r in each half of the stretched solutions matched separately and so the corresponding coefficients of each half could be equated separately also. This imposed two conditions that determined the two quantities B_1/A_- and B_2/A_- (and hence $B \equiv B_1/B_2$) uniquely. From equation (7.48) it is clear that the above limit of $\beta(n+1)$ depends on the particular choice $\mathscr{A} = \tilde{A}$. Use of the optimal value of the coefficient $\mathscr{A} = A_{opt}$ destroys the exact matching.

In order to have matching it is now necessary to impose a value of the radial coordinate at which the two asymptotic solutions are equated: $\Phi_{NH}(r_*) = \Phi_{FF}(r_*)$. Using equations (7.25) and (7.26) this translates to

$$\begin{aligned} A_- \left(\frac{r_H}{r_*}\right)^{\beta(n+1)} \frac{\Gamma(c)\,\Gamma(c-a-b)}{\Gamma(c-a)\,\Gamma(c-b)} + A_- \left(\frac{r_H}{r_*}\right)^{-1-\beta(n+1)} \frac{\Gamma(c)\,\Gamma(a+b-c)}{\Gamma(a)\,\Gamma(b)} \\ = B_1 \left(\frac{\omega r_H}{2}\right)^{\ell+\frac{n+1}{2}} \frac{\sqrt{r_H}}{\Gamma\left(\ell+\frac{n+3}{2}\right)} \left(\frac{r_*}{r_H}\right)^{\ell+\frac{n}{2}+1} - \\ \frac{B_2}{\pi} \left(\frac{2}{\omega r_H}\right)^{\ell+\frac{n+1}{2}} \sqrt{r_H}\,\Gamma\left(\ell+\frac{n+1}{2}\right) \left(\frac{r_H}{r_*}\right)^{\ell+\frac{n}{2}}. \end{aligned} \tag{7.54}$$

The presence of r_* in the above relation means it is now necessary to determine three quantities: B_1/A_-, B_2/A_- and r_* so that $B = B_1/B_2$ may be calculated uniquely. This requires imposition of a further two restrictions, in addition to (7.54). At this point a number of possible choices may be made. In order to achieve the smoothest possible matching it would be reasonable to impose equality of the first and second derivatives of the asymptotic solutions at r_* also. Unfortunately these conditions are rarely found to be satisfied for real values of r_* and lead to nonsensical values of the absorption probability. An alternative is to require that the two halves of the asymptotic solutions match separately, so that

$$\begin{aligned}
&\bullet\quad A_- \left(\frac{r_H}{r_*}\right)^{\beta(n+1)} \frac{\Gamma(c)\,\Gamma(c-a-b)}{\Gamma(c-a)\,\Gamma(c-b)} = B_1 \left(\frac{\omega r_H}{2}\right)^{\ell+\frac{n+1}{2}} \frac{\sqrt{r_H}}{\Gamma\left(\ell+\frac{n+3}{2}\right)} \left(\frac{r_*}{r_H}\right)^{\ell+\frac{n}{2}+1}, \\
&\bullet\quad A_- \left(\frac{r_H}{r_*}\right)^{-1-\beta(n+1)} \frac{\Gamma(c)\,\Gamma(a+b-c)}{\Gamma(a)\,\Gamma(b)} = \\
&\qquad\qquad -\frac{B_2}{\pi} \left(\frac{2}{\omega r_H}\right)^{\ell+\frac{n+1}{2}} \sqrt{r_H}\,\Gamma\left(\ell+\frac{n+1}{2}\right) \left(\frac{r_H}{r_*}\right)^{\ell+\frac{n}{2}}.
\end{aligned} \tag{7.55}$$

This would seem a sensible requirement since from equation (7.48) β is negative definite. The new value of B that results is identical to the previous version except for an additional r_*-dependent factor

$$B_{opt} = \left(\frac{r_H}{r_*}\right)^{2\beta(n+1)+2\ell+n+2} B\,, \tag{7.56}$$

where B is as defined in equation (7.31). Finally the new scalar absorption coefficient may be calculated as

$$|\mathcal{A}_\ell|^2_{sca} = 1 - \left|\frac{B_{opt}-i}{B_{opt}+i}\right|^2, \tag{7.57}$$

and the extreme low-energy expansion is given by

$$|\mathcal{A}_\ell|^2_{sca} = \left(\frac{r_*}{r_H}\right)^{2\beta(n+1)+2\ell+n+2} |\mathcal{A}_\ell|^2\,, \tag{7.58}$$

where $|\mathcal{A}_\ell|^2$ is the original low-energy expansion in equation (7.42), using the appropriate optimal values of β and G.

Since the two restrictions (7.55) automatically ensure (7.54) is satisfied, then one further constraint must be imposed to determine r_*. Again, the desire for a smooth matching would suggest that requiring the first derivative of both asymptotic solutions to match at r_* would be appropriate. Unfortunately this also produces mainly

complex values of r_* and unphysical predictions for the absorption coefficient. No reliable method of choosing r_* has yet been discovered based on analytic argument alone. At present, appropriate values are selected by direct comparison with the numerical solution.

Figure 7.4 shows absorption coefficients for $\ell = 2$ and n ranging from 1 to 8. In the uncorrected version the deviation from the numerical result increases rapidly with increasing n, however the corrected version is found to be in much better agreement for all n by imposing the fixed value $r_* = 1.62 r_H$. The agreement is most pronounced for larger n indicating that, in the case of the dominant mode $\ell = 2$, r_* is a weak function of the number of extra dimensions. Examining the situation for general ℓ reveals that as ℓ increases the dependence of r_* on n strengthens slightly and the constant value approximation begins to break down.

Figure 7.5 illustrates the corresponding situation for $n = 2$ and variable ℓ. The corrected absorption coefficient is found to be in excellent agreement with the numerical value out to $\omega r_H \approx 1$, but the required value of r_* is, in general, a strongly decreasing function of ℓ. Figure 7.6 illustrates the ω-dependence of r_* for the dominant mode $\ell = 2$ and the same range of n as in figure 7.4. The values of r_* displayed are accurate to three significant figures and reproduce the numerical results to within an error of at most 3%. Excluding the cases $n = 1$ and 2 (red lines marked in the figure) where more significant variation occurs, r_* is found to be approximately independent of ω over the range 0 to $\omega r_H \approx 1$, that may be safely considered "low-energy". For larger n the optimum matching region is found to be centred on the value $r_* = 1.62 r_H$, as illustrated in figure 7.4.

With this improved analysis for the scalar case, it is now possible to return to the main analytical result for gravitons in the bulk, equations (7.30)-(7.31) and examine the absorption coefficient in more detail. As in the case of emission on the brane [37, 111], the non-simplified analytical expression for $|\mathcal{A}_\ell|^2$ is found to be in excellent agreement with the exact numerical result in the low-energy regime and in a good – both quantitative and qualitative – agreement at intermediate energy. At high-energy the validity of approximations made in the analysis breaks down and reliability of the analytic expressions is compromised.

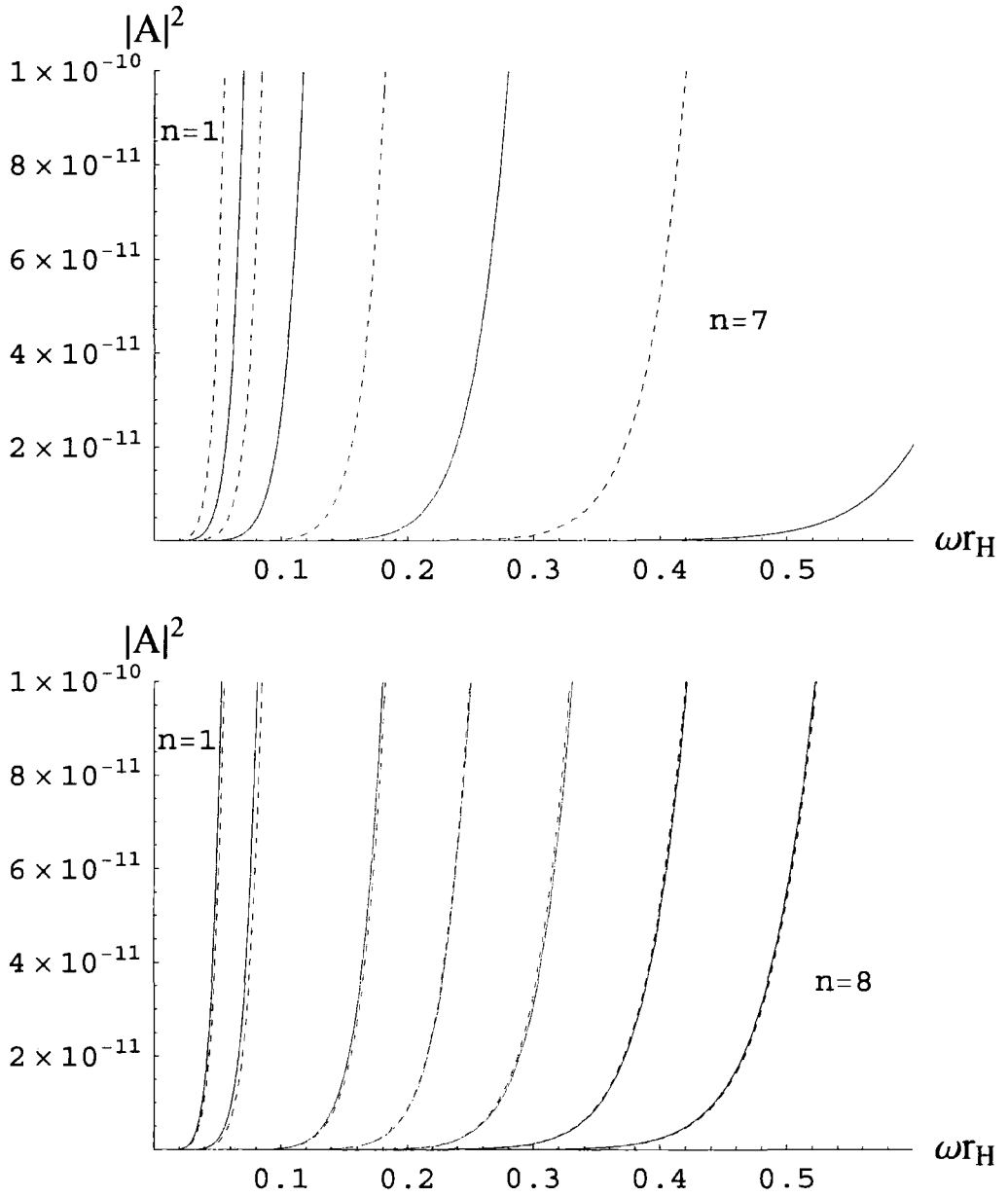

Figure 7.4: Comparison of the analytic gravitational scalar absorption probabilities (solid lines) with the numerical results (dashed lines) for $\ell = 2$ and variable n. The top figure (uncorrected) shows $n = 1$ (dark red), 2 (light red), 4 (green) and 7 (blue), while the bottom figure (corrected) presents $n = 1$ to 8 (n increasing from left to right) with $r_* = 1.62\, r_H$.

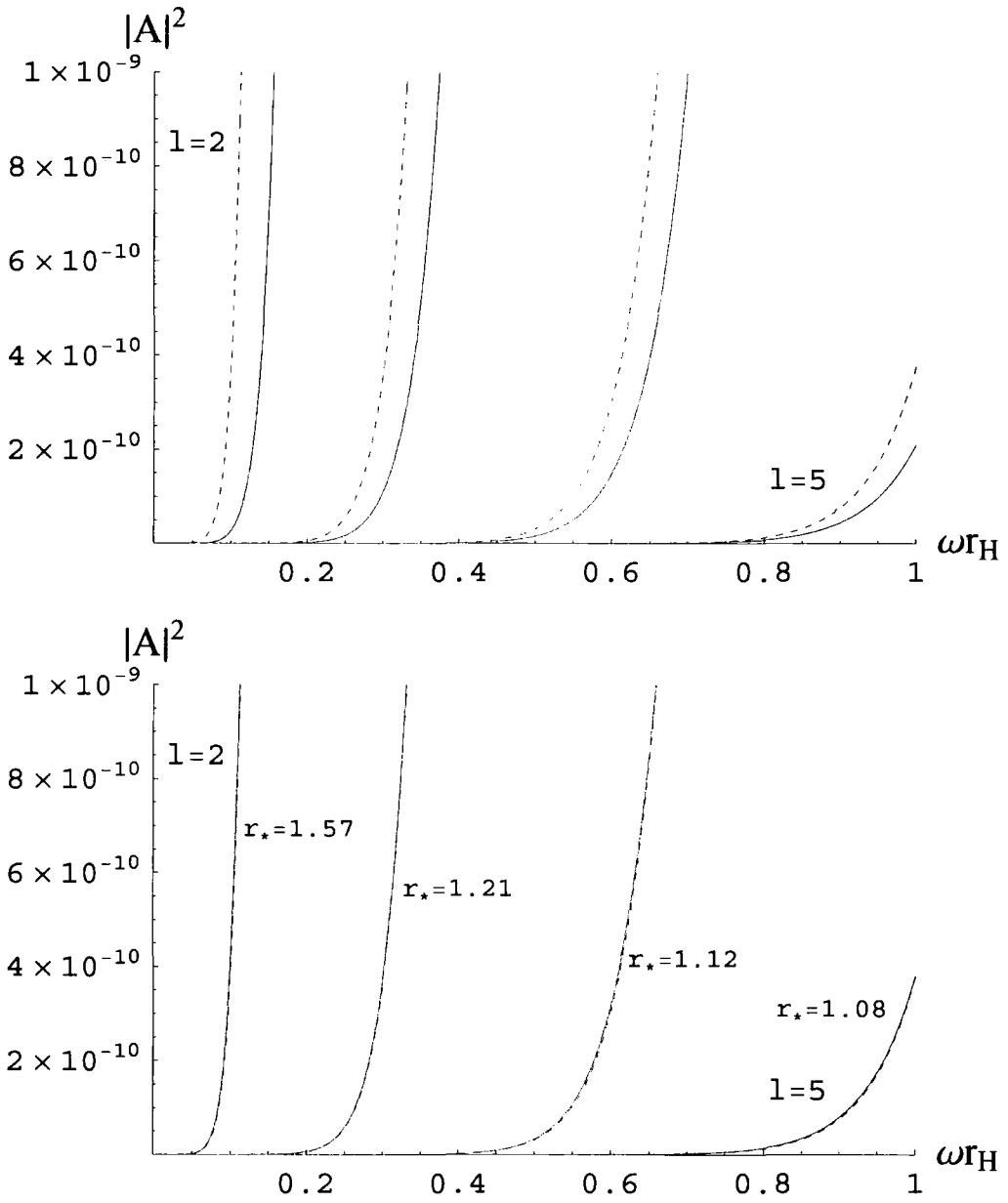

Figure 7.5: Comparison of the analytic gravitational scalar absorption probabilities (solid lines) with the numerical results (dashed lines) for $n = 2$ and variable ℓ and r_*. Both top (uncorrected) and bottom (corrected) figures show $\ell = 2$ to 5 (with ℓ increasing from left to right).

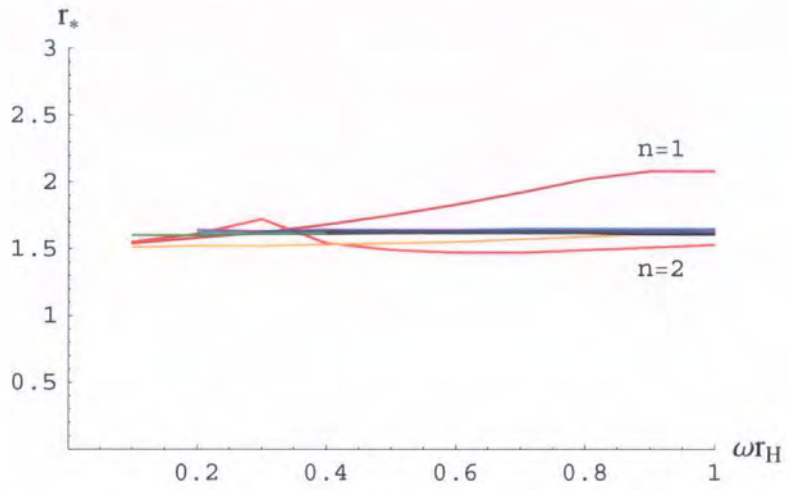

Figure 7.6: The value of r_* required to correct the absorption probability to within 3% of the numerical value as a function of ωr_H for $\ell = 2$ and $n = 1$ to 8.

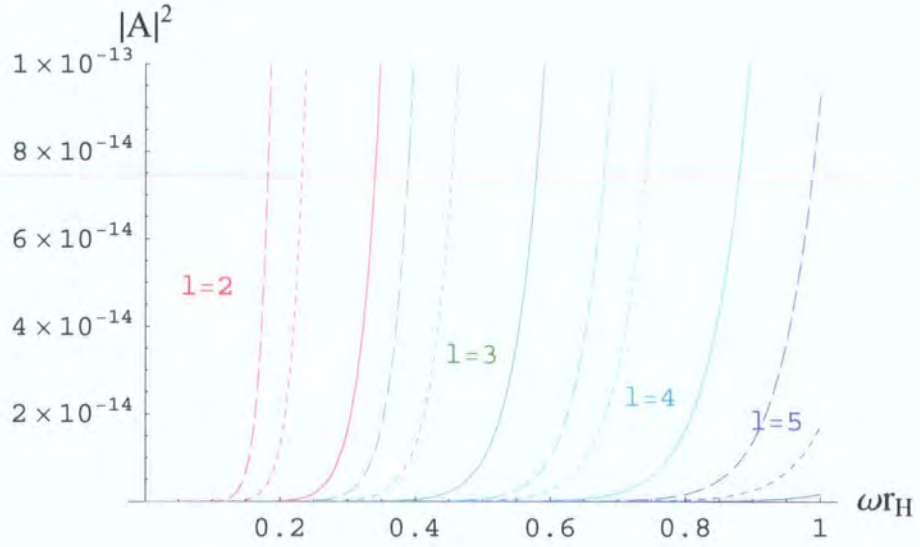

Figure 7.7: Analytic absorption probability $|\mathcal{A}_\ell|^2$ for tensor (solid lines), vector (short-dashed lines) and scalar (long-dashed lines) gravitational perturbations in the bulk for $n = 6$ and $\ell = 2, 3, 4, 5$.

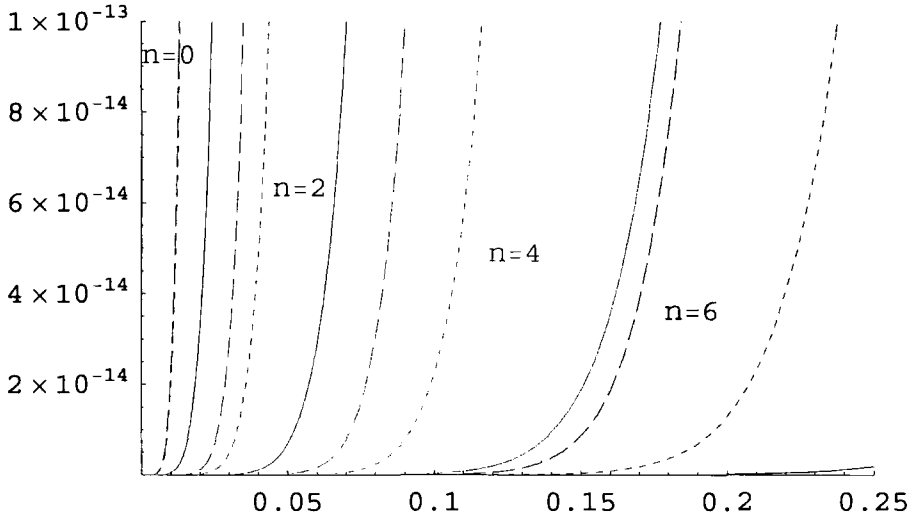

Figure 7.8: Analytic absorption probability $|\mathcal{A}_\ell|^2$ for tensor (solid lines), vector (short-dashed lines) and scalar (long-dashed lines) gravitational perturbations in the bulk for $\ell = 2$, and $n = 0, 2, 4, 6$.

In figure 7.7 the full analytic expressions for absorption probabilities for all types of gravitational perturbation are depicted for $n = 6$ and $\ell = 2$ to 5. The corresponding numerical results are no longer reproduced owing to their excellent agreement with the analytic values. Figure 7.8 displays the corresponding case for the dominant mode $\ell = 2$ and $n = 0$, 2, 4, 6. As should be expected, for all types of perturbation and values of ℓ and n the absorption probability vanishes when the energy of the propagating particle goes to zero, while it increases with ωr_H. Figure 7.7 reveals that, as ℓ increases, the absorption probability for all types of gravitational perturbation is suppressed, in accordance with the behaviour observed in the entries of table 7.1; although the results depicted correspond to the case $n = 6$, this behaviour holds for all values of n. Figure 7.8 shows that for fixed ℓ increasing n also causes significant suppression for all graviton types. This behaviour is observed for the lowest two partial modes with $\ell = 2$ and $\ell = 3$; for higher values of ℓ, $|\mathcal{A}_\ell|^2$ shows a temporary enhancement as n increases from 0 to 2 that returns to rapid suppression as n increases further.

As was noticed while studying the extreme low-energy regime, the absorption

n	ℓ	p	$\lvert\mathcal{A}_\ell^{(\mathbf{S})}\rvert^2$(corrected)
$n = 2$	$\ell = 2$	8	$3.9 \cdot 10^{-2}$
	$\ell = 3$	10	$5.9 \cdot 10^{-5}$
	$\ell = 4$	12	$1.1 \cdot 10^{-7}$
$n = 4$	$\ell = 2$	10	$2.5 \cdot 10^{-3}$
	$\ell = 3$	12	$1.1 \cdot 10^{-6}$
	$\ell = 4$	14	$4.3 \cdot 10^{-9}$
$n = 6$	$\ell = 2$	12	$5.7 \cdot 10^{-5}$
	$\ell = 3$	14	$5.0 \cdot 10^{-8}$
	$\ell = 4$	16	$4.2 \cdot 10^{-11}$

Table 7.3: The corrected asymptotic low-energy absorption probability for scalar gravitational perturbations in the bulk. As in table 7.1, entries represent coefficients of $(\omega r_H)^p$ and these values supersede those given previously for scalar modes.

probability for tensor gravitational perturbations is significantly suppressed in comparison to vectors and scalars. This behaviour is also found to extend to intermediate energy. The original expression for the scalar absorption coefficient (and the entries in table 7.1 derived from it) gave the misleading impression that the competition for dominance between vector and scalar perturbations depends on the particular values of ℓ and n. As can be seen from the corrected figures 7.7 and 7.8 and the corrected low-energy expansion given in table 7.3, scalar gravitons have an absorption coefficient that is individually dominant for every value of n and ℓ. However, for a given angular momentum quantum number ℓ, different types of perturbation are characterised by a different multiplicity of states and this fact must be accounted for before a reliable conclusion may be drawn on which type of gravitational degree of freedom is most likely to be emitted into the bulk by a static, higher-dimensional black hole.

	$N_\ell^{(T)}$		$N_\ell^{(V)}$		$N_\ell^{(S)}$	
	$n=1$	$n=6$	$n=1$	$n=6$	$n=1$	$n=6$
$\ell=2$	10	495	16	231	9	44
$\ell=3$	24	2574	30	910	16	156
$\ell=4$	42	8748	48	2772	25	450
$\ell=5$	64	23868	70	7140	36	1122

Table 7.4: Multiplicities of states corresponding to the same angular momentum number ℓ for tensor, vector and scalar gravitational perturbations, for $n = 1$ and $n = 6$.

7.4 The Energy Emission Rate

In a spherically symmetric higher-dimensional background the multiplicities of states corresponding to the same angular momentum number ℓ for tensor, vector and scalar perturbations are given by the expressions [158, 159]

$$N_\ell^{(T)} = \frac{n(n+3)(\ell+n+2)(\ell-1)(2\ell+n+1)(\ell+n-1)!}{2(\ell+1)!\,(n+1)!}, \tag{7.59}$$

$$N_\ell^{(V)} = \frac{\ell(\ell+n+1)(2\ell+n+1)(\ell+n-1)!}{(\ell+1)!\,n!}, \tag{7.60}$$

$$N_\ell^{(S)} = \frac{(2\ell+n+1)(\ell+n)!}{\ell!\,(n+1)!}. \tag{7.61}$$

Table 7.4 displays these multiplicities for some indicative values of ℓ and n, rendering the proliferation of states as either parameter increases immediately apparent. From this it is clear that the value of the absorption probability is not the sole factor important in determining the contribution of each type of gravitational perturbation to the total emission rate of the black hole.

Having obtained the absorption probability and multiplicities of states for each type of perturbation, it is now possible to calculate the corresponding low-energy power spectrum. The field theory calculation, analogous to that in §4.5, determining the energy emission rate of higher-dimensional gravitons has yet to be performed. However, given the similarity of the five-dimensional scalar energy emission rate [110] with the corresponding four-dimensional case and the close relation between

expressions for particles in four-dimensions with differing spin, it is reasonable to assume that the contribution of each type of gravitational perturbation to the total graviton energy emission rate is given by

$$\frac{d^2E^{(P)}}{dt\,d\omega} = \frac{1}{2\pi}\sum_{\ell} N_{\ell}^{(P)}|\mathcal{A}_{\ell}^{(P)}|^2 \frac{\omega}{\exp(\omega/T_H)-1}, \tag{7.62}$$

where the superscript $P = (T, V, S)$ denotes the type of perturbation. The total amount of energy emitted per unit time and unit frequency by the black hole in the form of gravitons is then given by summing over the three contributions. As an exact numerical analysis is required to calculate the full spectra (including the high-energy regime), here attention will be focused on the relative emission rates for the different types of gravitational perturbations and their magnitude in relation to that for bulk scalar fields.

A simple numerical calculation combining equation (7.62) with the entries of tables 7.1, 7.3 and 7.4, reveals that, in the asymptotic low-energy regime, scalar gravitons are the dominant type of gravitational degree of freedom emitted in the bulk. For example, for $n = 2$ and $\ell = 2$, scalar perturbations amount to 67% of the total gravitational degrees of freedom emitted, compared to 32% for vector and 1% for tensor modes. As n increases further, so does the dominance of the scalar-like perturbations that, for $n = 6$ and $\ell = 2$, reaches a magnitude of 77%. This dominance is significantly decreased and even over-turned at the level of higher partial waves: for instance, for $n = 6$ and $\ell = 4$, the vector, scalar and tensor perturbations correspond to 51%, 39% and 10%, respectively, of the total number of gravitational modes emitted.

The above results are strictly only valid at extreme low-energy so to gain a more reliable understanding of the behaviour of the radiation spectrum as the particle energy increases it is necessary to consider the full analytic expression (7.30)-(7.31). In figure 7.9 the energy emission rates for all types of gravitational perturbation, for $n = 1$ and $n = 6$ are plotted using the complete analytical expression (7.30)-(7.31) and the corrected gravitational scalar result. For comparison, the energy emission rate for bulk scalar fields is also included. In the summation over angular momentum quantum numbers in equation (7.62) all modes up to $\ell = 12$ have been

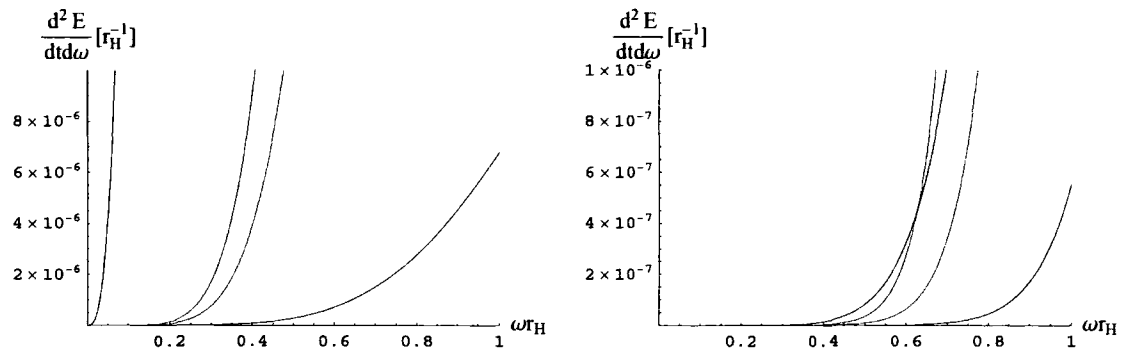

Figure 7.9: Energy emission rates for tensor (blue), vector (green) and scalar (red) gravitational perturbations and scalar fields (black) in the bulk, for $n = 1$ (left), and $n = 6$ (right).

included although, in the very low-energy region of the spectrum, the contribution of all modes with $\ell \geq 4$ is at least four orders of magnitude smaller than that of the $\ell = 2$ mode, regardless of the number of extra dimensions. Including such a large number of modes in the sum minimises the error that might otherwise be introduced in the intermediate energy regime.

The results depicted in figure 7.9 are in fact in excellent agreement with the conclusions derived using the simplified expression for $|\mathcal{A}_\ell|^2$. The scalar-type perturbations are indeed the dominant gravitational degrees of freedom emitted by the black hole in the bulk for all values of n. Likewise, the tensor modes are always the most suppressed although their relative magnitude increases as n increases owing to the large multiplicity of tensor states. Despite the above, the energy emission rates for all types of gravitational perturbations in the bulk, even when combined, remain well below that for scalar fields in the low-energy regime. This is due to the fact that the emission rate for scalar fields receives a significant enhancement at low energy from the dominant $\ell = 0$ and $\ell = 1$ modes that are absent from the spectrum of gravitational perturbations. However, it is apparent from the right-hand plot in figure 7.9 that as $\omega_\star$ increases, the higher partial waves gradually come into dominance and, for large n at least, cause graviton emission to supersede that of bulk scalar fields.

Finally, by comparing the vertical axes of the two plots in figure 7.9 it is possible

to conclude that the low-energy emission rate for all degrees of freedom in the bulk decreases as the number of extra dimensions increases. Although both the temperature of the black hole and multiplicity of states undergo a significant enhancement as n increases, the suppression of the absorption probability, depicted in figure 7.8, prevails, leading to overall suppression of the number of degrees of freedom emitted. This low-energy suppression for bulk scalar fields was first witnessed in [111, 113] but the exact numerical analysis performed in the latter work showed that at high energy the spectrum is actually enhanced with the number of extra dimensions. This is a result of a combination of factors – first the milder suppression of the absorption probability with n that occurs at higher energy, but also by the shift of the emission curve in accordance with Wien's law since a higher-dimensional black hole has a higher temperature. This latter effect leads to a preferential emission of higher-energy particles as n increases [111]. Due to the similarities observed in the behaviour of gravitational and scalar fields in the bulk, the same enhancement might be expected of gravitons in the high-energy regime.

7.5 Summary

In this chapter the emission of gravitons into the bulk from a $(4 + n)$-dimensional Schwarzschild black hole has been investigated. Working in the low energy regime, the field equations for tensor, vector and scalar-type gravitational perturbations have been solved analytically and the absorption probability computed in each case. Both a complete analytic expression and its asymptotic low-energy simplification have been studied in detail, and their dependence on the angular momentum number ℓ and number of extra dimensions n was examined. Although numerically different, as the energy increases these two expressions have qualitatively identical behaviours, revealing an increase in the absorption probability with increasing energy and suppression as the number of extra dimensions n and angular momentum number ℓ increase.

The complete analytical expression for the absorption probability has been used to derive the contribution of each gravitational degree of freedom to the total gravi-

ton emission rate of the black hole in the bulk. The results show that scalar gravitational perturbations are the dominant gravitational energy-carrying mode emitted in the bulk for all values of n and tensors are the most suppressed. The absence of the $\ell = 0, 1$ partial waves, dominant in the extreme low-energy regime, from all gravitational spectra causes even the total graviton emission rate to be less than that of scalar fields in the bulk. However, as energy increases and higher order modes come into dominance this situation appears to be reversed, particularly for larger n. Finally, as known from previous study of bulk scalar fields, the energy emission rates for all types of gravitational perturbations are suppressed with the number of extra dimensions throughout the low-energy regime.

Chapter 8

Conclusions

It is sometimes said that no worthwhile new theory resolves one problem without creating five more of significantly increased complexity. In this regard braneworlds are exceedingly worthwhile. Despite (or perhaps as a consequence of) the enormous volume of literature that has appeared on braneworld models in the last decade, there are now many more outstanding problems with these theories than the question of hierarchy amongst the fundamental forces they were proposed to resolve. It has been the task of this thesis to address and progress two of these problems in particular.

8.1 Randall-Sundrum Black Holes

The Randall-Sundrum braneworld black hole metric has proven elusive from the moment it was realised higher-dimensional warped geometries might render extra dimensions consistent with our standard four-dimensional view of the universe. Many different approaches have been applied and, while none has uncovered the complete solution, each has furthered understanding of the problem and revealed more about what may and may not be accomplished within the braneworld framework.

In chapter 3 a new approach to the Randall-Sundrum black hole was explored. In order to ensure a well-behaved metric from the five-dimensional perspective, the restrictions on embedding a four-dimensional hypersurface in a variety of five-dimensional bulks were derived for time-dependent brane trajectories containing perfect fluid distributions of energy-momentum. The complete set of time-dependent

restrictions are of sufficient complexity that, for the moment at least, analytic solution was only possible by seeking the subset of all possible trajectories for which the equation of state on the brane is $p(\tau, r) = -\rho(\tau, r)$, with p and ρ the pressure and energy density of perfect fluid on the brane respectively. Despite this restriction a rich variety of brane trajectories have been uncovered, with a given configuration specified by the values of five constants of integration. From a mathematical perspective these represent new solutions to classical general relativity where the full interaction between the bulk spacetime and an energy-momentum containing brane has been taken into account. From a physical perspective, these trajectories cannot represent the desired braneworld black hole. A consistency condition arose in the process of solution that restricts the form of bulk spacetime in which branes with the above equation of state may be admitted. The only permissible higher-dimensional metrics with physical interpretation are those of constant curvature, excluding the possibility of a black hole being present in the bulk. As such, the set of time-dependent solutions found represent a generalisation of the original Randall-Sundrum situation, but not a braneworld black hole.

A second possible simplification of the problem may be achieved by seeking time-independent trajectories. In this case the restrictions became completely integrable, being expressed analytically in terms of an implicit function of the radial variable. Most importantly, the assumption of time-independence removed the restriction on the form of the bulk metric, allowing static branes to be embedded in any $SO(4)$-symmetric five-dimensional spacetime. Two physically relevant backgrounds for which the brane trajectories and energy-momenta could be written in particularly convenient forms were the five-dimensional anti-de Sitter and Schwarzschild spacetimes. Again, a wide variety of brane shapes and energy distributions were discovered and analysed according to which might represent physically realistic configurations. For trajectories in pure adS the branes were characterised by constant energy density and their topology determined by the value of this energy density in relation to the critical value found in the Randall-Sundrum model, that exactly cancels the background negative energy density. Branes with super-critical energy density were closed, while critical or sub-critical branes were open. One feature of

of these branes that distinguishes them from the RS case is that in almost all circumstances they possess an excess pressure and are consequently not asymptotically flat.

Of particular interest were a class of solutions in a Schwarzschild bulk for which the brane extended to infinity and passed close to the black hole, bending away to just avoid touching the horizon in the region of closest approach. These branes were found to contain a localised accumulation of energy density in their central region that satisfied the dominant energy condition. In terms of their energy-momentum description they fulfilled most of the requirements of a braneworld star. Unfortunately, the gravitational potential witnessed by an observer in the vicinity of such a braneworld star would not be that of standard four-dimensional gravity since asymptotically the induced metric is the projection of the five-dimensional Schwarzschild metric, which has incorrect radial dependence. It was hoped that considering a bulk black hole in asymptotically anti-de Sitter spacetime might rectify this in the same manner that working in adS spacetime in the original RS model confined gravity to the brane. Unfortunately this was not to be the case. Analysis of brane trajectories in five-dimensional Schwarzschild-adS spacetime revealed that, while a satisfactory energy-momentum distribution was achievable in the central region, the problem of asymptotic excess pressure found for static branes in pure adS persisted.

Despite a configuration with all the desired properties of a braneworld star or black hole remaining undiscovered, it should be emphasised that the solutions found here represent the first completely consistent bulk-brane-black hole gravitational systems of lower symmetry than braneworld cosmologies. While the restrictions imposed to simplify the equations governing brane properties always introduced undesirable features, the possibility remains that the full set of time-dependent equations derived in chapter 3 may admit a braneworld black hole solution if some route, either analytic or numerical, can be found through the complexity of the full equations.

8.2 Higher-Dimensional Hawking Radiation

With the potential lowering of the fundamental scale of gravity suggested by brane-world models, the prospect of creating small black holes in high-energy collisions has become closer to reality. Much work has been conducted in the last five years on determining the spectra of Hawking radiation that might be witnessed in the laboratory as a microscopic black hole evaporates. Owing to the relative simplicity of the equations involved, the radiation from static Schwarzschild black holes has been studied extensively, both analytically and numerically. However, in high-energy particle collisions the non-zero impact parameter between parent particles renders production of black holes with angular momentum extremely likely.

As with the static case, the key to deriving emission spectra from a rotating black hole is to solve the field equations for particles propagating in the appropriate background. For all particle species the field equations are found to be separable, and it is solution to the radial component in particular that determines the probability of a particle being emitted. The key to achieving this has been use of a powerful technique involving matching of asymptotically accurate solutions in a intermediate regime to generate smooth radial solutions for each particle species that are approximately valid throughout all space. From these solutions the emission spectra may be derived. A limitation of the solution-matching technique is that it is only strictly valid in the limit of emission of low-energy particles from a slowly rotating black hole. That said, the expressions derived in chapters 5–7 have been tested, where possible, against exact numerical results and found to compare very favourably, even outside their strict range of validity.

In this thesis emission of scalars, fermions and gauge bosons onto the brane and scalar particles into the bulk from a higher-dimensional rotating black hole have been considered. Also the emission of gravitons into the bulk from a static black hole has been studied. Detailed conclusions about the emission of each particle species have been drawn at the end of each chapter, so the reader is referred there to avoid repetition. It should be mentioned, however, that in each case all analytic quantities derived compare well with their numerical counterparts in the appropriate low-energy and low-black-hole angular momentum limits and they all reduce to

known results existing in the literature for emission from Schwarzschild black holes. A number of features familiar from the static case, such as the cross-section for emission of scalar particles being equal to the horizon area of the black hole, have been shown to generalise to the rotating case. Also the high-energy cross-section has been found to reach a constant value, the same for all particle species, that may be calculated using a geometrical optics argument based on the minimum impact parameter a particle may possess without being absorbed by the black hole when it is incident from infinity along a path parallel to the black hole's axis of rotation.

An obvious avenue of further study is to consider the emission of gravitons into the bulk from a higher-dimensional rotating black hole. Given the detailed formalism required to study gravitational perturbations of the Schwarzschild metric, generalisation to the rotating case is anticipated to be a highly involved task. However, its study is essential before accurate estimates of the true fraction of a black hole's mass radiated on the brane may be obtained.

To conclude it is worth returning momentarily to reality. Although theoreticians are prone to talk about extra dimensions with an air of certainty, it should be remembered that they are still an extremely radical idea. To date, they have a problem far greater than any theoretical inconsistency: there is not a shred of experimental evidence to suggest they exist. That said, absence of evidence cannot be cause for exclusion and it is likely just such a radical idea is required to ease the friction between general relativity and quantum mechanics. With the Large Hadron Collider soon to generate data at the highest laboratory energies ever achieved, anything could be witnessed and it is important to be able to interpret whatever is found. The study of black holes in braneworld models ensures that if extra dimensions do indeed exist then, should their signature appear in high-energy experiment, one of the most radical discoveries in modern physics won't just pass unnoticed.

Bibliography

[1] S. Creek, R. Gregory, P. Kanti and B. Mistry, "Braneworld stars and black holes," Class. Quant. Grav. **23**, 6633 (2006) [arXiv:hep-th/0606006].

[2] S. Creek, O. Efthimiou, P. Kanti and K. Tamvakis, "Greybody factors for brane scalar fields in a rotating black-hole background," Phys. Rev. D **75**, 084043 (2007) [arXiv:hep-th/0701288].

[3] S. Creek, O. Efthimiou, P. Kanti and K. Tamvakis, "Greybody factors in a rotating black-hole background-II : fermions and gauge bosons," accepted for publication in Phys. Rev. D, arXiv:0707.1768 [hep-th].

[4] S. Creek, O. Efthimiou, P. Kanti and K. Tamvakis, "Scalar emission in the bulk in a rotating black hole background," Phys. Lett. B **656**, 102 (2007) arXiv:0709.0241 [hep-th].

[5] S. Creek, O. Efthimiou, P. Kanti and K. Tamvakis, "Graviton emission in the bulk from a higher-dimensional Schwarzschild black hole," Phys. Lett. B **635**, 39 (2006) [arXiv:hep-th/0601126].

[6] A. Einstein "The foundation of the general theory of relativity," Annalen Phys. **49**, 769 (1916)

[7] S. M. Carroll, "Spacetime and geometry: An introduction to general relativity," *San Francisco, USA: Addison-Wesley (2004) 513 p*

[8] R. M. Wald, "General Relativity," *Chicago, USA: Univ. Pr. (1984) 491p*

[9] M. H. Goroff and A. Sagnotti, "The ultraviolet behavior of Einstein gravity," Nucl. Phys. B **266**, 709 (1986).

[10] A. E. M. van de Ven, "Two loop quantum gravity," Nucl. Phys. B **378**, 309 (1992).

[11] S. Carlip, "Quantum gravity: A progress report," Rept. Prog. Phys. **64**, 885 (2001) [arXiv:gr-qc/0108040].

[12] J. Polchinski, "String theory. Vol. 1: An introduction to the bosonic string," *Cambridge, UK: Univ. Pr. (1998) 402 p*

[13] J. Polchinski, "String theory. Vol. 2: Superstring theory and beyond," *Cambridge, UK: Univ. Pr. (1998) 531 p*

[14] B. Zwiebach, "A first course in string theory," *Cambridge, UK: Univ. Pr. (2004) 558 p*

[15] E. Witten, "String theory dynamics in various dimensions," Nucl. Phys. B **443**, 85 (1995) [arXiv:hep-th/9503124].

[16] J. H. Schwarz, "The power of M theory," Phys. Lett. B **367**, 97 (1996) [arXiv:hep-th/9510086].

[17] M. J. Duff, "M theory (the theory formerly known as strings)," Int. J. Mod. Phys. A **11**, 5623 (1996) [arXiv:hep-th/9608117].

[18] T. Kaluza, "On the problem of unity in physics," Sitzungsber. Preuss. Akad. Wiss. Berlin (Math. Phys.) **1921**, 966 (1921).

[19] O. Klein, "Quantum theory and five-dimensional theory of relativity," Z. Phys. **37**, 895 (1926) [Surveys High Energ. Phys. **5**, 241 (1986)].

[20] N. Arkani-Hamed, S. Dimopoulos and G. R. Dvali, "The hierarchy problem and new dimensions at a millimeter," Phys. Lett. B **429**, 263 (1998) [arXiv:hep-ph/9803315].

[21] I. Antoniadis, N. Arkani-Hamed, S. Dimopoulos and G. R. Dvali, "New dimensions at a millimeter to a Fermi and superstrings at a TeV," Phys. Lett. B **436**, 257 (1998) [arXiv:hep-ph/9804398].

[22] N. Arkani-Hamed, S. Dimopoulos and G. R. Dvali, "Phenomenology, astrophysics and cosmology of theories with sub-millimeter dimensions and TeV scale quantum gravity," Phys. Rev. D **59**, 086004 (1999) [arXiv:hep-ph/9807344].

[23] C. D. Hoyle, D. J. Kapner, B. R. Heckel, E. G. Adelberger, J. H. Gundlach, U. Schmidt and H. E. Swanson, "Sub-millimeter tests of the gravitational inverse-square law," Phys. Rev. D **70**, 042004 (2004) [arXiv:hep-ph/0405262].

[24] S. J. Smullin, A. A. Geraci, D. M. Weld, J. Chiaverini, S. P. Holmes and A. Kapitulnik, "New constraints on Yukawa-type deviations from Newtonian gravity at 20-microns," Phys. Rev. D **72**, 122001 (2005) [Erratum-ibid. D **72**, 129901 (2005)] [arXiv:hep-ph/0508204].

[25] D. J. Kapner, T. S. Cook, E. G. Adelberger, J. H. Gundlach, B. R. Heckel, C. D. Hoyle and H. E. Swanson, "Tests of the gravitational inverse-square law below the dark-energy length scale," Phys. Rev. Lett. **98**, 021101 (2007) [arXiv:hep-ph/0611184].

[26] L. Randall and R. Sundrum, "A large mass hierarchy from a small extra dimension," Phys. Rev. Lett. **83**, 3370 (1999) [arXiv:hep-ph/9905221].

[27] L. Randall and R. Sundrum, "An alternative to compactification," Phys. Rev. Lett. **83**, 4690 (1999) [arXiv:hep-th/9906064].

[28] G. R. Dvali, G. Gabadadze and M. Porrati, "4D gravity on a brane in 5D Minkowski space," Phys. Lett. B **485**, 208 (2000) [arXiv:hep-th/0005016].

[29] G. R. Dvali, G. Gabadadze and M. Porrati, "Metastable gravitons and infinite volume extra dimensions," Phys. Lett. B **484**, 112 (2000) [arXiv:hep-th/0002190].

[30] J. D. Lykken and L. Randall, "The shape of gravity," JHEP **0006**, 014 (2000) [arXiv:hep-th/9908076].

[31] R. Gregory, V. A. Rubakov and S. M. Sibiryakov, "Opening up extra dimensions at ultra-large scales," Phys. Rev. Lett. **84**, 5928 (2000) [arXiv:hep-th/0002072].

[32] I. I. Kogan, S. Mouslopoulos, A. Papazoglou and G. G. Ross, "Multi-brane worlds and modification of gravity at large scales," Nucl. Phys. B **595**, 225 (2001) [arXiv:hep-th/0006030].

[33] A. Karch and L. Randall, "Locally localized gravity," JHEP **0105**, 008 (2001) [arXiv:hep-th/0011156].

[34] V. A. Rubakov, "Large and infinite extra dimensions: An introduction," Phys. Usp. **44**, 871 (2001) [Usp. Fiz. Nauk **171**, 913 (2001)] [arXiv:hep-ph/0104152].

[35] R. Dick, "Brane worlds," Class. Quant. Grav. **18**, R1 (2001) [arXiv:hep-th/0105320].

[36] R. Maartens, "Brane-world gravity," Living Rev. Rel. **7**, 7 (2004) [arXiv:gr-qc/0312059].

[37] P. Kanti, "Black holes in theories with large extra dimensions: A review," Int. J. Mod. Phys. A **19**, 4899 (2004) [arXiv:hep-ph/0402168].

[38] P. Horava and E. Witten, "Heterotic and type I string dynamics from eleven dimensions," Nucl. Phys. B **460**, 506 (1996) [arXiv:hep-th/9510209].

[39] P. Horava and E. Witten, "Eleven-dimensional supergravity on a manifold with boundary," Nucl. Phys. B **475**, 94 (1996) [arXiv:hep-th/9603142].

[40] C. Charmousis, R. Gregory and V. A. Rubakov, "Wave function of the radion in a brane world," Phys. Rev. D **62**, 067505 (2000) [arXiv:hep-th/9912160].

[41] L. Pilo, R. Rattazzi and A. Zaffaroni, "The fate of the radion in models with metastable graviton," JHEP **0007**, 056 (2000) [arXiv:hep-th/0004028].

[42] W. D. Goldberger and M. B. Wise, "Modulus stabilization with bulk fields," Phys. Rev. Lett. **83**, 4922 (1999) [arXiv:hep-ph/9907447].

[43] J. Garriga and T. Tanaka, "Gravity in the brane-world," Phys. Rev. Lett. **84**, 2778 (2000) [arXiv:hep-th/9911055].

[44] S. B. Giddings, E. Katz and L. Randall, "Linearized gravity in brane backgrounds," JHEP **0003**, 023 (2000) [arXiv:hep-th/0002091].

[45] C. Csaki, J. Erlich and T. J. Hollowood, "Graviton propagators, brane bending and bending of light in theories with quasi-localized gravity," Phys. Lett. B **481**, 107 (2000) [arXiv:hep-th/0003020].

[46] P. Binetruy, C. Deffayet and D. Langlois, "Non-conventional cosmology from a brane-universe," Nucl. Phys. B **565**, 269 (2000) [arXiv:hep-th/9905012].

[47] P. Binetruy, C. Deffayet, U. Ellwanger and D. Langlois, "Brane cosmological evolution in a bulk with cosmological constant," Phys. Lett. B **477**, 285 (2000) [arXiv:hep-th/9910219].

[48] C. Csaki, M. Graesser, C. F. Kolda and J. Terning, "Cosmology of one extra dimension with localized gravity," Phys. Lett. B **462**, 34 (1999) [arXiv:hep-ph/9906513].

[49] J. M. Cline, C. Grojean and G. Servant, "Cosmological expansion in the presence of extra dimensions," Phys. Rev. Lett. **83**, 4245 (1999) [arXiv:hep-ph/9906523].

[50] D. Ida, "Brane-world cosmology," JHEP **0009**, 014 (2000) [arXiv:gr-qc/9912002].

[51] S. Mukohyama, T. Shiromizu and K. i. Maeda, "Global structure of exact cosmological solutions in the brane world," Phys. Rev. D **62**, 024028 (2000) [Erratum-ibid. D **63**, 029901 (2001)] [arXiv:hep-th/9912287].

[52] P. Bowcock, C. Charmousis and R. Gregory, "General brane cosmologies and their global spacetime structure," Class. Quant. Grav. **17**, 4745 (2000) [arXiv:hep-th/0007177].

[53] D. J. H. Chung and K. Freese, "Cosmological challenges in theories with extra dimensions and remarks on the horizon problem," Phys. Rev. D **61**, 023511 (2000) [arXiv:hep-ph/9906542].

[54] T. Shiromizu, K. i. Maeda and M. Sasaki, "The Einstein equations on the 3-brane world," Phys. Rev. D **62**, 024012 (2000) [arXiv:gr-qc/9910076].

[55] R. Maartens, "Cosmological dynamics on the brane," Phys. Rev. D **62**, 084023 (2000) [arXiv:hep-th/0004166].

[56] P. Kanti, I. I. Kogan, K. A. Olive and M. Pospelov, "Cosmological 3-brane solutions," Phys. Lett. B **468**, 31 (1999) [arXiv:hep-ph/9909481].

[57] P. Kanti, I. I. Kogan, K. A. Olive and M. Pospelov, "Single-brane cosmological solutions with a stable compact extra dimension," Phys. Rev. D **61**, 106004 (2000) [arXiv:hep-ph/9912266].

[58] D. Brecher and M. J. Perry, "Ricci-flat branes," Nucl. Phys. B **566**, 151 (2000) [arXiv:hep-th/9908018].

[59] A. Chamblin, S. W. Hawking and H. S. Reall, "Brane-world black holes," Phys. Rev. D **61**, 065007 (2000) [arXiv:hep-th/9909205].

[60] R. Gregory and R. Laflamme, "Black strings and p-branes are unstable," Phys. Rev. Lett. **70** (1993) 2837 [arXiv:hep-th/9301052].

[61] R. Gregory, "Black string instabilities in anti-de Sitter space," Class. Quant. Grav. **17**, L125 (2000) [arXiv:hep-th/0004101].

[62] W. Israel, "Singular hypersurfaces and thin shells in general relativity," Nuovo Cimento Soc. Ital. Phys. B **44**, 4349 (1966).

[63] N. Dadhich, R. Maartens, P. Papadopoulos and V. Rezania, "Black holes on the brane," Phys. Lett. B **487**, 1 (2000) [arXiv:hep-th/0003061].

[64] M. Bruni, C. Germani and R. Maartens, "Gravitational collapse on the brane," Phys. Rev. Lett. **87**, 231302 (2001) [arXiv:gr-qc/0108013].

[65] R. Casadio, A. Fabbri and L. Mazzacurati, "New black holes in the brane-world?," Phys. Rev. D **65**, 084040 (2002) [arXiv:gr-qc/0111072].

[66] G. Kofinas, E. Papantonopoulos and I. Pappa, "Spherically symmetric braneworld solutions with (4)R term in the bulk," Phys. Rev. D **66**, 104014 (2002) [arXiv:hep-th/0112019].

[67] K. A. Bronnikov, V. N. Melnikov and H. Dehnen, "On a general class of brane-world black holes," Phys. Rev. D **68**, 024025 (2003) [arXiv:gr-qc/0304068].

[68] P. Kanti and K. Tamvakis, "Quest for localized 4-D black holes in brane worlds," Phys. Rev. D **65**, 084010 (2002) [arXiv:hep-th/0110298].

[69] R. Casadio and L. Mazzacurati, "Bulk shape of brane-world black holes," Mod. Phys. Lett. A **18**, 651 (2003) [arXiv:gr-qc/0205129].

[70] P. Kanti, I. Olasagasti and K. Tamvakis, "Quest for localized 4-D black holes in brane worlds. II: Removing the bulk singularities," Phys. Rev. D **68**, 124001 (2003) [arXiv:hep-th/0307201].

[71] S. S. Seahra, "Naked shell singularities on the brane," Phys. Rev. D **71**, 084020 (2005) [arXiv:gr-qc/0501018].

[72] C. Galfard, C. Germani and A. Ishibashi, "Asymptotically adS brane black holes," Phys. Rev. D **73**, 064014 (2006) [arXiv:hep-th/0512001].

[73] A. Flachi, O. Pujolas, M. Sasaki and T. Tanaka, "Dynamics of domain walls intersecting black holes," [arXiv:hep-th/0601174].

[74] T. Shiromizu and M. Shibata, "Black holes in the brane world: Time symmetric initial data," Phys. Rev. D **62**, 127502 (2000) [arXiv:hep-th/0007203].

[75] A. Chamblin, H. S. Reall, H. a. Shinkai and T. Shiromizu, "Charged brane-world black holes," Phys. Rev. D **63**, 064015 (2001) [arXiv:hep-th/0008177].

[76] T. Wiseman, "Relativistic stars in Randall-Sundrum gravity," Phys. Rev. D **65**, 124007 (2002) [arXiv:hep-th/0111057].

[77] H. Kudoh, T. Tanaka and T. Nakamura, "Small localized black holes in braneworld: Formulation and numerical method," Phys. Rev. D **68**, 024035 (2003) [arXiv:gr-qc/0301089].

[78] T. Banks and W. Fischler, "A model for high energy scattering in quantum gravity," [arXiv:hep-th/9906038].

[79] R. Emparan, G. T. Horowitz and R. C. Myers, "Black holes radiate mainly on the brane," Phys. Rev. Lett. **85**, 499 (2000) [arXiv:hep-th/0003118].

[80] P. D. D'Eath and P. N. Payne, "Gravitational radiation in high speed black hole collisions. 1. Perturbation treatment of the axisymmetric speed of light collision," Phys. Rev. D **46**, 658 (1992).

[81] P. D. D'Eath and P. N. Payne, "Gravitational radiation in high speed black hole collisions. 2. Reduction to two independent variables and calculation of the second order news function," Phys. Rev. D **46**, 675 (1992).

[82] P. D. D'Eath and P. N. Payne, "Gravitational radiation in high speed black hole collisions. 3. Results and conclusions," Phys. Rev. D **46**, 694 (1992).

[83] E. Berti, M. Cavaglia and L. Gualtieri, "Gravitational energy loss in high energy particle collisions: Ultrarelativistic plunge into a multidimensional black hole," Phys. Rev. D **69**, 124011 (2004) [arXiv:hep-th/0309203].

[84] H. Yoshino, T. Shiromizu and M. Shibata, "The close limit analysis for head-on collision of two black holes in higher dimensions: Brill-Lindquist initial data," Phys. Rev. D **72**, 084020 (2005) [arXiv:gr-qc/0508063].

[85] D. M. Eardley and S. B. Giddings, "Classical black hole production in high-energy collisions," Phys. Rev. D **66**, 044011 (2002) [arXiv:gr-qc/0201034].

[86] H. Yoshino and Y. Nambu, "High-energy head-on collisions of particles and hoop conjecture," Phys. Rev. D **66**, 065004 (2002) [arXiv:gr-qc/0204060].

[87] H. Yoshino and Y. Nambu, "Black hole formation in the grazing collision of high-energy particles," Phys. Rev. D **67**, 024009 (2003) [arXiv:gr-qc/0209003].

[88] E. Kohlprath and G. Veneziano, "Black holes from high-energy beam-beam collisions," JHEP **0206**, 057 (2002) [arXiv:gr-qc/0203093].

[89] S. B. Giddings and V. S. Rychkov, "Black holes from colliding wavepackets," Phys. Rev. D **70**, 104026 (2004) [arXiv:hep-th/0409131].

[90] H. Yoshino and V. S. Rychkov, "Improved analysis of black hole formation in high-energy particle collisions," Phys. Rev. D **71**, 104028 (2005) [arXiv:hep-th/0503171].

[91] D. C. Dai, G. D. Starkman and D. Stojkovic, "Production of black holes and their angular momentum distribution in models with split fermions," Phys. Rev. D **73**, 104037 (2006) [arXiv:hep-ph/0605085].

[92] H. Yoshino and R. B. Mann, "Black hole formation in the head-on collision of ultrarelativistic charges," Phys. Rev. D **74**, 044003 (2006) [arXiv:gr-qc/0605131].

[93] H. Yoshino, T. Shiromizu and M. Shibata, "Close-slow analysis for head-on collision of two black holes in higher dimensions: Bowen-York initial data," Phys. Rev. D **74**, 124022 (2006) [arXiv:gr-qc/0610110].

[94] D. Ida, K. y. Oda and S. C. Park, "Rotating black holes at future colliders: Greybody factors for brane fields," Phys. Rev. D **67**, 064025 (2003) [Erratum-ibid. D **69**, 049901 (2004)] [arXiv:hep-th/0212108].

[95] C. M. Harris, "Physics beyond the standard model: Exotic leptons and black holes at future colliders," [arXiv:hep-ph/0502005].

[96] S. W. Hawking, "Particle creation by black holes," Commun. Math. Phys. **43**, 199 (1975) [Erratum-ibid. **46**, 206 (1976)].

[97] P. C. Argyres, S. Dimopoulos and J. March-Russell, "Black holes and submillimeter dimensions," Phys. Lett. B **441**, 96 (1998) [arXiv:hep-th/9808138].

[98] S. B. Giddings and S. D. Thomas, "High energy colliders as black hole factories: The end of short distance physics," Phys. Rev. D **65**, 056010 (2002) [arXiv:hep-ph/0106219].

[99] S. B. Giddings, "Black hole production in TeV-scale gravity, and the future of high energy physics," *In the Proceedings of APS / DPF / DPB Summer Study on the Future of Particle Physics (Snowmass 2001), Snowmass, Colorado, 30 Jun - 21 Jul 2001, pp P328* [arXiv:hep-ph/0110127].

[100] R. C. Myers and M. J. Perry, "Black holes in higher dimensional spacetimes," Annals Phys. **172**, 304 (1986).

[101] R. P. Kerr, "Gravitational field of a spinning mass as an example of algebraically special metrics," Phys. Rev. Lett. **11**, 237 (1963).

[102] N. D. Birrell and P. C. W. Davies, "Quantum Fields In Curved Space," *Cambridge, Uk: Univ. Pr. (1982) 340p*

[103] B. S. Kay and R. M. Wald, "Theorems on the uniqueness and thermal properties of stationary, non-singular, quasifree states on spacetimes with a bifurcate Killing horizon," Phys. Rept. **207**, 49 (1991).

[104] A. C. Ottewill and E. Winstanley, "The renormalized stress tensor in Kerr spacetime: General results," Phys. Rev. D **62**, 084018 (2000) [arXiv:gr-qc/0004022].

[105] D. R. Brill, P. L. Chrzanowski, C. Martin Pereira, E. D. Fackerell and J. R. Ipser, "Solution of the scalar wave equation in a Kerr background by separation of variables," Phys. Rev. D **5**, 1913 (1972).

[106] Y. B. Zel'dovich, JETP Lett. **14**, 180 (1971).

[107] D. A. Leahy and W. G. Unruh, "Angular dependence of neutrino emission from rotating black holes," Phys. Rev. D **19**, 3509 (1979).

[108] M. Casals and A. C. Ottewill, "Canonical quantization of the electromagnetic field on the Kerr background," Phys. Rev. D **71**, 124016 (2005) [arXiv:gr-qc/0501005].

[109] E. Winstanley, "Hawking radiation from rotating brane black holes," arXiv:0708.2656 [hep-th].

[110] V. P. Frolov and D. Stojkovic, "Quantum radiation from a 5-dimensional rotating black hole," Phys. Rev. D **67**, 084004 (2003) [arXiv:gr-qc/0211055].

[111] C. M. Harris and P. Kanti, "Hawking radiation from a (4+n)-dimensional black hole: Exact results for the Schwarzschild phase," JHEP **0310**, 014 (2003) [arXiv:hep-ph/0309054].

[112] S. S. Gubser, "Can the effective string see higher partial waves?," Phys. Rev. D **56**, 4984 (1997) [arXiv:hep-th/9704195].

[113] P. Kanti and J. March-Russell, "Calculable corrections to brane black hole decay. I: The scalar case," Phys. Rev. D **66**, 024023 (2002) [arXiv:hep-ph/0203223].

[114] P. Kanti and J. March-Russell, "Calculable corrections to brane black hole decay. II: Greybody factors for spin 1/2 and 1," Phys. Rev. D **67**, 104019 (2003) [arXiv:hep-ph/0212199].

[115] M. Casals, P. Kanti and E. Winstanley, "Brane decay of a (4+n)-dimensional rotating black hole. II: Spin-1 particles," JHEP **0602**, 051 (2006) [arXiv:hep-th/0511163].

[116] C. M. Harris and P. Kanti, "Hawking radiation from a (4+n)-dimensional rotating black hole," Phys. Lett. B **633**, 106 (2006) [arXiv:hep-th/0503010].

[117] G. Duffy, C. Harris, P. Kanti and E. Winstanley, "Brane decay of a (4+n)-dimensional rotating black hole: Spin-0 particles," JHEP **0509**, 049 (2005) [arXiv:hep-th/0507274].

[118] D. Ida, K. y. Oda and S. C. Park, "Anisotropic scalar field emission from TeV scale black hole," [arXiv:hep-ph/0501210].

[119] M. Casals, S. R. Dolan, P. Kanti and E. Winstanley, "Brane decay of a (4+n)-dimensional rotating black hole. III: Spin-1/2 particles," JHEP **0703**, 019 (2007) [arXiv:hep-th/0608193].

[120] D. Ida, K. y. Oda and S. C. Park, "Rotating black holes at future colliders. II: Anisotropic scalar field emission," Phys. Rev. D **71**, 124039 (2005) [arXiv:hep-th/0503052].

[121] D. Ida, K. y. Oda and S. C. Park, "Rotating black holes at future colliders. III: Determination of black hole evolution," Phys. Rev. D **73**, 124022 (2006) [arXiv:hep-th/0602188].

[122] E. Jung and D. K. Park, "Bulk versus brane in the absorption and emission: 5D rotating black hole case," Nucl. Phys. B **731**, 171 (2005) [arXiv:hep-th/0506204].

[123] E. Newman and R. Penrose, "An approach to gravitational radiation by a method of spin coefficients," J. Math. Phys. **3**, 566 (1962).

[124] S. Chandrasekhar, "The mathematical theory of black holes," *Oxford, UK: Clarendon (1992) 646 p.*

[125] W. H. Press and S. A. Teukolsky, Astrophys. J. **185**, 649 (1973).

[126] A. A. Starobinskii and S. M. Churilov, Zh. Eksp. Teor. Fiz. **65**, 3 (1973).

[127] E. D. Fackerell and R. G. Crossman, J. Math. Phys. **18**, 1849 (1977).

[128] R. A. Breuer, *Gravitational perturbation theory and synchrotron radiation*, Lecture Notes in Physics Vol. 44 (Springer, Berlin, 1975).

[129] R. Breuer, M. Ryan Jr. and S. Waller, Proc. R. Soc. London A **358**, 71 (1977).

[130] M. Casals and A. C. Ottewill, "High frequency asymptotics for the spin-weighted spheroidal equation," Phys. Rev. D **71**, 064025 (2005) [gr-qc/0409012].

[131] A. A. Starobinskii and S. M. Churilov, *Sov. Phys.-JETP* **38**, 1 (1974).

[132] E. Seidel, "A comment on the eigenvalues of spin weighted spheroidal functions," Class. Quant. Grav. **6**, 1057 (1989).

[133] M. Abramowitz and I. A. Stegun, "Handbook of mathematical functions," *Dover, New York (1972)*

[134] S. A. Teukolsky, "Perturbations of a rotating black hole. 1. Fundamental equations for gravitational electromagnetic, and neutrino field perturbations," Astrophys. J. **185**, 635 (1973).

[135] W. G. Unruh, "Second quantization in the Kerr metric," Phys. Rev. D **10**, 3194 (1974).

[136] W. G. Unruh, "Absorption cross-section of small black holes," Phys. Rev. D **14** (1976) 3251.

[137] R. Gueven, "Wave mechanics of electrons in Kerr geometry," Phys. Rev. D **16**, 1706 (1977).

[138] S. L. Detweiler, Proc. Roy. Soc. Lond. A **349**, 217 (1976)

[139] S. S. Gubser, "Absorption of photons and fermions by black holes in four dimensions," Phys. Rev. D **56**, 7854 (1997) [arXiv:hep-th/9706100].

[140] C. W. Misner, K. S. Thorne and J. A. Wheeler, "Gravitation," *San Francisco 1973, 1279p*

[141] D. N. Page, "Particle emission rates from a black hole: Massless particles from an uncharged, nonrotating hole," Phys. Rev. D **13**, 198 (1976).

[142] N. G. Sanchez, "The wave scattering theory and the absorption problem for a black hole," Phys. Rev. D **16**, 937 (1977).

[143] N. G. Sanchez, "Absorption and emission spectra of a Schwarzschild black hole," Phys. Rev. D **18**, 1030 (1978).

[144] N. G. Sanchez, "Elastic scattering of waves by a black hole," Phys. Rev. D **18**, 1798 (1978).

[145] J. H. MacGibbon and B. R. Webber, "Quark and gluon jet emission from primordial black holes: The instantaneous spectra," Phys. Rev. D **41**, 3052 (1990).

[146] V. P. Frolov and I. D. Novikov, "Black hole physics: Basic concepts and new developments," *Dordrecht, Netherlands: Kluwer Academic (1998) 770 p*

[147] C. Muller, in *Lecture Notes in Mathematics: Spherical Harmonics* (Springer-Verlag, Berlin-Heidelberg, 1966).

[148] D. Ida, Y. Uchida and Y. Morisawa, "The scalar perturbation of the higher-dimensional rotating black holes," Phys. Rev. D **67**, 084019 (2003) [arXiv:gr-qc/0212035].

[149] E. Berti, V. Cardoso and M. Casals, "Eigenvalues and eigenfunctions of spin-weighted spheroidal harmonics in four and higher dimensions," Phys. Rev. D **73**, 024013 (2006) [Erratum-ibid. D **73**, 109902 (2006)] [arXiv:gr-qc/0511111].

[150] V. Cardoso, G. Siopsis and S. Yoshida, "Scalar perturbations of higher dimensional rotating and ultra-spinning black holes," Phys. Rev. D **71**, 024019 (2005) [arXiv:hep-th/0412138].

[151] F. R. Tangherlini, "Schwarzschild field in n dimensions and the dimensionality of space problem," Nuovo Cim. **27**, 636 (1963).

[152] H. Kodama and M. Sasaki, "Cosmological perturbation theory," Prog. Theor. Phys. Suppl. **78**, 1 (1984).

[153] H. Kodama, A. Ishibashi and O. Seto, "Brane world cosmology: Gauge-invariant formalism for perturbation," Phys. Rev. D **62**, 064022 (2000) [arXiv:hep-th/0004160].

[154] H. Kodama and A. Ishibashi, "A master equation for gravitational perturbations of maximally symmetric black holes in higher dimensions," Prog. Theor. Phys. **110**, 701 (2003) [arXiv:hep-th/0305147].

[155] V. Cardoso, M. Cavaglia and L. Gualtieri, "Black hole particle emission in higher-dimensional spacetimes," Phys. Rev. Lett. **96**, 071301 (2006) [Erratum-ibid. **96**, 219902 (2006)] [arXiv:hep-th/0512002].

[156] V. Cardoso, M. Cavaglia and L. Gualtieri, "Hawking emission of gravitons in higher dimensions: Non-rotating black holes," JHEP **0602**, 021 (2006) [arXiv:hep-th/0512116].

[157] A. S. Cornell, W. Naylor and M. Sasaki, "Graviton emission from a higher-dimensional black hole," JHEP **0602**, 012 (2006) [arXiv:hep-th/0510009].

[158] M. A. Rubin and C. R. Ordonez, "Eigenvalues and degeneracies for n-dimensional tensor spherical harmonics," J. Math. Phys. **25**, 2888 (1984).

[159] M. A. Rubin and C. R. Ordonez, "Symmetric tensor eigenspectrum of the laplacian on n-spheres," J. Math. Phys. **26**, 65 (1985).

Appendix A

Detailed Calculations

A.1 Extrinsic Curvature Components

If the spacelike vector n^A denotes the normal to a timelike hypersurface Σ and is normalised such that $n_A n^A = 1$, then the change in the normal vector when it is parallel transported along some vector T^A parallel to Σ must lie entirely in Σ since

$$n^B T^A \nabla_A n_B = \frac{1}{2} T^A \nabla_A \left(n^B n_B \right) = 0 \,. \tag{A.1.1}$$

Consequently the extrinsic curvature K_{AB} may be defined over Σ as the Ath component of the change in the normal one-form when parallel transported along the Bth coordinate curve

$$K_{AB} = h_A^M h_B^N \nabla_M n_N \,, \tag{A.1.2}$$

where h_{AB} is the projection tensor described in §3.1. If $U = \frac{d}{d\lambda}$ and $V = \frac{d}{d\nu}$ are two arbitrary vectors tangent to Σ then the extrinsic curvature K_{UV} in these directions may be evaluated by performing a geodesic-like calculation

$$\begin{aligned} K_{UV} &= U^A V^B h_A^M h_B^N \nabla_M n_N = U^M V^N \nabla_M n_N \\ &= -U^M n_N \nabla_M V^N \qquad \left(\text{since } V^N n_N = 0\right) \\ &= -n_N \left[\frac{d^2 x^N}{d\lambda d\nu} + \Gamma^N_{MS} \frac{dx^M}{d\lambda} \frac{dx^S}{d\nu} \right] \,, \end{aligned} \tag{A.1.3}$$

where Γ^N_{MS} are the connection coefficients associated with the metric of the bulk spacetime. It is now possible to apply this to the circumstances in §3.1 to calculate the extrinsic curvature components parallel to the brane tangent vectors (3.2).

Working with basis functions $x^A = (\tau, r, \chi, \theta, \phi)$, in terms of which the bulk metric may be written

$$ds^2 = -U(r)\,d\tau^2 + \frac{1}{U(r)}\,dr^2 + r^2(d\chi^2 + \sin^2\chi\,d\Omega_2^2)\,, \tag{A.1.4}$$

then the brane location may be specified by the constraint $\chi = \chi(\tau, r)$ and the normal takes the form

$$n_A = n(-\dot{\chi}, -\chi', 1, 0, 0) \qquad \text{where} \qquad \frac{1}{n^2} = \left(-\frac{\dot{\chi}^2}{U} + U\chi'^2 + \frac{1}{r^2}\right), \tag{A.1.5}$$

with overdot and prime denoting $\partial/\partial\tau$ and $\partial/\partial r$ respectively. With this notation the non-zero components of the extrinsic curvature may be evaluated using equation (A.1.3) as:

$$\begin{aligned} K_{TT} &= -n_N\left[\frac{d^2x^N}{d\tau^2} + \Gamma^N_{MS}\frac{dx^M}{d\tau}\frac{dx^S}{d\tau}\right] = -n_r\left[\Gamma^r_{\tau\tau} + \Gamma^r_{\chi\chi}\dot{\chi}^2\right] - n_\chi\left[\ddot{\chi}\right] \\ &= -n\left(\ddot{\chi} + Ur\chi'\dot{\chi}^2 - \frac{1}{2}UU'\chi'\right), \end{aligned} \tag{A.1.6}$$

$$\begin{aligned} K_{RR} &= -n_N\left[\frac{d^2x^N}{dr^2} + \Gamma^N_{MS}\frac{dx^M}{dr}\frac{dx^S}{dr}\right] = -n_r\left[\Gamma^r_{rr} + \Gamma^r_{\chi\chi}\chi'^2\right] - n_\chi\left[\chi'' + 2\Gamma^\chi_{r\chi}\chi'\right] \\ &= -n\left(\chi'' + \frac{2\chi'}{r} + \frac{U'\chi'}{2U} + Ur\chi'^3\right), \end{aligned} \tag{A.1.7}$$

$$\begin{aligned} K_{TR} &= -n_N\left[\frac{d^2x^N}{d\tau dr} + \Gamma^N_{MS}\frac{dx^M}{d\tau}\frac{dx^S}{dr}\right] = -n_\tau\left[\Gamma^\tau_{\tau r}\right] - n_r\left[\Gamma^r_{\chi\chi}\dot{\chi}\chi'\right] - n_\chi\left[\dot{\chi}' + \Gamma^\chi_{r\chi}\dot{\chi}\right] \\ &= -n\left(\dot{\chi}' + \frac{\dot{\chi}}{r} + Ur\chi'^2\dot{\chi} - \frac{U'\dot{\chi}}{2U}\right), \end{aligned} \tag{A.1.8}$$

$$\begin{aligned} K_{\Theta\Theta} &= -n_N\left[\frac{d^2x^N}{d\theta^2} + \Gamma^N_{MS}\frac{dx^M}{d\theta}\frac{dx^S}{d\theta}\right] = -n_r\left[\Gamma^r_{\theta\theta}\right] - n_\chi\left[\Gamma^\chi_{\theta\theta}\right] \\ &= -n\left(Ur\chi'\sin^2\chi - \sin\chi\cos\chi\right). \end{aligned} \tag{A.1.9}$$

$$\begin{aligned} K_{\Phi\Phi} &= -n_N\left[\frac{d^2x^N}{d\phi^2} + \Gamma^N_{MS}\frac{dx^M}{d\phi}\frac{dx^S}{d\phi}\right] = -n_r\left[\Gamma^r_{\phi\phi}\right] - n_\chi\left[\Gamma^\chi_{\phi\phi}\right] \\ &= -n\sin^2\theta\left(Ur\chi'\sin^2\chi - \sin\chi\cos\chi\right) = \sin^2\theta K_{\Theta\Theta}\,. \end{aligned} \tag{A.1.10}$$

A.2 The Time-Dependent Brane Equation of State

The Israel equations (3.16)-(3.18) may be written as

$$\frac{r^2\ddot{\alpha}}{U} - (\alpha' r - \alpha)\left(\frac{1}{2}U' r - U\right) + \alpha + \zeta A = 0\,, \tag{A.2.1}$$

$$U r^2 \alpha'' + (\alpha' r - \alpha)\left(\frac{1}{2}U' r - U\right) - \alpha + \zeta B = 0\,, \tag{A.2.2}$$

$$r^2\dot{\alpha}' - \frac{1}{2}\frac{U' r}{U} r\dot{\alpha} + \zeta C = 0\,, \tag{A.2.3}$$

where

$$A = \frac{1}{U}\left(-U + \frac{r^2\dot{\alpha}^2}{r^2 - \alpha^2}\right)\,, \tag{A.2.4}$$

$$B = \frac{U r^2 \dot{\alpha}^2 (\alpha' r - \alpha)^2}{(r^2 - \alpha^2)^2\left(-U + \frac{r^2\dot{\alpha}^2}{r^2 - \alpha^2}\right)}\,, \tag{A.2.5}$$

$$C = \frac{r\dot{\alpha}(\alpha' r - \alpha)}{(r^2 - \alpha^2)}\,, \tag{A.2.6}$$

$$\zeta = (1 + v)(U(\alpha' r - \alpha) + \alpha)\,, \tag{A.2.7}$$

and consequently $AB = C^2$. An additional constraint between the above Israel equations may be obtained by differentiating equation (A.2.1) with respect to r and equation (A.2.3) with respect to τ and then requiring consistency of the third-order mixed derivative $\ddot{\alpha}'$:

$$r\frac{\partial}{\partial r}(\text{A.2.1}) \quad \Rightarrow \quad \frac{2r^2\ddot{\alpha}}{U} + \frac{r^3\ddot{\alpha}'}{U} - \frac{r^2\ddot{\alpha}U' r}{U^2} - \alpha'' r^2\left(\frac{1}{2}U' r - U\right) - \tag{A.2.8}$$
$$(\alpha' r - \alpha)\left(\frac{1}{2}U'' r^2 - \frac{1}{2}U' r\right) + \alpha' r + \zeta' A r + \zeta A' r = 0\,,$$

$$r\frac{\partial}{\partial \tau}(\text{A.2.3}) \quad \Rightarrow \quad r^3\ddot{\alpha}' - \frac{1}{2}\frac{U' r}{U} r^2\ddot{\alpha} + \dot{\zeta} C r + \zeta \dot{C} r = 0\,, \tag{A.2.9}$$

$$\Rightarrow \quad (\alpha' r - \alpha)\left(-\frac{1}{2}U'' r^2 + U' r - U + 1\right) + \frac{\zeta}{U}(A + B)\left(\frac{1}{2}U' r - U\right) - \zeta A + \tag{A.2.10}$$
$$\zeta A' r + \zeta' A r - \frac{1}{U}(\dot{\zeta} C r + \zeta \dot{C} r) = 0\,.$$

A further constraint is obtained by performing a similar procedure but ensuring consistency of the other third-order mixed derivative $\dot{\alpha}''$:

$$r\frac{\partial}{\partial\tau}(\text{A.2.2}) \quad \Rightarrow \quad Ur^3\dot{\alpha}'' + \left(\frac{1}{2}U'r - U\right)(\dot{\alpha}'r^2 - \dot{\alpha}r) - \dot{\alpha}r + \dot{\zeta}Br + \zeta\dot{B}r = 0\,, \tag{A.2.11}$$

$$r\frac{\partial}{\partial r}(\text{A.2.3}) \quad \Rightarrow \quad 2r^2\dot{\alpha}' + r^3\dot{\alpha}'' - \frac{1}{2}\frac{U''r^2}{U}\dot{\alpha}r - \frac{U'r}{U}\dot{\alpha}r + \frac{1}{2}\left(\frac{U'r}{U}\right)^2\dot{\alpha}r - \frac{1}{2}\frac{U'r}{U}r^2\dot{\alpha}' + \zeta'Cr + \zeta C'r = 0\,, \tag{A.2.12}$$

$$\Rightarrow \quad \frac{r\dot{\alpha}}{U}\left(-\frac{1}{2}U''r^2 + U'r - U + 1\right) + \frac{2\zeta C}{U}\left(\frac{1}{2}U'r - U\right) - \zeta C + \zeta C'r + \zeta'Cr - \frac{1}{U}(\dot{\zeta}Br + \zeta\dot{B}r) = 0\,. \tag{A.2.13}$$

In the cases analysed in chapter 3 it was possible to solve the system of equations explicitly for the special cases of time independence or brane equation of state $w = -1$ since the conditions on the energy density could be integrated to give

$$\rho = \frac{\rho_0}{r^2}\left[U(\alpha'r - \alpha) + \alpha\right]\,, \tag{A.2.14}$$

for ρ_0 an arbitrary constant. In the more general case this is not possible, owing to the extra terms arising in equations (3.27) and (3.28). However, motivated by the result above some simplification can be obtained by assuming the above form for the energy density, but promoting ρ_0 to be an arbitrary function of τ and r: $\rho_0(\tau, r)$. In this case equations (3.27) and (3.28) may be written in the more compact form

$$\frac{\dot{\rho}_0 r}{\rho_0} = \frac{\zeta C}{(\alpha'r - \alpha)}\,, \tag{A.2.15}$$

$$\frac{\rho_0' r}{\rho_0} = \frac{\zeta B}{U(\alpha'r - \alpha)}\,. \tag{A.2.16}$$

Now, ensuring consistency of the mixed derivative $\dot{\rho}_0'$, found from taking the appropriate derivatives of the above two equations, and then substituting back for the first order derivatives of ρ_0 gives the condition

$$\zeta C'r + \zeta'Cr - \frac{1}{U}(\dot{\zeta}Br + \zeta\dot{B}r) = \zeta C\left[1 - \frac{1}{U}\left(\frac{1}{2}U'r - U\right) + \frac{\alpha}{U(\alpha'r - \alpha)}\right] - \frac{\zeta B\dot{\alpha}r}{U^2(\alpha'r - \alpha)}\left(\frac{1}{2}U'r - U\right)\,. \tag{A.2.17}$$

The left hand side of equation (A.2.17) is exactly the quantity appearing on the second line of (A.2.13) so the above may be used to substitute back into (A.2.13) to remove all derivatives of ζ, B and C. The resulting equation may be rearranged to give

$$\zeta = \frac{r\dot{\alpha}(\alpha' r - \alpha)\left(\frac{1}{2}U'' r^2 - U' r + U - 1\right)}{C\left[(\alpha' r - \alpha)\left(\frac{1}{2}U' r - U\right) + \alpha\right] - \frac{B\dot{\alpha} r}{U}\left(\frac{1}{2}U' r - U\right)}, \tag{A.2.18}$$

or

$$1+v = \frac{(r^2-\alpha^2)(\frac{1}{2}U''r^2 - U'r + U - 1)}{(U(\alpha' r - \alpha) + \alpha)[(\alpha' r - \alpha)(\frac{1}{2}U' r - U) + \alpha - \frac{r^2\dot{\alpha}^2(\alpha' r - \alpha)(\frac{1}{2}U'r - U)}{(r^2-\alpha^2)(-U + \frac{r^2\dot{\alpha}^2}{r^2-\alpha^2})}]}. \tag{A.2.19}$$

A.3 Convergence of the Series Solution to the SadS Brane

From the analysis of §3.5 two independent series solutions to the differential equation (3.49) governing the shape of the brane may be found. They can be written as

$$\alpha(r) = \sum_{n=0}^{\infty} a_n r^{2n+2} + \sum_{n=0}^{\infty} b_n r^{2n+1}, \tag{A.3.1}$$

where a_0 and b_0 are arbitrary constants and a_n and b_n satisfy the recurrence relations

$$a_1 = 0, \tag{A.3.2}$$

$$a_n = \frac{k^2(n-1)\left(n-\frac{3}{2}\right)}{\mu n\left(n+\frac{1}{2}\right)} a_{n-2} + \frac{(n-1)}{\mu\left(n+\frac{1}{2}\right)} a_{n-1} \qquad (\text{for } n \geq 2), \tag{A.3.3}$$

$$b_1 = -\frac{b_0}{2\mu}, \tag{A.3.4}$$

$$b_n = \frac{k^2\left(n-\frac{3}{2}\right)(n-2)}{\mu n\left(n-\frac{1}{2}\right)} b_{n-2} + \frac{\left(n-\frac{3}{2}\right)}{\mu n} b_{n-1} \qquad (\text{for } n \geq 2). \tag{A.3.5}$$

Considering first the "a" solution, from the above recurrence relation it is clear that all coefficients in the series have the same sign, so any radius of convergence that can be found to a sub-series must represent an upper limit to the radius of convergence of the full series. In particular, coefficients a_{2m}, for integer m, each contain a term of the form

$$a_{2m} \supset \frac{a_0 k^{2m}}{\mu^m} \prod_{j=1}^{m} \frac{(2j-1)\left(2j-\frac{3}{2}\right)}{2j\left(2j+\frac{1}{2}\right)} = \frac{a_0 k^{2m}}{\mu^m} \frac{(2m)!}{2^{2m}(m!)^2(4m+1)}. \tag{A.3.6}$$

Transforming to the dimensionless quantities $\sigma = \mu k^2$ and $\xi = kr$ the "a" solution contains a sub-series

$$\alpha(\xi) \supset a_0 \sum_{n=0}^{\infty} \frac{1}{\sigma^n} \frac{(2n)!}{2^{2n}(n!)^2(4n+1)} \xi^{4n+2} = \sum_{n=0}^{\infty} s_n \xi^{4n+2}, \tag{A.3.7}$$

the first three terms of which are visible in equation (3.92). Employing D'Alembert's ratio test, a limit may be placed on the radius of convergence of this sub-series by requiring

$$\begin{aligned} &\lim_{n\to\infty} \left| \frac{s_{n+1}}{s_n} \xi^4 \right| = \lim_{n\to\infty} \left| \frac{(2n+2)(2n+1)(4n+1)}{4\sigma(n+1)^2(4n+5)} \xi^4 \right| < 1 \\ &\Rightarrow \xi < \sqrt[4]{\sigma}. \end{aligned} \tag{A.3.8}$$

This consequently places the same upper limit on the radius of conversion of the full "a" series solution. It can similarly be shown that the "b" series contains a sub-series of the form

$$\alpha(\xi) \supset b_0 \sum_{n=1}^{\infty} \frac{1}{\sigma^n} \left(\frac{1}{2(2n-1)} \prod_{i=1}^{n} \frac{4i-5}{4i-3} \right) \xi^{4n-1} = \sum_{n=1}^{\infty} t_n \xi^{4n-1}, \tag{A.3.9}$$

where, again, the first three terms are apparent in equation (3.92). Utilising D'Alembert's ratio test

$$\begin{aligned} &\lim_{n\to\infty} \left| \frac{t_{n+1}}{t_n} \xi^4 \right| = \lim_{n\to\infty} \left| \frac{(2n-1)(4n-1)}{\sigma(2n+1)(4n+1)} \xi^4 \right| < 1 \\ &\Rightarrow \xi < \sqrt[4]{\sigma}, \end{aligned} \tag{A.3.10}$$

demonstrates that $\sqrt[4]{\sigma}$ is also an upper limit to the radius of convergence of the "b" solution.

The presence of this upper limit precludes the existence of any finite-term series solutions extending to the adS boundary. Moreover, it can be seen that for many values of the parameter σ the limit on the radius of convergence is far more restrictive. The value of the dimensionless coordinate ξ corresponding to the horizon radius in Schwarzschild-anti-de Sitter spacetime is given by $\xi_H = \sqrt{\frac{-1+\sqrt{1+4\sigma}}{2}}$. For $\sigma = 1$ it is apparent that the upper limit on the radius of convergence may be written as $\xi_{max} = 1.27\xi_H$. However, the low-order expansion (3.92) is only valid in the limit $\sigma \gg 1$ and as σ increases into this region then ξ_{max} tends rapidly to ξ_H, implying the solution is only valid inside the horizon.